Role of microtubule associated proteins in epithelial apico-basal polarisation and tissue architecture

Benjamin Rix

A thesis submitted in fulfilment of the requirements for the degree of Doctor of Philosophy

School of Biological Sciences

Norwich Research Park

University of East Anglia

March 2021

Word Count: 58,817

Abstract

The cytoskeleton is an integral aspect of many cellular functions and plays an important role in normal tissue development as well as in the pathologies of many diseases. One such function can be seen in the maintenance and formation of apico-basal polarised epithelial cells. Dysregulation of this epithelium causes many developmental diseases and cancers. In fact, 90% of all cancers develop in epithelial cells. As in many systems, microtubules are responsible for the asymmetrical distribution of polarity determinants in the epithelium which is ultimately controlled by the centrosome and microtubule associated proteins.

During apico-basal polarisation, the centrosome moves to an apical position where it nucleates microtubules, in kidney epithelium for example. The role and importance of the centrosome in this system is yet to be fully elucidated. Here, the centrosome was removed using the PLK4 inhibitor centrinone B in the MDCKII cell line and apico-basal polarisation was studied in these cells. The centrosome proved essential in the normal organisation of many key microtubule associated proteins in polarising epithelial cells. Amongst these were the relatively new CAMSAP family of proteins where CAMSAP2 and CAMSAP3 lost their non-centrosomal microtubule organising centre localisation in the absence of the centrosome. Markers of polarity were also perturbed in acentrosomal cells suggesting that the centrosome is essential for the formation of apico-basal polarised cells. Furthermore, centrosome removal led to a complete failure of 3D cyst formation further showing evidence of the centrosomes importance in the formation of apico-basally polarised cells.

During the differentiation of these apico-basally polarised cells the microtubule end binding protein EB2 is differentially expressed. Here the effect of EB2 overexpression in the MDCKII cell line is studied, analysing many aspects of apico-basal polarisation. EB2 overexpression caused many cellular changes such as mis localisation of the PAR3 polarity marker and a distinct change in junction integrity. Analysis of cell shape suggests these EB2 overexpressing cells became unjammed although it could not be determined if this was due to epithelial-mesenchymal transition or due to the unjamming transition. Cell jamming describes the stability of an epithelial layer with a normal mature layer being jammed with regular cell shape and low motility. Unjamming is a deviation from this solid like state giving more fluid characteristics to the cell layer. Analysis of the centrosome showed increased γ-tubulin and nucleation here although ninein and therefore MT anchorage remained unchanged suggesting that EB2 influences MT nucleation at the centrosome but not anchorage.

CRISPR-Cas9 KO of EB2 in MDA-MB-231 cells was attempted in an effort to explore EB2s effect on cell migration, and further distinguish between epithelial-mesenchymal transition and the unjamming transition. This yielded a heterogenous cell line with reduced EB2 expression which caused a significant decrease in cell migration.

Access Condition and Agreement

Acknowledgments

Table of Contents

List of Figures

Chapter VI

List of Tables

List of Abbreviations

+TIP	plus-end tracking protein
2D	Two-dimensional
3D	Three-dimensional
ACF7	Actin cross-linking factor-7
ADP	Adenosine-5'-diphosphate
APC	Adenomatous polyposis coli
ATP	Adenosine-5'-triphosphate
BCA	Bicinchoninic Acid
BSA	Bovine serum albumin
Ca2+	Calcium ions
CAMSAPs	calmodulin-regulated spectrin-associated protein
CAP-Gly	Cytoskeleton-associated Protein Glycine-rich
CDK1	Cyclin-dependent kinase 1
Cepx	Centrosomal protein x
CH	Calponin homology domain
DABCO	1,4-diazabicyclo[2.2.2]octane
DAPI	4',6-diamidino-2-phenylindole
ddH2O	double distilled water
DMEM	Dulbecco's modified eagle mediumXVIII
DMSO	Dimethyl sulfoxide
EB1/2/3	End binding protein 1/2/3
EDTA	Ethylenediaminetetraacetic acid
EMT	Epithelial mesenchymal transition

GAP	GTPase activating proteins
GDP	Guanosine-5'-diphosphate
GFP	Green fluorescent protein
HEPES	N-2-Hydroxyethylpiperazine-N-2-Ethanesulfonic Acid
IQGAP 1/2/3	IQ motif containing GTPase activating protein 1/2/3
KIFx	Kinesin-like protein x
MAP	Microtubule associated protein
MDCK	Madin darby canine kidney
MT	Microtubule
MTOC	Microtubule organising centre
ncMTOC	non-centrosomal microtubule organising centre
PAR3	Partioning defective-3
PAGE	Polyacrylamide gel electrophoresis
PBS	Phosphate buffered saline
PCM	Pericentriolar matrix
pEMT	Partial epithelial-mesenchymal transition
Plkx	Polo-like kinase x
RFP	Red fluorescent protein
SAS-5	Spindle assembly abnormal protein 5
SDS	Sodium dodecyl sulphateXIX
UJT	Unjamming transition
ZO-1	Zona occludins-1
γ-TuRC	gamma tubulin ring complex
γ-TuSC	gamma tubulin small complex

Chapter I:

Introduction

1.0 Chapter I: Introduction

1.1 The Cytoskeleton

The cytoskeleton is a network of filamentous proteins that is present in almost all cells including bacteria and archaea. Three main components make up the cytoskeleton – actin filaments, intermediate filaments and microtubules (MTs). Actin filaments are known for their ability to generate force with the aid of motor proteins, the most obvious example is a muscle sarcomere where actin with myosin generates the forces necessary for muscle contraction. Actin also plays a role in mitosis where it forms into a contractile ring at the later stages of division, contraction of this ring leads to cell separation and cytokinesis (Schroeder, 1973, Pelham and Chang, 2002). Intermediate filaments are the largest (8-10nm in diameter) and most varied of the cytoskeletal components as there are five main types of filaments that make up this family. They function to increase structural integrity by withstanding stress particularly in cells exposed to high levels of mechanical stress such as keratinocytes. Intermediate filaments are also important for the positioning of various cellular organelles such as the nucleus for example (Dupin et al., 2011). MTs have a range of functions within cells and most notably are responsible for the transport of proteins and vesicles around the cell, this in turn can led to asymmetric distributions essential for many cell processes such as migration and division (Kaltschmidt and Brand, 2002). In fact, MTs are involved in a vast array of cellular processes such as cell growth and size determination, mitosis, cell fate decisions, movement of the cell and organelles and intracellular signalling.

1.1.1 Actin Filaments

Actin is the most abundant protein in many eukaryotic cells and is the smallest of the cytoskeletal filaments at ~5-9nm in diameter. Filamentous actin (F actin) is formed of monomers that are globular (G-actin), each G-actin subunit consists of 2 lobes separated by an incomplete cleft. The cleft being the site of enzymatic activity (ATPase fold) where ATP and $Mg2^+$ bind prior to hydrolysis to ADP. G-actin is only considered as functionally active when ATP is bound. Binding of ADP or ATP determines which state (F-actin or G-actin) actin is found within the cell (Murakami *et al.,* 2010, Merino *et al.,* 2018). F-actin is a single stranded dextrorotatory helix with a cross over within 350-380Å, meaning that a complete helix is formed every 350-380Å. G-actin arranges in a head to tail fashion to form F-actin that has polarity due to this repeating arrangement. The end that has its ATP binding site exposed is known as the minus end whereas the opposite end which has the cleft obscured by the adjacent bound G-actin is called the plus end. These ends may also be referred to as pointed and barbed respectively due to their appearance under transmission electron microscope along with myosin S1 fragments fixed with tannic acid (Dominguez and Holmes., 2011).

Nucleation of G-actin to form F-actin requires the aid of nucleating factors to form the initial structure that is to become the F-actin. The most researched of these nucleating factors is the Arp2/3 complex, which is a 7-subunit protein that mimics the structure of a G-actin dimer to allow binding of new molecules to this structure. Once an F-actin has nucleated, polymerisation can occur at the plus-end to extend the length of the filament (Mullins *et al.,* 1998, Amann and Pollard., 2001). Control of this process is essential to maintain the actin organisation within the cell, inhibitors and activators of actin mediate this process. Thymosin is a protein that slows the process of polymerisation by directly binding to G-actin monomers, preventing their incorporation into the filament (Heintz *et al.,* 1993). Profillin is an activator of actin polymerisation assisting in the exchange of ADP to ATP at the monomer cleft which can then bind to the plus end where the ATP is hydrolysed to ADP (Markey and Lindberg., 1978, Walders-Harbeck *et al.,* 2002). Actin polymerisation is also carried out by the formin family of proteins which have been shown to be involved in cell polarity including during migration and many other processes. The formin mDia 1 has been shown to have mechanical force sensing ability for the induction of actin polymerisation (Kubota *et al.,* 2017). There is also a stochastic element to actin polymerisation, a concentration of ~0.1µM G-actin is required for nucleation and continued polymerisation. This stochastic relationship is the cause of the treadmilling effect, as monomers are lost from the filament, the concentration increases which causes more monomeric addition to the plus end. This effect maintains filament length through an even exchange of subunits with loss at the minus end and addition at the plus end (Welch and Mullins., 2002, Robin *et al.,* 2021).

1.1.2 Intermediate Filaments

Intermediate filaments are important for the positioning and stabilisation of organelles such as the nucleus and contribute to some junctional structures such as the desmosomes and hemidesmosome. Intermediate filaments are most abundant in cells that encounter mechanical stress such as the skin where the intermediate filaments provide structural integrity. The composition of intermediate filaments depends on the cell/tissue type, keratins have high expression in epithelial cells whereas mesenchymal cells express vimentin. Compared to the other cytoskeletal components they are larger (8-10nm) in diameter and can be categorized into types I-VI. There are more than 70 genes that are expressed in human tissue and many pathologies related to mutation and mis regulation of these genes (Hesse *et al.,* 2001). The common feature of these intermediate filaments is a central α helical rod domain formed from four smaller helices. This structure wraps in an antiparallel pattern with another intermediate filament to form a dimer which then form a staggered tetramer with other dimers, lining up head to tail. Post translational modifications (PTMs) of intermediate filaments occur mainly at the head or tail domain, likely due to their importance in the dimerization

process. Modifications include phosphorylation, sumoylation, acetylation and glycosylation. Phosphorylation is the most common modification with many functions. It regulates axonal transport when neurofilaments are phosphorylated, cell migration where vimentin and keratins may become phosphorylated and cell growth where keratin phosphorylation is important (Snider and Omary, 2014). In particular, phosphorylation of keratin 18 was studied by Ku *et al.,* (2002), here mutation of a single phosphorylation site on keratin 18 led to disrupted filament organisation in a tissue dependent manner. Here, it was observed that mutation of the keratin phosphorylation site caused increased mitotic events in a tissue specific manner (Ku *et al.,* 2002).

Intermediate filaments form a rich network that underlies the apical membrane in many apico-basal polarised epithelial cells. An example of this is the intermediate filament IFB-2 which accumulates near the gut lumen in *C. elegans* during development and in adulthood. Using immunolabelling of a gut specific IFB-2 protein, it was shown that IFB-2 was confined to a discrete circumferential apical layer directly tethered to junctional structures. These are in turn joined to adjacent cell for increased structural integrity. Control of the localisation of IFB-2 was shown to be due to LET-143 by RNAi which is suggested to be responsible for the majority of intermediate filament apical web formation (Bossinger *et al.,* 2004).

1.2 Microtubules

MTs are cylindrical protein filaments conserved in all eukaryotic organisms and play a critical role in a variety of cellular process. These functions include cell division, cell motility and cell polarity (Garcin and Straube., 2019, Forth and Kapoor., 2019, Meiring *et al.,* 2020). They also provide structural support and transport of organelles, vesicles (cargo) and regulate the movement of some signalling molecules (Ross *et al.,* 2008). Importantly for this work, MTs are involved in the formation of apico-basal polarised cells such as in polarised kidney epithelia (Goldspink *et al.,* 2017).

1.2.1 Microtubule Structure and dynamics

MTs are composed of heterodimers each containing one α-tubulin monomer and one β-tubulin monomer. These heterodimers stack head to tail in a repeating manner to form what is known as a protofilament, a single stand of heterodimers. Thirteen of these protofilaments form the hollow tube structure of the MT although this can vary between 11 and 16 protofilaments (Mandelkow and Mandelkow, 1994, Nogales *et al.,* 2015). The head to tail formation of αβ heterodimers creates two distinct ends, one has exposed α-tubulin (minus end) and the other β-tubulin (plus end) (see Fig. 1.1). These two ends are structurally and functionally diverse, the minus end is slow growing and usually

anchors to a Microtubule Organising Centre (MTOC) such as the centrosome and the plus end is fast growing and extends out to the cell periphery (Akhmanova and Steinmetz, 2015). This polarity of MTs allows for the direction specific transport of proteins to and from the site of anchorage to the termination of the plus end.

MT dynamics are defined as the speed of MT polymerisation, the speed of depolymerisation, the rate of catastrophes and the rate of rescues within single MTs (Howard and Hyman, 2003, Roostalu and Surrey., 2017, van der Vaart *et al.,* 2009). In summary dynamic instability of MTs refers to the constant cycles of growth, pausing and shrinkage of the MT plus tip. MT polymerisation is not an energy dependent process as MT polymerisation still occurs in the presence of non-hydrolysable GTP to form stable MTs (Nogales., 1999). Polymerisation is ultimately driven by the high affinity of tubulin dimers even against compressive forces as seen when MTs do work. However, these MTs are slow to depolymerise and cannot function in this state, therefore GTP hydrolysis to GDP increases the rate of depolymerisation significantly, which increases turnover of MTs to allow them to function. At the dynamic plus tip, GTP binds αβ-heterodimers as they are incorporated into the MT, subsequently the GTP bound to the β tubulin monomer becomes hydrolysed to form GDP (Geyer *et al.,* 2015). The presence of GDP is a marker of instability and causes an increase in MT dynamics. A GTP cap exists at the plus end of the MT, GTP bound to tubulin here causes a straighter conformation compared to that of GDP decorated tubulin which has increased curvature and torsional stress at this point, increasing the likelihood of depolymerisation, increasing MT dynamics (Nawrotek *et al.,* 2011). The control of this GTP cap is one of the key elements to the control of MT dynamics (Ohi and Zanic., 2019).

There are many aspects that influence the dynamics of MTs such as post translational modification of the tubulin structure itself. This in turn either directly influences MT stability through conformational change or indirectly as it alters the binding affinity of MT associated proteins (MAPs) such as the end binding (EB) proteins which have a drastic effect of plus tip dynamics. These aspects are described below.
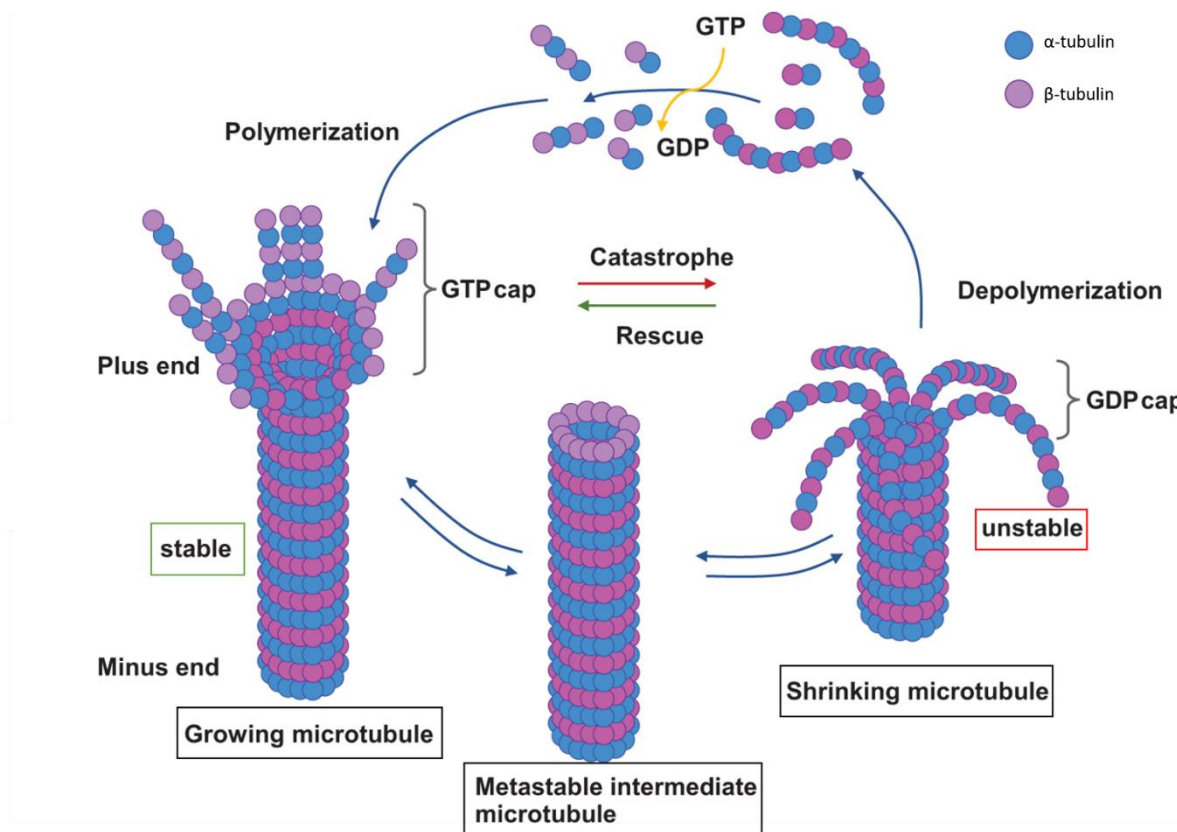
Figure 1.1 Microtubule structure and dynamics. MTs show a property called dynamic instability meaning they undergo a constant transition between growth, pausing and shrinkage. This is driven by hydrolysis of GTP at the plus tip. GTP bound tubulin dimers are added to the GTP cap of these growing MTs. Loss of this GTP cap via hydrolysis leads to depolymerisation or catastrophe (rapid depolymerisation). It is thought that GTP is also found in islands in the MT lattice to rescue this catastrophe. Adapted from Mierke., (2018).

1.2.2 Microtubule Nucleation

MT nucleation is the formation of a new MT from its subunits, it is a process that can naturally occur in the absence of cellular machinery but is greatly enhanced with this machinery present. In flat cells, nucleation mainly occurs at the centrosome via γ-tubulin localised there. At the centrosome a γ-tubulin structure resembles a MT as a template for the initiation of MT nucleation and polymerisation by the recruitment of αβ-tubulin to this site. This structure is known as the γ-tubulin ring complex (γ-TuRC) and consists of a small γ-tubulin complex (γ-TuSC) with γ-tubulin complex proteins (GCPs) (Oakley an Oakley., 1989, Oakley *et al.,* 2015). There are 6 GCPs (GCP1-6) arranged in the γ-TuRC which consists of 13 γ-tubulin molecules. Lateral interactions of GCP 4, 5 and 6 are thought to be responsible for the arrangement of this complex (Kollman *et al.,* 2011). Recently using cryo-EM it has been shown that the γ-TuRC is an asymmetric cone shaped structure with an actin like bridge within its lumen (Wieczorek *et al.,* 2020). The γ-TuRC ability to nucleate and its localisation is influenced by other proteins. NEDD1 has been shown to be a key regulator for MT anchorage as Nedd1-γ-tubulin promotes MT anchorage. Cep215-γ-tubulin is a complex known to induce nucleation at the centrosome as well

as augmin which induces nucleation during mitotic spindle formation (Muroyama *et al.,* 2013, Goshima *et al.,* 2008, Luders *et al.,* 2006).

1.3 Microtubule post-translational modifications

Post translational tubulin modification (PTM) of microtubules heavily influences the binding of MAPs along the MT and dictates the stability and behaviour of the MT. Most PTMs modify residues within the highly flexible C-terminal tail of the tubulin dimers, which extends from the MT, regulating MAPs there (Lessard *et al.,* 2019, Wall *et al.,* 2018).

1.3.1 Acetylation and deacetylation

MT acetylation has long been accepted as a marker of older, more stable MTs (Portran et al., 2017, Xu *et al.,* 2017). The acetylation PTM of MTs occurs within the hollow space or luminal surface of the MT at a location denoted as the K40 or the αK40 loop. More specifically this modification occurs at the Lys40 residue within the integrated α-tubulin monomer. The enzyme responsible for causing this modification is α-tubulin acetyltransferase (αTAT1). One theory of this enzymes activity is that it gains access to the MT luminal surface when a MT undergoes torsional stress leading to spaces forming within the MT lattice structure, hence stabilising the MT which is under load. In addition to this, αTAT1 has 100 times greater catalytic activity towards polymerised tubulin compared to the monomeric or dimeric forms. Alternatively, αTAT1 may simply gain access to the MT lumen via the MT open ends although the exact mechanism remains to be determined. Eshun-Wilson et al., (2019) used cryo-electron microscopy with reconstructions of αTAT1 acetylated MTs to visualise the structural consequences of this modification. Here they found that acetylation reduced the amount of disorder within the lattice resulting in a restricted state with less movement, likely reducing bending and therefore increasing strength and stability of the MT. The amount of acetylation within a MT can be correlated to its stability. The resistance of MTs to MT depolymerising drugs has been correlated with the degree of acetylation present within the MTs (Eshun-Wilson et al., 2019).

MT acetylation is now known to be a reversible modification in a process called deacetylation. The enzymes responsible for this process have been known for some time in comparison to the relatively newly discovered acetylating agents. Histone deacetylase 6 (HDAC6), a class II histone deacetylase and SIRT2, a class III NAD-dependent histone deacetylase form a cytoplasmic complex and most likely co-function as deacetylation agents (Hubbert *et al.,* 2002). Either acting together or independently the enzymes remove the acetyl group from the luminal MT surface to form more dynamic less stable MTs. Histone deacetylase 6 (HDAC6) in particular not only influences MT dynamics via deacetylation, it has

also been shown to effect MT stability just by its presence, likely via a +TIP interaction although this is yet to be elucidated (Zilberman et al., 2009). Inhibition of HDAC6 yields a decrease in MT dynamics, a characteristic which decreases focal adhesion turnover due to decreased MT dynamics (Tran *et al.,* 2007). One possibility is EB1 which has been shown to be important for HDAC6 to exert its activity in migrating endothelial cells during angiogenesis (Li et al., 2011). The motor protein kinesin-1 has also been found to preferentially bind acetylated tubulin for the polarised trafficking. Drug induced increased MT acetylation caused a redirection of kinesin-1 transport due to acetylation oversaturation and lack of distinction (Reed *et al.,* 2006, Kaul *et al.,* 2014).

1.3.2 Tyrosination and detyrosination

Another MT post translational modification is the tyrosinated or detyrosinated state of the C-terminus of the α-tubulin subunit within the MT. Detyrosination exposes the glutamate at the newly formed C-terminus, MTs in this formation are known as Glu-MTs and tyrosinated MTs are designated Tyr-MTs. The conformational change that occurs to expose/conceal the glutamate residue in detyrosination and tyrosination respectively confers the binding ability of certain +TIPs to that region. In mammalian cells, cytoskeletal associated proteins Gly-rich domain (CAP-Gly) containing +TIPs such as CLIP-170 bind the tyrosinated tubulin form whereas motor proteins such as some kinesin-2 has increased motility at detyrosinated MTs (Sirajuddin *et al.,* 2014). This difference in binding affinities is one mechanism in which the cell can modify MT behaviour. Carboxypeptidases (CCPs) are responsible for the detyrosination of MTs. Clearly the tyrosination/detyrosination state of MTs are important for many cellular processes. The identification of tubulin CCPs have been an elusive subject with little progress until the recent years where some have been identified. One such example is tyrosination state which influences neuron differentiation. Aillaud et al., (2017) described how the CCP vasohibin along with its small interacting partner SVBP are tubulin CCPs, this study used knock outs and inhibitors of the vasohibin and SVBP complex formation. In summary, when these tubulin CCPs were knocked out or complex formation was prevented and the amount of tubulin detyrosination decreased, leading to neurons with severe differentiation defects as well as disrupted neuronal migration when taken to the in vivo mouse model (Aillaud *et al*, 2017).

1.3.3 Glutamylation and glycylation

Glutamylation and glycylation are highly enriched in axonemes of most eukaryotes and are thought to influence cilia and flagella maintenance and formation due to their presence at the basal body (Bosch Grau et al., 2013). They are also important in spindle MTs, stabilising MTs detached from

the spindle pole (Bobinnec et al., 1998). These two modifications result in the formation of side chains emanating from the glutamate/glycine residues of the C-terminal tail of both MT monomers. The TTLL family of proteins are responsible for the production of these modifications that usually occurs in a repeated pattern to give polyglutamylation for example. The TTLL enzymes differ in preferred subunit substrate, to begin with these enzymes imitate side chain growth (TTLL1 and TTLL4) via glutamic acid or glycine addition. Then the chain is elongated (TTLL6) to form the maturely modified MT with complete interlinking side chains (van Dijk *et al.,* 2007).

1.4 Microtubule binding proteins

1.4.1 Microtubule +Tips

Plus tip binding proteins or plus end tracking proteins (+TIPs) are a group of proteins defined by their ability to accumulate to the plus tip of growing MTs, which include MT motor proteins as well as non-motor MT binding proteins such as the EBs. +TIPs were first described using CLIP-170-GFP which was shown to move at the MT plus tip with growth (Perez et al., 1999). The binding pattern of these +TIPs are defined by the temporal and spatial attachment at the MT plus tip. For example, a +TIP may bind to the recently polymerised tubulin at the plus tip exclusively, via this mechanism as tubulin addition occurs the protein disassociates from the older MT structure and binds to the newer regions at the plus tip, a behaviour that when observed appears as moving comets tracking the MT plus tip. This process, known as treadmilling has been demonstrated with the use of fluorescent speckle microscopy which uses a low concentration of fluorescently labelled subunits that mix with unlabelled assembly units to give an uneven distribution of fluorescence. This causes the appearance of bright puncta against a dark background at the assembly structure which can be analysed for movement and turnover (Grego *et al.,* 2001). Although currently there is no known mechanism for this behaviour, it is suggested that phosphorylation of proteins in older MT regions occurs to cause disassociation there. This theory arose as tumour suppressor genes APC and CLASP1/2 are targeted by GSK3β, which decreases their affinity for MTs in migrating cells (Watanabe *et al.,* 2009). Alternatively, phosphorylation may be required for the binding of MT associated proteins such as in the case of CLIP-170. CLIP-170 has two states, a folded binding inhibitory state and an unfolded bonding capable state. Phosphorylation by the kinase mTOR induces formation of the unfolded state hence increasing MT affinity (Nirschl *et al.,* 2016).

Treadmilling is not the only possibility for +TIP accumulation, alternatively the accumulation of a particular protein at the plus tip may be due to active transport to that region with the aid of motor proteins or via binding to existing +TIPs. The majority of the studies of this mechanism are in budding and fission *saccharomyces cerevisiae* yeast models. In this model it was shown that kinesin motor proteins Kip2p and Tea2p were responsible for the directional movement of 2 MT binding proteins, Bik1p and Tip1p (CLIP-170 homologues) (Caudron *et al.,* 2008). Mammalian models of this system are scarce, one study used a human foetal brain cDNA library and the yeast two-hybrid screening approach to identify APC binding partners. Results showed interaction of APC and 3A-KIF3B of the kinesin superfamily. Further experimentation concluded that this interaction was required for its clustered accumulation. Interestingly the truncated form of APC seen in many cancers was unable to be transported into these clustered due to a possible lack of interaction with motor proteins (Jimbo et al., 2002). The final possibility is that +TIPs may be attracted to particular structures that are present at the MT plus tip such as the beta sheet. As the beta sheet becomes closed into the lattice of the MT MAPs may disassociate as the beta no longer exist at that location.
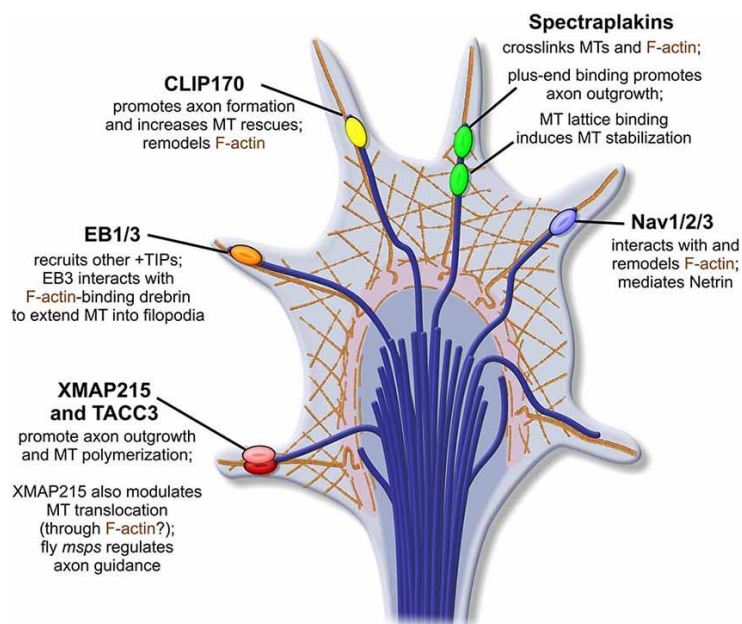
Figure 1.2 MT +Tips. MT +TIPs are a group of proteins that bind to the plus end of MTs. The example shown here depicts a MT bundle entering the growth cone of an axon. MT +TIPs have a wide variety of functions such as MT polymerisation (XMAP215), protein transit, and cortical docking (EB1). Adapted from Bearce *et al.,* (2015).

1.4.2 End binding proteins

In mammals, end binding proteins (EBs) are a family of 3 proteins, EB1, EB2 and EB3, encoded by the MAPRE genes. Of all the +TIPs, EBs are considered to be the master controller as they recruit many factors to the plus end and to a lesser extent the minus end. Structurally, EBs have a calponin homology (CH) domain at the amino terminal. Next to this is the linker region which varies in length

depending on the EB in question. Followed by the protein interaction coiled-coil domain which allows for the homo/heterodimerization exhibited by the EB proteins, this region terminates with a carboxy-terminal EEY/F motif which is a target for many CAP-Gly domain containing proteins. Finally, at the C terminal there is an EB homology domain which along with the linker region dictates the MT binding affinity of the protein (Hayashi and Ikura., 2003, Slep., 2010, Akhmanova and Steinmetz, 2015). A study by Buey et al., (2011) using chimera EB3 proteins with vary charges of at the C-terminal found that the C-terminal EB domain supressed binding of EBs to the MT lattice, increasing bias for the plus end and is controlled by the charge of this region. Further control of EBs ability to bind to MTs comes from the potential for phosphorylation, an event that leads to dissociation from the MT. This phosphorylation occurs at the linker region of the EB proteins at the Serine, thymidine and tyrosine residues. EB2 is temporally phosphorylated by the kinase Aurora B and CDK1 at multiple sites of the linker region upon initiation of mitosis to reduce MT binding. Exogenous expression of an EB2 mutant without the ability to become phosphorylated led to dominant kinetochore MT structures delaying the formation of the spindle MT network (Limori et al., 2016). As mentioned, EBs have the ability to form homodimers with the same protein or hetero dimers with other members if the EB protein family. Another difference between the EBs is that EB2 lacks the ability to form heteromdimers whereas EB1 and EB3 can form both hetero and homodimers. Dimerization of EBs leads to the formation of a hydrophobic cavity, a requirement for MT binding and the binding of other +TIPs that require EBs for their transport (Roth *et al.,* 2019).

EB1 and EB3 in particular show preferential affinity to the plus end of a growing MTs as a result of high affinity for the GTP bound tubulin (Komarova *et al.,* 2009). Using tubulin with blocked GTP hydrolysis, Roostalu *et al.,* (2020) demonstrated that EBs bind to the GTP conformation of MTs and that slowing down GTP hydrolysis caused extended GTP caps. Binding may also occur along the lattice of MTs at so called GTP islands, remnants of GTP tubulin within the lattice left over from when the plus tip occupied that space. These islands may act as points of rescue in the case of catastrophe to switch from the depolymerisation to polymerisation state. Dimitrov *et al.,* (2008) showed the presence of GTP islands/remnants through the use of a GTP-tubulin specific antibody (hMB11), here it was also shown that these islands stopped MT depolymerisation although only one-third of these islands effectively prevented the depolymerisation of the MT (Dimitrov *et al.,* 2008, Cassimeris., 2009). It is still unknown what mechanism determines the frequency of GTP island formation and how this effects MT stability and transport. Structural arrangement analysis of EB binding to MTs show that EBs bridge protofilaments and make contacts with four tubulin monomers (except at the seam) that are in a particular conformational state with high CH domain affinity due to the presence of GTP (Maurer *et al.,* 2012). Recent work created a photo deactivated (functionally) variant of EB1 where exposure

to blue light caused MT disassociation. Exposure of blue light and the subsequent dissociation of EB1 caused substantial depolymerisation at the plus end of the MT even in the presence of the MT polymerising agent XMAP215 (van Haren *et al.,* 2018).

Several +TIPs contain the SxIP motif within their structure including the cytoplasmic linker associated proteins (CLASPs). The region is conserved in all CLASP proteins and is needed for the binding of EB1 via the EBH domain, an interaction shared by many other +TIPs that rely on EB1 for transport along MTs (Buey et al., 2011, Galjart, 2010). The interaction between EB1 and CLASP 1 and 2 is not only essential for plus end directed transport but also influences EB binding. The SxIP can be post-translationally modified via phosphorylation to alter binding, expression of CLASPs has been shown to exclude EB binding from the lattice to maintain localisation to the plus tip of the MT (Grimaldi et al., 2014, Galjart, 2005). This behaviour not only influences the binding of EB1 to MTs but also acts as a regulator for plus end directed transport. Another domain that has been shown to interact with the EBs is the CAP-Gly domain. Proteins containing the CAP-Gly domain include CLIP proteins, the dynactin subunit p150[glued], centrosome associated protein 350 and the kinesin HIF13b. The CAP-Gly domain of these proteins interact with EBs via the C terminal EEY/F domain.

Table 1.1 Common microtubule associated protein functional domains. Table showing the most common domains of +TIPs including examples and interactions with other +TIPs. Adapted from Galjart., (2010)

Classification	+TIP*	Homologs†	Interaction with other +TIPs
'Core' +TIPs	EB1-like proteins	Bim1 (*Sc*)	Most known +TIPs
		Mal3 (*Sp*)	
CAP-Gly domain	CLIP-170	CLIP-190 (*Dm*)	EB1, CLIP-170, CLIP-115, p150^{glued}, CLASP1,2, MCAK, LIS1
		Bik1 (*Sc*)	
		Tip1 (*Sp*)	
	CLIP-115	–	EB1, CLIP-170, CLASP1,2
	p150^{glued}	NudM (*An*)	EB1, CLIP-170
		Ssm4 (*Sp*)	
SxIP motif	CLASP1,2	Orbit/Mast (*Dm*)	EB1, CLIP-170, CLIP-115, ACF7
		Stu1 (*Sc*)	
		Peg1 (*Sp*)	
	APC	Kar9p (*Sc*)	EB1, MCAK
	ACF7	Shot/Kakapo (*Dm*)	EB1, CLASP1,2
	STIM1	–	EB1
	MCAK	Klp10A (*Dm*)	EB1, CLIP-170, APC, Tip150
		XKCM1 (*Xl*)	
	Tip150	–	EB1, MCAK
	Navigators	–	Unknown
	Melanophilin	–	EB1
	p140Cap	–	EB1
	CDK5RAP2	–	EB1
	RhoGEF2 (*Dm*)	–	EB1
	DDA3	–	EB1
TOG domain	Ch-TOG	Msps (*Dm*)	EB1
		XMAP215 (*Xl*)	
		Stu2 (*Sc*)	
Not classified	LIS1	NudF (*An*)	CLIP-170, p150^{glued}
	NudA (*An*)	Dynein heavy chain	p150^{glued}, LIS1

Despite their high sequence conservation, EBs are functionally distinct in both their MT binding behaviour and +TIP partner binding. It has been shown that EBs compete with each other for binding along the MT and as such expression level of each EB family member has the ability to influence the binding and behaviour of the others. Goldspnk *et al.,* (2013) used siRNA to knock down EB2, causing EB1 to not only form comets but also decorate the MT lattice, a domain usually occupied by EB2. This suggests to some extent EBs are self-limiting in their position and also possibly behaviour (Goldspink et al., 2013). EB2 in particular has reduced affinity for the plus end of the MT compared to EB1 and EB3. It also binds to binding partners such as APC to a lesser extent than that of EB1 and EB3 and is far less likely to be involved in the sequestering of proteins along the plus end. Moreover, it is thought that EB2 does not act as a plus end mediator for plus end attachment to the cell cortex, organelles and the kinetochores which EB1 has been shown to do (Goldspink et al., 2013). Another key difference is that EB2 is localised toward the MT lattice whereas EB1 and EB3 form comet like structures at the plus tip (Roth *et al.,* 2019). Another difference is their influence on MT dynamics, generally EB1 and EB3 reduce MT dynamics, producing a more stable MT. Overexpression of these EBs causes the formation of MT bundles, a marker of stable MTs (Bu and Su, 2001). EB2 on the other hand, induces less stable MTs and increased dynamics (Goldspink et al., 2013).

Currently, EB2 is a very under studied protein with the majority of focus on EB1 and to a lesser extent EB3. Previous research by the Mogensen lab found that at the base of intestinal crypts where undifferentiated cells reside, there is a very high level of EB2 expression compared to more differentiated cells higher up the crypt. This suggests that in this system, EB2 expression has a role in maintaining the undifferentiated state of these cells and its down regulation is needed for differentiation to occur. This work was carried out on adult mice small intestinal crypts using immunolabelling and was also confirmed using *in vitro* tissue culture techniques. Here mIMCD-3 cells where grown to increasing levels of confluence to mimic differentiation level and showed less confluent (differentiated) cells expressed higher levels of EB2 that decreased with increasing confluence (Goldspink et al., 2013). It is still unknown what the role of EB2 is in these undifferentiated cells and its effect on the cytoskeleton.

1.4.3 CLIP-170

CLIP-170 is a +TIP that binds to MTs through their CAP-Gly domain but mainly associates to MTs through interaction with EB1 (Bieling *et al,* 2008). CLIP-170 has been shown to associate with the growing MT plus tip and along with family member CLIP-115 act as rescue factors in the event of MT catastrophe as dominant negative mutants of CLIP-170 cause no rescue and total MT catastrophe

(Komarova *et al.,* 2005). Importantly for this work, CLIP-170 plays a role in the association of vesicles with MTs for their transport. It is thought that CLIP-170 binds to p150^{GLUED} (subunit of the dynactin complex) for binding of the dynein motor protein (Liu., 2017). Formation of this complex leads the MT minus end directed transport of vesicles to the apical regions in apico-basal polarised cells for example.

1.4.4 Microtubule motor proteins

The motor proteins, kinesins and dyneins are MT motor proteins that move along MTs in an ATP dependent manner. Kinesins are a family of mainly plus end directed motor proteins involved in several cellular functions such as mitosis, meiosis and the transport of cellular cargo such as in apico-basal polarised cells. Kinesins play wide range of roles depending on the family member e.g. kinesin-1,2 and 3 are all involved in the transport of vesicles whereas kinesin 6 is involved in the positioning of spindle poles and cytokinesis. In particular kinesin-2 has been shown to mediate the apical endosome transport for the formation of the lumen. Li *et al.,* (2014) showed that kinesin-2 interaction with the FIP5 on endosomes transports these endosomes from the centrosome to the apical cleavage furrow during lumen formation. Kinesins are also very important regulator of MT dynamics and act as MT depolymerises (kinesin 8, 13 and 14). Kinesin 13 achieves this through the ATP hydrolysis as a driver for tubulin sub unit removal (Hunter *et al.,* 2003). Kinesin 8 destabilises the MT GTP cap which normally stabilises this site, this appears to occur as the kinesin moves pass this site and remove these GTP subunits (Gardner *et al.,* 2011).

The dynein family are minus end directed MT motor proteins which also play a wide range of roles including in the formation of apico-basal polarisation. An example of this is the dynein mediated localisation of the crumbs complex to the apical membrane in apico-basal epithelial tissue (Li *et al.,* 2008). More recently, Jouette *et al.,* (2019) showed that dynein mediated transport and membrane trafficking control PAR3 polarised distribution. This study showed that dynein transported RAB11 positive vesicles were needed for the delivery of PAR3 to the anterior cortex. It was suggested that dynein mediated membrane trafficking was essential for the maintenance of PAR3 asymmetry, a key characteristic of apico-basal polarised epithelial tissue (Jouette *et al.,* 2019).

Table 1.2 Kinesin family and known functions. Table showing list of kinesin family members with known functions and the sub family member responsible. In brackets is the species used for identification/functional study. Adapted from Verhey and Hammond., (2009).

Family	Functions	Commonly studied family members
Kinesin-1	Vesicle, organelle and mRNA transport	• KIF5 (Mm), KHC (Dm and Nc) and UNC-116 (Ce)
Kinesin-2	Vesicle, melanosome and intraflagellar transport	• Heterotrimeric subfamily: KIF3 (Mm), KLP64D (Dm), KLP68D (Dm), KRP85 (Ce), KRP95 (Ce), Kin1 (Tt), Kin2 (Tt) and FLA10 (Cr) • Homodimeric subfamily: KIF17 (Hs), OSM-3 (Ce) and Kin5 (Tt)
Kinesin-3	Vesicle transport	• Subfamily: KIF1 (Hs), UNC104 (Dm), UNC-104 (Ce) and Kin3 (Nc) • Subfamily: KIF13 (also known as GAKIN; Hs), KIN73 (also known as KHC73; Dm) and KLP-4 (Ce) • Subfamily: KIF28 (Hs) and KLP-6 (Ce) • Subfamily: KIF16 (Hs) and KLP98A (Dm) • Subfamily: KIF14 (Hs)
Kinesin-4	Chromosome positioning	• KIF4 (Hs), chromokinesin (Gg), KLP3A (Dm) and KLP1 (also known as KIF4; Xl)
Kinesin-5	Spindle pole separation and spindle bipolarity	• KIF11 (also known as Eg5; Hs), KIF11 (Mm), Eg5 (Xl), KLP61F (Dm), BimC (An)BMK-1 (Ce), Cin8 (Sc), Kip1 (Sc) and Cut7 (Sp)
Kinesin-6	Central spindle assembly and cytokinesis	• Subfamily: MKLP2 (also known as KIF20A; Hs), KIF20A (also known as Rab6 kinesin; Mm) and Subito (Dm) • Subfamily: MKLP1 (also known as KIF23; Hs), KIF23 (Mm), CHO1 (Cg), Pavarotti (Dm) and ZEN-4 (Ce)
Kinesin-7	Kinetochore–microtubule attachment and chromosome congression	• KIF10 (also known as CENPE; Hs), KIF10 (Mm) and KIP2 (Sc)
Kinesin-8	Chromosome congression	• Subfamily: KIF18 (Hs) and KLP67A (Dm) • Subfamily: KIF19 (Hs), KLP13 (Ce), KIP3 (Sc), KLP5 (Sp) and KLP6 (Sp)
Kinesin-10	Chromosome positioning	• KIF22 (also known as KID; Hs and Xl) and Nod (Dm)
Kinesin-12	Spindle pole organization	• KIF12 (Mm), KIF15 (Mm), KLP54D (Dm) and KLP2 (also known as KIF15A; Xl)
Kinesin-13	Kinetochore–microtubule error correction and chromosome segregation	• Subfamily: KIF2A (Hs), KIF2B (Hs), MCAK (also known as KIF2C; Hs), MCAK (Cg), KCM1 (also known as KIF2C; Xl), KLP10A (Dm), KLP59C (Dm), KLP59D (Dm) and KLP7 (Ce) • Subfamily: KIF24 (Hs) and Kin1 (Pf)
Kinesin-14	Spindle pole organization and cargo transport	• Subfamily: KIFC1 (also known as HSET; Hs), CHO2 (Cg), NCD (Dm), CTK2 (Xl) and Kar3 (Sc) • Subfamily: KIFC2 (Hs), KIFC3 (Hs), KLP3 (Ce) and a large number of plant-specific isoforms

1.5 The Centrosome

The centrosome is the most studied of all MTOCs, many cell types exhibit MTs with minus ends anchored at the centrosome, which is located close to the nucleus and the MTs extend peripherally in all directions. This formation is known as a radial array of MTs and is indicative to cells with no directionality and still have centrosome organised MTs (Bartolini and Gundersen, 2006). The centrosome consists of a pair of centrioles surrounded by a protein scaffold called the pericentriolar material (PCM). Generally, the PCM contains components necessary for the nucleation of MTs such as γ-tubulin and augmin whereas the centrioles are responsible for MT anchorage (Lin et al., 2015, Mennella et al., 2014, Delgehyr et al., 2005). The two centrioles are distinct from one another with one being the older and relatively immotile mother and the other being the younger motile daughter centriole. The mother centriole features distal and sub-distal appendages that allow for the anchorage of MT minus ends, these appendages recruit several factors such as the γ-tubulin ring complex (γ − TuRC), dynactin and ninein (Mogensen et al., 2000).

1.5.1 The Centrosome Cycle and Duplication

Centrosome replication is dependent on the cell cycle, daughter cells that have just separated possess a single pair of centrioles (Bornens., 2021). These centrioles are tightly bound (engaged) in an orthogonal fashion, early in the G_1 stage of the cell cycle the centrioles pair disengage and gain some distance from one another but still maintain a fibrous proteinaceous link. In late G_1 to early S phase the separated centrioles form procentrioles upon and perpendicular to the existing centriole. These procentrioles elongate during G_2 to match the size of the mother centrioles heading into division where they separate and move to opposite poles to form the spindle poles. Like many cellular processes linked to the cell cycle, centrosome duplication is mediated by cyclin dependant kinases (Cdks) and cyclins. In particular Cdk2 and cyclin E are key regulators of centrosome duplication (Meraldi *et al.,* 1999). This was shown experimentally with the use of Cdk-cyclin E repressors derived from p57 which prevented centrosome duplication in *xenopus* egg extracts. The same result is observed when injection of general Cdk inhibitors p21 or p27 is performed into *xenopus.*

Engaged centrioles become disengaged in the G1 stage of the cell cycle, this is the separation of the mother and daughter centrioles. This process begins with the transposition of cohesin, a centriole engagement factor which is found in a ring structure at the distal centriole. Seperase has been reported to have a role in centriole disengagement amongst other proteins, ectopic activation of seperase or depletion of SGO1 which protects cohesin from the action of seperase causes premature disengagement (Schöckel et al., 2011). Astrin is another inhibitor of seperase that also prevents the premature disengagement (Gruber *et al.,* 2002). As well as inhibition of seperase,

pericentrin also prevents premature disengagement via its mechanical support around the centrioles as it is a major structural component of the PCM. Once seperase has induced centriole disengagement the centriole remains attached via a proteinaceous link consisting of rootletin, C-Nap1, CEP68 and LRRC45.

Procentrioles form at a particular site of existing centrioles. Three main proteins have been identified as mediators for initiation of procentriole formation at this site, polo like kinase 4 (PLK4), SASS6 and STIL. PLK-4 recruitment is facilitated by Cep252 and Cep192 which are found in rings around the circumference of the centriole (Sonnen *et al.,* 2013, Hatch *et al.,* 2010). These proteins are found at the site of procentriole assembly at the G1-S transition stage of the cell cycle, the stage when assembly occurs. The core of the assembly known as the cartwheel is a nine-fold symmetric template structure at the proximal end of the centrioles. Here the protein SASS6 is found as a structural component with STIL association. STIL is phosphorylated by PLK4 to enhance th recruitment of SASS6 to form the cartwheel (Kratz *et al.,* 2015). However, before these two proteins are recruited to the assembly point on the mother centriole, PLK4 is recruited which is an essential event for the replication of the centriole. Unlike the others that localise at the cartwheel site, PLK4 localises to a dot like structure and recruits SASS6. From work carried out on the crystal structure of SASS6 it appears to self-oligomerise to form the backbone of the cartwheel structure upon recruitment (van Breugel *et al.,* 2011). As centriole elongation occurs the centrin protein is also incorpoaratied as a structural unit within the centriole and is required as centrin removal causes duplication defects (Salisbury *et al.,* 2002). At the early G1 stage can be seen localised in a ring around the centriole and only forms the dot structure when the cell enters the G1-S transition stage. The exact model of these interactions is yet to be elucidated, it is likely that PLK4 phosphorylates downstream proteins in the assembly pathway.

Specialised MTs (A, B and C) are nucleated from the cartwheel structure on the mother centriole, cryoelectron tomography of procentrioles discovered that A-tubulin are capped by the γ-TURC which is responsible for its nucleation and localises it to the core the centriole during this process. B- and C-tubules show no γ-TURC cap and so are likely nucleated in another way yet to be elucidated. The final stage of this nucleation process is capping by CPP110 and CPAP once the desired length of the centriole has been reached (Schmidt *et al.,* 2009).

Once the centriole is formed the centrosome then undergoes maturation in the G2 stage of the cell cycle. The γ-tubulin accessory factor, Cep215 (CDK5RAP2) is phosphorylated by PLK1 for recruitment around the centrioles for MT oragnsiation (Conduit *et al.,* 2014). Maturation includes the recruitment of the PCM components, a process reliant on the recruitment of Aurora-A kinase to the

centrosome via Src activation at the golgi. Aurora A kinase then phosphorylates the centrosomal protein TACC which ultimately recruits the γ-TURC and PCM proteins to form the PCM (Brittle and ohkura *et al.,* 2005, Hannak *et al.,* 2001, Baretta *et al.,* 2016). At this stage the newly formed centriole is attached to the mother centriole, separation occurs at the G2/M stage in preparation for mitosis and the formation of the spindle poles. Centrosome separation occurs when the proteinaceous linker connecting the centrioles is severed. Nek2 is an important effector here, phosphorylating CEP68, CEP250, Rootletin and NINL (man *et al.,* 2015). The separation of centrioles is then mediated by MT motor proteins via GAS2L1 binding to MTs (via EB proteins) and actin as this linker is separated (Au *et al.,* 2017, Jiang *et al.,* 2012). Kinesin (Eg5) provides the force required for centrosome separation, activated by phosphorylation by Nek6 resulting in centrosome separation (Mardin and Schiebel, 2012, Bertran *et al.,* 2011).
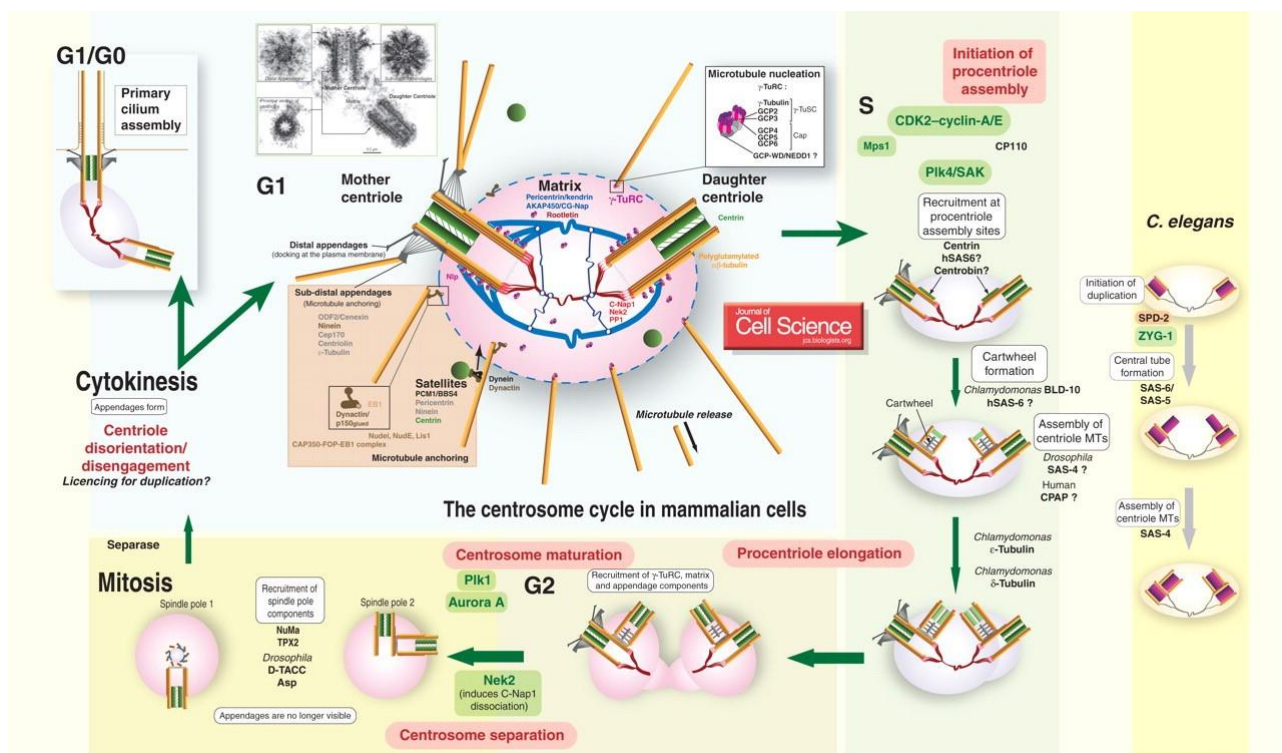
Figure 1.3 Structure and duplication of the centrosome. (G1) Two distinct centrioles connected via a proteinaceous linker. These previously engaged centrioles where disengaged in a cell cycle dependent manner regulated by PLK1 and CDK1. (G1/S) Centriole duplication is initiated by PLK4 recruitment to the centriole allowing for the cartwheel structure assembly. This forms the procentriole from the body of the existing centriole. (G2) Maturation of the centriole and separation of the linker by Nek2A. (Mitosis) centrosome movement and bipolar spindle formation to ensure daughter cells maintain a centrosome. Adapted from Azomzadeh and Bornens., (2007).

1.6 Epithelial Tissue

1.6.1 Structure and function

Epithelial tissue is a strong lining tissue that supports organs and usually surrounds organs or the functional area of the organ such as the lumen of the gut. The purpose of the epithelium is varied depending on the location. Skin epithelium for example acts as a barrier against potential toxins and pathogens. In the gut the epithelium is also responsible for the exchange of molecules to and from the body. In general, the functions are selective absorption, secretion, protection and environmental sensing. Epithelium differs slightly in shape depending on its location and function within the body. The three basic shapes of epithelium are columnar, cuboidal and squamous. These may be arranged as single monolayers known as simple epithelium where every cell contacts the basement membrane such as in the walls of the capillaries, an example of simple squamous epithelium or epithelium may be arranged into layer two or more cells deep. Layered epithelium can be stratified (consisting of layers) or pseudostratified (a layer of cells with uneven alternating nuclei positioning) that gives the illusion of layered cells.

The familiar polygonal honeycomb shape of an epithelial monolayer (as seen from the apical side) is a result of three edges (cell membranes) meeting at one vertices, usually 2 from one cells and one from another. The application of short term external stress deforms the shape in a reversible manner with the edges and vertices maintain their pattern. Longer term forces alter the arrangement of cell-cell contacts, creating and dissolving the contacts as needed, depending on the direction and amount of force applied. Junctional remodelling in an epithelial monolayer may result from cell extrusion such as ankiosis at the tip of microvilli of the intestine, as a result of cell death or during cell division (Guillot and Lecuit, 2013). Epithelial tissue is supported by the basement membrane, the basement membrane provides the substrate for epithelial layer binding. It consists of fibrous extracellular matrix in two layers; the basal lamina and the underlying reticular connective tissue. These layers are connected via collagen VII anchoring fibrils and fibrillin microfibrils to form the basement membrane. The basement membrane attaches the epithelium to the basal loose connective tissue via substrate adhesion molecules such as those present in hemidesmosomes of the basal membrane of epithelial cells (Leblond and Inoue., 1989).

1.7 Epithelial cell junctions

Due to the dense intercalating nature of epithelial tissue, cell contacts are very abundant in this cell type. Generally speaking a cell junction is a proteinaceous bridge between neighbouring cells or between a cell and the surrounding ECM. Cell junctions have three classifications; occluding

junctions that form a seal to prevent even small molecules passing through, anchoring junctions that attach cells to neighbours or the ECM and finally communicating junctions that allow transmission of signals from one cell to another.

1.7.1 Tight Junctions

As part of the function of the epithelium, occluding junctions known as tight junctions in vertebrates prevent leakage of molecules, creating an effective barrier. Not only do tight junctions function to prevent the leakage of molecules from the lumen, they also maintain the position of various membrane bound proteins such as the channels required for nutrient transport. Apically located membrane bound proteins are prevented from moving basally and *vice versa*. Disruption of the tight junctions via the chelation of calcium (Ca^{2+}) has been found as their formation and maintenance is calcium dependent and leads to a loss of membrane bound protein polarity. Experimental analysis using a low molecular weight tracers placed one side of the epithelial layer was used to show diffusion only occurs as far as the tight junctions and did not diffuse across the layer (Friend and Gilula, 1972). The permeability of these tight junctions can be modified for the selective absorption of some key nutrients from the intestinal lumen such as amino acids. Tight junctions mainly consist of two families of proteins, claudins and occludins. The composition of the proteins varies depending on the tissue type, for example a specific occludin called paracellin-1 is required for the reabsorption of Mg^{2+} from the urine into the blood (Simon et al., 1999).

1.7.2 Gap junctions

Gap junctions are transmembrane channels formed from proteins called connexins. These channels provide direct intercellular communication ability through the rapid exchange of ions and metabolites. Gap junctions are formed of ~20 connexins of which there are many isoforms suggesting that gap junctions have the ability to selectively allow intercellular transport. The communication that exists through gap junctions is still and area of research as little is known about this area (Evans and Martin *et al.,* 2002).

1.7.3 Adherens junctions

Adherens junctions consist of E-cadherin and intracellular components, p-120-catenin, β-catenin, α-catenin. E-cadherin, a trans-membrane protein that links to actin intracellularly, spans the membrane and forms cis and trans homophillic clusters with the same structure of the

neighbouring cell. This actin-E-cadherin link relies on proteins that act as adapters such as α-catenin and β-catenin along with vinculin amongst others (Ishiyama *et al.,* 2013). These E-cadherin structures are concentrated at the adherens junctions arranged in a horizontal adhesive belt in the apical regions of the epithelial monolayer. Recently the apico-basal machinery in particular has been shown to have a critical role in the regulation and remodelling of adherens junctions. Formation of adherens junctions is induced from neighbouring cells making actin-based contacts with trans E-cadherin. This causes the formation of small E-cadhern clusters, engagement of these with neighbouring cells activates Rac signalling via activation of the Rac guanine exchange factor (GEF) TIAM1. This Rac activation promotes branched actin network formation, expanding the E-cadherin clusters. Evidence is also present suggesting that Nectin engagement between neighbouring cells recruits E-cadherin complexes (Indra *et al.,* 2013, Sato *et al.,* 2006). PAR3 and α-catenin are recruited to the expanding junction to inhibit Rac signalling and activate Rho to form stable actin bundles and a stable junction (Matsuzawa *et al.,* 2016).

The PAR complex has been shown to be a key regulator in this process. Arora *et al.,* (2020) shows that E-cadherin polarity is maintained by aPKC in development and E-cadherins presence is key for polarisation to occur in a stepwise manner. Importantly for this study this study also showed that E-cadherin at the junction increases as cell height increases and polarisation is established in the peridermis of zebrafish (Arora *et al.,* 2020). The presence of PAR3 has been shown to be essential as it inhibits TIAM1 to prevent Rac activation and maintain stable adherens junctions (Nishimura *et al.,* 2005). MTs also play an important role in the maintenance of adherens junctions as p120-Ctn at the adherenes interacts with kinesins and CLASP2 to regulate MT dynamics and CLASP2 loss destabilizes adherens junctions (Shahbazi *et al.,* 2013, Chen *et al.,* 2003).

Within the monolayer of cells there is a balance of forces, the adhesive belt provides resistance to cortical tension forces generated by actomyosin network that overall reduces the amount of cell contacts to act as an indirect mediator of cell junction formation. Although the maintenance of the contacts via actin with its adapters is crucial, showing the balance that exists within this system and is a determinant of cell shape. In non-epithelial tissue, adherens junctions occur as punctate or streak like structures between cells making contact. In epithelium they are far more abundant, forming the adhesion belt or zonula adherens that lies just beneath the tight junctions and adheres cells to all surrounding epithelia in the layer (Saloman *et al.,* 2017).

1.8 Apico-basal Polarisation

In vertebrates, apico-basal polarised epithelial cells use cues from neighbouring cells and through interactions with the ECM to orient the directionality of their polarisation and localisation of key polarity complexes. In mature organs the apical surface is found at the contact-free outside facing surface, toward the external environment in skin and toward the lumen in tubular organs. Apico-basal polarity arises from extrinsic and intrinsic cue to define this polarity. Extrinsic cues come mainly from the surrounding cells, ECM and basement membrane. It has been shown that interactions with the ECM are essential for determining polarity. Yu *et al.,* (2005) show that collagen 1 and β1-integrin orientate polarity and inhibition of this interaction leads to inverted polarity. This could be rescued by the addition of activated Rac1 showing the importance of Rho GTPases in cell polarity (Yu *et al.,* 2005). Intrinsic cue includes junction formation as well as the asymmetrical positioning of polarity complexes. The centrosome also gives intrinsic cues for polarisation, the centrosome or midbody in MDCK cells defines the site for apical protein targeting and lumen formation. The mammalian process of epithelial polarisation has many similarities to the *Drosophila,* in fact most discoveries were made in the fly due to its ease of use particularly when analysing phenotypes of mutants. These experiments along with genetic screens have identified three major protein complexes, the apical Par (Par3, Par6, Cdc42 and aPKC), crumbs (Crumbs, PALS1 and PATJ complex) and scribble complex (scribble, lgl and Discs large) (see figure 1.4 for protein interactions) (Margolis and Borg., 2005). Interaction between adjacent cells is the first known event and involves the Ig superfamily cell-adhesion molecule nectin and a junctional protein called JAM-A (Fukuhara et al., 2002). This interaction leads to recruitment of the Par complex and the assembly of the adherens and tight junctions. The crumbs complex is recruited more apically in comparison whereas the scribble complex defines the basolateral surface. Mutation experiments of the Par complex proteins show that it is essential in the polarisation process, therefore the Par complex is known as the master regulator (Hurd *et al.,* 2003). Genetic mutation of the Scribble complex sees the expansion of the apical domain and the opposite was found when the Crumbs complex was mutated, highlighting the antagonistic relationship exhibited by these complexes (Fletcher *et al.,* 2012).

As MDCK cells are used as a model for apico-basal polarisation in this study, nephron polarisation is described here. Here, PAR3 localises to cortical areas and the basolateral protein NCAM is seen uniformly at the cell cortex (Yang *et al.,* 2013, Pickett *et al.,* 2019). As apico-basal polarity and morphogenesis progresses, PAR3 colocalises with aPKC at the apcal cortex. PAR3 is moved basally of aPKC at canonical adherens junctions. PAR3 has been shown to localise even in the absence of PAR6 and aPKC suggesting that PAR3 is an upstream regulator of this process. Several other proteins such as CDC42, afadin, PAR6 and CRB have also been shown to be essential and possible upstream as their

removal prevent polarisation occurring (Tang *et al.,* 2013). Many questions still remain in this process and little is known about the role of the cytoskeleton in this process. The centrosome moves apically in this process and is a process yet to be elucidated. Evidence suggests that Rac1 and more downstream proteins such as CDC42 activation is involved as inhibition leads to mis localisation of the basal body (Hashimoto *et al.,* 2010). This positioning is also affected by the inhibition of actin polymerisation. Similarly, nocodazole depolymerisation of MTs leads to basal body mis localisation (Turner and Adler., 1998, Carvajal-Gonzalez *et al.,* 2016). Following the establishment of polarisation, extensive cytoskeletal reorganisation occurs. As described in more detail in section 1.8.1, lateral MTs orient their minus ends toward the apical domain with more MTs running perpendicular just below the microvilli and at the cell base. This organisation is key for the transport of membrane proteins from the Golgi (trans Golgi network) to the relevant membrane.
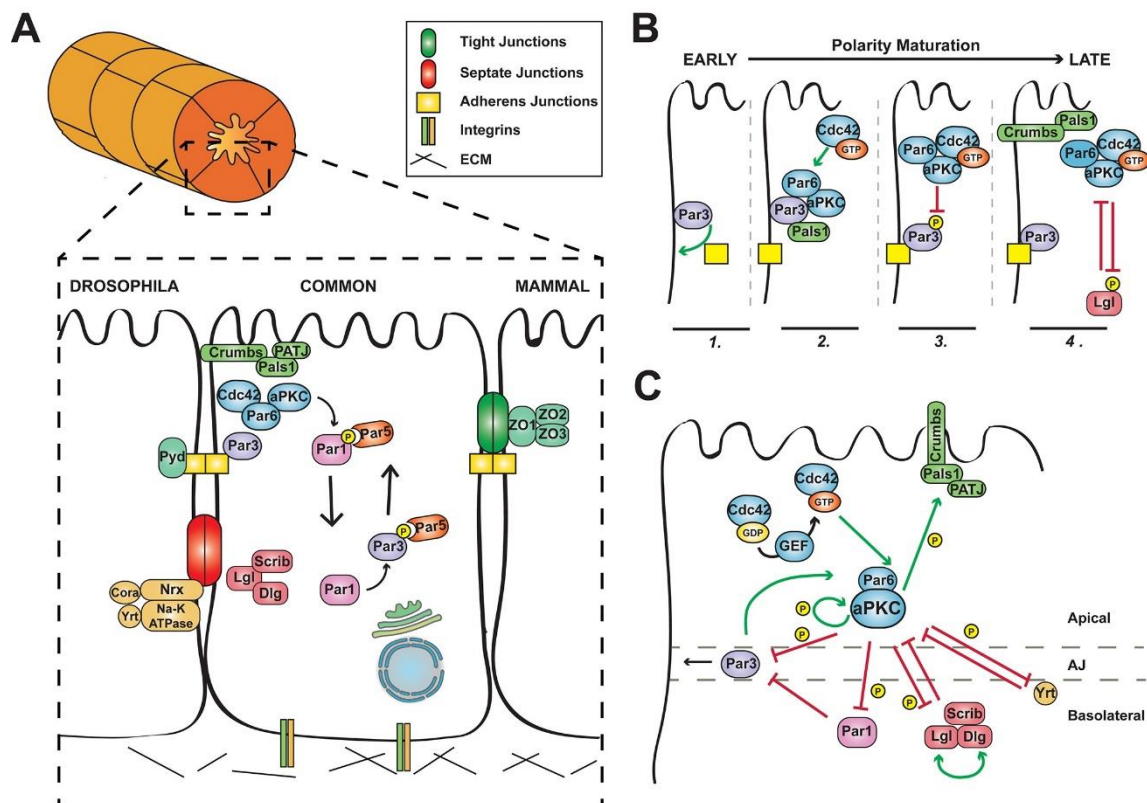
Figure 1.4 Polarity establishment in epithelial cells. (A) Polarity of epithelial cells is determined by the apical PAR complex. Interactions between this PAR complex with the basal scribble complex and the apical Crumbs complex leads to establishment of epithelial apico-basal polarisation. (B) Successive polarity complex interactions. 1. PAR3 recruits E-cadherin for the establishment of adherens junctions. 2. Activated Cdc42 and PAR3 recruits Pals1, PAR6 and aPKC. 3. aPKC phosphorylates PAR3, excluding it from the apical membrane to define the apical-lateral border. 4. Phosphorylated PAR3 prevent interaction with Pals1 to stabilise Crumbs in the apical membrane. PAR6-aPKC and the scribble complex maintain polarity through reciprocal inhibition. (C) Cdc42 binds to PAR6 via GEF mediated activation. Apical Cdc42-aPKC-PAR6 exclude PAR3 from the apical domain. aPKC is inhibited entering the basolateral by the determinants there ensuring it apical localisation. Adapted from Roman-Fernandez and Bryant., (2016).

1.8.1 Reorganisation of microtubules to non-centrosomal MTOCs

During epithelial cell differentiation and polarisation MT reorganisation follows several distinct but transient steps that are not yet fully understood. MTs are released from the centrosome, captured at the cell periphery (cortical capture), translocated to new anchoring regions and ncMTOCs form with the localisation of many anchoring and possibly nucleation proteins (Sanchez and Feldman, 2016). In some cell types, the centrosome may disaggregate completely (e.g. enterocytes) and therefore the centrosome no longer anchors or nucleates MTs (Toya and Takeichi, 2016). These processes are highly regulated by the cell cycle; which determines many centrosomal behaviours such as centriole duplication and disengagement (Doxsey et al., 2005). In the intestinal crypt for example, decreased Wnt signalling with increased distance from the stem cell niche reduces proliferation, this decrease in cell cycle rate induces reorganisation of the MT pattern and polarisation begins although the pathways involved here are yet to be elucidated (Muroyama et al., 2016). During the differentiation of epithelial cells, the centrosome acts as an inhibitor of polarisation if active and therefore requires attenuation of its anchorage ability before polarity can be established (Noordstra et al., 2016). The release and transport of MTs from the centrosome was first observed by Keating et al., (1997), here it was shown that MTs nucleated at the centrosome detached and moved peripherally with their plus ends leading, suggesting that minus end directed motors most likely dynein were responsible (Keating et al., 1997).

MT release and capture is thought to be the mechanism for this redistribution of MTs, with MTs being released from the centrosome and captured at the adherens junctions for organisation there (Bellet *et al.,* 2009, Mogensen., 1999). MT release from the centrosome is not yet fully understood, centrosomal associated proteins such as pericentrin and centrin are differentially lost from the centrosome to varying degrees during differentiation, to reduce MT affinity (Muroyama et al., 2016, Bartolini and Gundersen, 2006). It is reported that two γ-tubulin accessory factors are differentially lost from the centrosome during the differentiation process of epidermal cells. The γ-tubulin accessory factors Nedd-1, an enhancer of MT anchorage and CDK5RAP2, an enhancer of MT nucleation was differentially lost as differentiation occurs. The effect of this is the accumulative inactivation of the centrosomes ability to anchor MTs leading to their re-localisation to ncMTOCs (Muroyama et al., 2016). In addition, the MT anchorage protein ninein is also released from the centrosome during differentiation and relies on MTs for its transport bi-directionally from the centrosome to ncMTOCs possibly leading to reduced centrosomal MT affinity at the centrosome, although this remains to be determined (Goldspink *et al.,* 2017, Moss et al., 2007). As well as loss of centrosomal anchorage, MT loss from the centrosome may occur due to active cleavage of MTs. Two

enzymes found at the centrosome with the ability to cleave MTs are katanin and spastin. Katanin and Spastin are AAA family proteins that sever MTs in an ATP dependant manner. Centrosomal factions and other MT dense regions are enriched in these MT severing proteins to fulfil this possible function (Errico et al., 2004, McNally et al., 1996, Zhang et al., 2011, Brodu et al., 2010, Svenson et al., 2005). A recent study highlighted the release of MTs from the centrosome via katanin in conjunction with the binding of the MT stabilising protein CAMSAP3 (Dong et al., 2017). Once released from the centrosome the MTs require positioning to their new ncMTOC, cortical capture may aid in this process.

Cortical capture is important for the localisation of many proteins, the translocation of MTs and for the formation and maturation of cell junctions. Likely models of this system rely on MT bound +TIPs docking with cortical receptors as the MT grows toward the periphery, a process that may be aided by the guidance of filamentous or F-actin in association with bridging proteins such as ACF7 (MACF1) (Gundersen et al., 2004, Ning et al., 2016, Mimori-Kiyosue and Tsukita, 2003). Previous studies have identified CLIP-170, CLASPs and EB1 accumulate at the plus end of MTs and facilitate cortical capture by binding the cortical receptor IQGAP1 (Fukata et al., 2002, Akhmanova et al., 2001, Ligon et al., 2006, Bellett et al., 2009). The cortical receptor IQGAP1 and its activators Rac1 and Cdc42 are thought to capture the +TIP complex to the cortex and to cell junctions to allow protein delivery and MT anchorage (Fukata et al., 2002, Watanabe et al., 2004). Once captured it is suggested that the adenomatous polyposis coli (APC) protein stabilises MT binding at the cortex (Watanabe et al., 2004). EB1, CLIP-170, dynein and β-catenin co-localise at junctional sites, proposing that MTs are captured to this region or transferred here after cortical capture occurs (Bellett et al., 2009). Additionally, at the MT plus tip the LIS1/NUDEL complex localises with the dynein/dynactin motor complex via interaction with CLIP-170 to possibly generate pulling forces for MT positioning (Kardon and Vale, 2009). Dynein is a good candidate for the translocation of MTs from the cortex to the adherens junctions after cortical capture and MT release, dynein/dynactin is localised to the MT plus ends, astral MTs to position them during mitosis and at the cortical regions of polarised cell cultures (Dujardin and Vallee, 2002). Dynein is recruited to the adherens junctions via direct β-catenin binding where it potentially positions MTs to this ncMTOC while anchored at the cortex (Kardon and Vale, 2009, Ligon et al., 2001, Bellett et al., 2009). A clear pathway is yet to be implemented for the positioning of MT organisation though cortical capture although it remains likely.
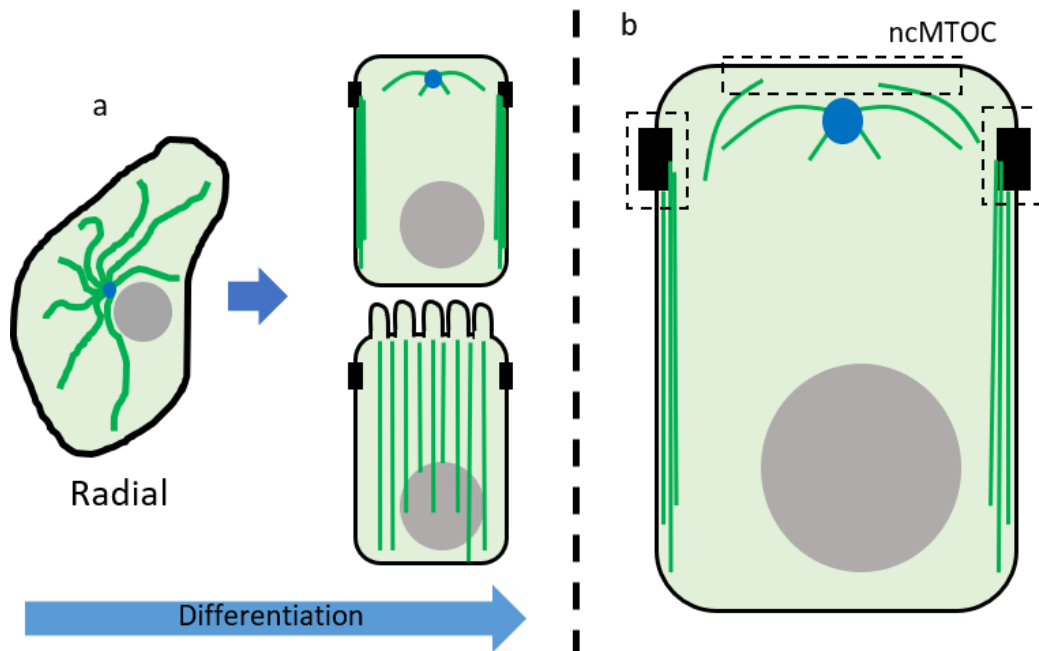
Figure 1.5 Diagram depicting apico-basal polarisation. (a) Undifferentiated cells exhibit a highly dynamic radial array of MTs (Green). As differentiation occurs, the dynamics of MTs reduces and more role specific MT patterns are implemented. In the case of polarisation, a radial array is replaced by an apico-basal array of MTs that form a directional specific transport system. The centrosome (Blue) may remain as the primary nucleation site or be non-existent and nucleation occurs at the sub apical membrane as in intestinal epithelial cells. (b) An apico-basal polarised cell exhibits an apical surface that faces the lumen, a basal membrane bound to the basement membrane and many cell-cell contacts such as the adherens junctions shown here. In this example, the MTOC is at the sub apical membrane however in polarised cells that retain the centrosome the MTOC resides primarily at the adherens junction.

1.8.2 The unjamming transition

The conversion from sedentary to migratory behaviour has been attributed to the recently discovered unjamming transition (UJT) (Mitchel *et al.,* 2020). The UJT involves the collective transition from what's known as a jammed phase, often compared to the solid elemental state as cells in this formation show little movement. Unjammed cells migrate cooperatively in swirls in a fluid like fashion (Park *et al.,* 2015, Park *et al.,* 2016). Within a jammed layer cells are anchored in all directions by neighbouring cells and the dysregulation of this leads to heterogenous changes in jamming within the layer. This is a new and poorly understood concept but has been identified in many systems and pathologies such as asthma and cancer (Kim *et al.,* 2020). Unjamming is able to overcome the kinetic and cell cycle arrest of terminally differentiated epithelial cells to promote collective mobility in carcinoma by increased actin nucleation for example (Palamidessi *et al.,* 2019).

A recent study by Mitchel *et al.,* (2020) attempted to define the differences between UJT and partial EMT (pEMT) although there are similarities. It is unclear how much overlap exists in this system

as the UJT may carry characteristics of pEMT and *vice versa.* Induction of pEMT through TGF-β shows diminished junctional tension, decreased E-cadherin and ZO-1 expression as well as expression of some EMT markers such as vimentin. In comparison, UJT shows no loss of E-cadherin and no increased expression of vimentin or N-cadherin. Overall, the epithelial behaviour appears to persist during UJT but is lost during pEMT. There is also a difference in cell cooperativity where UJT involves the movement of large packs of cells of around 45 cells which increased to 237 cells as UJT proceeds whereas pEMT showed movement of much smaller packs of cells of around 5-10 cells consistently. Although this work shines some light on this area, the use of external mechanical cues to induce UJT may not be a true representation of its natural occurrence *in vivo* or even *in vitro* (Mitchel *et al.,* 2020). This is an area that warrants further study to define these characteristics of epithelial layers.

EMT is a developmental process important for many processes such as neural crest cell migration for the formation of some organs and tissues as well as in wound healing, it also is involved in the metastasis process in many cancers. EMT requires distinct changes in cell morphology such as loss of cell-cell adhesion, loss of apico-basal polarity and the acquisition of a migratory and invasive behaviour which is ultimately driven by differential gene expression. Snail and Twist are central to EMT, these transcription factors promote expression of genes involved in cell migration, downregulation of adhesion factors and increased production of proteins that digest the basement membrane for cell release (Thiery *et al.,* 2009).

A relatively new method for the analysis of epithelial monolayers is shape index which uses the perimeter and area to define a value against a threshold value representing jammed or unjammed layers. (Bi *et al.,* 2015, Park *et al.,* 2015, Mitchell *et al.,* 2020). According to the shape index the UJT occurs at 3.81 with values below this representing a jammed layer and above this is considered an unjammed layer. This is an *in silico* model based on the vertex model and experimentally validated (Park *et al.,* 2016). A cell within an epithelial layer has a preferred perimeter determined by 3 factors: an energy associated with cell area and attributable to its compressibility; an energy associated with the cell perimeter maintained by the stiffness and contractility of the apical actomyosin ring; and an energy associated with interfaces of cell–cell contact, including the effects of adhesion molecules (Park *et al.,* 2015). As described by Mitchell *et al.,* (2020), the shape index is also called rescaled preferred cell perimeter, when there is a mismatch between the cell perimeter and the preferred shape, tensions arise on the cell edges as a result, inducing further deformation.
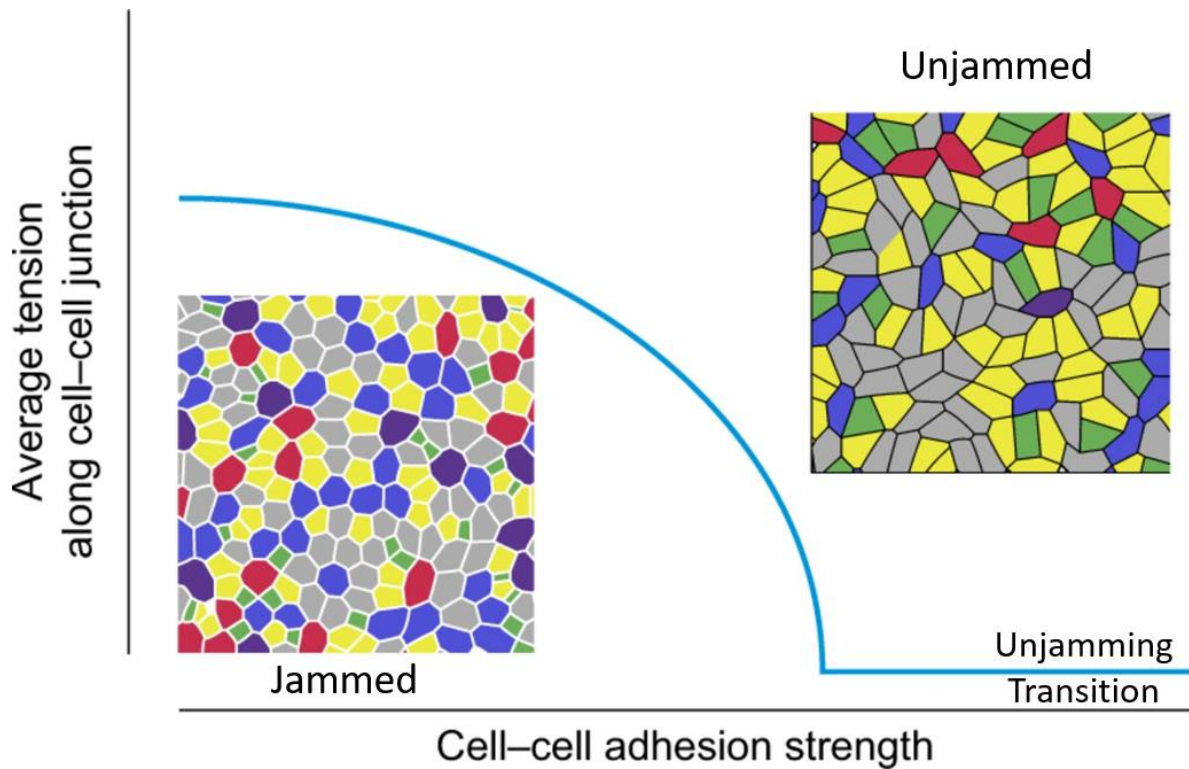
Figure 1.6 The unjamming transition. The UJT is often compared to the solid and liquid physical states, a jammed layer being solid and an unjammed layer being liquid. The threshold between these states is known as the UJT. There are two main factors that determine this in an epithelial layer, junction strength and the forces applied to them. A reduction in strength or increased force from propulsion causes unjamming, this can be quantified using the shape index where the UJT is represented by the value 3.81 and values above this are unjammed. Adapted from Park *et al.,* (2016).

1.8.3 CAMSAPs and ncMOCs

There are many differences between the CAMSAP family members, CAMSAP1 decorates the extreme minus end of the MT and has no effect on tubulin addition at this site, simply moving as new tubulin is added, whereas CAMSAP 2 and 3 show a far more extensive decoration with CAMSAP2 being the longest in length (Hendershot and Vale., 2014). All CAMSAPs bind to the free minus end of MTs that are slowly growing and protect the MT from depolymerisation as shown by attaching GFP-patronin to glass coverslips and adding fluorescently labelled MTs in a cell free system, MTs bound to GFP-patronin by one end only (Goodwin and Vale ., 2010). In the same experiment it was shown that CAMSAP3 protects against depolymerises such as kinesin 13, purified kinesin 13 was added to fixed MTs in the presence or absence of GFP-patronin, in the absence of patronin depolymerisation occurred from both MT ends whereas in the presence of patronin MT depolymerisation occurred only from the exposed plus end and never extended past the patronin decorated area preserving an area to act as a seed for later polymerisation (Goodwin and Vale, 2010). CAMSAP2 and 3 where shown to

co-localise at the minus end, interestingly in this study, siRNA of these CAMSAPs forced a radial array motif suggesting that CAMSAPs are needed for MT relocation from the centrosome, a characteristic necessary for epithelial polarisation (Tanaka et al., 2012).

At ncMTOCs, CAMSAPs have been found to interact with many other proteins such as the spectraplakin ACF7, which links MTs to the apical cortical actin network via CAMSAP3 to organise the MT network in the absence of a centrosome at this site (Noordstra et al., 2016). As the name suggests CAMSAPs share an interaction with the spectrin family of proteins that are found in a criss-cross pattern on the underside of the cell membrane. Using the *Drosophila* ovarian follicle cells, it was found that the spectrins, α-spectrin in particular, was necessary for the asymmetrical distribution along with the spectraplakin shot (ACF7/MACF1 in human) which has both actin binding and MT binding (via CAMSAP3) properties. Mutation of α-spectrin led to some perturbation in follicle cells, a mislocalisation of shot from the apical membrane and also negatively affected the transport of Rab11 vesicle, a key contributor to the formation of a polarised apical membrane. Loss of polarity determinants CDC42 and Lgl caused the most dramatic loss of disruption to polarity suggesting that apical-basal polarity determinants act upstream of Spectrin polarisation to control Patronin and Shot localisation and microtubule polarisation, which then directs apical trafficking of Rab11 for microvilli biogenesis (Khanal et al., 2016). Furthermore Nashcheckin *et al.,* (2016) reported shot as a cortical MT anchor in the *Drosophila* oocyte and that γ-tubulin does not localise here suggesting that no nucleation occurs in this region and only pre-formed MTs became anchored at this site. Here, PAR-1 excluded Shot and MTs from the posterior of the oocyte which has not been studied in mammalian cells. This was achieved firstly with the use of mutant PAR-1 which resulted in shot localisation and MT growth from the posterior cortex, an area that sees no MT growth in WT ooctyes likely due to the presence of PAR-1. To confirm this, a symmetric PAR-1 mutant that localises to all oocyte membranes was used and showed that MT growth did not occur from these areas showing a mechanism for asymmetrical MT localisation (Nashchekin et al., 2016).

In human, ACF7 has been shown to be important for both epithelial polarisation and for cell migration. ACF7 appeared to be more influential than CAMSAP2 or 3 as KO of ACF7 caused perturbation of epithelial architecture whereas KO of CAMSAP2 or 3 alone did not in a 3D system. This is most likely due to the fact that ACF7 was shown to participate in the apical recruitment of CAMSAP3 by a direct interaction demonstrated by a pull-down assay, interestingly this study failed to show spectrin association with CAMSAP although this may be cell line specific (Noordstra et al., 2016). However, it should be mentioned that there is some conflicting evidence here as Toya et al., (2016) describes a slightly different situation where KO of CAMSAP3 leads to a disruption of the MT architecture in both the models with perturbation of the nucleus and Golgi apparatus. However, in

these systems, removal of CAMSAP3 did not led to a more radial array of MTs as seen in 2D systems by Noordstra et al., (2016).

Using the CaCo-2 human intestinal adenocarcinoma cell line it was found that non centrosomal MTs crosstalk with F-actin through their minus ends and this contributes to control of the focal adhesion size and overall cell migration. Here ACF7 interacted with CAMSAP3 to facilitate this MT/actin interaction anchoring these non centrosomal MTs to the actin network (Ning *et al*., 2016). As well as the MT network, Patronin/CAMSAP3 influences the actin cytoskeleton which is also very important for apical basal polarisation. The formin (actin polymerising proteins) orthologue CYK-1 was found to bind directly to PTRN-1 which promotes CYK-1 mediated actin polymerisation (Gong et al., 2018). This highlights the possibility that CAMSAPs also influence the actin cytoskeleton although this is currently an understudied area. As previously described, it is likely that any influence on actin may be due to the ACF7 crosslinking actin and MTs.

As well as ncMTOC organisation, CAMSAPs have been implemented in the release of MTs from the centrosome. MT release from the centrosome is an important step in the polarisation process and the translocation of MTs. There is evidence that MT release from the centrosome occurs via both a change in centrosome composition and by active cleavage of MTs by katanin (Jiang et al., 2014, Jiang et al., 2018, Muroyama et al., 2016). This cleavage by katanin and possibly centrosomal release (not tested) relies on a pericentrosomal cloud of CAMSAP3. It was found that CAMSAP3 accumulates in the pericentrosomal area (around centrosome) in single non-differentiated/polarised cells and this accumulation was dependent on the minus end directed motor Dynein. Furthermore, there is a direct interaction between CAMSAP2 and 3 and katanin and that CAMSAP interaction with katanin was essential for MT cleavage here. Loss of CAMSAP3 caused a strictly radial centrosome bound array of MTs and overexpression of CAMSAP3 leads to a loss of centrosome bound radial MTs again suggesting that CAMSAP3 is required for release and transport of MTs from the centrosome (Dong et al., 2017, Jiang et al., 2018).

More evidence of the MT organising ability of CAMSAP3 comes from the early mouse embryo. In this system it has been shown that early embryo cells were connected in pairs via a MT bridge known as a cytokinetic bridge that does not undergo stereotypical abscission after cell division. This bridge becomes a site for CAMSAP3 accumulation and acts as an ncMTOC during interphase and is crucial for the movement of key proteins such as E-cadherins transport to cell membranes which is essential to maintain inner mass pluripotency (Zenker et al., 2017). CAMSAP3 also plays a role in maintaining neuronal polarity and shows preferential binding depending on MT acetylation (Pongrakhananon et al., 2018). Here it was shown that CAMSAP3 was enriched in axons and mainly

bound to non-acetylated MTs despite axonal MTs being mainly acetylated. CAMSAP3 mutation leads to supernumerary axons with increased MT acetylation. Tissue culture repeated this result as CAMSAP3 was depleted MT acetylation increased. Therefore, CAMSAP3 maintained a population of non-acetylated MTs and prevented their acetylation from the MT acetylating protein αTAT1 (Pongrakhananon et al., 2018).

1.9 Cell Migration

The cytoskeleton plays an important role in the process of cell migration which occurs during normal physiological processes such as wound healing and immune responses. Of course, cell migration is also a major factor in the metastasis of tumours, an example of pathological cell migration. Migration can occur as single cells in the case of immune cells such as leukocytes migrating toward an immune response or a collective movement of cells in sheets seen in development and wound healing. Migration is usually a collection of processes that ultimately leads to the movement of the cell or cells, although the exact method varies depending on cell type. One of the early stages involves protrusion of the lamellipodia toward the direction of intended travel which then form cell substrate adhesions, providing the traction required for cell movement. This is them followed by contraction of the cell body toward the leading edge and finally retraction of the tail that has formed due to the cells movement (Vicente-Manzanares *et al.,* 2005, Ridley, 2001).

1.9.1 Lamellipodia protrusion

Formation of the lamellipodia usually results from the detection of a chemokine gradient. It consists of a wave like extension to the plasma membrane, usually ~0.1-0.3µm thick and 1-5µm in length. It defines the leading edge of the cells where adherence to the substarte occurs. The lamellipodia contains a dense network of branched actin filaments, this branching is key to the formation of the lamellipodia. The Arp2/3 complex is responsible for this branching in the presence of specific nucleation-promoting factors (NPF). However molecular genetic approaches have the Arp2/3 complex is not essential, instead formins are the essential factor in this process (Yamaguchi and Condeelis, 2007).

1.9.2 Focal adhesions

At the level of the lamellipodia, adhesions form that make contact with the ECM, mostly via the integrin protein family. At this site, as the cell moves, a turnover of these adhesions occurs to

maintain traction at this leading edge. Plaques of adhesions known as focal adhesions provide the majority of traction in this system. Focal adhesions are multi-protein structures that link the actin cytoskeleton to the ECM, the formation and maturation of these focal adhesions is a regulated process aided by MTs. The formation of focal adhesions involves initiation, clustering of key proteins, growth, maturation and ultimately disassembly. Initiation occurs via the activation of β3-integrins achieved via an allosteric conformational change as the integrin makes contact with the ECM (outside-in activation) or integrin binding to intracellular adapters (inside-out activation). Focal adhesion formation relies on protein scaffolding assembly made up of new focal adhesion components controlled stochastically. Disassembly of the focal adhesion is controlled by internal factors such as physical stress changes, external substrate degradation but also via calpain cleavage of talin and ubiquitin degradation (Wehrle-Haller, 2012).

Very little is known about the function of EB2 and its effect on migration, preliminary work from our lab suggests that increased EB2 expression causes an increase in cell migration. Liu *et al.,* (2015) studied the interaction of EB2 with HAX1 and the subsequent effect on focal adhesion turnover, an important factor in cell migration. Using coimmunoprecipation and immunolabelling HAX1 was found to localise at focal adhesions and EB2 recruited HAX1 to MTs for its delivery. Knock down of either EB2 or HAX1 caused reduce focal adhesion turnover which in turn reduce cell migration *in vitro* and wound healing *in vivo* (Liu *et al.,* 2015). Yue *et al.,* (2014) also describes a role for EB2 in focal adhesion disassembly where MTs deliver MAP4K4 to focal adhesions via EB2 recruitment. This MAP4K4 localisation indirectly activates Arf6 which then enhances focal adhesion dissolution (Yue *et al.,* 2014).

1.9.3 Golgi organised microtubules

It is emerging that the MT minus end CAMSAPs and the +TIP EBs (EB1 and 3) have an interaction. Wei et al., (2017) described an EB1- CAMSAP2 crosstalk between non-centrosomal MTs and the autophagosome. Here it was shown that in HeLa cells CAMSAP2 cooperates with EB1 by regulating its binding to the MT plus end and therefore effecting MT dynamics. This CAMSAP2 EB1 interaction was suggested to occur in the cytoplasm rather than at the MT level. Interestingly here it was also shown that CAMSAP2 was found mainly at the Golgi, binding MT minus ends anchored here. In addition to this research Yang et al., (2017) used CRISPR KO of specific EBs in HeLa, HEK293T, HT1080 and RPE1 cells and found that disruption of EBs decreases the length of CAMSAP2 decoration at the opposite end of the MT and this in turn led to more detached MTs from the Golgi membranes and a more compact Golgi complex, likely caused by a lack of mechanical forces from fewer MTs attached

to the Golgi. Furthermore, it was found that the interaction of the MT minus ends with the Golgi was reliant on EB1/EB3-myomegalin complex and minus end CAMSAP2 (Figure 2). Disruption of EB1 and EB3 also reduced cell migration and focal adhesion assembly and distribution most likely due to a lack of MT binding at the Golgi which is a well-documented phenotype of a migrating cell.

Recently the CAMSAPs have been implemented in cell migration, in particular they have been shown to organise MTs at the Golgi for the formation of a polarised array of MTs that extend toward the leading edge and the direction of migration. Interestingly Martin et al (2018) found that the centrosome had little effect on cell polarity as removal with the drug Centrinone B failed to prevent cell polarization and movement in 2D or 3D systems. Here it appeared to be non centrosomal MTs organised and stabilised by CAMSAP2 that was essential for this. However, a complex interaction is present in these HUVEC endothelial cells where loss of CAMSAP2 prevents polarisation only when the centrosome is present. In the absence of both CAMSAP2 and the centrosome polarisation could occur although in a flawed manner. As well as cell migration Pongrakhhananon et al., (2018) discovered a role of CAMSAP3 in EMT in lung carcinoma cells (NCI-H460 and A549). Here it was found that CAMSAP3 is necessary to main a cells epithelial morphology as loss of CAMSAP3 via CRISPR KO caused an increase in EMT in these cells. This fits with previous research that shows CAMSAP3 organises MTs at epithelial, non centrosomal sites whereas KO disrupts this and precedes a more radial array of MTs, closer to that of a migrating cell.

1.10 Rationale

MTs are responsible for a diverse range of cellular activities and importantly for this work are key regulators of apico-basal polarity and cell migration. The centrosome is a major organiser of MTs and strongly influence their behaviour and dynamics. The role of the centrosome during apico-basal polarisation is not known nor is it known if it is essential for this process to progress. The EBs are also strong regulator of MTs, influencing their dynamics and interactions. Limited research suggests that high EB2 expression is an indicator of undifferentiated cells and its overexpression has been found in invasive cancers although these has not been explored fully. The role of EB2 in these situations is not known and warrants further study.

1.11 Aims and Objectives
1. Chapter III: Investigating the effect of centrosome loss on apico-basal epithelial polarisation. The aim of this chapter is to:
    a. Evaluate the effectiveness of centrinone B centrosome removal in MDCKII cells

b. Determine the localisation of CAMSAP2 and CAMSAP3 in MDCKII cells and determine the effect of centrosome loss on these proteins

c. Compare markers of polarity such as cell height and PAR3 localisation in control and acentrosomal cells

d. Determine if the centrosome is required for the formation of 3D cysts.

2. Chapter IV: Investigating the effect of EB2 overexpression on cell apico-basal polarisation. The aim of this chapter is to determine the effect of EB2 overexpression on:

a. Epithelial apico-basal polarisation

b. Centrosome composition and function

3. Chapter V: Generation of a MDA-MB-231 MAPRE2 KO Cell Line using CRISPR Cas9. The aim of this chapter is to:

a. Generate a MAPRE2 (EB2) KO/KD MDA-MB-231 cell line with genomic and proteomic validation. Specifically, validation of loss of EB2 protein expression and MAPRE2 mRNA

b. Analyse the effect of EB2 KO on MDA-MB-231 cell migration.

Chapter II:

Materials and Methods

2.0 Chapter II: Materials and Methods

2.1 Cell Lines

The MDCKII cell line was used as a model of epithelial cells in this study, they are non-cancerous and are commonly used for virus infection studies as well as a model of epithelial tissue. MDCK cells were originally isolated from kidney tissue of an adult female cocker spaniel in 1958. The MDCK II cell line is a subclone of the heterogenous MDCK cell line. It is thought that this cell line is derived from the distal tubule or collecting duct of the nephron. MDCKII cells easily form polarised layers in 2D cultures and form cysts when embedded in 3D matrices. The MDCK II cell lines used in this study were previously generated in the Mogensen lab and were transfected with the pmCherry-C1 plasmid (see section 7.1 for plasmid map), either containing the mouse MAPRE2 gene in the multiple cloning site (MCS) or with no addition. This plasmid also contained the neoR gene for positive selection of cells containing the plasmid, for this G418 (geneticin) was used. To reduce heterogeneity of plasmid number and ultimately the amount of mChery-EB2 or mCherry-EMPTY, serial dilution was carried out to create clonal populations. These clonal population are maintained under antibiotic selection at all times to ensure construct expression.

The Panc-1 cell line was also briefly used in this study, this cell line is a human pancreatic cancer cell line derived from carcinoma of ductal pancreatic cell. It was isolated from a 56-year-old male, are epithelial in nature, have poor differentiation ability and metastasize easily. Previous work in the Mogensen lab identified heterogenous expression of EB2 in this cell using immunolabeling. Some cells expressed very little EB2 whereas others expressed a very high amount compared to the majority of Panc-1 cells. Serial dilution of the Panc-1 cell line was used to isolate and expand single clones with homogenous expression of EB2. This study used two such clones, one expressing high amounts of EB2 and the other expressing low amounts of EB2 both relatively and absolutely.

The MDA-MB-231 cell line is a highly invasive cell line commonly used as a model of late-stage breast cancer. It is a triple negative epithelial cell line and therefore has mutated oestrogen, progesterone receptors and low human epidermal growth factor receptor 2 (HER2). The cell line was established from pleural effusion of a 51-year-old Caucasian woman with metastatic mammary adenocarcinoma. Work from the Mogensen lab has identified high EB2 in this cell line compared to less invasive cell lines such as the MCF-7s (Amodu, 2018, thesis).

2.2 Tissue Culture

2.2.1 Passaging Cells

Cell lines were maintained in DMEM high glucose (4.5mg/L) (Gibco) supplemented with 10% FBS (Gibco), 1% L-Glutamine (2mM) (Gibco) and 1% PenStrep (100 units/ml) (Gibco). Cells were incubated at 37°C and 5% CO_2 in a humidified environment. Cell lines were routinely maintained, passage was carried out twice weekly and media change was not normally carried out (except for MDA-MB-231 and Panc-1 cells) to aid in the epithelial morphological preservation. Aseptic technique was used throughout and all reagents were prewarmed to 37°C. Passage was carried out when cells reached ~90% confluence by removing media, washing in 2ml 0.25% trypsin (Gibco), detaching with 3ml 0.25% trypsin and incubating for 20 minutes for MDCK IIs, 5 minutes for MDA-MB-231s or 10 minutes for Panc-1 cells at 37°C. Trypsin was then neutralised with 3 ml full media and centrifuged at 300g for 5 minutes to pellet cells. The supernatant was then discarded, and the cell pellet was suspended in 2ml full media, the desired amount was then removed and pipetted into a new T75 flask containing 10ml full media. MDCKII cells were split 1:20-1:25, MDA-MB-231 cells were split 1:5-1:10 and Panc-1 cell were split 1:4-1:8. The MDCK II cell lines containing plasmids were grown in media containing 1mg/ml G418 (Sigma-Aldrich).

2.2.2 Cell Counting

Cells counts were carried out using a haemocytometer by adding 15µl to the haemocytometer with a glass cover slip and all four corners were counted and an average was taken. This gave X x 10,000 cells/ml, which was then used to calculate volume of cell suspension needed to give desired concentration or number of cells to be seeded.

2.2.3 Freezing and Thawing Cells

Long term cell storage was carried out in liquid nitrogen containing Dewar's or a drystore system. To freeze cells, cells were detached as above and 1 million cells in 1ml of full media containing 10% dimethylsulfoxide (DMSO) was placed in cryovials (Corning). These cryovials were then placed into Mr. Frosty freezing container (Fisher) containing isopropanol and stored at -80°C overnight to slowly lower the temperature. Cell vials were then transferred into boxes stored in liquid nitrogen or the dry store system. When thawing these cells, 5ml full media was prewarmed and placed into a T25 flask. The cryovial containing the cells was then thawed by rubbing between the hands until liquid, the media containing the cells and DMSO was then added to the flask and the media was changed the following day to remove the DMSO that was contained in the freezing media.

2.2.4 2D Monolayer Culture

Many variations of 2D monolayer cultures were used in this study to form partially polarised layers of varying polarity and differentiation, cells were grown directly on plastic, on glass coverslips or on polycarbonate tissue culture inserts (Anopore 0.4μm, Thermo Fisher). For this, cells were trypsinised and counted as above, to obtain fully confluent cultures 500,000 cells were seeded into 35mm dishes containing glass coverslips or per well of a 6 well plate. To obtain ~60% confluency 150,000 cells were seeded and to study single cells 25,000 cells were seeded for 24 hours. Cells were suspended in full media and applied directly to the culture surfaces, tissue culture inserts were placed in wells containing full media without cells. For analysis of polarisation 40,000 cells were seeded and fixed and stained at increasing time points.

2.2.5 3D Cyst Culture

Polarised MDCK II 3D cysts were generated as part of this study according to Goldspink *et al*., (2017). For this, cover slips were placed into wells of a 24 well plate; cells were then detached and counted as above. Following this 5,000 cells/25μl of undiluted ~9mg/ml matrigel (Corning) was mixed by agitation (avoiding bubbles). Over each coverslip, 25μl of this suspension was spread using a sterile pipette tip and allowed to set at 37°C for 30-60 minutes. Finally, 500μl 5% serum DMEM media was placed on top, fixation and immunolabelling was then carried out after 10 days after cyst formation.

2.3 Drug Treatments

2.3.1 Centrinone B Treatment

Centrinone B selectively inhibits PLK4, a serine-threonine protein kinase that initiates centriole assembly. Developed by Wong *et al*., (2015), centrinone B was found to inhibit the activity of PLK4 in HeLa cells and prevented the assembly of new centrioles without disassembling existing centrioles. Therefore, after successive cell divisions, many cells in culture would have no centrosomes and some would possess only a single centrosome. As centrinone B does not disassemble existing centrioles, cell cultures were seeded at low density before treatments were added, ensuring as little centrosomes as possible were present in the population. Centrinone B was stored as a stock of 50mM in DMSO at -20°C. Centrinone B was then added at 500nM in full media and cultured for 7 days to allow for adequate cell proliferation. Cell were then seeded as needed after these steps. Centrinone B concentration was based on work by Wong *et al.,* (2015) which showed that 500nM effectively

removed the centrosome while showing good cell survival. Subsequent research show lower concentrations (125nM) of centrinone B are effective and these lower concentration should be considered for future work (Guizzunti and Seeman., 2016, Dudka *et al.,* 2019).

2.3.2 Nocodazole Treatment (MT regrowth assay)

MTs were depolymerised using a combination of cold and drug treatment. Nocodazole was stored as a stock of 10mg/ml in DMSO at -20°C. Firstly, cells were incubated on ice for 1 hour with 5 µg/ml nocodazole in full media, followed by a further incubation for 1 hour at 37°C. Cells were then washed in ice cold media before fresh media was added and cells were allowed to recover. Before recovery, one sample was fixed to ensure proper depolymerisation had occurred then the recovery timepoints were fixed separately. The recovery times in this study were 2, 4 and 6 minutes.

2.3.3 Blebbistatin Treatment

Blebbistatin treatment was used to inhibit the activation of the motor protein myosin. Blebbistatin was stored as a stock of 5mg/ml in DMSO at -20°C. Cells were seeded and grown for 5 days as above. Blebbistatin treatment was then carried out by adding 50μM blebbistatin in full media and incubated for 4 hours at 37°C and 5% CO_2. Note: longer treatment periods caused multi nucleated cells due to cytokinesis failure during mitosis. Cells were then methanol fixed and immunolabelling was carried out as in section 2.4.

2.3.4 Y27362 Treatment

The Y27362 ROCK inhibitor was used in this study to further explore the effect of EB2 overexpression on cell junctions and shape index. Y27362 was stored as a stock of 1mM in DMSO at -20°C. Y27362 treatment was carried out adding 10μM in full media and incubated for 24 hours at 37°C and 5% CO_2. Cells were then methanol fixed and immunolabelling was carried out as in section 2.4.

2.4 Indirect Fluorescent Immunolabelling

Indirect fluorescent immunolabelling was carried out in accordance to Goldspink *et al.,* (2017).

2.4.1 Methanol Fixation

Samples were fixed using cold methanol at -20°C. Fixation time varied depending on sample thickness, cells on glass were fixed for 5 minutes, TC inserts for 10 minutes and 3D samples for 20-30

minutes. Samples were then washed with PBS to remove excess methanol and blocked using 10% goat serum in PBS for 30-45 minutes. The antibody was then diluted to the desired dilution in 1% goat serum in PBS, 50µl of diluted antibody was then applied onto parafilm in a droplet per coverslip/sample. The 3D samples were kept in 24 well plates throughout and only removed for mounting, here 200µl antibody solution was used instead of 50µl. The 2D samples were then placed cell side down onto this droplet and incubated for at least 1 hour at room temperature or overnight at 4°C. Primary antibody was then washed for 6 x 5 minutes with 1% goat serum in PBS or 4 x 30 minutes for 3D samples. The secondary antibody was then applied in the same fashion as the primary except for 30 minutes only at room temperature. Samples were then washed for a final time in PBS for 3 x 10 minutes or 6 x 20 minutes for 3D samples. The penultimate wash contained 300nM DAPI as a nuclear counter stain. The samples were then mounted onto a glass microscope slides with hydromount (National Diagnostics) (supplemented with 2.5% w/v DABCO). Samples were then stored at 4°C overnight before being visualised using fluorescent microscopy.

2.4.2 PHEMO Fixation

PHEMO fixation is a very good method for the preservation of the cytoskeleton although some loss of antigen can occur. Samples were first washed with PBS warmed to 37°C and fixation was carried out using PHEMO fix solution (3.7% Paraformaldehyde, 0.05% Glutaraldehyde and 0.5% Triton X100) prepared in PHEMO buffer solution (68mM PIPES, 25mM HEPES, 15mM EGTA and 3mM Magnesium chloride) for 10 minutes at room temperature. Sample was then washed with PHEMO buffer twice for 10 minutes each and a final wash with PBS for 5 minutes. Blocking, immunolabelling and mounting were all carried out as above.

2.4.3 Antibodies
Table 2.1 List of antibodies used in this study.

Antibody against	Company	Product code(s)	Dilution (Concentration)	Raised in
Primary Antibodies				
Ninein (PEP3)	In-house	N/A	1:1,000	Rabbit
Tubulin (YL 1/2)	Abcam	Ab6160	1:150 (6.7 µg/ml)	Rat
Ninein (N5)	Abcam	Ab52473	1:1,000 (1 µg/ml)	Rabbit
CAMSAP2 (1L1)	ProteinTech	CAMSAP1L1	1:500 (2 µg/ml)	Rabbit

CAMSAP3	Sigma-Aldrich	SAB4200415	1:200 (5 µg/ml)	Rabbit
IQGAP1	BD BioSciences	610611	1:50 (5 µg/ml)	Mouse
CLIP-170	Abcam	Ab61830	1:50 (20 µg/ml)	Mouse
PCM1	Gift	Gift	1:400	Rabbit
E-cadherin	BD BioSciences	610181	1:500 (0.5 µg/ml)	Mouse
γ-tubulin	Abcam	Ab16504	1:1,000 (1 µg/ml)	Mouse
Pericentrin	Gift	Gift	1:500	Rabbit
Villin	BD BioSciences	610358	1:500 (0.5 µg/ml)	Mouse
Centrin	Millipore		1:500	Mouse
ZO-1	ThermoFisher	61-7300	1:200 (1.3 µg/ml)	Rabbit
GM130	Abcam	Ab52649	1:250	Rabbit
PAR3	Millipore	07-330	1:500 (1 µg/ml)	Rabbit
α-tubulin	Abcam	Ab15246	1:300 (3.3 µg/ml)	Rabbit
β-catenin	BD	610153	1:500 (0.5 µg/ml)	Mouse
RFP	Abcam	Ab62341	1:1,000 (WB) (5 µg/ml)	Rabbit
B-actin	Abcam	Ab8227	1:500 (2 µg/ml)	Rabbit
Cep215 (CDK5RAP2)	Millipore	06-1398	1:250	Rabbit
EB2	Absea	010614A11	1:200 (5 µg/ml)	Rat
Secondary Antibodies				
Rabbit (Alexafluor 488, 568 or 647)	Thermo Scientific	A11008 A11011 A21245	1:1,000 (2 µg/ml)	Goat
Rat (Alexafluor 488, 568 or 647)	Thermo Scientific	A11006 A11077 A21247	1:1,000 (2 µg/ml)	Goat
Mouse (Alexafluor 488, 568 or Cy5)	Thermo Scientific (488 and 568)	A11001 A11004	1:1,000 (2 µg/ml)	Goat
	Jackson (Cy5)	115-175-003		

Mouse (HRP)	Thermo Scientific	62-6520	1:1,000 (1.5 µg/ml)	Goat
Rat (HRP)	Thermo Scientific	31470	1:1,000 (0.8 µg/ml)	Goat
Rabbit (HRP)	Thermo Scientific	65-6120	1:1,000 (1 µg/ml)	Goat

2.5 Microscopy

The study utilised three forms of microscopy, which were optical light, widefield fluorescence and confocal scanning microscopy (Zeiss AxioObserver Z1, Zeiss Axioplan 2ie and Zeiss LSM510-META/Zeiss LSM980 Airyscan respectively). Illumination was as follows, Colibri7 LEDs for Zeiss AxioObserver Z1, mercury lamp for Zeiss Axioplan 2ie and blue diode (405nm), argon (458, 477, 488, 504nm), helium-neon 543nm and helium-neon 633nm lasers for Zeiss LSM510-META. Confocal pinhole dimension was 1 A.U. Objectives used were 20x (NA=0.75 and XY=0.397µm) and 63x oil immersion (NA=1.4 and XY=0.213). Image processing was carried out using ImageJ software and Microsoft PowerPoint. Widefield fluorescence microscopy was utilised to collect data from a larger z area such as in the case of the junctional imaging to capture a better overview of the junction. Confocal microscopy was primarily used for measurements such as cell height and also for imaging of 3D cysts.

2.6 Western Blotting

Western blotting was carried out in accoradance to Goldspink *et al.,* (2017). Lysates were collected using the M-PER (Thermo Scientific, USA) lysis reagent with 15-minute incubation on ice and scraping of cell layers. Lysate was the spun a 13,000 rpm at 4°C and supernatant was collected and stored at -20°C. Lysate concentration was quantified using the Pierce BCA protein assay kit (Thermo Scientific, USA). Briefly, a standard curve was generated using bovine serum albumin of known concentrations from 0-2000µg/ml. BCA working reagent was added for colorimetric reaction and incubated for 30 mins at 37°C. Absorbance at 560nm was then measured using a spectrophotometer (Promega, USA). Unknown lysate absorbance was then plotted against this to determine concentration.

Lysate samples were resolved on either 10% or 4-8% gradient SDS polyacrylamide gels (Expedeon, UK) using PageRuler prestained protein ladder (Thermo Scientific, USA) at 120-200V for ~45 minutes. Samples were then transferred to nitrocellulose membrane using the semi-dry transfer system at 15V for 45 minutes. Membranes were initially blocked with 5% skimmed milk in TBST (137mM NaCl, 2.7 mM KCl and 19mM Tris Base with 1ml Tween-20 per litre) for 1 hour at room temperature. Incubation with primary antibody was then carried out in 5% milk TBST at 4oC overnight,

followed by 6 x 5 minute washes in 5% milk TBST. Chemiluminescence was used, secondary HRP conjugated antibodies were then incubated at room temperature for 1 hour followed by 6 x 5 minutes washes. Finally, membranes were imaged using ChemiDoc XRS+ imaging technology (BIO-RAD, USA) and quantified using ImageJ.

For re-probing of blots membranes were first stripped, this was accomplished by incubating membrane at room temperature in stripping buffer (1 litre H2O, 15g Glycine, 1g SDS and 10ml Tween20 adjusted to pH 2.2 with concentrated HCl) for 10 minutes. Fresh stripping buffer was replaced and incubated for further 10 minutes; membrane was washed twice for 10 minutes with PBS then twice for 5 minutes in TBST. ECL western blotting substrate was then applied and imaged with the ChemiDoc to confirm removal of antibodies, membrane was then blocked as before and re probed.

2.7 Image and Data Analysis

2.7.1 Fluorescence Intensity Analysis
For pixel intensity analysis of centrosomes, junctions, asters and total intensity, ImageJ was used. Samples were imaged using the same exposure for direct comparisons to be made. If automated analysis was to be carried out then intensity thresholding was used by creation of a binary image by setting predetermined thresholds. This binary image was then used as a measurement mask for measurement of original image. Pixel intensity values are relative and are therefore arbitrary. If manual areas were to be measured, then whole fields of view (FOV) or smaller selected areas were highlighted using the freehand tool and pixel intensity and area were measured. See section 2.7.2 for pixel intensity analysis at junctions.
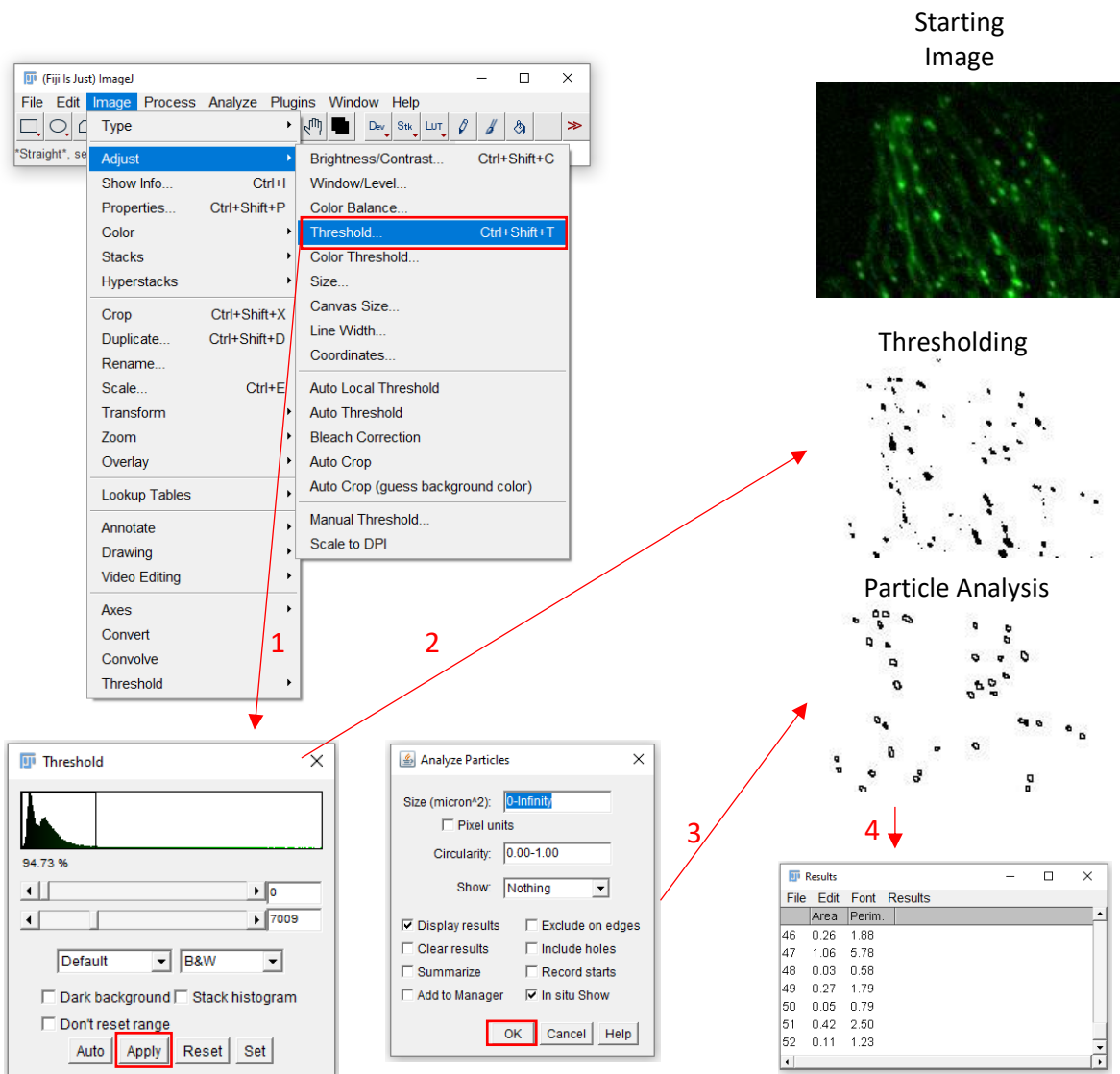
Figure 2.1 Example workflow of intensity analysis of comets using ImageJ. 1) The image threshold was set to produce a binary mask for measurements by selecting Image>Adjust>Threshold. The Thresholding options were then used to select pixel intensity ranges to be measured. These values were kept the same within experiments. 2) Once these settings were applied a binary image was created based on the threshold set. 3) Particle analysis was then carried out based on the binary mask by selecting Analyze>Analyze Particles. Size exclusion was used to prevent measurements of unwanted objects. 4) Table of results obtained from this analysis.

2.7.2 Junction Analysis

Cell junction analysis was carried out on confocal or widefield fluorescent images after immunolabelling. All images to be compared were imaged using the same exposure values and treated exactly the same. This was completed by firstly manually drawing a 10μm straight line across junctions in a perpendicular to the junction itself. This was done blind using a second antibody against a protein not to be measured such as actin. Note that these lines were then centred manually over the channel to be measured to ensure peak intensity occurs at the centre of the line. Intensity measurements were then taken every 0.1μm along the line to give continuous measurement across the junction. These profiles were then plotted as pixel intensity at distances along this line. All analysis was carried out using ImageJ.
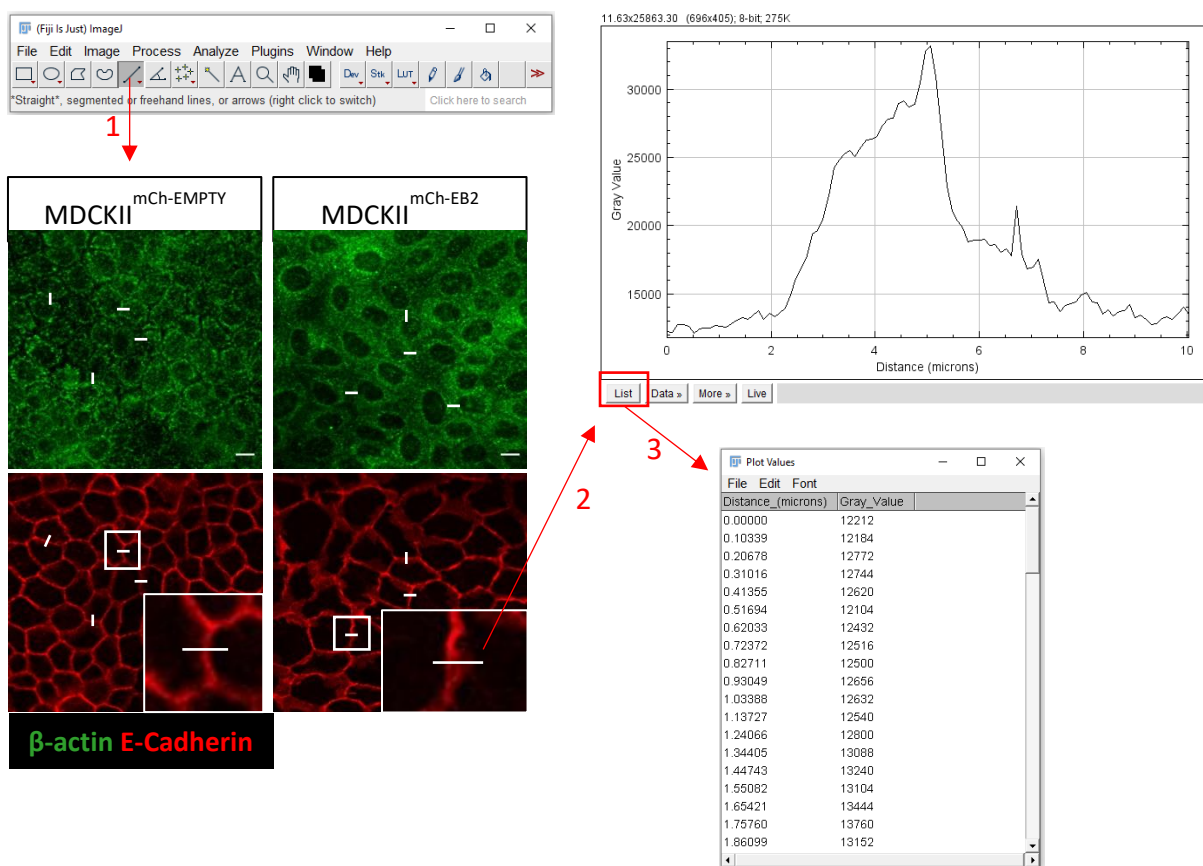
Figure 2.2 Example workflow of junction intensity analysis using ImageJ. 1) Using a label other than the stain of interest, a 10μm line is manually drawn across random junctions in a perpendicular manner, using the straight-line tool. 2) The pixel intensity profile of this line was then seen by selecting Analyze>Plot Profile. 3) Values from this plot were then generated by selecting list to show values from every 0.1μm across the line.

2.7.3 Jamming Analysis

Cell jamming was analysed using ImageJ, the cells were first labelled with E-cadherin to highlight the cell periphery and imaged using either widefield or confocal fluorescence microscopy. Using this staining, the freehand line tool was used to draw around the perimeter of the cell. This gave the measurement of the cell area and perimeter used to calculate the shape index which is used as a quantification of cell jamming. The formula used was shape index= perimeter/√area. This method was adapted from Park *et al.,* (2015).
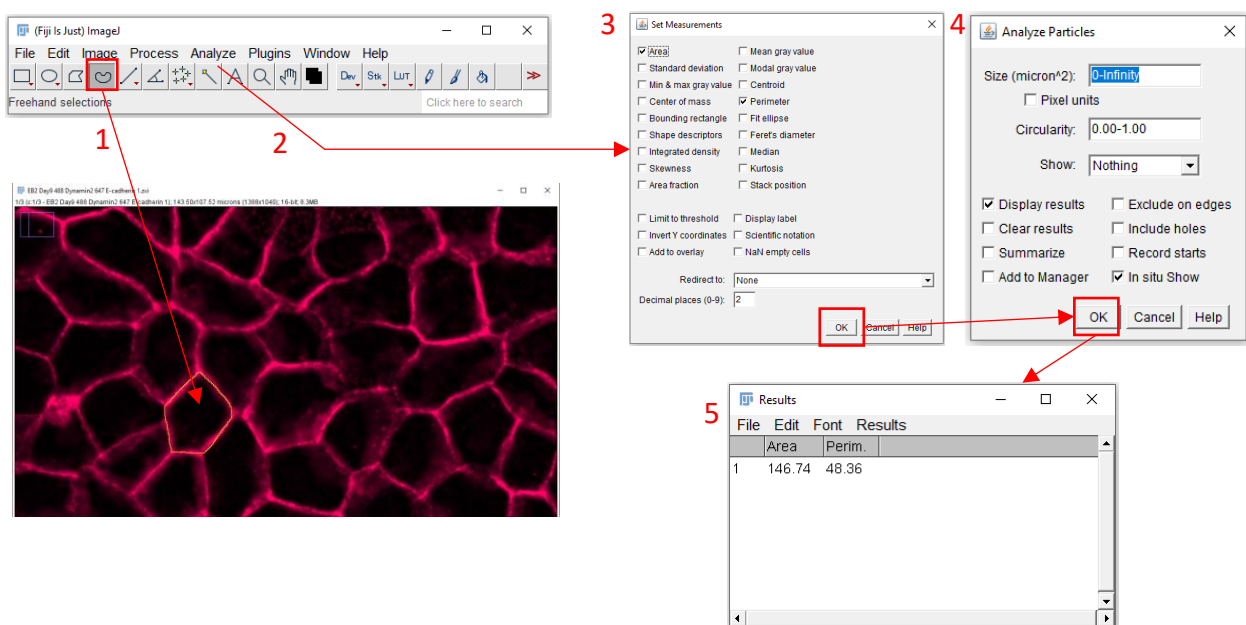
Figure 2.3 Example workflow of shape index analysis using ImageJ. 1) Using a cell-cell contact marker, the periphery of the cell was drawn using the freehand selection tool. 2) The measurements were then set by selecting Analyze>Set Measurements. 3) The area and perimeter were selected. 4) Particle analysis was then carried out without any size exclusion. 5) Values from the results table were then used to calculate shape index.

2.7.4 Statistical Analysis

Statistical analysis was carried out using SPSS statistical software, mostly for experiments containing 2 groups a T test was carried out for parametric data sets. Non-Parametric data sets with two groups were subjected to Mann Whitney U tests. For experiments with more than 2 groups, ANOVA was carried out with post hoc Tukey tests. All statistical testing was carried out at a confidence level of 95%.

2.8 CRISPR

CRISPR mutation of the MAPRE2 gene in MDA-MB-231 cell line was carried out with validation of protein and mRNA loss/reduction. This was achieved using knock-in mutagenesis with simultaneous insertion of a GFP marker and puromycin resistance as follows. The MDA-BM-231 cell line was used because they have been shown to express high levels of EB2 which work from the Mogensen lab has identified to induce increased invasiveness (Amodu, 2018, thesis). Therefore, the effects of EB2 KO would likely be more dramatic in this cell line compared to others with normal EB2 expression. The construct used for this work contained the guide (sgRNA) with the Cas9 contained within the same construct to increase efficiency as transfected these separately would decrease efficiency.

2.8.1 Guide Design Validation

To ensure the commercially designed guides were appropriate for the knockout of EB2 in MDA-MB-231, it was first essential to analyse the MAPRE2 gene. Transcripts and exons positioning were analysed using the NCBI genome database and Ensembl.

2.8.2 Transfection

The sgRNA and Cas9 sequence were delivered into cells contained within the pCas-Guide construct. Two variations of these constructs were used, one containing guide 1 and the other containing guide 2 (Origene). In addition to this, a linear donor was used containing the turboGFP and puromycin resistance gene (pac) (Origene). The guides were not transfected together, each guide was transfected with the linear donor. The co-transfection of these components was carried out using the lipofectamine 3000 (ThermoFisher) transfection method as follows.

Cells were seeded into 24 well plates at 40,000 cells per well in 0.5ml of full media and incubated overnight at 37°C and 5% CO_2, the next day cells were visualised and were ~70% confluent. The transfection was carried out as per manufacturer's instructions using two volumes of lipofectamine 3000 reagents. Two solutions were made containing guide 1 or guide 2 containing constructs with the linear donor. This solution was then added to the 24 well plates in a drop wise manner. The cells were then incubated for 4 days at 37°C and 5 % CO_2 before selection and further validation.

2.8.3 Puromycin Selection

Puromycin was used as a selection drug for successful linear donor transfection and genome integration. Puromycin was stored as a stock of 10mg/ml in 20mM HEPES buffer at -20°C. A dose curve was carried out and showed that 7µg/ml effectively killed all control MDA cells within 48 hours. Therefore, transfected cells were treated with 7µg/ml puromycin in full media for 72 hours. Cells were treated 4 days after transfection to select for the presence of the integrated or unintegrated donor then 3 weeks later to select for the integrated donor only.

2.8.4 Flow cytometry and FACS

The GFP positive and larger cells were selected from the puromycin resistance population as these more likely containing linear donor integration at MAPRE2. Cells were trypsinised for 25 minutes and EGTA treated for 5 mins to ensure only single cells were present for analysis. Cells were analysed using flow cytometry to assess the GFP expression levels within the guide 2 treated cell population and compared to MDA WT control cells. Cells in suspension where then analysed using the BD FACSAria II cell sorter (BD Biosciences) equipped with a 488 nm laser. Fluorescence activated by the 488 nm laser was measured at the detector between 505 and 550. Cells sorting was carried out simultaneously and 2627 cells were sorted, of which 105 were kept and grown prior to sorting. These cells were then used in future experiments. FlowJo was used for graph production and analysis of data. All flow cytometry and cell sorting techniques were carried out under the guidance of Dr Ernst Poschl.

2.8.5 Sub Cloning

Two methods for the isolation of single cells was used. Firstly, serial dilutions were carried out with the goal of isolating single cells within wells of a 96 well plate. Here, 4000 cells were pipetted into the first well (A1) then consecutive 1 in 2 dilutions were carried out in each well of the first column, resulting in a decreasing number of cells in each well. This was then followed by more consecutive 1 in 2 dilutions along the rows of the 96 well plate going from left to right of all wells. The result of this is the theoretical lowest number of cells are within the bottom right well and this number increases moving to the top left well of the plate. A more selective method was used were 5,000 cells were seeded into 100mm petri dishes and individual cells were pipetted from this into individual wells of a 96 well plate. Collagen I coating and increased serum concentration were used in the 96 well plate to attempt to increase survival rates of single cells. Conditioned media produce by growing WT MDA-

MB-231 cells in media for 3 days. This media was then filtered using a 0.2μm syringe filter, conditioned media was then pipetted into 96 well plates.

2.8.6 PCR

Genomic DNA (gDNA) extraction was carried out using the PureLink Genomic DNA Mini Kit (ThermoFisher) as per manufacturer's instructions. As many cells as possible were used for this process with a maximum of 5,000,000. These were pelleted as suspended in PBS along with proteinase K and RNase A to remove protein and RNA contaminants and cells were lysed using the PureLink Genomic Lysis/Binding Buffer and incubating at 55°C for 10 minutes. DNA was then precipitated using 100% ethanol. The gDNA was the collected in a PureLink Spin Column and washed twice with provided wash buffers. Finally, the gDNA was eluted using 25 μl of the water-based DNA elution buffer. Collected gDNA quantified using the nanodrop method (NanoDrop 1000, ThermoFisher) and stored at -20°C.

Amplification and analysis of target sites was achieved using PCR. For amplifications under 1kb then the GoTaq Green (Promega) kit was used that only contains Taq polymerase. For amplifications over 1kb, the OneTaq DNA polymerase kit (NEB) was used which included the proof reading DeepVent DNA polymerase. OneTaq was used with 10mM dNTP (N0447, NEB) with the recommended increased polymerase concentration of 2.5units/50 μl reaction. All PCR reaction were carried out in 50 μl reaction volumes. GoTaq green was used as per manufactures instructions. PCR cycle setting for each polymerase can be seen below.

Table 2.2 Thermocycler settings used for GoTaq Green DNA polymerase amplification

GoTaq Green	Temperature	Duration	
Initial Denaturation	95°C	2 mins	
Denaturation	95°C	30 secs	
Annealing	55-65°C	30 secs	X30
Extension	72°C	1 min	
Final Extension	72°C	5 mins	

Table 2.3 Thermocycler settings used for OneTaq DNA polymerase amplification

OneTaq	Temperature	Duration	
Initial Denaturation	94°C	30 secs	
Denaturation	94°C	30 secs	
Annealing	55-68°C	30 secs	X30
Extension	68°C	1 min per kb	
Final Extension	68°C	5 mins	

Amplicons were visualised using electrophoresis on 2% agarose gels run at 100-150V for 1-1.5 hours using 20 µl of sample along with 5 µl of ladder (Generuler 100bp plus, ThermoFisher). Gels were then bathed in TAE solution containing ethidium bromide (0.6µg /ml) on a shaker for 30 minutes. The gel was then analysed on a UV transilluminator (BioRad).

Table 2.4 List of primers and their use

Primer Sequence	Use
TGTTGATGGACACTTAGGTTGC	MAPRE 2 guide 2 site forward primer
GGGAGTTTGCATGGTGAGAC	MAPRE 2 guide 2 site reverse primer
TCCAGTGGAGAAGCTAGTGA	MAPRE 2 guide 2 site forward primer
ATTGCATCTTGCCCTTGTCG	MAPRE 2 guide 2 site reverse primer

2.8.7 Band Extraction and Sequencing
For further analysis of amplicons bands were excised from agarose gels. Using a sterile scalpel, the band was cut from the gel under illumination from a table top UV lamp box. The excised gel was place into a sterile 1.5ml Eppendorf tube and purified using a commercially available gel extraction kit (Qiagen). Purified DNA was then quantified using the NanoDrop method and if possible reamplification using PCR was carried out.

Sequencing of these purified bands was carried out using next generation sequencing via Eurofins Genomics. The Mix2Seq (Eurofins) kit was used, DNA sample (concentration varied by length) was combined with either the forward or reverse primer and sent to eurofins for sequencing.

2.8.8 cDNA synthesis

RNA was extracted from cells pelleted using an RNA extraction kit (Quick-RNA Mini prep plus kit, Zymo, Cat no. R1058), according to manufacturer's guidance. Samples were eluted in 25 uL of nuclease free water; RNA concentration and purity quantified on a Nanodrop 1000 and 1 uL was checked on a 2% agarose gel. cDNA was synthesised with qPCRBIO cDNA Synthesis Kit (PB30.11-02) as per manufacturer's instructions with 500 ng of total RNA. cDNA was diluted 1:40 prior to use.

2.8.9 qRT-PCR

Reactions for qPCR were prepared as follows:

4 uL of cDNA

1 uL of Quantitect primer (18s or MAPRE2) (QT00199367, QT00199521, Qiagen)

5 uL of SybrGreen (4309155, Applied Biosystems)

Into a 96 well plate (Applied Biosystems; cat. no. N8010560) on a 7500 Standard PCR instrument (Applied Biosystems) following the cycling program (2 mins 50°C; 10 mins 95°C; 45 cycles (10 secs 95°C; 1 min 60°C); with melt curve analysis (15 secs 95°C; 1 min 60°C; 30 secs 95°C, ramp rate 1%; 15 secs 60°C). Raw CT values were analysed, with the delta delta CT method to calculate fold change. Values were normalised to expression of 18s. Experiments were set up in biological triplicate and technical triplicate with no template controls too.

2.9 Random Migration Assay

To assess the migration of the cells generated above a random migration assay was carried out with comparisons made to MDA-MB-231 WT cells. To achieve this 24 well plates were first coated with collagen 1, WT MDA-MB-231 cells or clone 6 was then seeded at 25,000 cells per well with 0.5ml media and incubated overnight at 37°C and 5% CO_2. The next day, cell well then transferred to an inverted incubating microscope (Axio Observer) and left to settle for 1 hour at 37°C and 5% CO_2. Three

positions per well were then set and verified and images were taken every 10 minutes for 18 hours using phase visible light microscopy. The ImageJ manual tracking plugin was used to collect raw cell positional data which was then analysed using the Ibidi chemotaxis migration analysis tool.

Chapter III:

Effect of centrosome loss on apico-basal epithelial polarisation

3.0 Chapter III: Effect of centrosome loss on apico-basal epithelial polarisation

3.1 Overview

In relatively flat cells the centrosome is the major MTOC where it anchors and nucleates MT generating a radial pattern. During apico-basal polarisation the centrosome function and positioning changes and in some cell types it is eliminated completely. Loss of centrosomal MTOC activity has been noted as differentiated cells reorganise their MTs to a non-centrosomal array, but it is currently unclear if the centrosome is essential in this process. Here, MDCKII cells were used as a model of apico-basal polarisation due to their ease of polarisation *in vitro.* The PLK4 inhibitor centrinone B was used to produce an acentrosomal population of MDCKII cells and the polarisation process was studied at several stages.

3.2 Introduction

During apico-basal epithelial polarisation the centrosome moves to an apical position where it may or may not nucleate and anchor MTs, depending on the cell type (see section 1.8) (Sanchez and Feldman., 2016). It is not known if the centrosome is essential for cells to polarise and reorganise their MT array, so the aim of this study is to analyse acentrosomal cells during apico-basal polarisation and particularly to analyse what happens to key centrosomal and MT associated proteins during this process. Previous research in *C. elegans* nematodes show that γ-tubulin redistributes from the centrosome to the lateral then apical membrane as it moves apically. It was also stated that laser ablation of the centrosome prevented this (Feldman and Priess, 2012). However, whether this is also the case for mammalian cells remains to be determined. Complete redistribution of γ-tubulin is not universal for all apico-basal polarity models as the centrosome retains its nucleation ability in some polarised cells such as in kidney epithelium from which the MDCKII cell line were isolated (Werner *et al.,* 2017). Therefore, γ-tubulin positioning alone is not a sufficient marker for the study of polarisation. Here we study several consequences of acentrosomal cell generation including CAMSAP localisation, cell height (elongation) and MT organisation.

Removal of the centrosome is the obvious strategy for determining its importance in the apico-basal MT reorganisation and polarisation process. There are many methods available for the removal of the centrosome such as laser ablation, microsurgery, chemical inhibition or genetic modification. Laser ablation is one of the most common methods used and involves the use of a high energy microbeam to destroy the centrosome. Although commonly used, the potential side effects of laser ablation are not well known and warrant further study. It is rapid and doesn't require long term treatments although for the removal of the centrosome it may not be effective long term due to the

de novo centriole assembly pathway (Uetake *et al.,* 2007). This may result in the generation of centrosomes when carrying out longer term experiments such as those used here and as such is unsuitable for this study. Gene mutation/KO of key centriole regulatory factors such as mutation of CEP152 (molecular scaffold for interaction of PLK4 and CENPJ) and STIL (structural element of the cartwheel formation) have been used to produce stable acentrosomal cell lines (Sir *et al.,* 2013). Although genetic modification methods of course carry the risk of off target mutagenesis. CRISPR makes this method very easy but off-target effects are always a consideration. Removal of the centrosome via drugs has become more popular recently due to the discovery of centrinone B. Its ease of use and long-term effects through continuous treatment may explain its popularity as previous methods require advanced equipment such as multi-photon microscopes and genetic studies. Here centrinone B was used and applied to MDCKII cells continuously ensuring centriole loss throughout experimental periods. Although as with any drug treatment cell toxicity may exert an effect.

Centrinone B was developed by Wong *et al.,* (2015) as a selective PLK4 inhibitor based on the VX-680 compound which is a non-selective aurora kinase inhibitor. Inhibition of PLK4 prevented new centriole assembly which caused the progressive loss of centrioles from a dividing population of cells. This effect was reversible as centrinone washout led to recovery of centrioles via the *de novo* centriole assembly pathway. Centrosome loss via centrinone B in some immortalised and primary cells led to arrest of the cell cycle due to activation of p53 in response to the activation of the cell cycle checkpoint. Transformed or cancerous cells with mutations in p53 do not arrest the cell cycle but a decrease in proliferation was observed in all cell lines studied (Wong *et al*., 2015).

The Madin Darby Canine kidney (MDCK II) cell line was used as a model of epithelial tissue in this study. MDCKII cells were derived from the distal tubules/collecting duct epithelia of the canine kidney nephron (Leighton et al., 1969). They are considered normal e.g. non-cancerous and are used commonly as a model of epithelial tissue as they easily polarise. So, although they do contain normal p53 they were used as a model for these studies. When grown to high confluence they partially polarise, a process that is aided by the use of semi-permeable tissue culture inserts/filters which allow for closer to *in vivo* basal membrane interactions. In this configuration MDCKII cells show characteristics of epithelial tissue such as continuous cell junctions, increased cell height and apico-basal arrays of MTs. MDCKII, when polarised, contains ncMTOCs associated with apical adherens junctions and the MTs extend basally from here. The centrosome remains as the major nucleation site proximal to the apical membrane (Bellet et al., 2009). Additionally, MDCKII cells form cysts when embedded into 3D matrices such as Matrigel (Goldspink et al., 2017). These cysts consist of a hollow sphere of cells with a central lumen. The apical surface of the cells faces the lumen while the basal surface faces the ECM. These 3D cysts also show many hallmarks of epithelial tissue such as junction

formation, elongation, apical/basal membrane formation and apical-basal organised MTs. They are considered a more representative model due to closer morphology to *in vivo* architecture.

Rationale and gaps in knowledge

- The centrosome plays a role in the establishment of ncMTOCs during apico-basal polarisation but the extent of this is unknown
- Is the centrosome essential for epithelial apico-basal polarisation to occur?
- Does centrosome removal effect the localisation of key ncMTOC proteins such as CAMSAP2 and CAMSAP3?
- Does centrosome loss effect the ability of MDCKII cells to form 3D cysts?

Hypothesis

Centrosome loss will prevent apico-basal polarisation and perturb the normal distribution of certain MT organising proteins.

Aims

- Evaluate the effectiveness of centrinone B centrosome removal in MDCKII cells
- Determine the localisation of CAMSAP2 and CAMSAP3 in MDCKII cells and determine the effect of centrosome loss on these proteins
- Compare the localisation of markers of polarity such as PAR3 in control and acentrosomal cells
- Analyse possible effects on cell elongation in control and acentrosomal cells
- Determine if the centrosome is required for the formation of 3D cysts.

3.3 Results

3.3.1 CAMSAP 2/3 characterisation in MDCKII cells

The general characteristics of polarised MDCKII cells has been well studied and the relocation of key MT associated and centrosomal proteins such as ninein and CLIP-170 has been reported previously (Goldspink *et al.,* 2017, Muroyama *et al.,* 2016, Pickett *et al.,* 2019). A summary of MT and associated protein organisation can be seen in figure 3.1. Confirmation of these results was carried out in our system (Fig. 3.2). Here, γ-tubulin remains at the centrosome in both 2D and 3D cells with some apical staining in 3D whereas ninein relocated to cell-cell contacts in 2D cells seeded under Matrigel and in cysts.
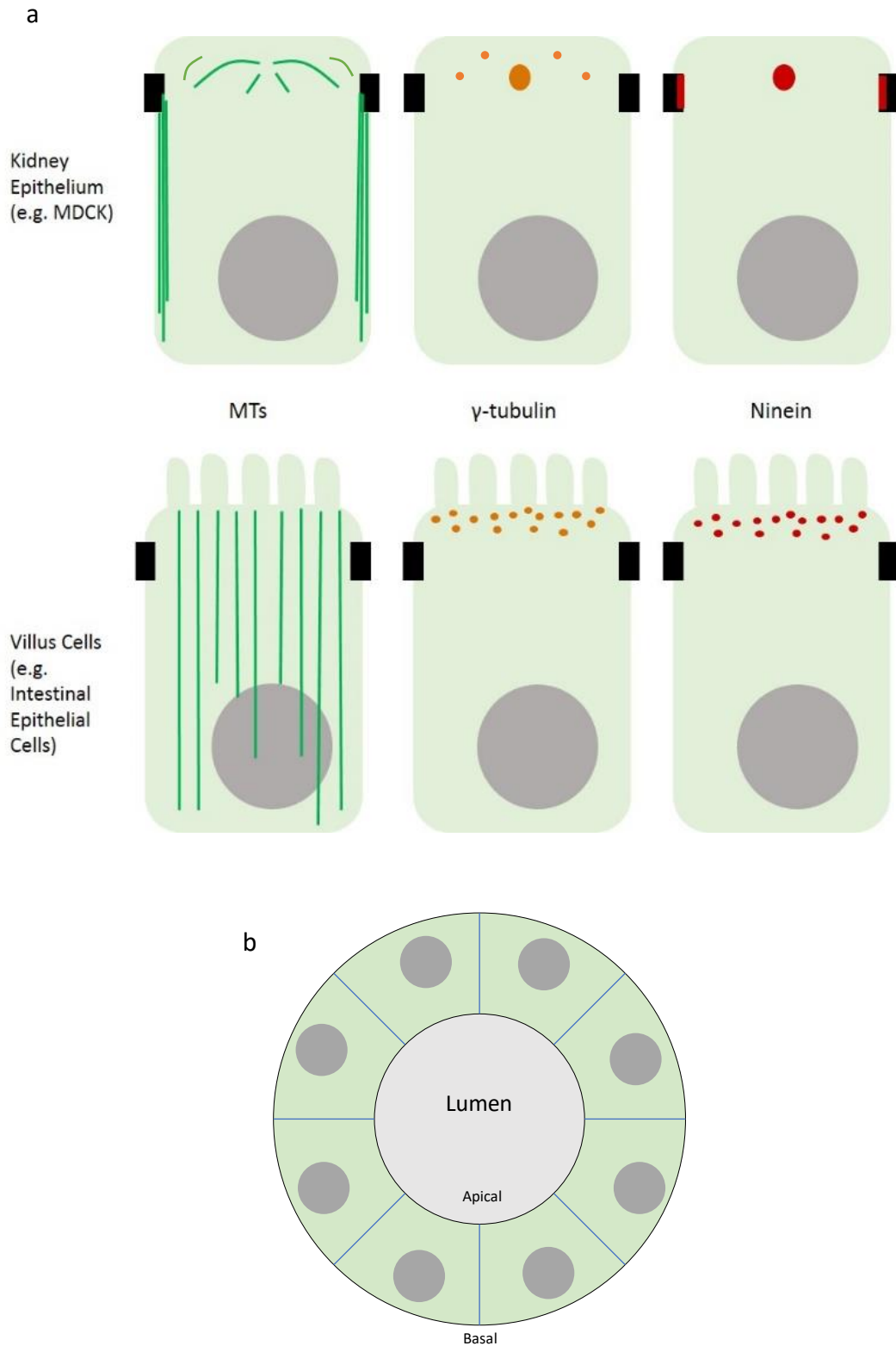
Figure 3.1 Overview of apico-basal polarisation. (a) Diagrams depicting polarised epithelial cells with MTs, key centrosomal and junctional proteins. MT anchorage and nucleation sites differ depending on the cell line, 2 examples are shown here. (b) Diagram depicting a cross section of a 3D cyst that forms from MDCKII cells embedded in Matrigel. Cells in a cyst show a lumen facing apical membrane and a basal membrane.
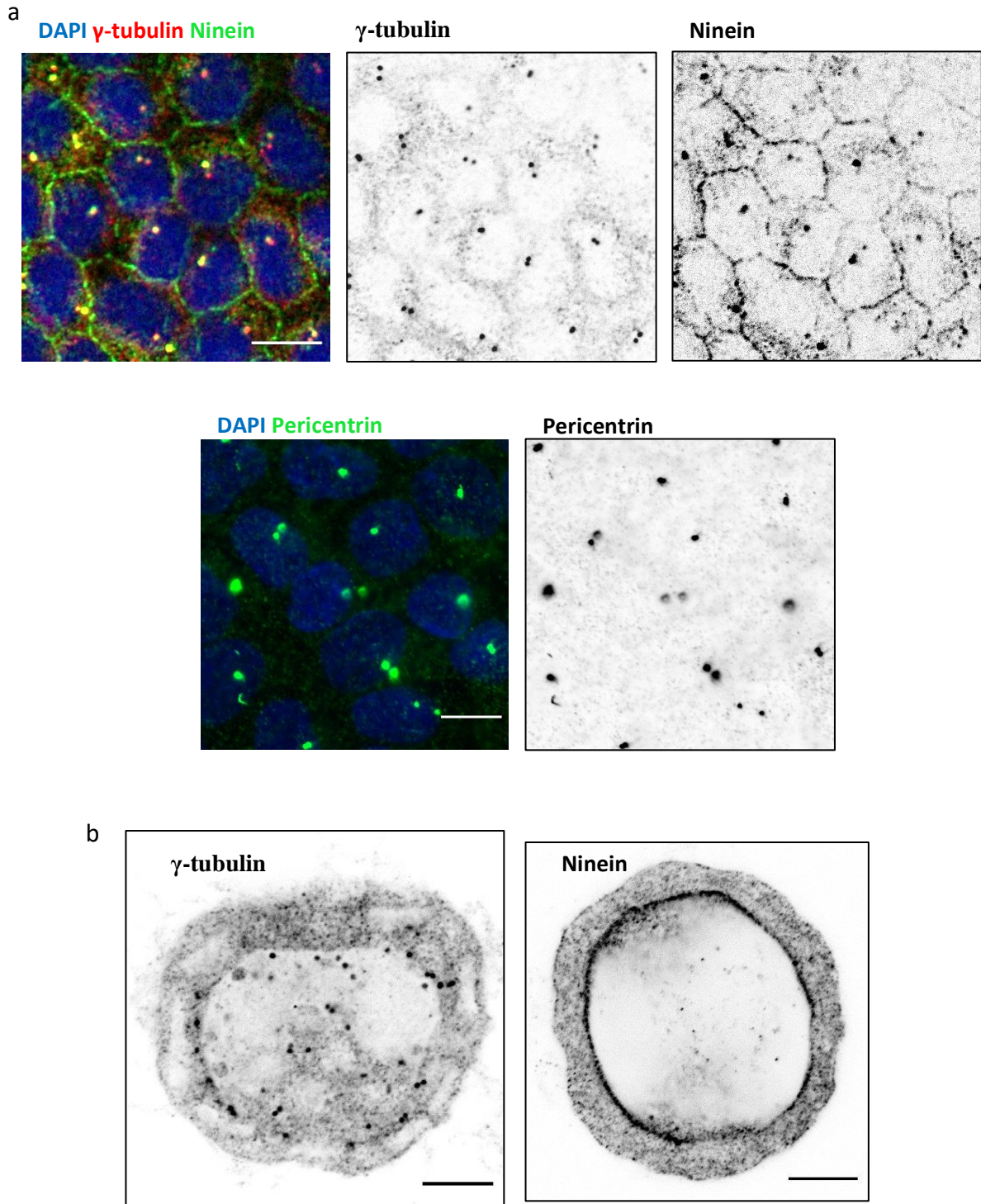
Figure 3.2 Centrosomal protein localisation during apico-basal polarisation. (a) MDCKII cells seeded densely under a Matrigel layer and cultured for 7 days. Single Z optical sections of double immunolabelling shows γ-tubulin (red) and ninein (green) and single immunlobelling shows pericentrin (green) imaged via confocal microscopy. Pericentrin and γ-tubulin staining shows distinct puncta indicative of centrosomes and ninein shows single mother centriole labelling. (b) MDCKII cells embedded in Matrigel and grown for 10 days to form cysts. Single Z optical sections, iImmunolabelled for ninein and γ-tubulin and imaged using fluorescent confocal microscopy. Ninein can be seen in at centrosome and decorating apical membrane whereas γ-tubulin shows centrosomal staining. Scale bars= 10µm.

As the CAMSAP family is yet to be studied in the MDCKII cell line it was first necessary to elucidate the distribution of CAMSAP2 and CAMSAP3 in these cells. To achieve this MDCKII cells were seeded densely on semi-permeable filters and grown for 12 days to induce partial polarisation. Immunolabelling and confocal microscopy was then used to study the spatial orientation of these proteins. In MDCKII cells, CAMSAP 2 was seen decorating the apical membrane in distinct puncta (Fig. 3.3). These aggregations of CAMSAP2 could be seen throughout the apical membrane in an evenly space manner. Whereas, CAMSAP 3 showed very strong localisation at the cell junctions and some co-localisation with CAMSAP2 in these apical puncta. Although this colocalization was not evident in every apical punctum as some consisted of CAMSAP2 alone. MDCKII cells were also formed into 3D cyst structures to study CAMSAP2 and CAMSAP3 in a closer to *in vivo* model. As in 2D, MDCKII cysts exhibited extensive CAMSAP2 apical puncta with no obvious junctional staining and CAMSAP3 showed strong junctional staining and clear co-localisation with apical CAMSAP2 in puncta. There appeared to be more co-localisation of CAMSAP2 and CAMSAP3 in apical puncta as little CAMSAP2 only puncta were present (Fig. 3.3b).
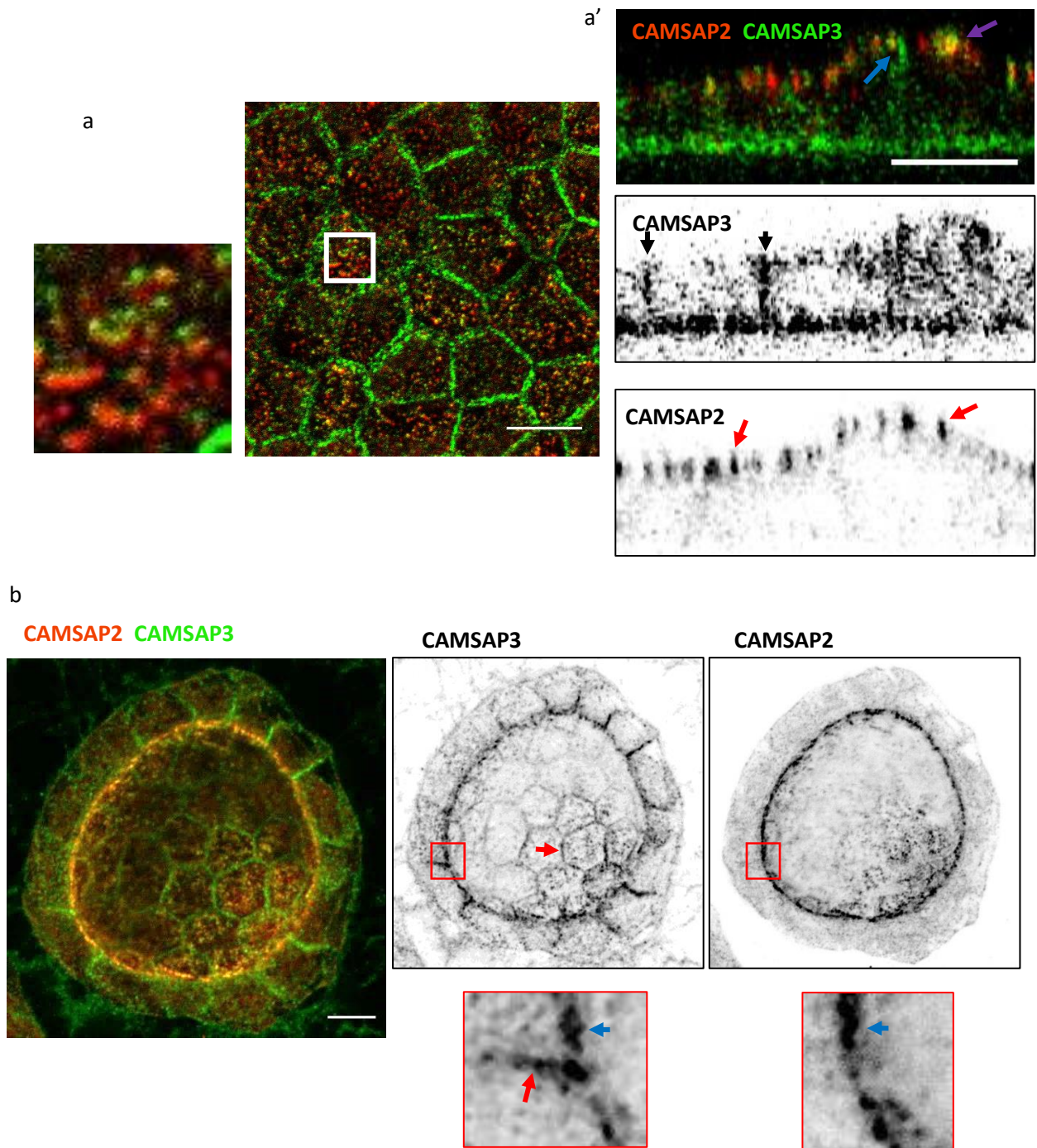
Figure 3.3 CAMSAP 2/3 analysis in confluent MDCKII cell layers. (a) MDCKII cells grown for 12 days on semi-permeable filters and double immunolabelled for CAMSAP2 and CAMSAP3. CAMSAP3 can be seen decorating the cell-cell contacts (blue and black arrows) whereas CAMSAP2 can be seen along the apical membrane in distinct puncta (blue and red arrows) with some co-localisation with CAMSAP3 (purple arrow). (a') Orthogonal views of images shown in (a). (b) MDCKII cells embedded in Matrigel and grown for 10 days to form cysts. Double immunolabelled for CAMSAP2 and CAMSAP3 imaged using fluorescent confocal microscopy. Enlargements show apical (blue arrows) and junctional (red arrows) staining. Scale bars= 10µm.

3.3.2 Centrinone B treatment effectively prevented centrosome replication in MDCK cells

The centrosome was analysed in MDCKII cells to confirm its loss after centrinone B treatment with comparisons made to DMSO controls. Cells were seeded at very low density and treated with 500nm centrinone B for at least 7 days prior to seeding for subsequent experiments. Centrinone B treated cells showed almost complete loss of key centrosomal proteins including pericentrin, centrin, ninein and γ-tubulin at the centrosome. Pericentrin lost its dense accumulation at the centrosome and instead became distributed throughout the cytoplasm although larger accumulations were present in some cells (Fig. 3.4). Similarly, centrin, γ-tubulin and ninein became dispersed throughout the cytoplasm (Fig 3.4 and 3.5). Quantification of centrosome presence shows centrosome loss in 93% of 68 centrinone B treated cells when labelled with above markers from one experiment (Fig 3.5b).

To assess the further effects of Centrinone B treatment on MDCKII cells both cell size and cell proliferation was measured. Cell size was measured using widefield fluorescence imaging using the tight junction marker ZO-1 (Fig 3.6a), which was then measured manually using the freehand draw tool in ImageJ. Mean cell size was significantly increased by ~7 fold with centrinone B treatment with much increased deviation when compared to the control (Fig 3.6b). Cell proliferation was measured by seeding cells and counting every 24 hours using a haemocytometer, based on 3 individual experiments. Centrinone B treated cells showed significantly reduced proliferation rates when compared to DMSO control throughout the experimental time period. This difference increased with time most likely due to the exponential nature of cell growth (Fig 3.6c).
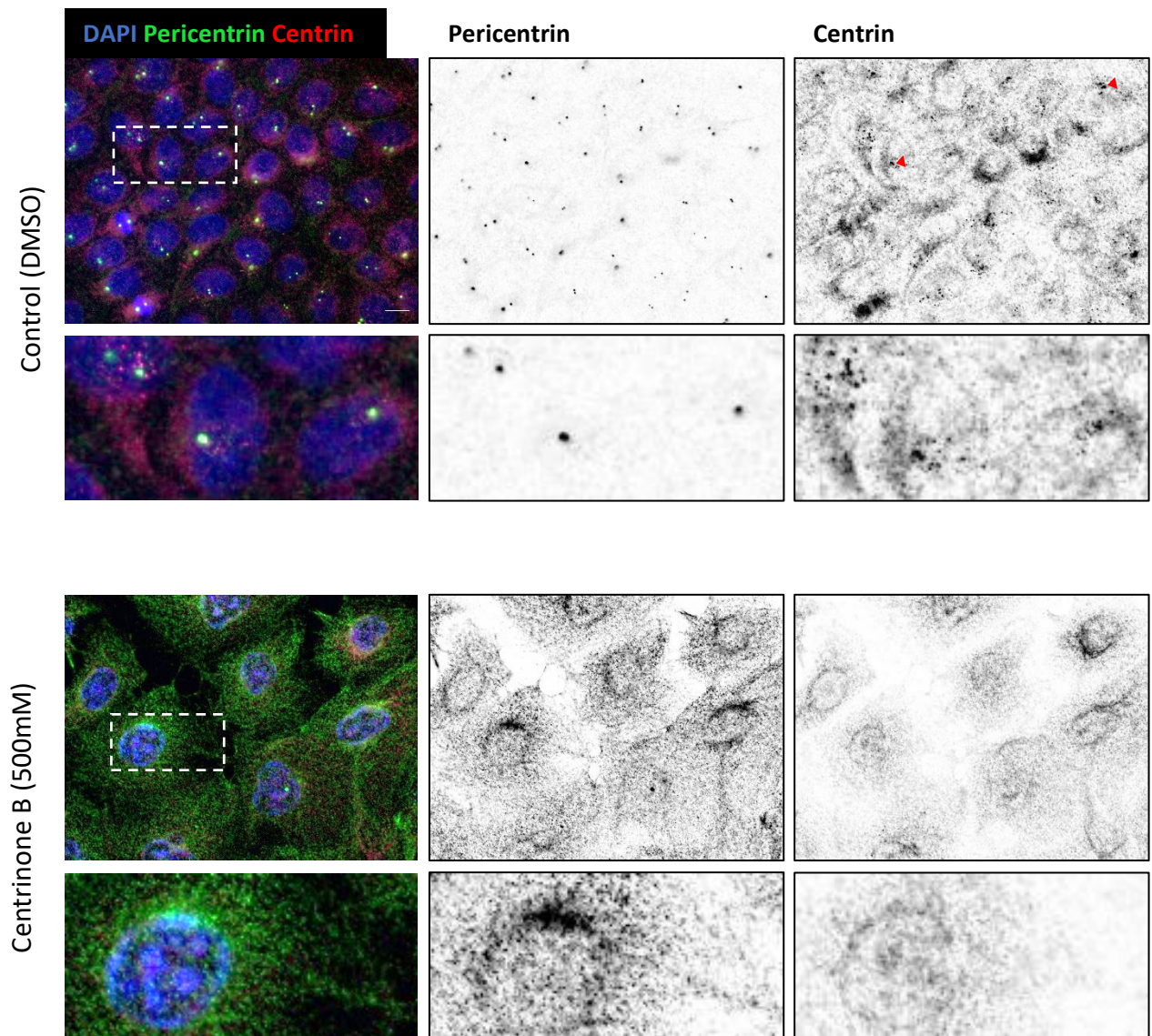
Figure 3.4 Pericentrin and centrin analysis after centrinone B treatment. Double immunolabelling of MDCKII cells cultured on glass treated with DMSO/centrinone B for 7 days and imaged using widefield fluorescent microscopy. Staining in DMSO or centrinone B treated cells of key structural centrosomal proteins pericentrin (green) and centrin (red). In DMSO treated cells pericentrin shows distinct staining at puncta at centrosomes as does centrin with some non centrosomal staining. Centrinone B treated cells show distinct loss of single puncta staining. Some accumulation of pericentrin can be seen close to the nucleus in some cells with centrin showing primarily cytosolic staining. Scale bar= 10µm.
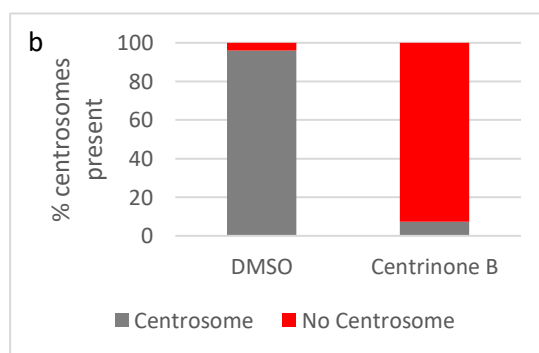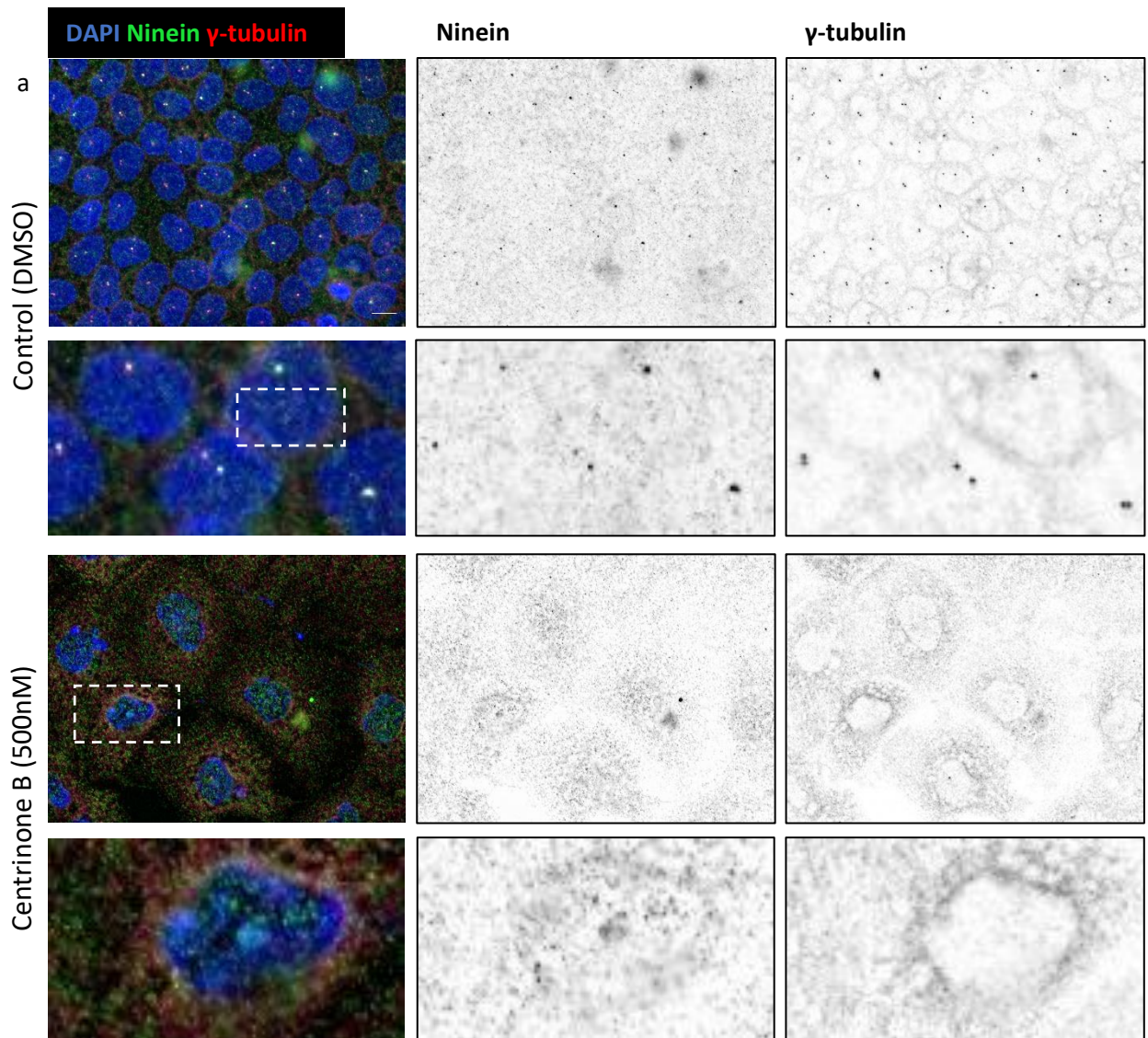
Figure 3.5 Ninein and γ-tubulin analysis after centrinone B treatment. (a) Double immunolabelling of MDCKII cells cultured on glass treated with DMSO/centrinone B and imaged using widefield fluorescent microscopy. Staining in DMSO or centrinone B treated cells of key functional centrosomal proteins ninein (green) and γ-tubulin (red). In DMSO treated cells γ-tubulin shows staining of both centrioles whereas ninein only labelled the mother centriole. (b) Cells were manually counted to determine if γ-tubulin puncta was present to determine % centrosomes present in the population. Centrinone B treated cells show distinct loss of single puncta staining. γ-tubulin shows some accumulation around the nucleus possibly at Golgi with cytosolic labelling. Ninein shows no clear accumulations and appears cytosolic. DMSO n=102 cells, Centrinone B n=68 cells, 1 experiment. Scale bars= 10μm.
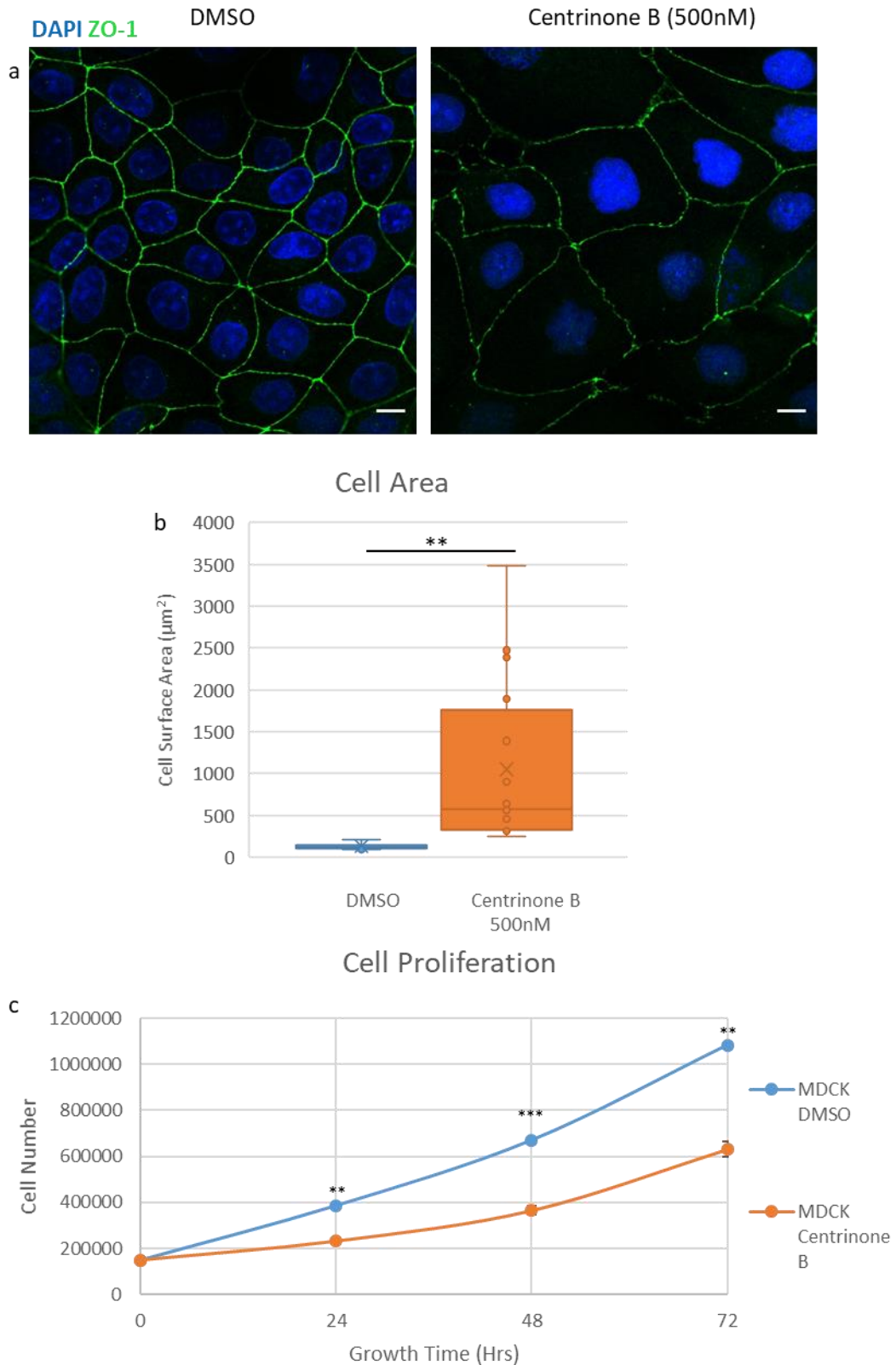
Figure 3.6 Cell size and proliferation analysis with Centrinone B treatment. (a) Confocal images of MDCKII cells immunolabelled for ZO-1 (green) for analysis of cell size. (b) Cell periphery was manually selected and the area was obtained using ImageJ. MDCKII cells treated with centrinone B show a significant (p=0.003) increase in cell size compared to control of around 7 fold (n=19). (c) Cell proliferation was significantly reduced with centrinone B treatment, this difference increased with time. p= 24Hr 0.002, 48Hr <0.001, 72Hr 0.008. n=3 for each group (biological repeats). Error bars= +/- 1 SE. Scale bar = 10μm.

3.3.3 MT and associated protein organisation following Centrinone B treatment

The effect of centrinone B treatment may vary depending on differentiation/polarisation of cells. To analyse this, MDCK cells were grown as single/double cells (Fig 3.7-3.8), in islands (Fig 3.9) or fully confluent on semi-permeable filters (Fig 3.10-3.14). In single control cells treated with DMSO, CAMSAP 2 and CAMSAP 3 is evenly distributed throughout the cytoplasm with no accumulations (Fig 3.7). This was also true for CAMSAP 2 in double/recently divided cells however CAMSAP 3 showed immediate localisation to the cell-cell contact (Fig 3.7). In these single cells treated with centrinone B, some accumulations of CAMSAP 2 and more so CAMSAP 3 were seen in a perinuclear position with reduced CAMSAP3 remaining at the cell-cell contacts compared to DMSO treated. This CAMSAP 2 labelling was not shown to be co-localised at the Golgi although there was significant localisation of CAMSAP3 at the Golgi (Fig. 3.8). There also appeared to be a difference in morphology with centrinone B treated cells appearing flatter and more mesenchymal compared to the DMSO treated control cells as cells appeared flatter and more irregular in shape.

In cells allowed to grow for 3 days to form islands, CAMSAP 2/3, E-cadherin and PAR-3 localisation was assessed to identify possible ncMTOC sites as before but also changes in junction structure and polarity markers. Adherens junctions appeared very irregular and abnormal in acentrosomal cells labelled using E-cadherin when compared to control DMSO treated cells. The polarity marker PAR3 was present and localised at these junctions in both groups but this appeared reduced in acentrosomal cells (Fig. 3.9). DMSO treated cells showed cytoplasmic CAMSAP 2 without obvious puncta with CAMSAP 3 decorating the junctions. In centrinone B treated cell islands, CAMSAP3 lost the majority of its localisation at the junctions whereas there was no difference seen in CAMSAP2 localisation between groups (Fig. 3.9).
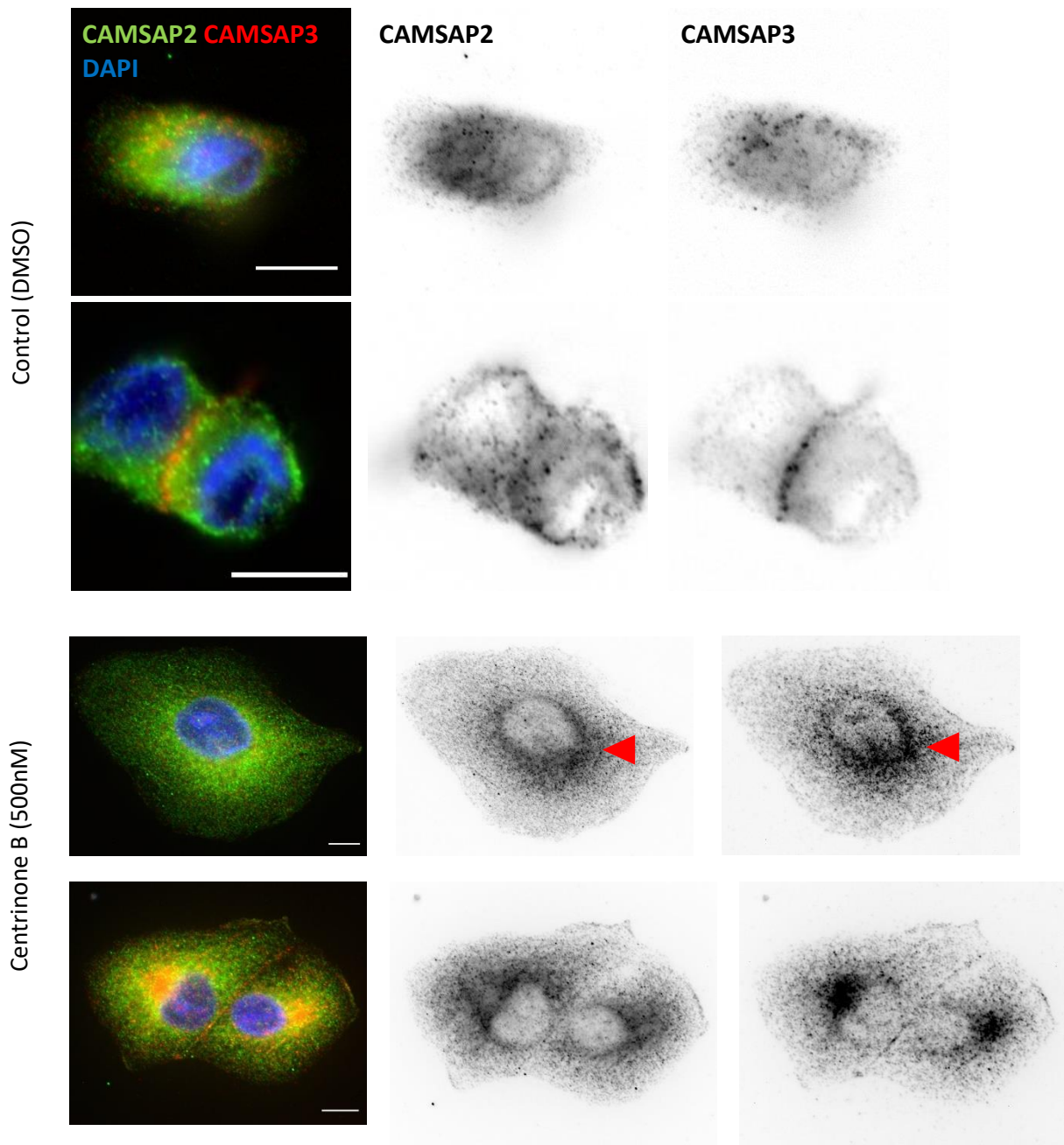
Figure 3.7 CAMSAP 2/3 localisation in single/double cells without a centrosome. MDCKII cells treated with DMSO/centrinone B seeded sparsely onto glass for 18 hours, immunolabelled for CAMASP2 (green) and CAMSAP3 (red) and imaged using widefield microscopy. More aggregations of CAMSAP 2 and CAMSAP 3 can be seen in single cells treated with centrinone B (red arrows). These aggregates can also be seen in double cells and CAMSAP 3 shows reduced junctional localisation. Scale Bars= 10μm.
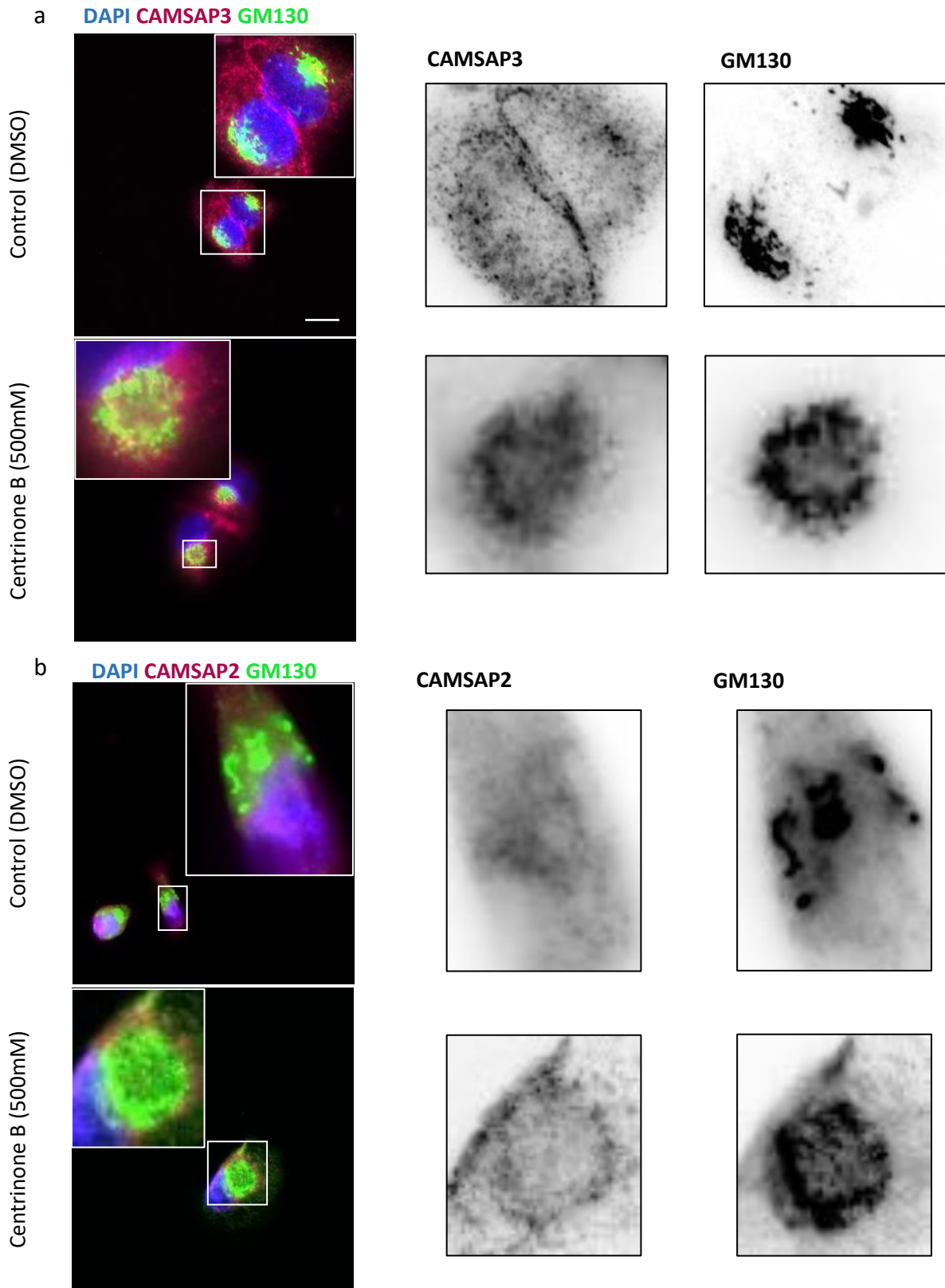
Figure 3.8 CAMSAP 2/3 colocalization at the Golgi. MDCKII seeded sparsely and treated with DMSO/centrinone B then double immunolabelled for CAMSAP 3 (a) or CAMSAP 2 (b) (purple) and GM130 (green). Imaged using widefield fluorescent microscopy. CAMSAP3 showed no localisation with GM130 at the Golgi in DMSO treated cells whereas clear co-localisation was seen in acentrosomal cells treated with centrinone B. CAMSAP2 showed no co-localisation with GM130 in both the DMSO and centrinone B treated cells. Scale bars= 10µm.
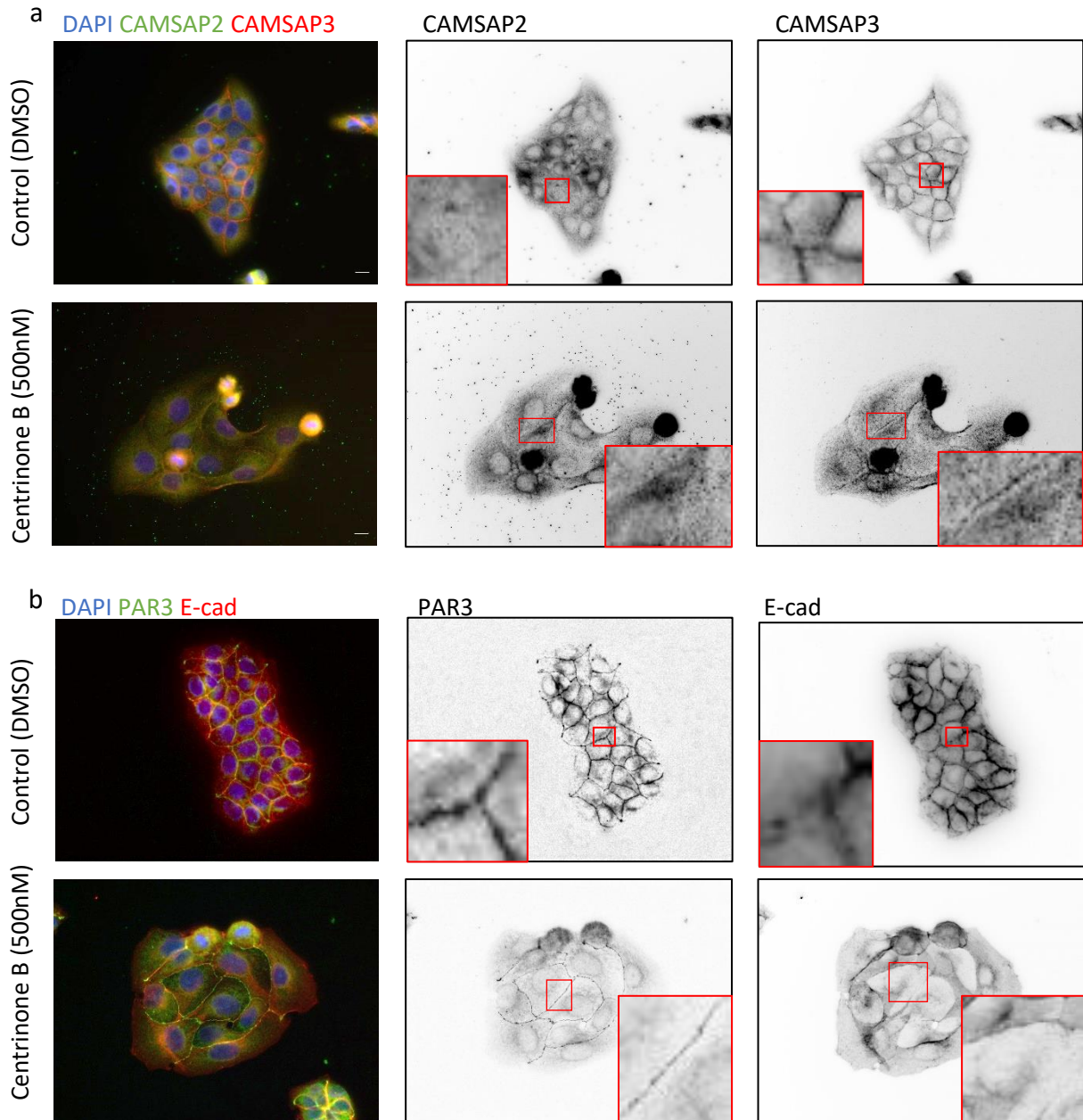
Figure 3.9 Microtubule and polarisation associated proteins in cell islands treated with centrinone B. DMSO/Centrinone B treated MDCKII cells were grown on glass for 3 days to form islands and visualised using widefield microscopy. (a) Double immunolabelling for CAMSAP2 and CAMSAP3 showing localisation in MDCKII cell islands. Few CAMSAP 2 puncta can be seen in DMSO treated cells and little in acentrosomal cells although more staining can be seen throughout the cytoplasm. (b) Double immunolabelling for PAR3 and E-cadherin localisation in MDCKII cell islands. Acentrosomal cells show abnormal junction formation with reduced PAR3 at this site. Scale bars= 10µm.

Partially polarised MDCKII cells treated with Centrinone B were then assessed by seeding cells at high density on semi-permeable membranes. As before, DMSO treated control cells showed CAMSAP3 at junctions while CAMSAP2 staining was seen at puncta. This puncta formation appeared here for the first time in this polarisation series suggesting that CAMSAP2 puncta formation is a marker of later stage polarisation. When these cells were treated with centrinone B, all CAMSAP 3 was lost from the junction, instead it was distributed throughout the cytoplasm without any clear aggregations. CAMSAP 2 also lost most of its accumulation with almost no apical puncta again being distributed throughout the cytoplasm (Fig. 3.10). CAMSAP 2 localisation was further analysed in the confocal microscope. Optical sections were taken from the apex to the base of the cells and Z sections were analysed (Fig. 3.11). Centrinone B treated cells showed some apical CAMSAP 2 puncta although these were very much reduced in size and intensity when compared to DMSO treated control cells. Control MDCKII cells showed very uniform E-cadherin staining at cell-cell contacts whereas this uniformity was lost in acentrosomal cells with some contacts having very little E-cadherin present. PAR3 labelling was absent from most cell-cell contacts with far more visible within the cytoplasm when compared to control cell (Fig. 3.12).

MT organisation was analysed in these fully confluent partially polarised cells by labelling the MTs and using CAMSAP 2/3 as marker for MT minus end accumulation and ncMTOC detection. This showed a dramatic change in MT organisation, removal of the centrosome caused a more radial MT array to be adopted. DMSO treated control cells exhibited a mainly peripheral MT organisation with some MT organisation around the Golgi suggesting some organisation at this site. Whereas, in cells treated with centrinone B, MTs can be seen organised at a ncMTOC close to the nuclei in a position that the centrosome would likely usually occupy. This organisation site was present in a majority of treated cells and co-labelling for the Golgi shows co-localisation of MT and Golgi at this site (Fig. 3.13).
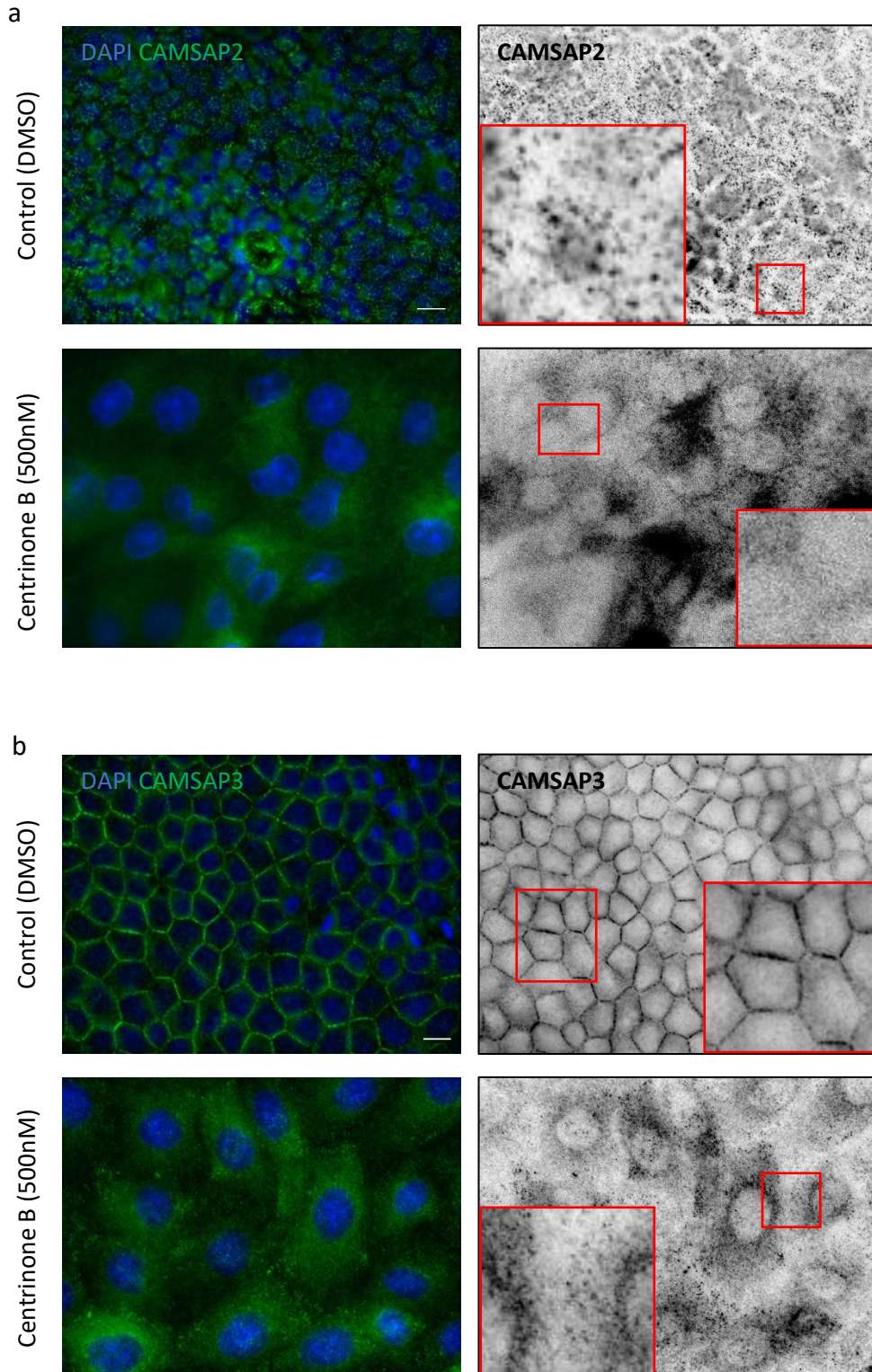
Figure 3.10 CAMSAP2/3 localisation in acentrosomal cells. DMSO/centrinone B treated MDCKII cells were seeded densely on tissue culture inserts and grown for 12 days. (a) In DMSO treated cells distinct puncta can be seen in likely apical cap regions. However, CAMSAP2 labelling showed complete loss of puncta with cytosolic staining in centrinone B treated cells. (b) DMSO treated cells show clear CAMSAP3 junctional labelling with little cytosolic staining. However, centrinone B treated cells shows complete loss of CAMSAP3 junctional staining with mainly cytosolic labelling. Scale bars= 10μm.
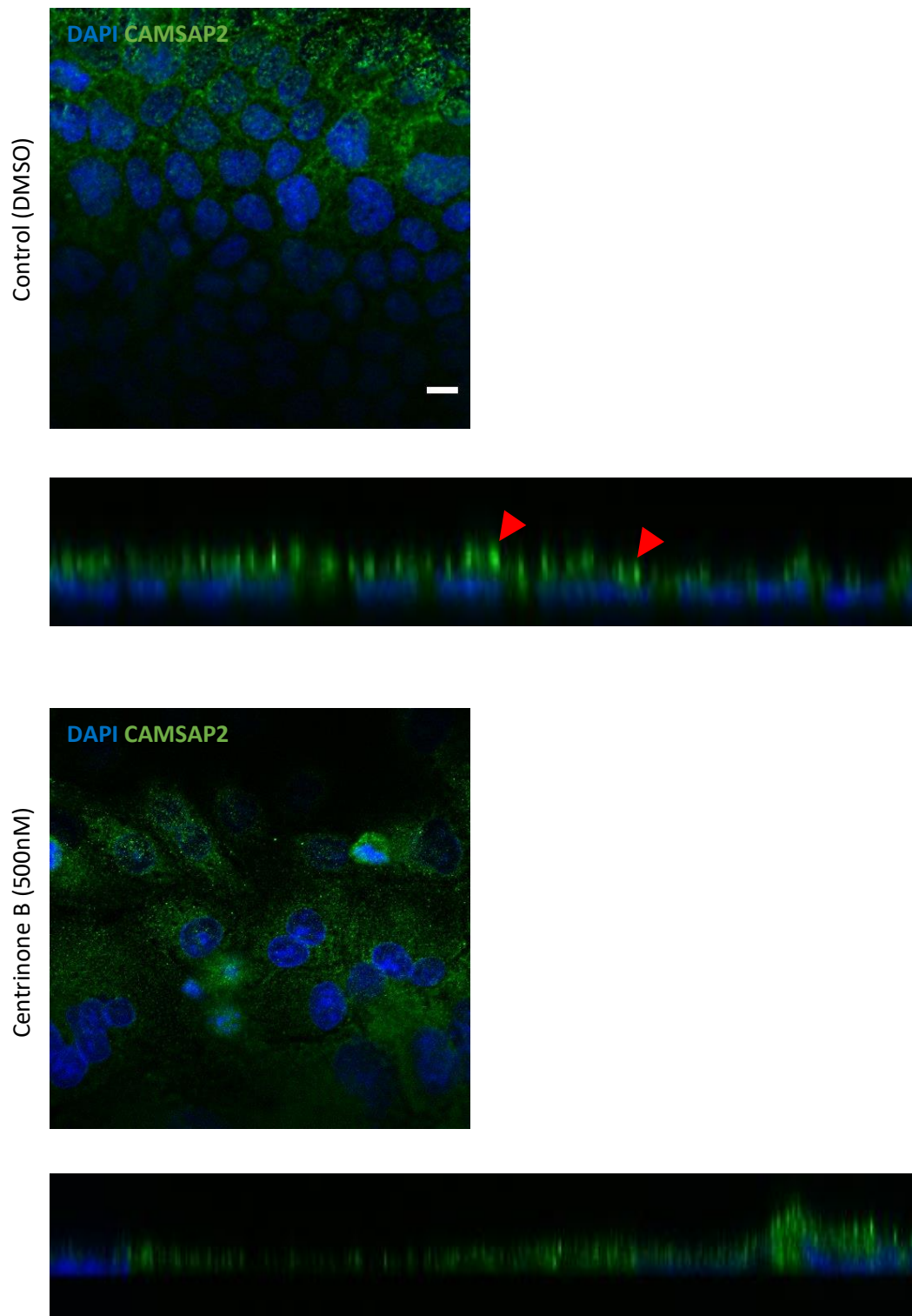
Figure 3.11 CAMSAP2 apical puncta in confluent MDCKII cells. Confocal images single immunolabelling of CAMSAP2 (green) in cells grown for 12 days on tissue culture inserts. Orthogonal views shown were reconstructed using z slices taken every 0.2µm compiled in ImageJ. Clear CAMSAP2 puncta can be seen in the apical regions of control DMSO treated cells (red arrows). Centrinone B treated MDCKII cells show a distinct reduction in puncta size. Scale bar= 10µm.
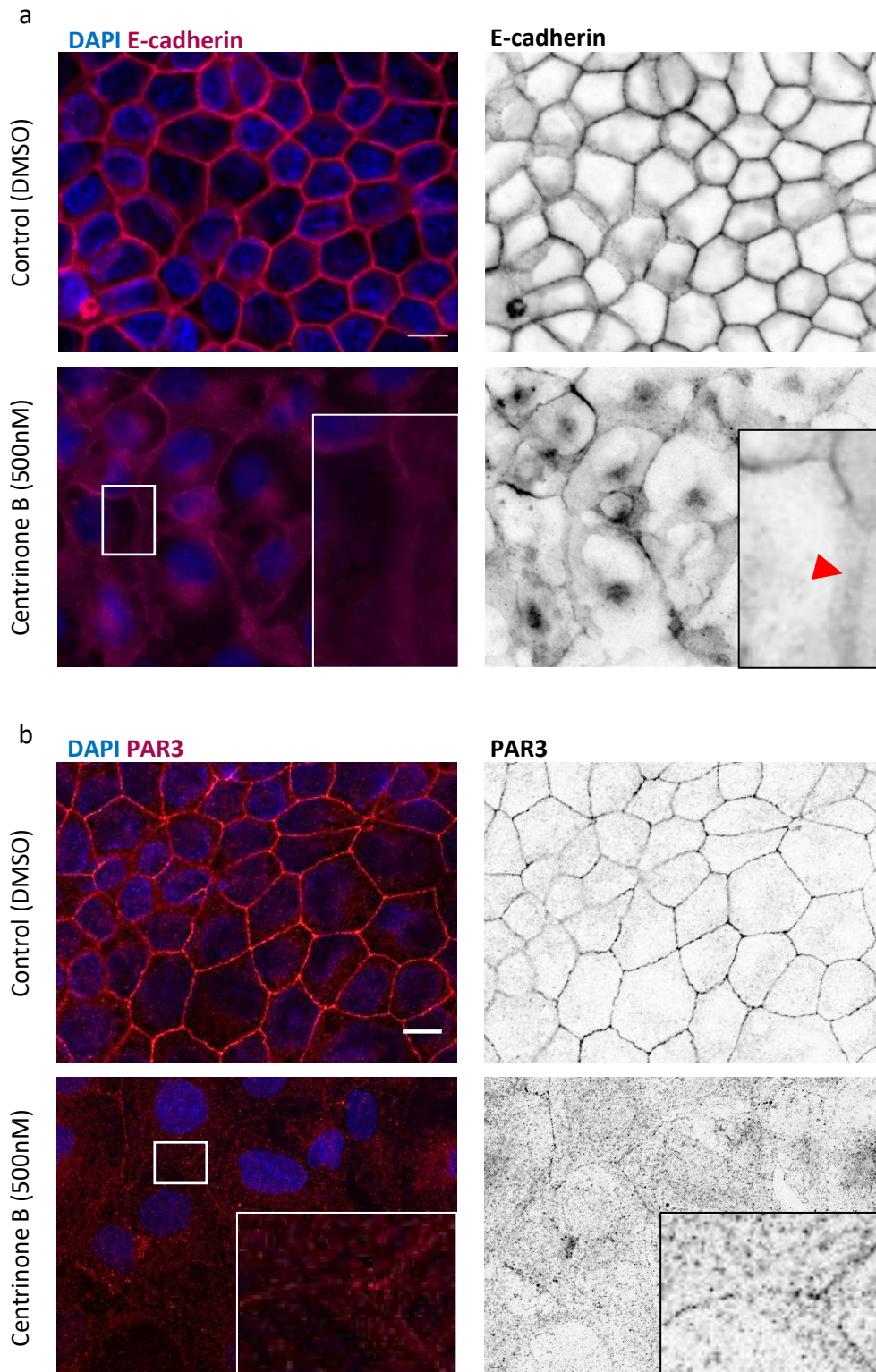
Figure 3.12 Acentrosomal cells show abnormal adherens junctions and PAR3 localisation. MDCKII cells seeded densely on tissue culture inserts for 12 days, single immunolabelled and visualised using widefield microscopy. (a) DMSO treated MDCKII cells show clear junctional staining with little diffusion whereas centrinone B treated cells show irregular and abnormal E-cadherin staining with extensive diffusion around the junction (red arrow). (B) In DMSO treated MDCKII cells PAR3 shows normal localisation to cell-cell contacts and little cytosolic staining. In centrinone B treated MDCKII cells PAR3 labelling shows almost complete loss of localisation at cell-cell contacts with extensive cytosolic labelling. Scale bars=10µm.
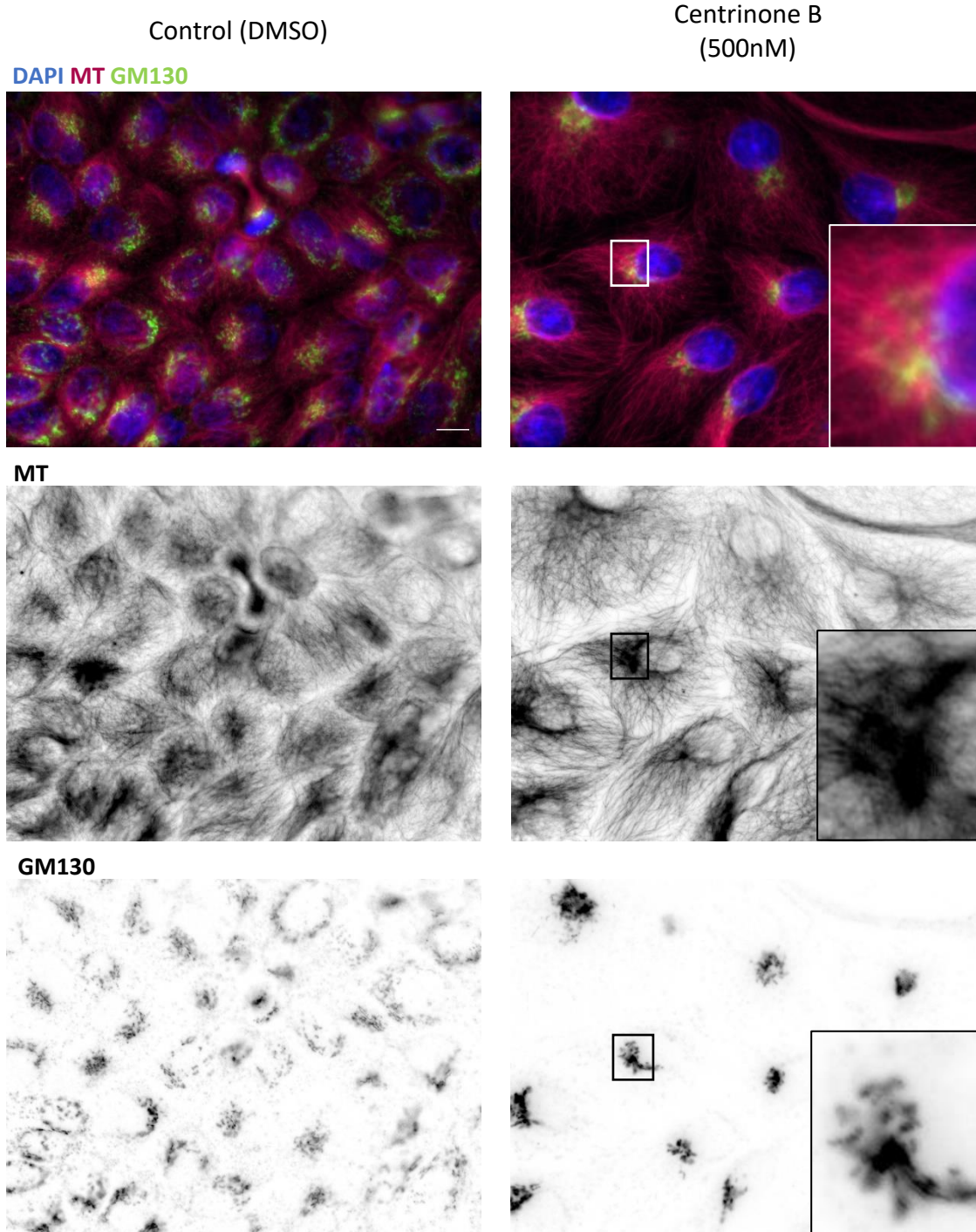
Figure 3.13 Microtubule organisation after centrinone B treatment. Double immunolabelling of α-tubulin (red) and GM130 (green) in MDCKII cells treated with DMSO/centrinone B, imaged using widefield microscopy. DMSO treated MDCKII cells show little MT organisation at Golgi whereas centrinone B treated cells show seemingly exclusive Golgi organised MTs in a radial array pattern. Scale bar= 10μm.

3.3.4 Centrinone B treated cell had comparable height to DMSO treated controls

To assess if removal of the centrosome via centrinone B treatment effects the cell ability to polarise and elongate normally, cell height analysis was carried out. This was done by seeding cells on filters for 12 days, immunolabelling and finally confocal microscopy to capture z slices every 0.2μm of the cell layer (Fig. 3.14). There was no significant difference in the cell height between the two groups although the centrinone B treated group showed a mean increase of 33% in height. Data based on 4 separate z stacks from 1 experiment analysed in ImageJ.

3.3.5 Centrinone B treated cells did not form 3D cysts

MDCKII cells form cysts with a central lumen, adjacent apical membrane and an ECM facing basement membrane when embedded in Matrigel. As before CAMSAP2 decorates the apical membrane in puncta with some CAMSAP3 co-localisation here. The majority of CAMSAP3 was seen at junctions. However, cells treated with centrinone B failed to form 3D cysts and very few cells survived after 10 days. Cells that did survive became very large but remained as single cells or formed small clusters with no cyst formation. Immunolabelling for ninein and γ-tubulin showed no distinct centrosome with extensive cytoplasmic staining in the cells that did survive (Fig. 3.15).
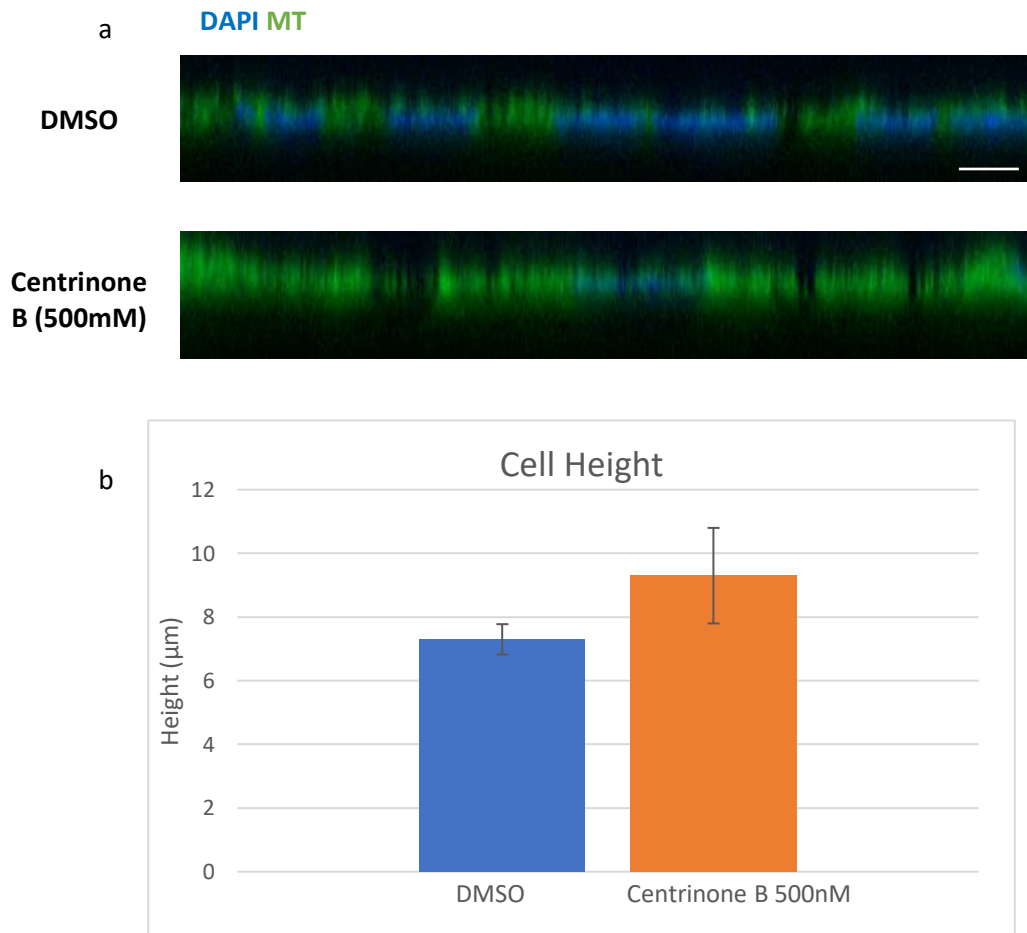
Figure 3.14 Analysis of cell height. MDCKII cells seeded densely on tissue culture inserts for 12 days, single immunolabelled and visualised using confocal microscopy. (a) Orthogonal views show z slices taken every 0.2μm reconstruction and height measurements were made using ImageJ. Z stacks were constructed from 75 optical sections per image. (b) Cell height was measured using α-tubulin staining by counting z slices containing intensities above a set threshold. Quantification of height analysis shows centrinone B treated cells showed a 33% increase in cell height although this wasn't significant (p=0.07). N=4 FOV per group with 3 measurements taken per FOV in 1 experiment. Scale Bar= 10μm. +/- 1 SE shown.

CAMSAP3 CAMSAP2

Control

β-cat γ-tub DAPI **B-cat γ-tub DAPI** **MT Ninein DAPI**
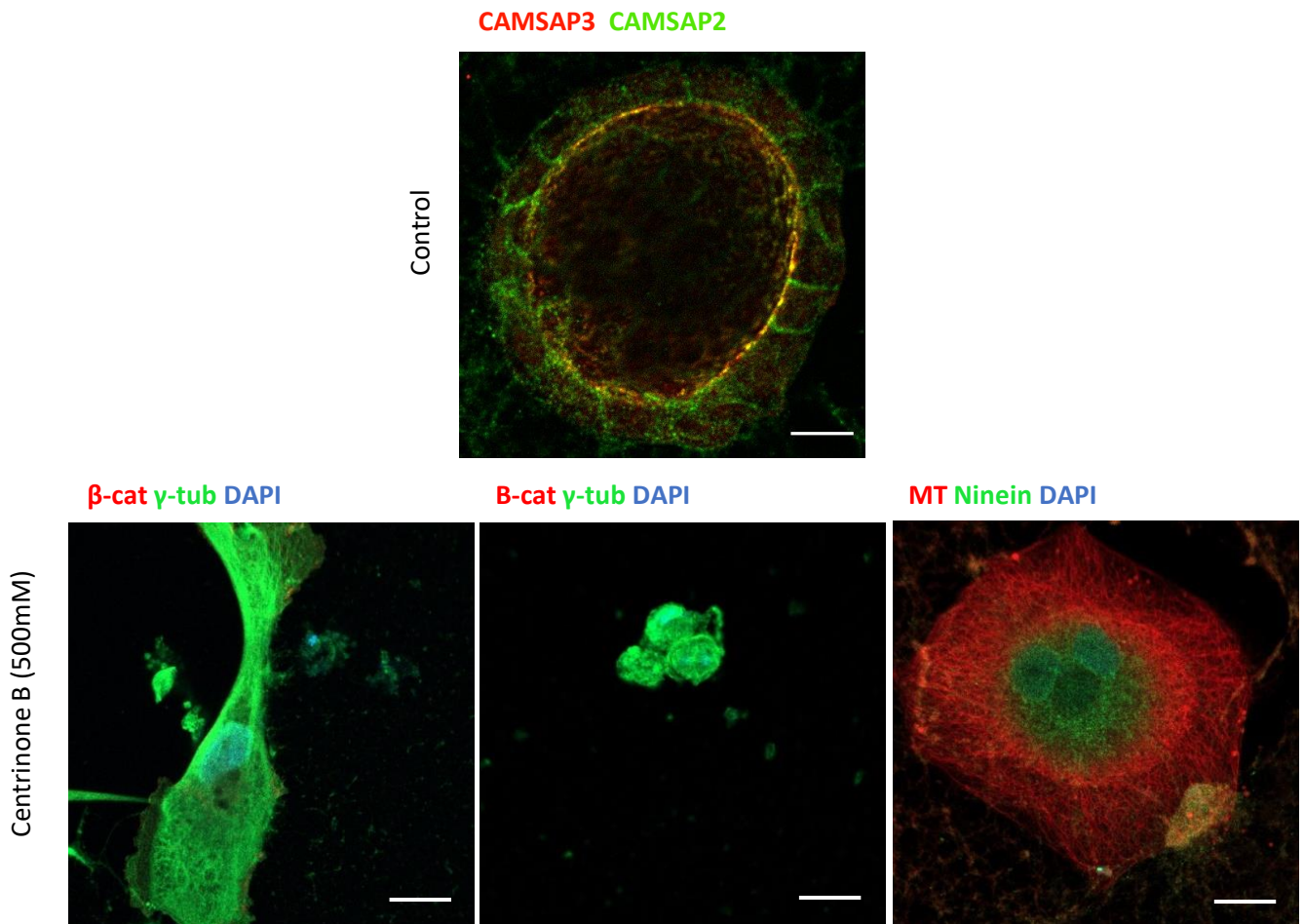
Centrinone B (500mM)

Figure 3.15 Centrinone B treated cells did not form cysts. MDCKII Cells were embedded into Matrigel and grown for 10 days to form cysts. Various labelling shows DMSO treated cells clearly formed mature cysts containing a defined lumen. Centrinone B treated cells did not form cysts. In fact cell survival was extremely low, these cells either became extremely large or likely cell death occurred when embedded into Matrigel. Scale bars= 10μm.

3.4 Discussion

3.4.1 MDCKII and CAMSAP Characterisation

To confirm that our MDCKII polarisation system works well and is representative of *in vivo* behaviour, γ-tubulin and ninein localisation was assessed in 2D cell layers and 3D cysts. As supported by previous research it was shown that γ-tubulin remains at the centrosome as this is the major site of MT nucleation with some apical labelling, this also occurs as some nucleation occurs here in fully polarised MDCKII cells (Bre *et al.,* 1990). Goldspink *et al.,* (2017) showed ninein moved to junctional sites via MTs in polarising cells, this was also shown by our experiments (Fig. 3.1). Although ninein movement to these cortical sites only occurred with the aid of Matrigel layered on top of cells. As Matrigel induces further polarisation and based on previous work in our lab, ninein cortical localisation occurs only in the later stages of polarisation. Therefore, ninein was not assessed during the early stages of polarisation.

As CAMSAP 2 and CAMSAP 3 localisation has yet to be studied in MDCKs it was first necessary to confirm their localisation in this cell line, this was carried out in fully polarised 3D cysts and partially polarised layers on tissue culture inserts. The consensus from previous research is that CAMSAP2 and CAMSAP3 decorate the minus end of MTs (Jiang *et al.,* 2014, Hendershott and Vale., 2014). Although there is some conflicting evidence to CAMSAP3s ncMTOC localisation where it is not always reported at the junctions (Meng *et al.,* 2008, Toya *et al* 2016, Noordstra., *et al* 2016). In this work, CAMSAP3 was clearly present at junctions likely due to the fact that MDCKIIs are known to have primarily junction organised MTs (Fig. 3.3). Any conflict in the literature is likely due to the primary organisation site of MTs which varies depending on cell line or differentiation level such as in enterocyte differentiation for example. CAMSAP2 was seen in puncta in MDCKII cells which were at the apical sites with some CAMSAP3 co-localisation, likely due to some MT organisation in this sub apical position (Bre *et al.,* 1987). This CAMSAP 2 and CAMSAP 3 localisation was also evident in 3D cysts suggesting CAMSAP2 and CAMSAP 3 localise early in polarisation as there was no difference between partially and fully polarised samples. Although subsequent experiments showed CAMSAP2 puncta only formed in fully confluent MDCKII monolayers likely due to some MT anchorage here during late polarisation. In summary, as expected CAMSAP2 and 3 decorated the known ncMTOCs in this cell line.

3.4.2 Centrinone B treated cells as an *in vitro* model for examining the role of the centrosome during MDCKII apico-basal polarisation

Here, the role of the centrosome in the epithelial polarisation process was examined using the PLK4 inhibitor centrinone B. Based on the method from Wong *et al.,* (2015) cells were treated with

500mM centrinone B for 7 days after seeding at low density. This method began with a few cells to ensure that few centrosomes were present in the treated population, as inhibition of PLK4 leads to a prevention of replication rather than an elimination of the centrosomes present. Previous research has shown that centrinone B treatment leads to a progressive reduction in foci containing centriolar and pericentriolar material with each round of cell division until a complete absence is noted in HeLa cells (Wong *et al.,*2015). The initial question to be answered is do MDCKII cells survive and proliferate without the centrosome as the characterising paper for centrinone B casts some doubt on this. Wong *et al.,* (2015) found that the 3 cell lines and 3 primary cells they tested arrested the cell cycle whereas cancerous (transformed) cells were able to survive, due to p53 mutations. This was studied using shRNA targeting of p53 which increased survival in cells treated with centrinone B. Further research identified three more genes (*TP53BP1, USP28 and TRIM37*) that prevented p53 elevation in response to centrinone treatment, sequencing of these genes in MDCKII has not been carried out (Meitinger *et al.,* 2016). Despite this, MDCK cells did survive and actively proliferated without the centrosome, previous research has also shown that the centrosome is not essential for cell survival and proliferation using laser ablation and microsurgery (Khodjakov *et al.,* 2000, Hinchcliffe *et al.,* 2001). As MDCKII cells survived and proliferated we were able to culture cells as needed although further investigations are needed to explore the factors that determine acentrosomal cell survival with centrinone B.

The cell cycle was not arrested with centrinone B treatment as continual cultivation was possible in treated cells. Centrinone B treated cells did however show decreased proliferation suggesting a slowing of the cell cycle. There were other indications that the cell cycle was affected with cell size increased. An increase in cell size was not reported by the Wong paper or other subsequent papers using this drug, although the decrease in proliferation rate was found (Wong *et al.,* 2015, Chinen *et al.,*2020, Gheiratmand *et al.,* 2019). Gheiratmand *et al.,* (2019) does appear to show an increase in cell size in a figure although this isn't mentioned in the text. The most common effector of cell size is the timings of the cell cycle. Analysis of proliferation rates showed a decrease in proliferation with centrinone B treatment therefore the increase in cell size may have been caused by extended periods spent in the growth phases (G_1 and G_2) of the cell cycle. To confirm this, several experiments could have been carried out to determine the cell cycle stage of these cells. Most commonly DNA dyes (commonly PI) are used with flow cytometry with the intensity of the signalling determining if cells are pre or post-S phase. Unfortunately, these experiments were not carried out due to time constraints, but the decreased proliferation rate offers a good explanation for the increase in cell size. Another potential contributor is MT dynamics which also influence cell size although no

study has elucidated the effect of centrosome removal on MT dynamics, therefore it is unclear to what extent this plays a role (Lacroix *et al.,* 2018).

To confirm that centrinone B treated cells are a good model for the study of acentrosomal polarisation, several centrosomal proteins were analysed with and without treatment. This included the presence of the main structural and functional proteins at this site. A common marker for centrioles is centrin (Centrin-2) and an antibody against centrin2 was therefore was used to test for the presence of the centrosome in these cells. Centrin-2 plays an important role in the determination of centrosome position and segregation. It is one of the first proteins to be incorporated into centrioles and is continually present throughout the cell cycle (Salisbury *et al.,* 2002). In both control and centrinone B treated cells, immunolabelling of centrin2 produced some staining not specific to the centrosome (likely due to its presence at other sites such as distal striated fibres), but clear centrosomal staining is seen when overlaying with other centrosomal markers in control cells (Paoletti *et al.,* 1996). Centrinone B treatment led to a loss of these focused centrin points which indicated a loss of centrioles as it is a core component of these structures (Fig. 3.4). Therefore, centrioles were not present within cells treated with 500mM centrinone B for 7 days. This is supported by the absence of focused ninein centres with centrinone B treatment as ninein is located within the PCM and at the sub distal appendage of mother centrioles where it anchors MTs (Mogensen *et al.,* 2000). This result suggests that there is no anchorage of MTs at these sites, a key function of the centrosomal MTOC. Importantly there was also no accumulation of ninein at other potential organising sites such as the cell cortex as found in epithelial layers and 3D structures further suggesting that ninein is not acting as a MT anchor in these cells (Goldspink *et al.,* 2017). The lack of distinct foci of ninein localisation suggests cells are not forming alternate ncMTOCs and it is likely free MT minus ends are protected by CAMSAP2 and CAMSAP3 either free floating or at ncMTOCs such as the Golgi as previous;y reported in some cells (Yang *et al.,* 2017).

Another function of the centrosome is MT nucleation which occurs via γ-tubulin within the PCM (Moritz *et al.,* 2000). Here, γ- tubulin was also lost from the centrosome suggesting that MT nucleation is no longer possible at this site. Staining of γ-tubulin in centrinone B treated cells shows dispersal throughout the cytoplasm signifying that MT nucleation may occur in the cytoplasm potentially via MT-dependent nucleation (Fig 3.5) (Petry *et al.,* 2013). MT regrowth assays on centrinone B treated cells would elucidate if this is the case or determine whether MT nucleation occurs from a distinct site. Previous research has shown that the PCM is recruited by the centrioles and is greatly expanded during the cell cycle (Giansanti *et al.,* 2008, Conduit *et al.,* 2010). Therefore, the lack of centrioles shown by centrin loss suggests no centriole focused PCM could be recruited and act as a site of nucleation. To assess if the PCM has been dispersed in centrinone B treated cells,

pericentrin was labelled for and again showed that it was lost from centrosomes and dispersed throughout the cytoplasm with some accumulation at the nuclear membranes in some cells (Fig 3.3). This is a site of nucleation in some cells but there was no evidence that this becomes a site of MT organsiation here except for the presence of pericentrin (Fant *et al.,* 2009). Pericentrin is known as the scaffold of the PCM where many proteins rely on interactions here for their localisation at this site such as γ-tubulin (Zimmerman *et al.,* 2004). Therefore, centrinone B treatment in MDCK II cells allowed for proliferation leading to a cell population of mainly acentrosomal cells. These did not contain centrioles where MT anchorage would normally occur, nor did they possess PCM in single aggregates for MT nucleation. All functional aspects of the centrosome are lost, making this a good method for the functional ablation of the centrosome.

Ultimately centrinone B treatment resulted in an acentrosomal MDCK cell population removing the centrosome in 93% of cells, although the unknown effect on the cell cycle and cell size should be considered when drawing conclusions from further experiments.

3.4.3 MT organisation and MDCKII polarisation in the absence of the centrosome

To assess the importance of the centrosome in the polarisation process a polarisation series was carried out. This series used single or recently divided cells as a model for low polarisation, cell islands as a level of higher polarisation and finally confluent cell layers as the highest level of partial polarisation in 2D. This model appeared to work well with each stage showing different characteristics of increasing polarisation, an example of this is the fact the CAMSAP2 apical puncta was only present in the fully confluent cells. This fits with previous research that shows these puncta as ncMTOCs in fully polarised/differentiated epithelial cells (Goldspink *et al.,* 2017). By using this model in combination with CAMSAP2/3 labelling and analysis of height and polarity markers we can study polarisation. Although CAMSAP localisation does not always confer MT minus end accumulation, it can be used to detect this at known sites such as the junctions, apical caps and Golgi as this is now a well characterised concept (Meng *et al.,* 2008, Toya *et al* 2016, Noordstra., *et al* 2016).

Previous research shows MDCKII cells exhibit nucleation from the centrosome and the apical sites, with the major site of anchorage being at the adherens junctions where minus ends attach (Bre et al., 1987, Meads et al., 1995). It is known that during apico-basal polarisation the centrosome moves to an apical position, exactly how this occurs, and the importance of the centrosome in polarisation is not yet known. It is known that cell junction formation is one of the first steps toward polarisation in any apical-basal polarisation event (Bellet *et al.,* 2009, Yamada *et al.,* 2015). E-cadherin labelling of adherens junctions was carried out in cell islands and confluent layers to qualitatively analyse their

architecture in acentrosomal cells. In cell islands, junctions were irregular in both DMSO and centrinone B treated groups (Fig. 3.7b). This highlights a potential flaw in the use of islands as a model. Here, some cells had full peripheral cell-cell contacts with neighbours whereas outer cells did not. This means it is likely that outer cells cannot properly organise their polarity complexes as this relies on the PAR complex interaction at the adherens junctions of the cell (Weng and Wieschaus., 2017).

In comparison, E-cadherin staining in confluent control cells shows complete cell-cell contact coverage due to their uniformity and polarised nature. However, acentrosomal cells continued to show junctional abnormalities at this stage which suggests the centrosome plays an important role in the maintenance of junction architecture and this is likely to be linked to abnormal MT organisation. MTs are an essential regulator for the maintenance of E-cadherin at adherens junctions with de novo synthesis of E-cadherin rather than recycling (Le Drougen *et al.,* 2015). Centrosome anchored MTs are likely to be important for this E-cadherin transport due to the centrosome proximity to rough ER where E-cadherin is synthesised. Acentrosomal cells likely have different MT organisations and dynamics as MTs are not anchored to the centrosome. Previous research has also shown that E-cadherin is trafficked along MTs and that the adherens junctions are maintained by a highly dynamic population of centrosomal bound MTs (Stehbens et al., 2006, Reilein et al., 2005, Ekaterina and Citit., 2018). Although it is unclear from these experiments if MT dynamics are affected, this previous research does offer evidence for the junctional abnormalities seen in acentrosomal confluent cells. Nonetheless junction formation was affected in cell islands and confluent layers which therefore likely effected the ability of these cells to polarise normally as positioning of the polarity complexes relies on this. The lack of E-cadherin from this site alone most likely effects the initiation of cell surface polarity due to PAR3 mis-localisation (Nejsum *et al.,* 2007, Le Droguen *et al.,* 2015).

To assess this further PAR3 labelling was carried out to identify its localisation in acentrosomal cells. PAR3 is part of the PAR complex which is known as the master regulator because it is essential in organising the crumbs and scribble complexes (Riga *et al.,* 2020). Therefore, mis-localisation or a reduction in its localisation may suggest a lack of polarisation in these cells. Indeed, in both acentrosomal cell islands and confluent cells normal PAR3 localisation to the junctions was reduced. Therefore, it is possible that the junctional disruption seen here is enough to prevent the proper localisation of the PAR polarity complex although this needs more work for confirmation. Analysis of the trafficking of fluorescently tagged E-cadherin and subsequent localisation of the polarity markers may elucidate this further.

Interestingly CAMSAP3 showed a complete loss of labelling in confluent cell-cell contacts but not in cell islands when treated with centrinone B. This suggests that at the later stages of polarisation

the junctional MT organising centre is lost in the absence of the centrosome. The question is why does this only occur in fully confluent layers and not in cell islands? The lack of PAR3 at the junction suggests these cells are not polarised and therefore the CAMSAP3 decorated MTs would not anchor at this junctional site. MT staining in these acentrosomal cells support this as MTs appear more radial compared to control cells that exhibit a more peripheral MT organisation (Fig 3.11). Based on colocalization alone it appeared that radial arrays were organised by the Golgi in acentrosomal cells, suggesting that this is the primary MTOC in the absence of the centrosome and not the adherens junctionsr as in DMSO treated cells. Confirming this, some CAMSAP3 was found to colocalise with the Golgi marker GM130 showing MT organisation here although this colocalization was weak (data not shown). Previously, CAMSAP3 has been shown to bind to CG-NAP at the Golgi, CG-NAP is usually a centrosomal protein which offers a site for nucleation (Wang *et al.,* 2016). The presence of CAMSAP3 and MTs at the Golgi suggests that this becomes the site of MT organisation and nucleation in these acentrosomal cells. It appears that the apico-basal MT organisation is lost in favour of this more radial Golgi centred network. To confirm this a nocodazole recovery assay could have been carried out to confirm nucleation from the Golgi. From these results the cause of the CAMSAP3 loss from junctions could not be determined but it is possible that the junction localisation is lost as a result of lack of MT organisation at the junction. Alternatively, CAMSAP3 may not be recruited to this site which is unlikely as CAMSAP3 is essential for MT organisation here (Noordstra *et al.,* 2016). Therefore, it is most likely that the upstream events such as PAR3 localisation to the junction, which is disrupted in acentrosomal cells is the cause of the abnormal CAMSAP3 decoration. Observation of the MT pattern via immunolabelling of tubulin and high-resolution microscope would elucidate this further.

More evidence for this loss of apico-basal polarisation comes from CAMSAP2 puncta not being present in acentrosomal cell layers signifying a distinct lack of polarisation. This is seen in greater detail in orthogonal views where CAMSAP2 puncta is almost completely lost at the apical sites. These signs point to a distinct lack of polarity in these acentrosomal cells. A further measure of this was carried out by analysing the cell height of these confluent cell layers. As cell height is an indicator of polarity because cells elongate with polarisation it was expected that acentrosomal would have been significantly shorter than controls. Although the opposite was true as acentrosomal cells were in fact taller although not significantly. The most likely explanation for this is the increase in cell size seen with centrinone B treatment rendering this method for assessing cell polarisation inaccurate. It should be mentioned that control cells were not as tall as expected based on previous experiments from the Mogensen lab and therefore did not fully elongate. This experiment should be repeated, and comparisons should be made to elongated control cells.

Taken together these results suggest the centrosome is essential for the formation of apico-basal-polarisation, as acentrosomal cells appear to form a more radial array MT networks. This work suggests E-cadherin localisation to the junctions is perturbed which may subsequently prevent proper polarity complex position. Much more work is needed here to determine the sequence of events that takes place in acentrosomal cells.

3.5 Acentrosomal cells did not form 3D cysts

The use of 3D culturing is considered to be the most representative method for the formation of polarised tissue *in vitro*. Untreated MDCKII cells easily form these cyst structures when embedded into ECMs such as Matrigel. The fact that cysts did not form from acentrosomal cells informs us that the differences seen here in 2D cultures is enough to prevent cyst formation. Due to the complete lack of cyst formation it was impossible to explore the full reasons behind this. The most likely explanation is lumen initiation failure in acentrosomal cells, as this is one of the fist events in cyst formation. MDCKs embedded in Matrigel form lumens via the cord hollowing method. Trafficking of proteins such as Rab27 target vesicles to the apical membrane, a process reliant on MTs. The fact that CAMSAP3 was not present at polarised 2D junctions suggests that MT positioning is abnormal in acentrosomal cells. This potentially prevents the normal protein trafficking from the trans Golgi network to the apical sites. PAR3 and aPKC kinase activity are required for apical trafficking to the lumen initiation site (Bryant *et al.,* 2010, Ruch *et al.,* 2017). As PAR3 was shown to be mis-localised in acentrosomal cell this suggests that lumen initiation fails in these cells.

3.6 Summary

In summary, centrinone B treatment led to centrosome loss in MDCKII cells. Centrosome loss caused several aberrations of key polarisation events such as adherens junction and ncMTOC formation. This in combination with a loss of PAR3 from the junctions suggested that these cells did not polarise normally, and that the centrosome is indeed essential. MT analysis suggests a radial array of MT was present instead of an apico-basal array in acentrosomal cells. This can be seen more dramatically in 3D cultures as acentrosomal cysts failed to form.

To improve these results, several experiments needs to be carried out. One major improvement would be the continual and parallel testing for the presence of the centrosome when analysing results as some centrosomes remain in the population. The cell cycle should also be analysed to shed light on the increase in cell size seen with centrinone treatment. To further expand on these results MT dynamics should be measured as this likely plays an important role and potentially cause many of the differences seen through disruption of E-cadherin trafficking. This in combination with nocodazole regrowth assays would prove very useful for studying how MTs behave in these acentrosomal cells. Arguably the best model for the further study here would be gut organoids with centrinone B treatment. This model is very close to *in vivo* and shows the polarisation process from stem cell to terminally differentiated enterocytes in a single system.

Chapter IV:

Effects of EB2 overexpression on tissue architecture and MTOC integrity in MDCKII cells

4.0 Chapter IV: Effects of EB2 overexpression on tissue architecture and MTOC integrity in MDCKII cells

4.1 Overview

Previous published work shows that EB2 is important for MT reorganisation during the apico-basal polarisation of epithelial cells, while EB2 downregulation is associated with MT bundle formation. *In vivo* data from inner ear and intestinal epithelial tissue showed a correlation between low EB2 expression and presence of MT bundles and lack of such bundles when EB2 is elevated. This was supported by *in vitro* data which revealed that EB2 is downregulated with increasing confluency and polarisation of mouse kidney cells (mIMCD-3) (Goldspink *et al.,* 2013). Currently the function of EB2 in apico-basal polarisation is not known but it appears to be an important one. This chapter explores the effect of increased EB2 expression on several cell characteristics such as maintenance of normal tissue architecture and MTOC integrity. This was achieved using MDCKII cells overexpressing EB2 with comparisons made to an empty vector control.

4.2 Introduction

Epithelial tissues are commonly found in layers which act as barriers to separate internal and external environments. These internal and external interfaces include, for example, the intestine, kidney and lungs. Loss of epithelial architecture leads to many pathological conditions such as cancer. In fact, 90% of all cancers derive from epithelial tissue. For metastasis of tumours, epithelial tissue must change shape and polarity through the EMT process to become migratory, a process that involves MT reorganisation although this is not fully elucidated (Hinck and Nathke., 2014, Brabletz *et al.,* 2018). Therefore, understanding the intricacies of epithelial tissue polarity and integrity may increase the therapeutic pathways available for the treatment of cancers and of course add to the base of scientific knowledge.

MTs are very important for establishment of the apico-basal axis and are responsible for the asymmetric distribution of key polarity determinants (see section 1.8). However, the role of EB2 in this process is very understudied. Published work from our lab has studied the role of EB2 in polarised cells *in vitro* and *in vivo* using immunolabelling of mouse intestinal sections. Goldspink *et al.,* (2013) showed that EB2 is highly expressed during the early stages of apico-basal epithelial differentiation but, is then downregulated as differentiation continues. The *in vitro* work was carried out using the mouse inner medullary kidney (mIMCD-3) cells at increasing levels of confluence, mimicking the polarisation/differentiation effect and EB2 expression was analysed via western blotting. Higher EB2 expression was evident in less confluent cells. To mimic this decrease in EB2 expression seen in polarised cells, siRNA was carried out in human retinal pigment epithelial cells (ARPE-19). ARPE-19

typically display the classical radial array of MTs anchored at the centrosome. Unfortunately, this is a poor model for studying apico-basal polarisation but may suggest what effect EB2 is having in relation to MT organisation. Depletion of EB2 leads to the formation of straight, less-dynamic MT bundles which is a marker of differentiation in many systems including epithelial apico-basal polarisation (Goldspink *et al.,* 2013).

Goldspink *et al.* (2013)*,* also showed that depletion of EB2 leads to EB1 association along the MT lattice, a domain usually occupied by EB2. This EB1 decoration may explain the decrease in MT dynamics as EB1 stabilizes the MT plus end, although this was not explored further in the study. In relation to apico-basal polarisation, another study found that EB2 depletion led to ACF7 (MACF1) recruitment to the MT lattice and co-alignment with actin filaments which is a characteristic of apico-basal polarisation (Antonellis *et al.,* 2014, May-Simera *et al.,* 2016). ACF7 is a spectraplakin that possess actin and MT binding domains and it is an essential integrator of MT-actin dynamics with depletion of ACF7 preventing bundle formation (Kodama *et al.,* 2003). EB2 depletion studies have shown that ACF7 becomes associated along MT bundles and co-localisation between ACF7 and EB1 was seen, suggesting EB2 prevents this in this system (Goldspink *et al.,* 2013). siRNA experiments of EB1 and EB2 individually suggest that EB2 but not EB1 expression is important for the initial MT reorganisation that occurs early in polarisation while both EB2 and EB1 are required for epithelial cell elongation. EB2 has also been found to have a role in mitosis where it is phosphorylated by Aurora B kinase and CDK1. Here, phosphorylation occurs at multiple sites within the amino terminus and within the linker region to disassociate EB2 from the MTs. Phosphorylation of EB2 is strictly associated with the onset of mitosis and prevention of this effect delays spindle formation and MT formation at the kinetochore (Limori *et al.,* 2016). Whether EB2 is phosphorylated during differentiation has not been explored but potentially it could have a role in the stabilisation of MTs during differentiation in combination with the decrease in expression or phosphorylation as differentiation occurs.

As EB2 decreases with differentiation and remains low in fully differentiated cells it is possible that changes in the level of EB2 could influences the dynamics and packing behaviour of cells and thus the overall tissue architecture. Cell packing can be quantified by measuring cell shape known as the shape index (Park *et al.,* 2015). Cellular jamming/unjamming is often described through the liquid and solid elemental states with a solid layer being a highly organised and polarised epithelial layer known as a jammed layer. The liquid state of an unjammed layer arises from some pathological cause and involves a collective turbulent movement and lack of consistency of cell shape and organisation, the point at which this change occurs is known as the unjamming transition (UJT) (see section 1.8.2) (Park *et al.,* 2016). Cell jamming, or shape is controlled by opposing forces of junctional contraction and cortical tension. Junctional contraction is heavily influenced by the zonula adherens band and changes

to this structure alters the forces generated or resisted. Cortical tension forces are generated mainly by actin and myosin motor proteins that are heavily influenced by MTs. Unjamming has been identified in epithelial systems *in vitro* and *in vivo* in developmental processes as well as in the pathology of asthma and cancer (Atia *et al.,* 2018, Fredberg *et al.,* 2016, Haeger *et al.,* 2014). Recently questions have arisen about the meaning of the UJT with the consensus that UJT and partial EMT (pEMT) are distinct although do overlap and remains undefined. Recent work has shown that cell-cell junctions and apico basal polarity remains intact with the UJT whereas for pEMT this was not the case and included diminished junctional tension. UJT involves the movement of cells in large packs caused by irregular force generation within the monolayer whereas pEMT involves the movement of smaller packs or individual cells that break away from the monolayer due to diminished junctional tension (Mitchel *et al.,* 2020). It is currently thought that pEMT and UJT may work sequentially or cooperatively within an epithelial layer to effect processes such as morphogenesis, wound healing and tissue remodelling as well as cancer progression (Mitchel *et al.,* 2020). More work is needed to define the cooperation that exists between pEMT and UJT and further define the causes and behaviour of these characteristics.

The MDCKII cell line was used in this study as a model of epithelial polarisation with overexpression of EB2 or an empty vector control. The MDCK II cell lines used in this study were previously generated in the Mogensen lab and were transfected with the pmCherry-C1 plasmid, either containing the mouse MAPRE2 gene in the multiple cloning site (MCS) or with no addition. The mCherry fluorescent protein was used to allow for the easy confirmation of plasmid presence and therefore EB2 overexpression, with mCherry alone being used in control cells to eliminate any effects seen from high expression of mCherry rather than EB2. The MDCKII cell line easily forms apico-basal polarised layers in 2D and cyst structures in 3D. They have a primarily peripheral apico-basal MT organisation and generate ncMTOC at apical adherens junctions during differentiation. Additionally, the Panc-1 subclones with high or low EB2 expression were also used. These are sub clones isolated from the parental Panc1 cell line which showed heterogony for EB2 expression. Although not a model of apico-basal polarisation, some insights may be gleamed into EB2 function from this model.

Rationale and gaps in knowledge

- Differential EB2 expression during apico-basal polarisation and differentiation suggests that EB2 plays a role in the control of cell differentiation and polarisation
- Does high EB2 expression alone confer a lack of differentiation?
- What aspects of apico-basal polarisation are affected by differential EB2 expression?

- o Cell height?
- o PAR3 positioning?
- o Cell junction formation and structure?
- o Cell shape (jamming/unjamming)?

Hypothesis

Overexpression of EB2 perturbs normal differentiation of MDCKII cells including cell elongation, localisation of the key polarity marker Par3 and cell shape and overall tissue structure.

Aims

The aims of this chapter are to investigate the effects of EB2 overexpression on:

1. Epithelial apico-basal polarisation and differentiation

2. Centrosome/ncMTOC integrity and function

4.3 Results

4.3.1 EB2 Overexpression Model

The sub-clones containing mCherry/mCherry-EB2 used in this study were previously generated by Jonathan Gadsby, a previous member of the Mogensen lab (see section 2.1 for details). This mCherry expression can be seen in methanol fixed cells imaged using widefield fluorescence microscope (Fig 4.1a). To confirm that these sub clones were stably expressing mCherry-EB2 and mCherry-EMPTY and represents a good model of EB2 overexpression, Western blotting was used to confirm the presence of these vectors (Fig 4.1b). Endogenous expression of EB2 could not be visualised as the anti-EB2 antibody showed no reactivity to canine EB2 during the Western blot technique, whereas the exogenous mouse EB2 (mCherry-EB2) did show reactivity. The western blot clearly showed the presence of the exogenous mouse EB2 in the MDCKII cells containing mCherry-EB2 (MDCKII$^{mCh-EB2}$), no exogenous expression was seen in the MDCK cells expressing mCherry-EMPTY (MDCKII$^{mCh-EMPTY}$). Expression of mCherry was also measured using an antibody against RFP. Expression of mCherry was present in both cell lines and was around 1.8 fold higher in the MDCK$^{mCh-EMPTY}$ cells. Note that mCherry bands in the MDCKII^{mC-EB2} cells were larger (~65kDa) due to the attached EB2.

4.3.2 Analysis of cell height and PAR3 localisation shows perturbation in MDCKII$^{mCh-EB2}$ cells

To determine the effect of EB2 overexpression on epithelial cell elongation and polarisation, MDCKII$^{mCh-EMPTY}$ and MDCKII$^{mCh-EB2}$ cells were seeded on glass and allowed to grow for up to 14 days generating populations with increasing confluency and polarity (Fig. 4.2a). Height analysis of these layers was used to quantify partial-differentiation. From 1 experiment, 4 z stacks per group were taken with 9 height measurements taken per z stack. Both MDCKII^{mChEMPTY} and MDCKII$^{mCh-EB2}$ cells followed the same overall pattern of cell height, reducing initially at day 3 then increasing until day 9 when it then plateaued at ~22-24µm. In the early stages of the polarisation series MDCKII$^{mCh-EMPTY}$ were significantly taller than MDCKII$^{mCh-EB2}$ cells. This significant difference was seen until day 7, then at day 9 and 14, heights were comparable with no significant difference. In these early stages, MDCKII$^{mCh-EB2}$ cell height was decreased by 34% at day 1, 32% at day 3, 60% at day 5 and 22% at day 7.
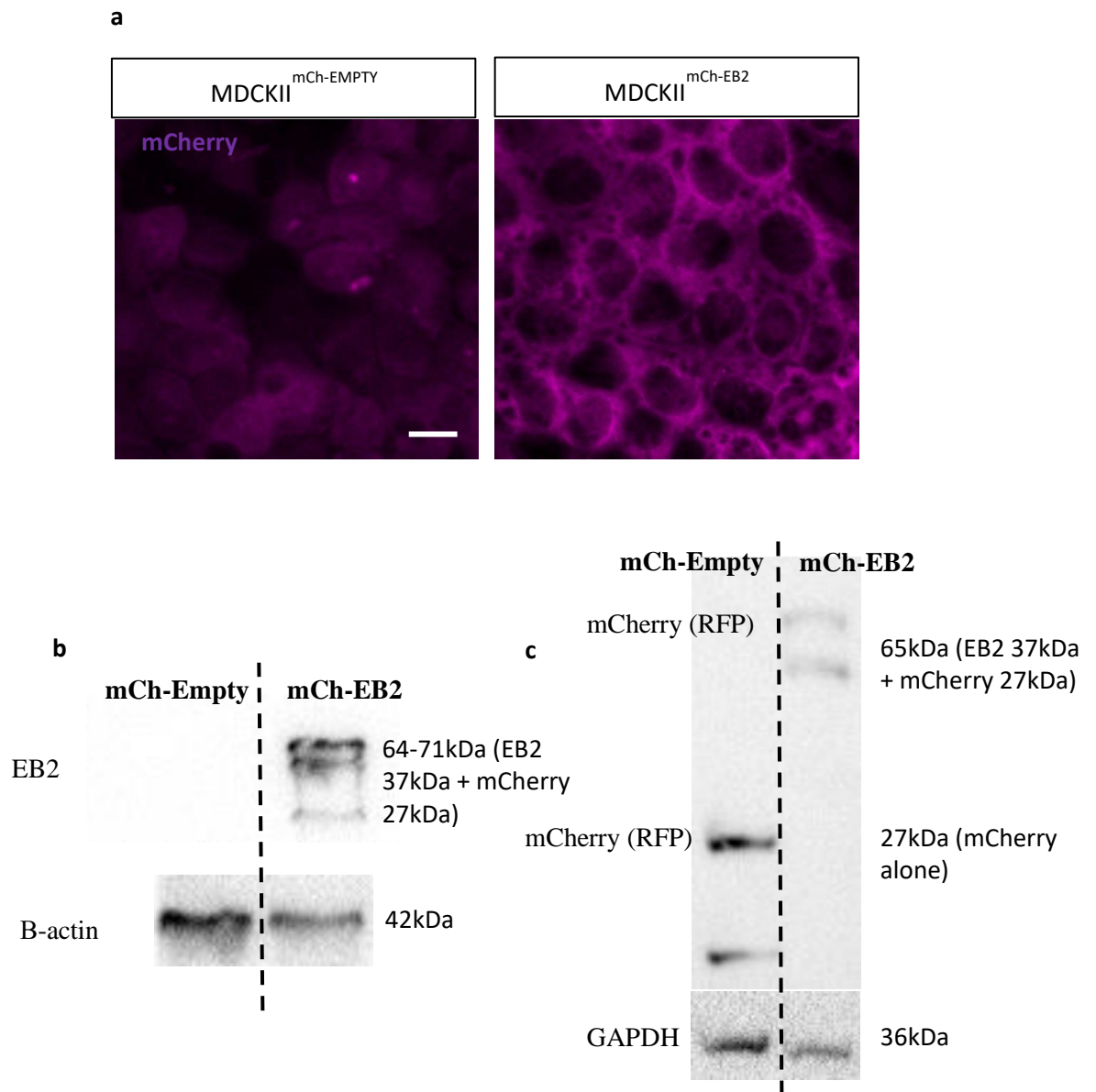
Figure 4.1 Model of epithelial EB2 overexpression. (a) MDCKII cells expressing mCherry-EB2 (overexpression) or mCherry-EMPTY (empty vector control). Cells seeded on glass and imaged using widefield fluorescence microscopy showing mCherry fluorescence. Scale bar= 10μm (b) Western blot using an EB2 antibody showing exogenous EB2 (37kDa) conjugated to mCherry (27kDa) with several bands at ~64-71kDakDa in the MDCKII^mCh-EB2 cell line only, EB2 antibody showed no reactivity to endogenous EB2. β-actin used as a loading control and shows band at 42kDa (c) Western blot using an RFP antibody showing presence of mCherry expression in both cell lines. MDCKII^mCh-EMPTY shows mCherry band at expected 27kDa and MDCKII^mCh-EB2 cells shows mCherry conjugated to EB2 at 64-70kDa. A smaller unknown band was also present in both groups. GAPDH antibody used as a loading control and shows band at expected 36kDa.
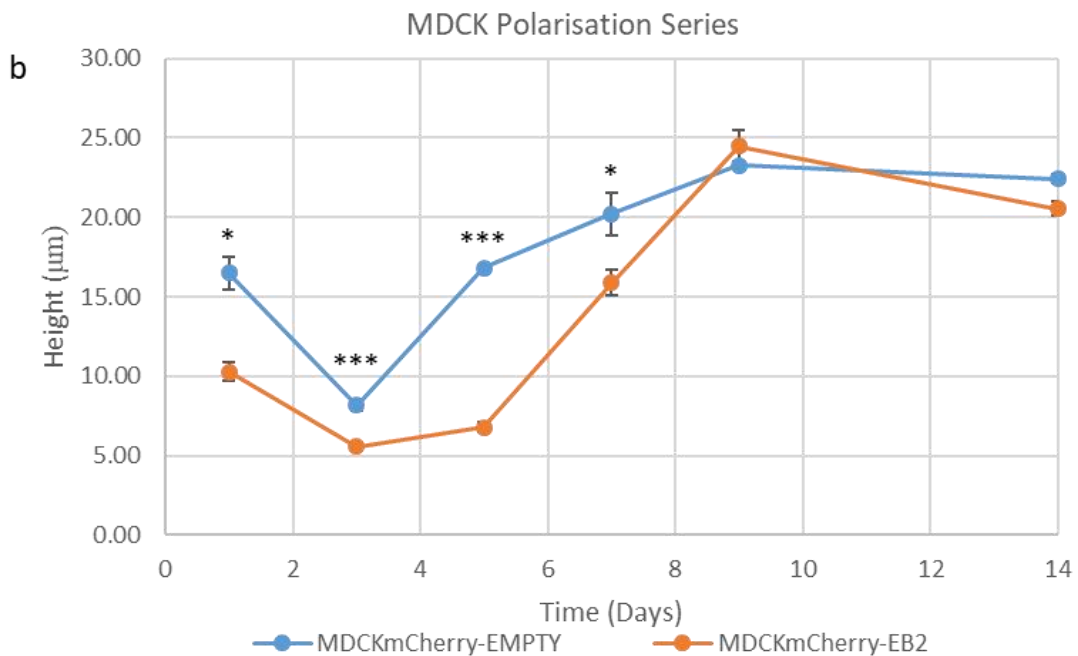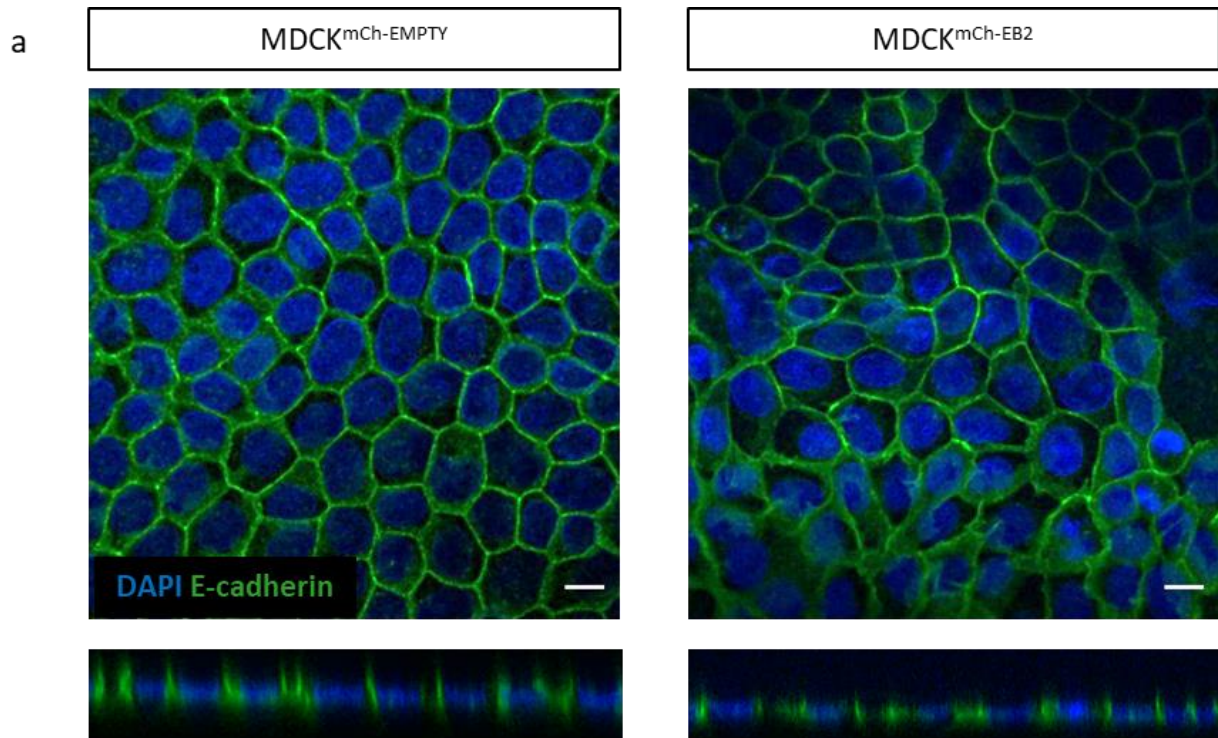
Figure 4.2 Cell height analysis in polarising MDCKII cells. (a) MDCKII cells seeded on glass for 5 days and immunolabelled for E-cadherin (green) and counter stained with DAPI (blue). Orthogonal views show layer/cell height used for quantification. Scale bars= 10µm. (b) Quantification of cell height with increasing time/confluence. In both cell lines cell height initially decreased at day 3 then increased until plateauing at day 9 and 14. MDCKII$^{mCh-EB2}$ cells showed significantly decreased height until day 9. +/- 1 SE shown. N= 4 z slices with 9 measurements taken per z slice, 1 experiment. P values: day 1=0.029, day 3= <0.001, day 5= <0.001, day 7= 0.041.

The polarity marker PAR3 was localised by immuno-labelling in cell layers grown for 7 days to assess their positioning in MDCKII[mCh-EMPTY] and MDCKII[mCh-EB2] cells (Fig. 4.3a). MDCKII[mCh-EB2] cells showed very incomplete PAR3 coverage at cell-cell junctions whereas MDCKII[mCh-EMPTY] cells showed uniform and complete coverage of cell-cell contacts. In order to analyse and compare the accumulation of PAR3 at apical cell-to-cell junctions between the two subclones, 10µm bars were blindly positioned perpendicular to cell-cell contacts using the β-actin labelled channel. The fluorescence intensity was then measured every 0.1µm along these line profiles in the PAR3 channel. PAR3 showed a significant reduction in mean peak fluorescence intensity of 71% at junctional sites in MDCKII[mCh-EB2] compared to MDCKII[mCh-EMPTY] cells. Junction adjacent PAR3 intensity appeared similar between groups and a significant difference was only seen at the peak (Fig 4.3b). Data was gathered from 36 line profiles for MDCKII[mCh-EMPTY] and 25 line profiles for MDCKII[mCh-EB2] from a single experiment.

4.3.3 Cells overexpressing EB2 showed increased size and slightly decreased proliferation rate

To analyse the effect of EB2 overexpression on cell size, confluent layers of MDCKII[mCh-EMPTY] and MDCKII[mCh-EB2] cells were immuno-labelled for E-cadherin and analysed in ImageJ. The cell borders were manually traced using E-cadherin to demarcate the circumference of the cells and the cell areas could then be determined using ImageJ (Fig 5.4a). MDCKII[mCh-EB2] cells showed a significant (p=<0.001) 29% increase in size compared to MDCKII[mCh-EMPTY] cells (Fig. 4.4b). The effect of EB2 overexpression on proliferation rate was analysed by seeding a known number of cells and counting cells at 24-hour time periods using a haemocytometer. Here it was shown that the MDCKII[mCh-EB2] cells had slightly decreased proliferation at the 24 and 48-hour time period although this proved not to be significant. However, at 72-hours, proliferation rate was significantly decreased (p=0.043) in MDCKII[mCh-EB2] cells by 18% (Fig. 4.4c). Data was gathered from 3 biological repeats one cell count per experiment.
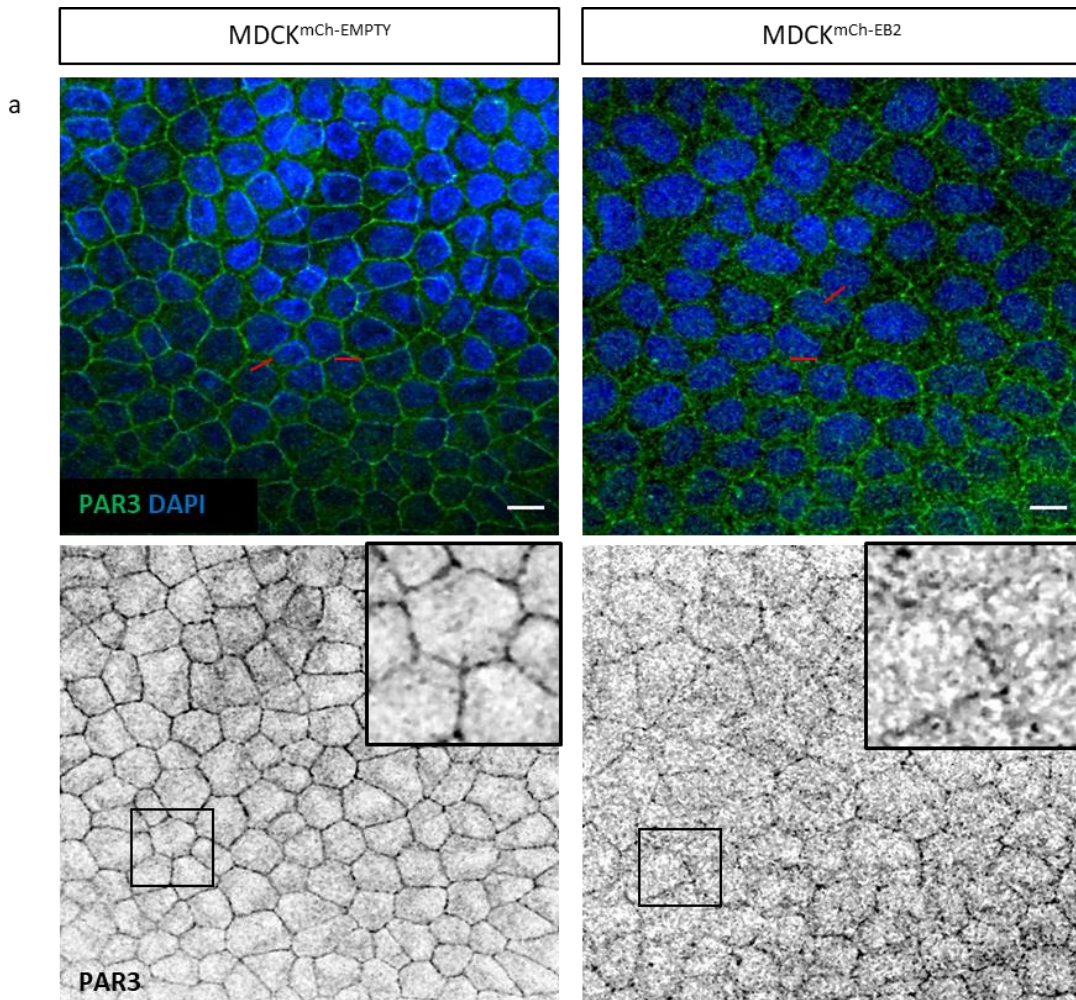
PAR-3 Junctional Intensity Profiles
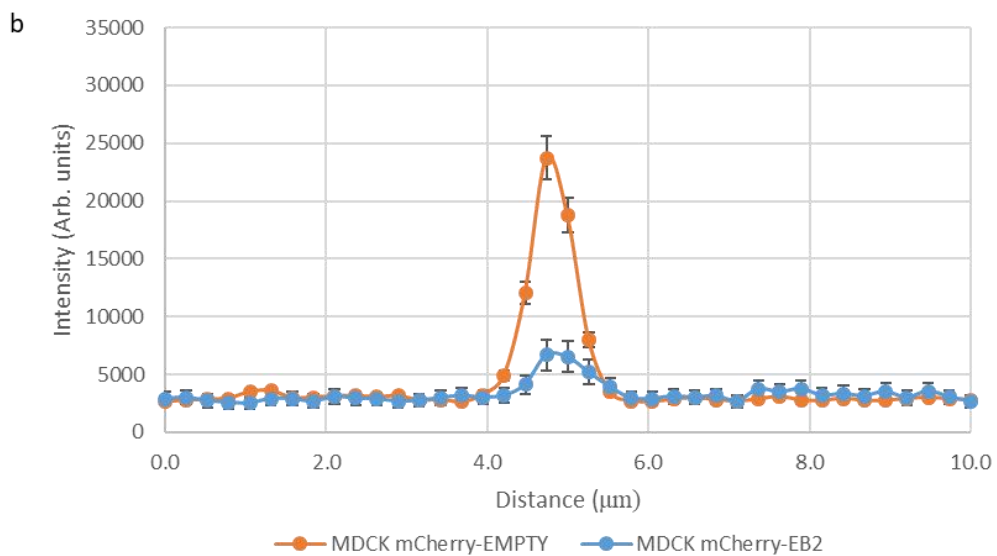
Figure 4.3 Analysis of PAR3 polarity marker localisation. (a) MDCKII cells seeded on glass and grown for 7 days. Methanol fixation and immunolabelling for PAR3 (green) was carried out and cells were imaged using fluorescent widefield microscopy. The red lines represent line profiles that were used for junction quantification. PAR3 labelling in MDCKII^mCh-EMPTY shows clear localisation at cell-cell contacts whereas MDCKII^mCh-EB2 cells shows a reduction in this localisation with more cytosolic staining present. (b) Fluorescence intensity analysis based on line profiles across PAR3 staining at cell-cell contacts. +/- 1 SE shown. MDCKII^mCh-EMPTY n=36, MDCKII^mCh-EB2 n=25 cells, 1 experiment.

a

| MDCKII^mCh-EMPTY | MDCKII^mCh-EB2 |

E-cadherin DAPI

b

Mean Cell Size

***

Mean Cell Size (μm^2)

■ MDCKIImCh-EMPTY ■ MDCKIImCh-EB2

c

Cell Counts Over Time

*

Mean Cell Count

Time (Hours)

MDCKIImCh-EMPTY
MDCKIImCh-EB2
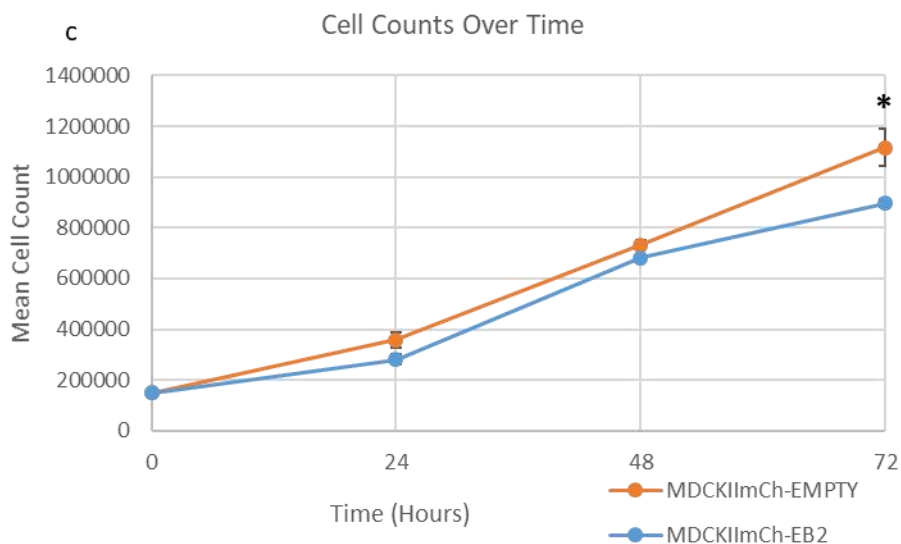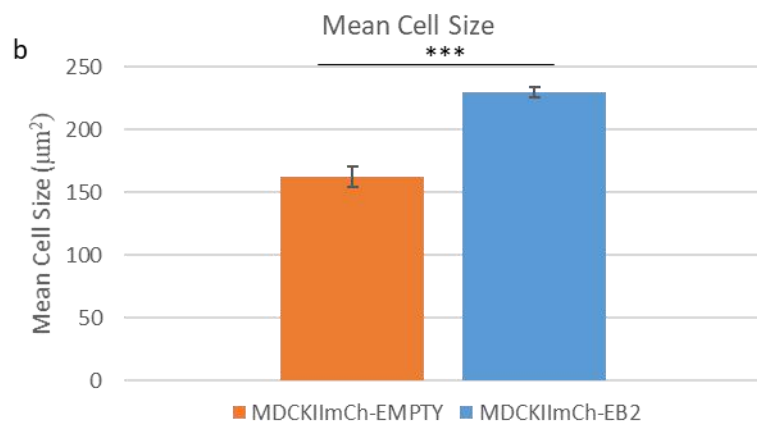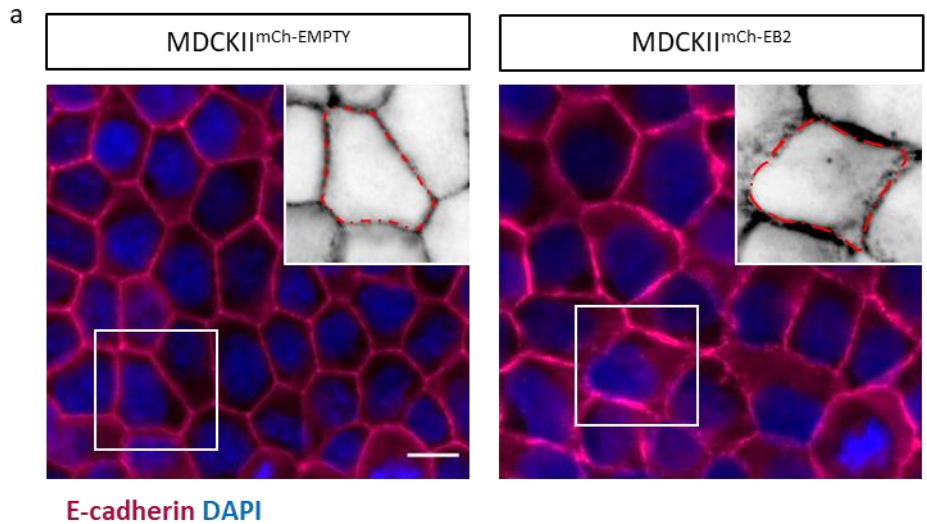
Figure 4.4 Analysis of cell size and proliferation. (a) MDCKII cells seeded on glass and grown for 9 days, fixed in methanol and immunolabelled for E-cadherin (red) with DAPI counterstain (blue) then imaged using widefield fluorescence microscopy. Scale bar= 10µm. (b) Cell size based on surface area was measured using E-cadherin as a peripheral marker in ImageJ. MDCKII^mCh-EB2 show a significant increase in cell size of 29%. +/- 1 SE shown. n= 100 cells per group, 3 experiments. (c) Cell growth based on cell number over time. There was no significant difference in cell proliferation until 72 hours when MDCKII^mCh-EB2 cells showed a significant decrease. +/- 1 SE shown. n=3 haemocytometer counts from 3 experiments.

4.3.4 EB2 overexpression causes adherens junction abnormalities

To quantify the effect of overexpression of EB2 on E-cadherin localisation, cells were immunolabelled for E-cadherin and actin and fluorescence intensity line profiles were obtained as described for PAR3 (see 4.3.2) (Fig. 4.5a). Initially this was carried out in cells seeded on glass for 7 days. Peak intensities across the line profiles were also analysed and showed no significant difference in the peak intensity between MDCKII[mCh-EMPTY] and MDCKII[mCh-EB2] cells. The mean line plot profiles mirrored this result with both groups having a single peak representing the junction. However, the EB2 overexpressing cell line had an increased area under the curve (data not shown) representing the increased E-cadherin staining either side of this peak intensity, as seen in the immunolabelled images (Fig. 4.5 a and b). This effect was visualised in more detail by looking at selected representative single plots as averaging of this data smoothed out the aberrations seen in the MDCKII[mCh-EB2] cells. These individual line plots showed multiple diffuse peaks in the MDCKII[mCh-EB2] group whereas the MDCKII[mCh-EMPTY] control group showed single peaks with low adjacent intensity. This analysis also showed that junctional E-cadherin was greatly diffused in the MDCKII[mCh-EB2] cells compared to empty vector controls (Fig. 4.5 d and e). Here junction size/width is used as a measure of E-cadherin diffusion at the junction. Data was gathered from 20 line profiles per group in a single experiment.

To assess whether E-cadherin localisation is affected in polarising cells, a polarisation series was carried out by analysing cell junctions at different time periods in confluent cells. MDCKII[mCh-EMPTY] cells showed relatively uniform fluorescent intensity line profile structure with a single peak and low adjacent intensity. In these control cells, peak intensity was markedly reduced after day 1 and then no significant differences were seen at subsequent time points. MDCKII[mCh-EB2] confluent layers also showed increased peak intensity in the earlier stages with day 1 and day 3 having similar intensity which then decreases at subsequent time points by 46% at day 5 and then decreased by a further 29%. By day 9 this peak was decreased significantly with relatively high adjacent intensity (Fig. 4.6). The diffuse junctions may be due to imaging of out of focus deviations of the lateral membranes that are seen as part of the junctions when imaged using widefield microscopy. To assess if this is occurring here, E-cadherin 3D structure was observed by reconstructing z-slices into a stack taken using a confocal microscope, the junctional angles were compared qualitatively where no distinct difference was seen in angle or overall shape of E-cadherin staining at cell-cell contacts (Fig. 4.7).
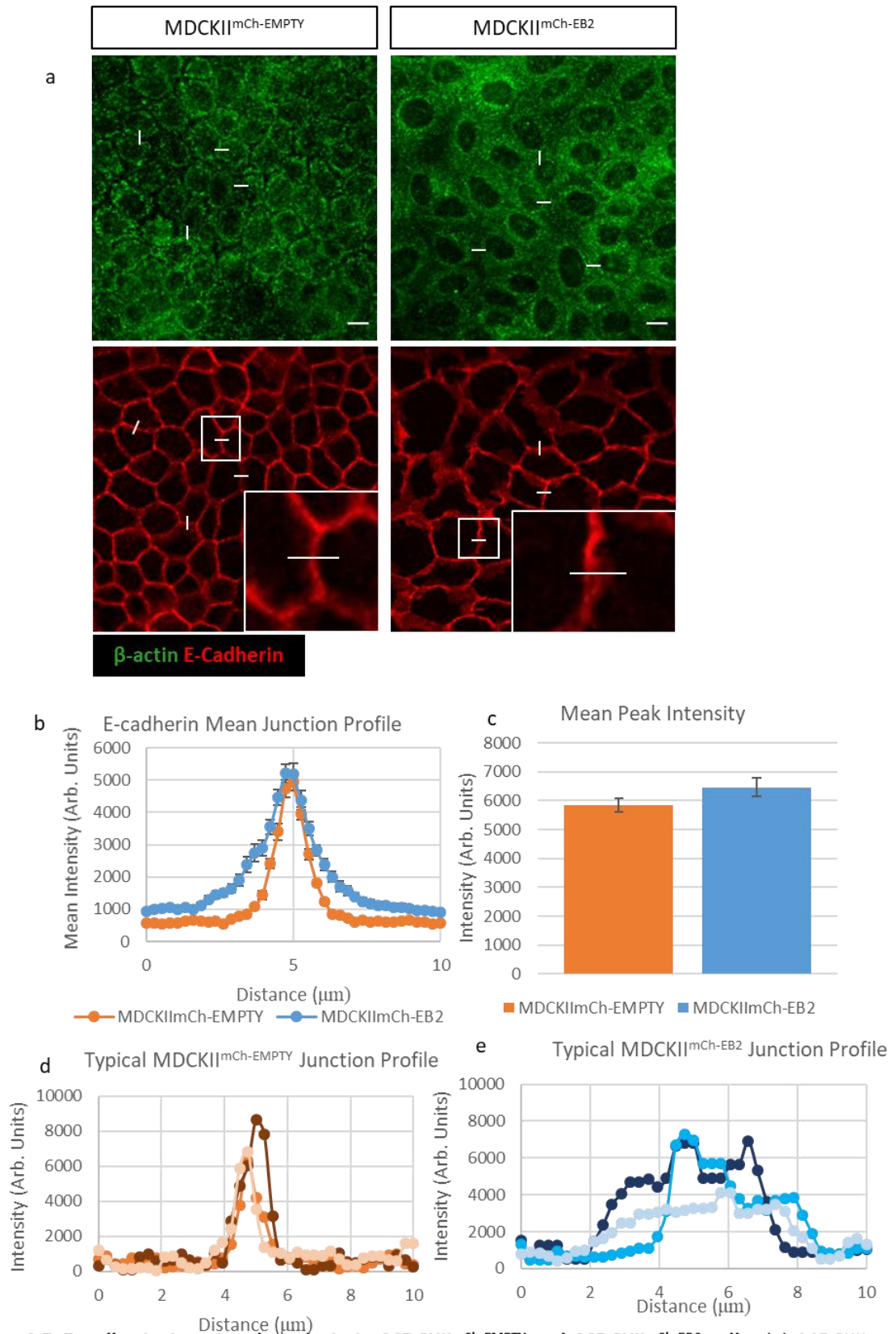
Figure 4.5 E-cadherin junctional analysis in MDCKII^mCh-EMPTY and MDCKII^mCh-EB2 cells. (a) MDCKII cells seeded onto glass and grown for 7 days were immunolabelled for β-actin (green) and E-cadherin (red), imaged on a widefield fluorescence microscope. White bars represent line profiles along which intensity measurements where taken. Scale bars= 10μm. (b) Fluorescence intensity analysis showing mean line profile intensity of E-cadherin staining at junctions. +/- 1 SE shown. N= 20 line profiles, 1 experiment. (c) Quantification of mean peak intensity of E-cadherin staining at junctions. No significant difference was seen in peak junction intensity. +/- 1 SE shown. n=55 line profiles, 1 experiment. (d,e) Fluorescent intensity profiles of a single representative line profile measuring intensity across cell-cell contacts.
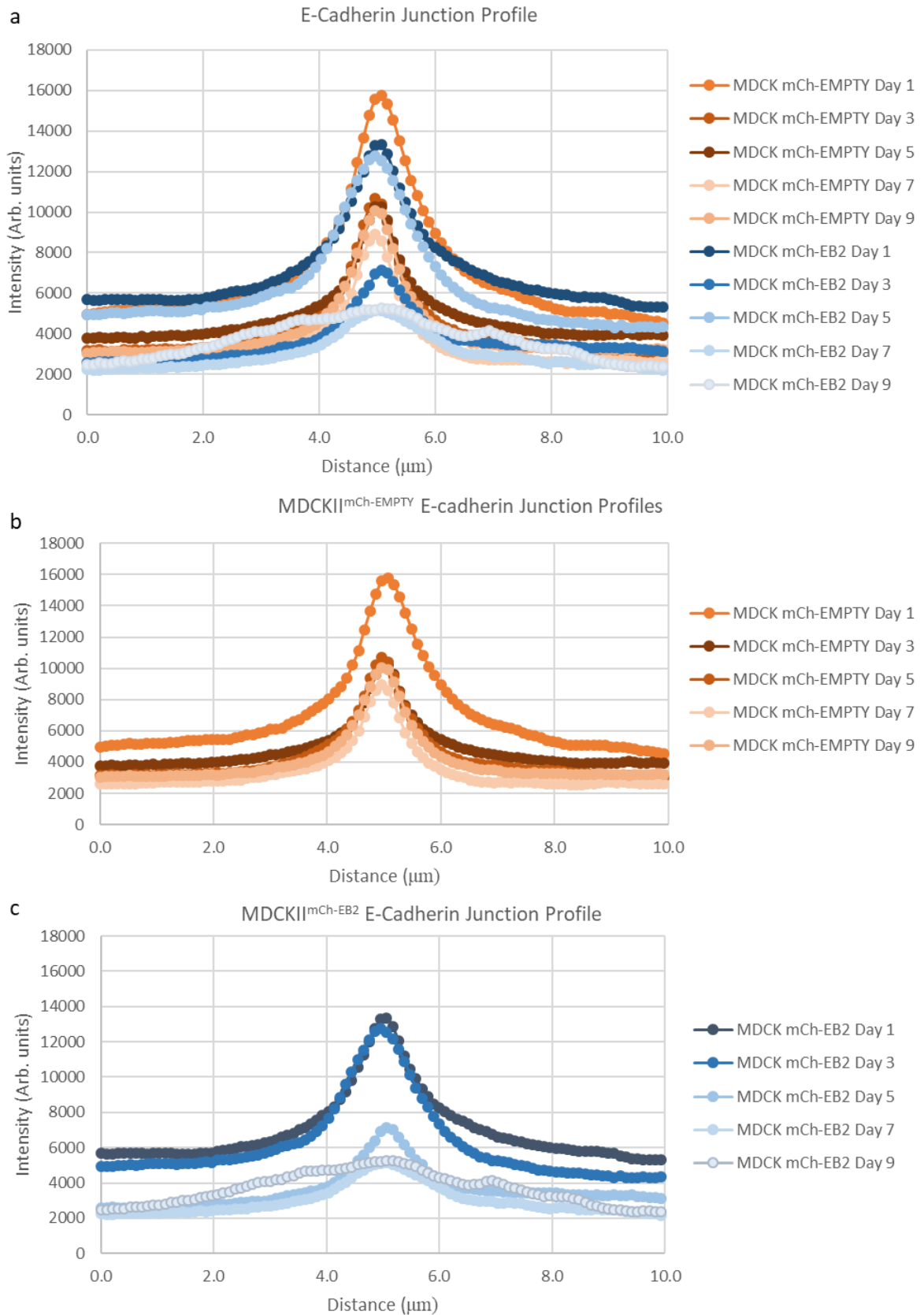
Figure 4.6 Junction profile analysis during polarisation. (a) Quantification of mean line profile intensity of E-cadherin staining at junctions at increasing days of differentiation. (b,c) Data showing MDCKII$^{mCh-EMPTY}$ or MDCKII$^{mCh-EB2}$ separately. MDCKII$^{mCh-EB2}$ cells show a distinct decrease in intensity and definition as time proceeds, particularly at days 7 and 9. Control empty vector cells showed initial decrease in intensity while maintaining definition after day 1, this was delayed in MDCKIImCh-EB2 cells and only occurred at after day 3. n= 80 line profiles per group from 3 experiments.
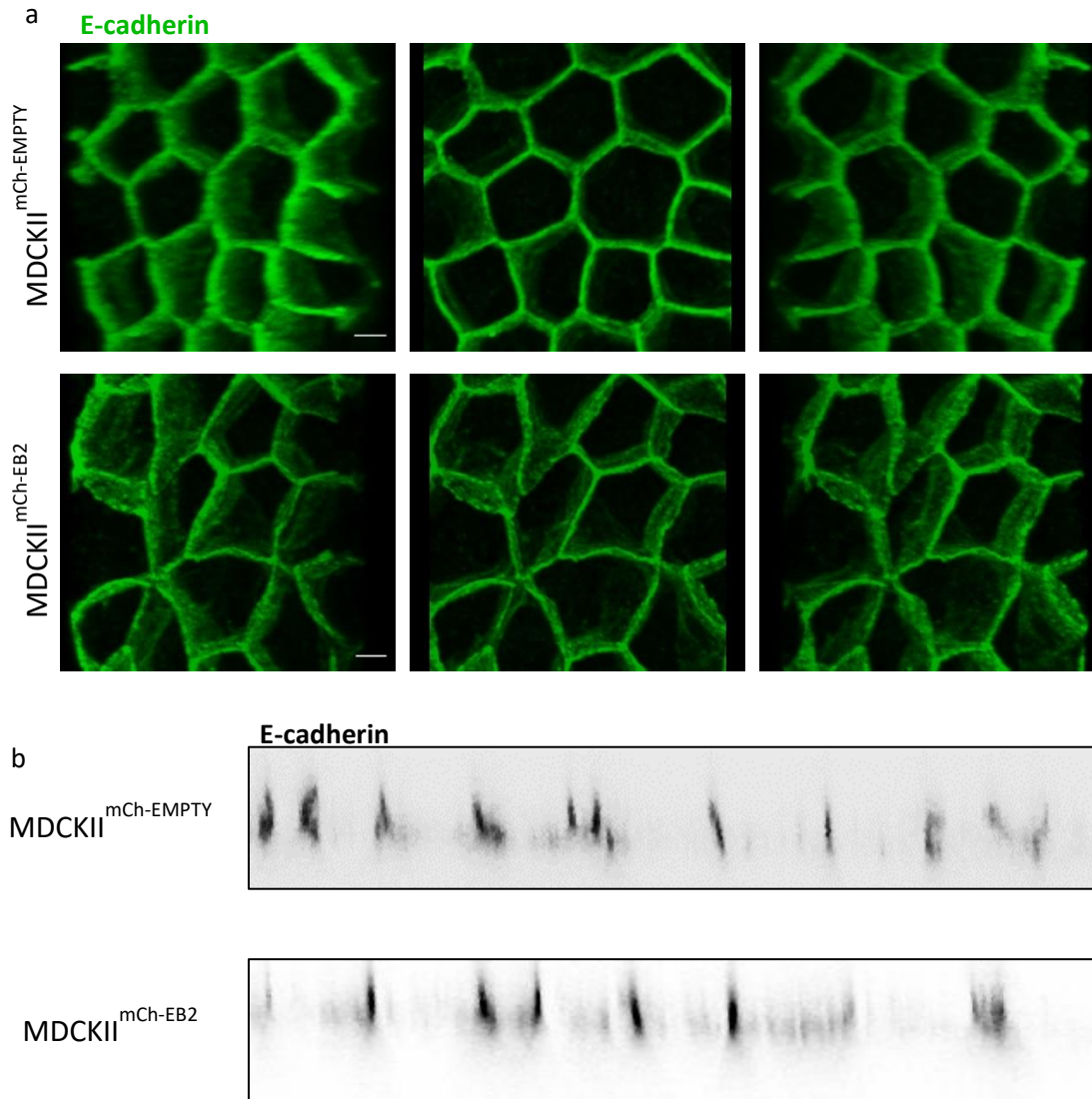
Figure 4.7 Analysis of E-cadherin 3D localisation at cell-to-cell junctions in MDCKII^{mCh-EMPTY} and MDCKII^{mCh-EB2} cells. (a) MDCKII cells seeded on glass and grown for 5 days. Cells were methanol fixed, immunolabelled for E-cadherin and imaged using fluorescent confocal microscopy. Reconstructed z stacks show 3D layer from 3 viewing angles to give an overview of junction structure. Slightly more deviation in E-cadherin junction structure is seen in MDCKII^{mCh-EB2} cells compared to the empty vector control Scale bar= 10µm. (b) Orthogonal views of E-cadherin stained z stacks to visualise junction structure. Junctions appear straight in both groups with no obvious difference.

4.3.5 EB2 overexpression promotes unjamming

Cell jamming/unjamming was analysed by using the shape index and the 3.81 threshold to determine whether EB2 overexpression caused changes in the UJT of these cells. Based on previous research, cells above this threshold are considered unjammed while cells below are jammed. A normal fully polarised layer *in vivo* is considered jammed and increases in shape index represent disease phenotypes. Shape index is calculated using the formula shape index=perimeter/√area, see section 2.7.3 for more details. Here, analysis was carried out on days 7, 9 and 14 as this show increasing degrees of confluency compared to early time points which represents less confluent/sub confluent populations. At these time points no layers were below the threshold of 3.81 suggesting that they were all unjammed. However, MDCKII^mCh-EB2 cells had a significantly higher shape index at every time point. The mean shape index of these EB2 overexpressing cells showed very little change with time, in these cells the shape index was 4.02 at day 7, 3.97 at day 9 and 4.01 at day 14. Whereas control empty vector cells showed decreased mean shape index with increasing time going from 3.88 at day 7, 3.83 at day 9 then to 3.81 at day 14. MDCKII^mCh-EMPTY cells had significantly (p=<0.001) lower shape index at every time point when analysed using a T test. Data was gathered from 190 MDCKII^mCh-EMPTY cells and 150 MDCKII^mCh-EB2 cells taken from 3 biological repeats.

4.3.6 MyosinII and ROCK inhibition rescued some junctional abnormalities

To attempt to elucidate potential mechanisms behind the abnormalities seen in jamming and junction structure with EB2 overexpression, myosinII and Rho-associated protein kinase (ROCK) inhibition was carried out in cell layers seeded at high density and grown for 7 days. Cells were then immunolabelled for E-cadherin for junction and shape index analysis as well as Myosin LC S20 to assess blebbistatin treatment effectiveness (Fig. 4.9).

Mean fluorescence intensity analysis of E-cadherin line profiles across cell junctions showed little change following 4-hour treatment with blebbistatin in both MDCKII^mCh-EMPTY and MDCKII^mCh-EB2 cells (Fig. 4.9a and b). However, MDCKII^mCh-EB2 cells treated with blebbistatin did show a significant increase in shape index with a mean increase of 10% (p=0.03, n= MDCKII^mCh-EMPTY 106, MDCKII^mCh-EB2 77) (Fig. 4.11c). MDCKII^mCh-EMPTY cells showed no significant difference in shape index upon blebbistatin treatment. Activated myosin was evaluated by immuno-labelling for phosphorylated myosin LC (S20). MDCKII^mCh-EMPTY cells showed a significant decrease of 18% and MDCKII^mCh-EB2 cells showed a significant decrease of 32% in myosin LC (S20) intensity suggesting blebbistatin treatment was effective (p=0.03, n= 4 FOVs per group) (Fig. 4.9d). As previously showed junction profile averaging mutes true E-cadherin junctional structure. Therefore, analysis of 4 individual representative fluorescence intensity line profiles are shown in figure 5.10. This shows that blebbistatin rescued the effect of EB2

overexpression of junction width, with the width being much closer to the control cells. Absolute size/width measurements of E-cadherin diffusion at junctions were made but due to the difficulty in this measurement they are only shown in figure S4.

ROCK inhibition was used to determine if changes in the shape index and E-cadherin positioning are due to the difference in monolayer tension caused by ROCK. The shape index was analysed following treatment with the ROCK inhibitor Y27632 for 24 hours in MDCKII$^{mCh-EMPTY}$ and MDCKII$^{mCh-EB2}$ cells (Fig 4.11 a and b). No significant changes in shape index was observed following ROCK inhibition in EB2 overexpressing cells while a significant increase was observed in the control MDCKII$^{mCh-EMPTY}$ cells (n=60 cells per group) (Fig4.11c). In accordance to previous results, control (DMSO) MDCKIIm^{Ch-EB2} cells had an increase in shape index compared to empty vector cells. Fluorescence intensity analysis of individual E-cadherin line profiles across cell junctions showed a slight recovery of junction size/width of E-cadherin diffusion seen in the EB2 overexpressing cell (Fig. 4.12). As before absolute values were taken from these width measurements and these measurements can be seen in figure S4.
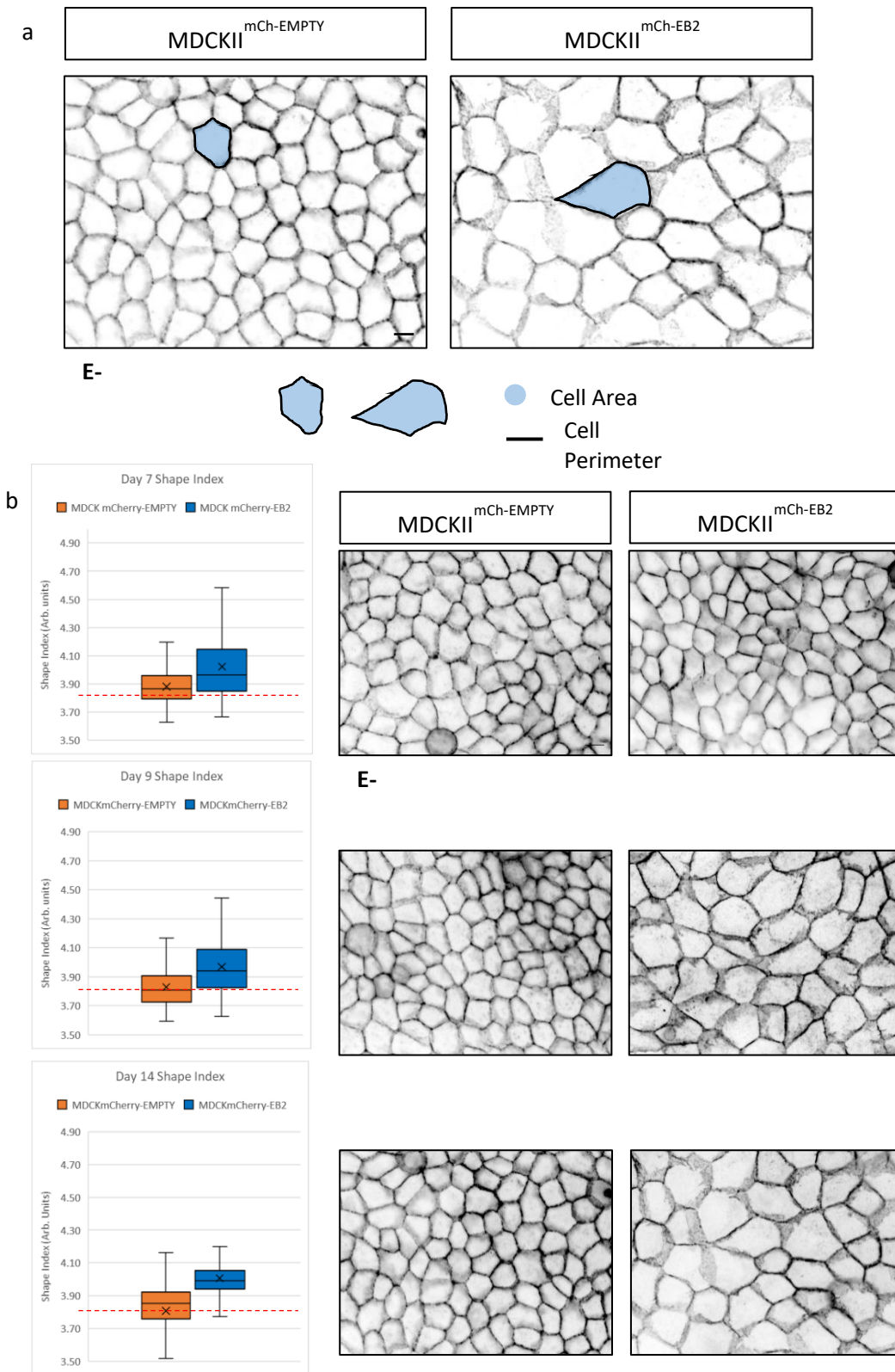
Figure 4.8 Analysis of shape index in MDCKII[mCh-EMPTY] **and MDCKII**[mCh-EB2] **cells at different time points.** (a) Example of cell jamming analysis showing measurements of cell area and cell perimeter. Shape index was calculated using the formula: shape index= perimeter/$\sqrt{area}$. (b) Epithelial jamming analysis in cells grown for 7, 9 and 14 days on glass, immunolabelled for E-cadherin and imaged using widefield fluorescence microscopy. Mean shape index is shown as x and red dotted line represents the threshold at which cells are jammed/unjammed (UJT). In MDCKII[mCh-EMPTY] cells show decreasing shape index with time whereas MDCKII[mCh-EB2] cells showed a constant shape index of ~4.00 which was consistently higher than control cells. Due to size difference, less cells are present in EB2 overexpressing cell per FOV. Scale bars= 10μm. n=150-190 cells per group, 3 experiments.
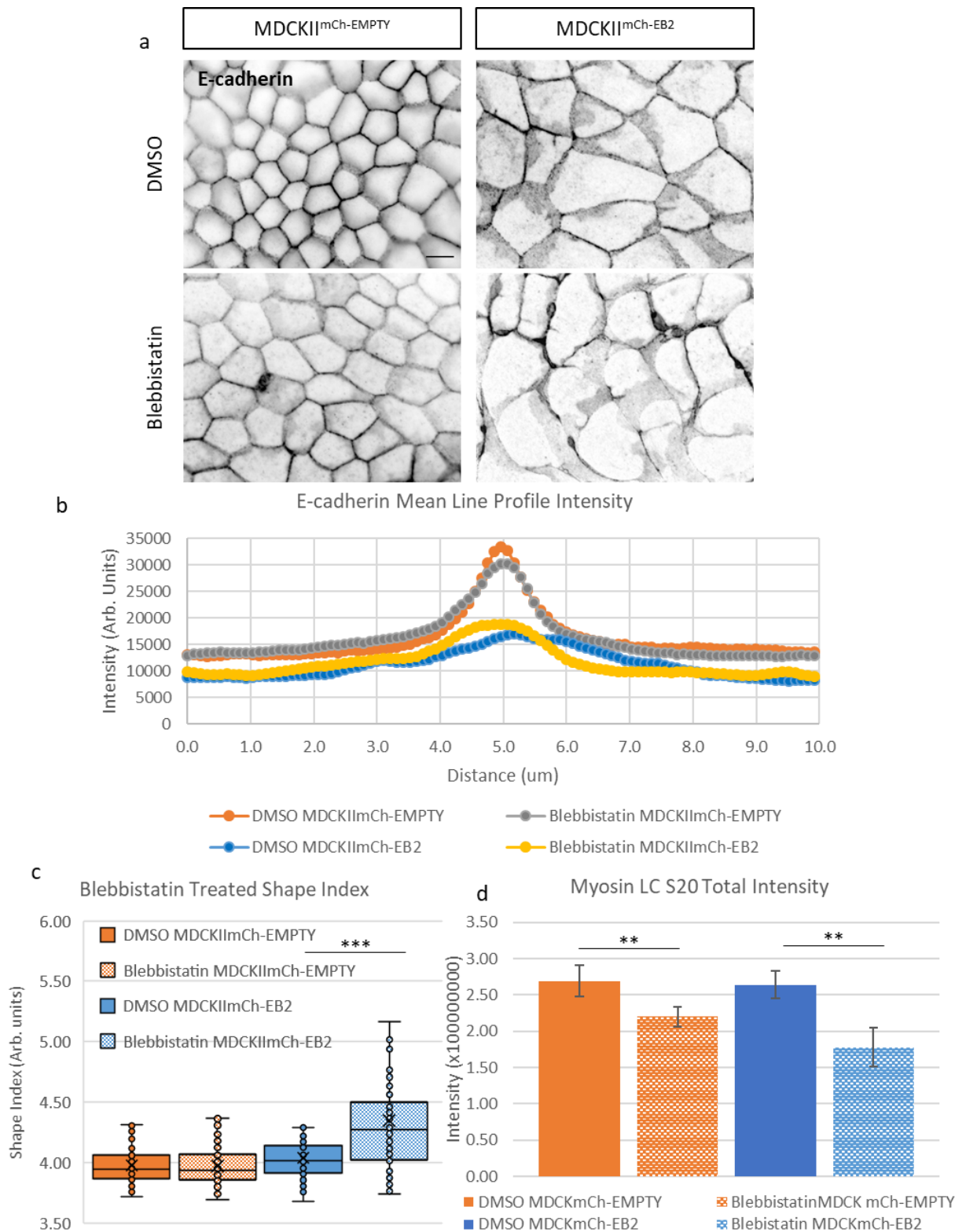
Figure 4.9 Myosin inhibition of MDCKII^{mCh-EMPTY} and MDCKII^{mCh-EB2} cells. (a) MDCKII cells seeded on glass for 7 days then treated with DMSO/blebbistatin for 4 hours, immunolabelled for E-cadherin and imaged using fluorescent widefield microscopy. Scale bar=10µm. (b) Quantification of line profile measuring E-cadherin across cell-cell contacts. Blebbistatin treatment had little effect on E-cadherin junction profile. N=8 cells per group, 1 experiment. N=8 line profiles per group, 1 experiment. (c) Cell shape index with DMSO/blebbistatin (50µM) treatment for 4 hours. Blebbistatin treatment had no significant effect on MDCKII^{mCh-EMPTY} cells but caused a significant increase of 10% in shape index in MDCKII^{mCh-EB2} cells (p=<0.001). N=106 MDCKII^{mCh-EMPTY} cells and 77 MDCKII^{mCh-EB2} cells, 1 experiment. (d) Mean myosin LC S20 total intensity measurements using ImageJ showed activate myosin was significantly reduced 18% (p=0.04) in control cells and 32% (p=0.03) in EB2 overexpressing cells. N=4 FOV, 1 experiment. +/- 1SE shown.
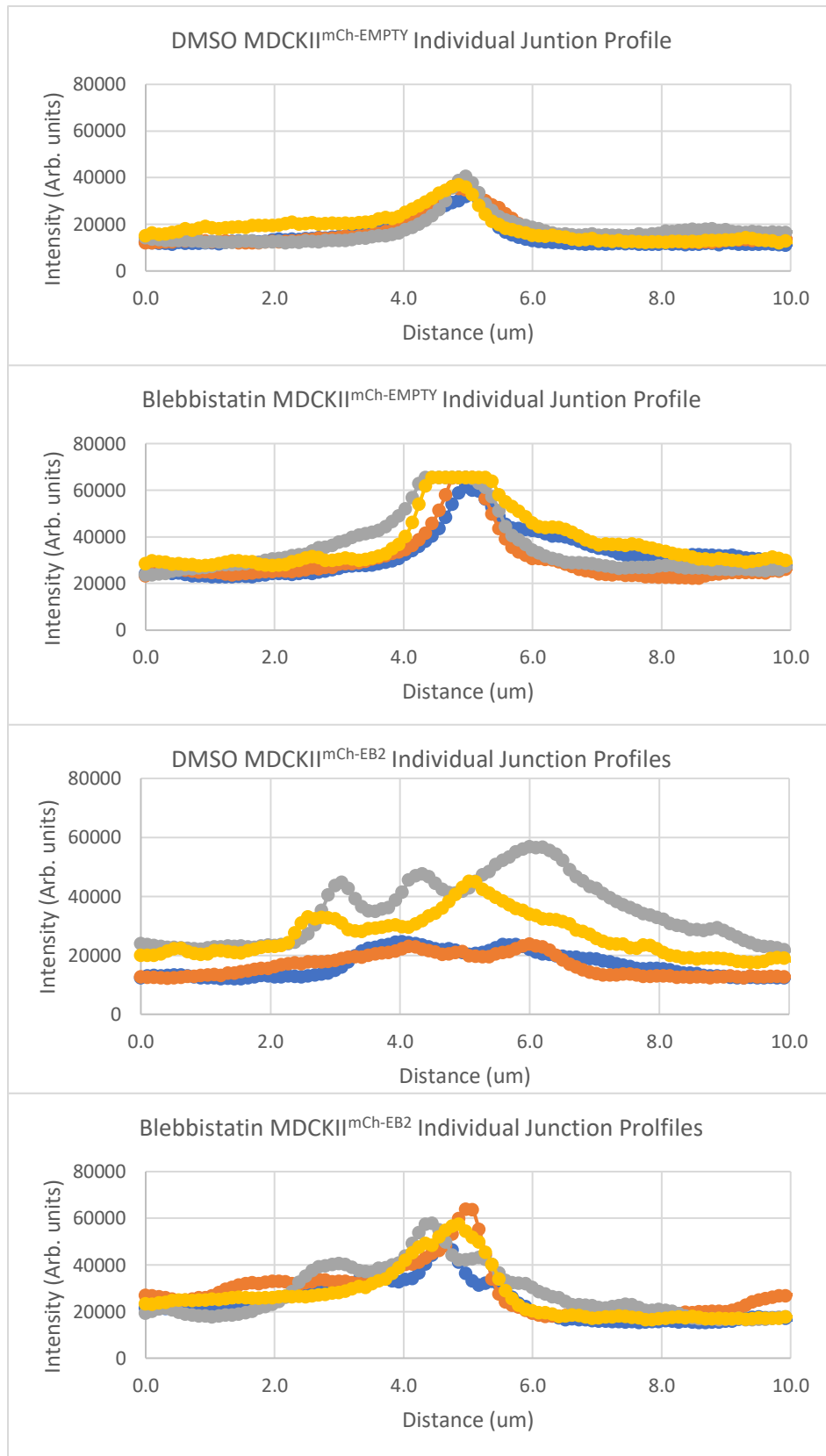
Figure 4.10 Junction width analysis with myosin inhibition. Each graph shows four individual and representative E-cadherin junction profiles with DMSO or 50μM blebbistatin treatment. Each colour represents a random single junction profile from each treatment group for qualitative assessment of junction width and E-cadherin diffusion. DMSO treated MDCKII^mCh-EB2 show much increased junction width compared to MDCKII^mCh-EMPTY control cells. Blebbistatin treatment caused partial recovery of this phenotype in MDCKII^mCh-EB2 cells. Quantification can be seen in appendix figure S4.
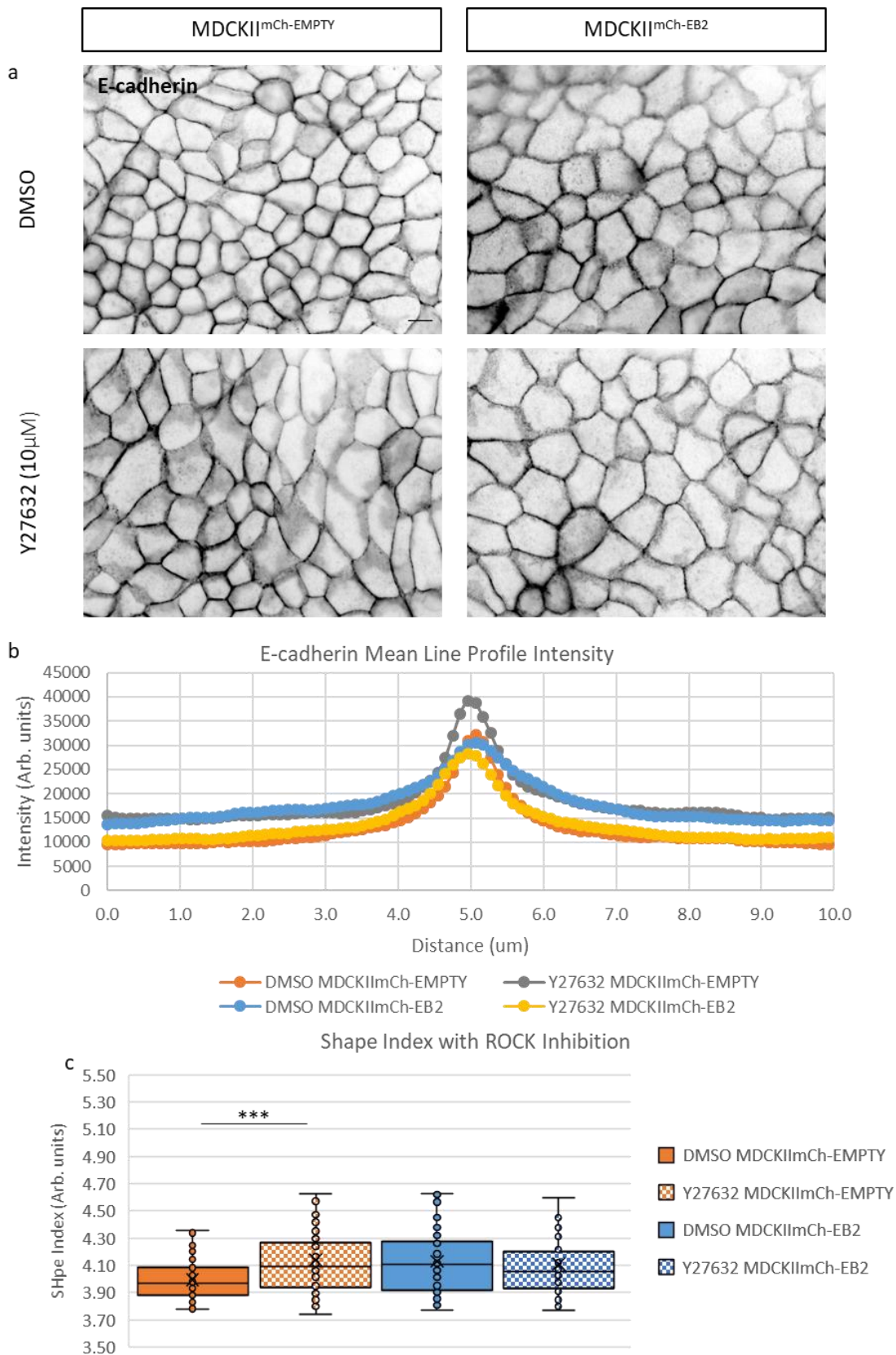
Figure 4.11 Rock inhibition with shape index and junction analysis. (a) MDCKII cells seeded for 5 days on glass, immunolabelled for E-cadherin and imaged using widefield fluorescence microscopy. Scale bar= 10μm. (b) Mean line profile intensity analysis of E-cadherin at cell-cell junctions with DMSO/Y27632 (10μM) treatment. ROCK inhibition appeared to improve junction definition by reducing intensity of E-cadherin adjacent to the junction. N=12 junctions, 1 experiment. (c) Shape index quantification with DMSO/Y27632 treatment. ROCK inhibition cause a significant (p=<0.001) increase in MDCKII[mCh-EMPTY] and there was no difference in shape index MDCKII[mCh-EB2] cells. N=60 cells per group, 1 experiment.
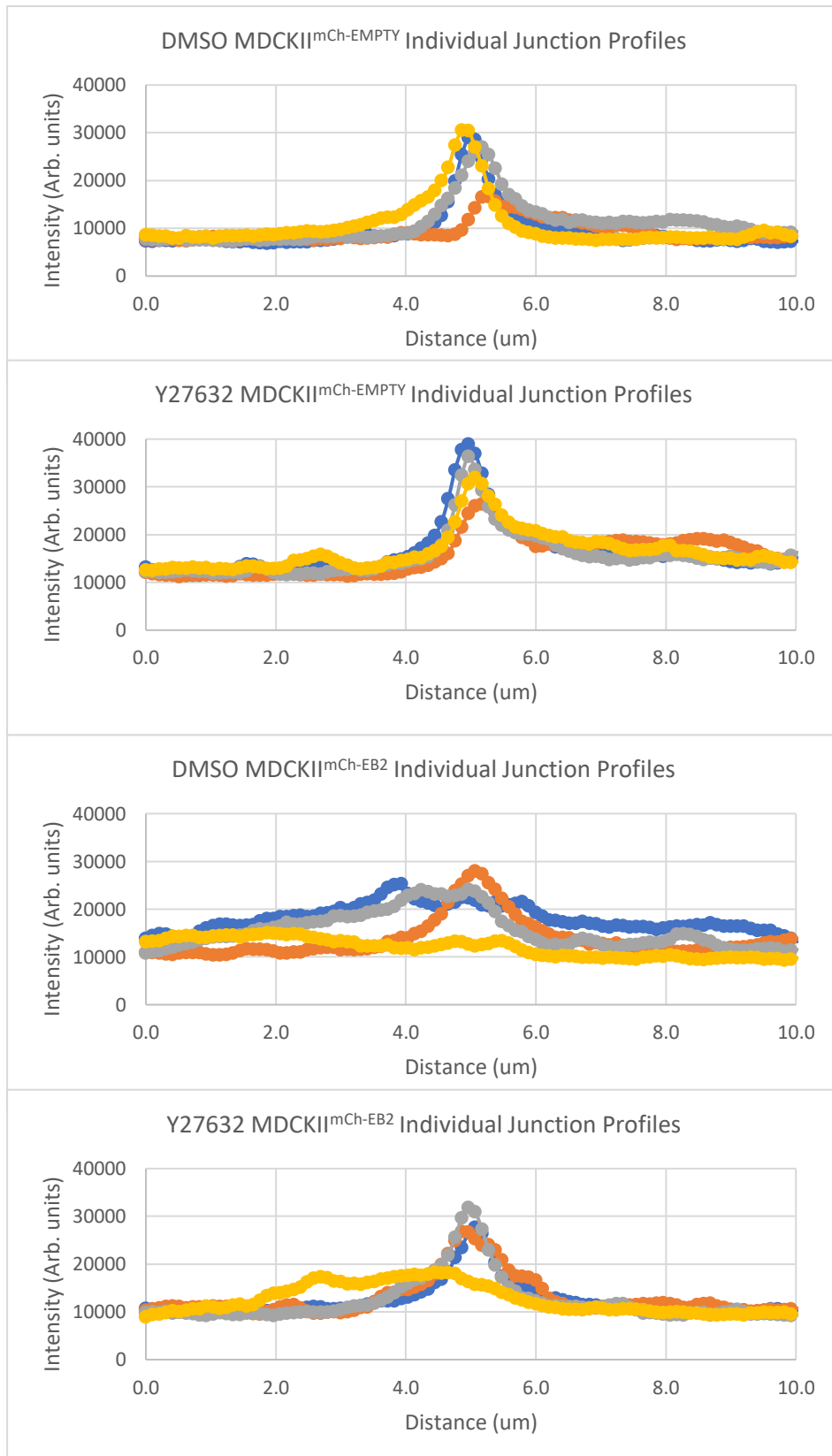
Figure 4.12 Junction width analysis with ROCK inhibition. Each graph shows four individual and representative E-cadherin junction profiles with DMSO or 10μM Y27632 treatment. Each colour represents a random single junction profile from each treatment group for qualitative assessment of junction width. Each colour represents a random single junction profile from each treatment group, to be used for qualitative assessment of junction width and E-cadherin diffusion. Junction width appeared to be unaffected in MDCKII[mCh-EMPTY] control cells whereas partial recovery was seen with Y27632 treated MDCKIImCh-EB2 cell as width more closely resembled that of the DMSO treated MDCKII[mCh-EMPTY] cells. Quantification can be seen in appendix figure S4.

4.3.7 EB2 overexpression increased γ-tubulin and MT nucleation at the centrosome but reduced the number of Cep215 comets.

The total cell expression and centrosomal localisation of key centrosomal proteins was analysed using Western blotting and fluorescent intensity analysis. Firstly, γ-tubulin was analysed due its importance in nucleation. There was no significant difference in the intensity of γ-tubulin measured at the centrosome between MDCKII$^{mCh\text{-}EMPTY}$ and MDCKII$^{mCh\text{-}EB2}$ cells but there was a significant increase of 40% in the γ-tubulin centrosomal area in MDCKII$^{mCh\text{-}EB2}$ cells (n=72 cell, 3 repeats) (Fig. 4.13 a,b and c). Additionally, an overall increase of 48% in total γ-tubulin expression in MDCKII$^{mCh\text{-}EB2}$ compared to MDCKII$^{mCh\text{-}EMPTY}$ cells was estimated based on two Western blot experiments (n=2 experiments) (Fig. 4.13d). As γ-tubulin is a key nucleation factor, MT nucleation/elongation was then studied using a Nocodazole regrowth assay to quantify and localise MT growth after nocodazole recovery. This was carried out and cells were fixed and labelled for α- and γ-tubulin at 0, 2, 4 and 6 minutes after nocodazole removal. Aster size was analysed manually by drawing around the α-tubulin stained aster using the circle tool in ImageJ and area was measured. This showed that aster size and therefore MT length was initially reduced by 18% at 2 minutes but increases by 128% and 89% in the MDCKII$^{mCh\text{-}EB2}$ cells compared to MDCKII$^{mCh\text{-}EMPTY}$ cells at 4 and 6 minutes respectively. There was only a significant difference at 4 and 6 minutes when analysed using a T test which gave a p value of <0.001 at both of these time points (Fig 4.14b). Fluorescence intensity measurements were also taken of the aster areas to evaluate the relative amount of α-tubulin present. This showed that at 2 and 4 minutes, the MDCKII$^{mCh\text{-}EB2}$ cells showed a decrease of 41% and 13% respectively with only the 2-minute time point being significant when analysed using a T test (p=<0.001) (Fig. 4.14c). At 6 minutes MDCKII$^{mCh\text{-}EB2}$ cells had an increase in intensity of 73% at 6 minutes, this was significant when analysed using a T test (p=0.015).
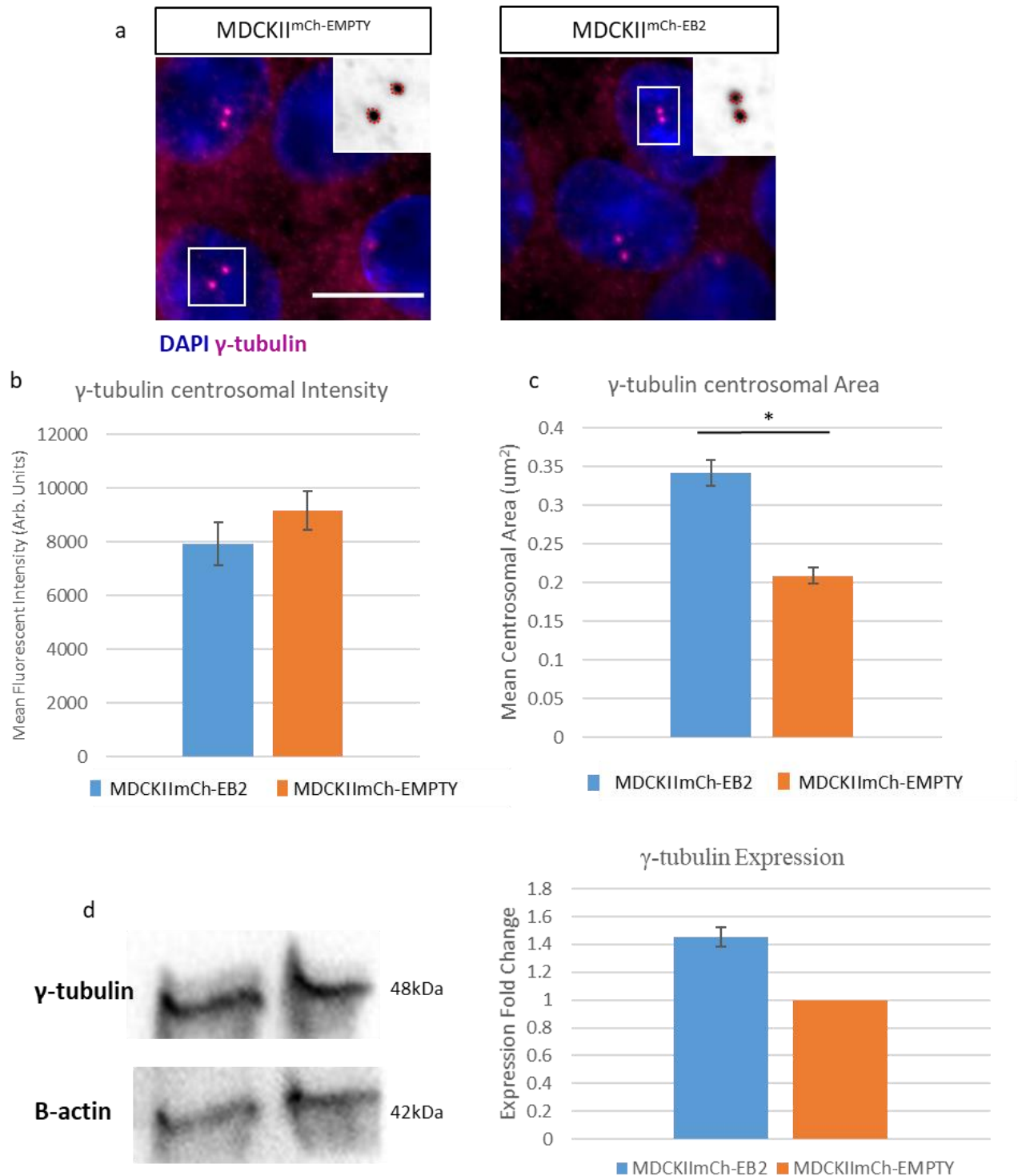
Figure 4.13 γ-tubulin analysis in MDCKII^mCh-EMPTY and MDCKII^mCh-EB2 cells. (a) MDCKII cells seeded sub-confluent on glass and immunolabelled for γ-tubulin with DAPI counterstain, imaged using fluorescence widefield microscopy. Enlargements show centrosomes with red dotted line representing measured area. Scale bar= 10μm. (b) Quantification of γ-tubulin intensity at the centrosome. No significant difference was seen in measured intensity at the centrosome. N=72 centrosomes, 3 experiments. +/- 1 SE shown. (c) Quantification of centrosome area labelled with γ-tubulin. MDCKIImCh-EB2 showed a significant (p=0.015) increase in centrosomal area when labelling for γ-tubulin. n=72 centrosomes, 3 experiments. +/- 1 SE shown. (d) Expression analysis of γ-tubulin using western blot with normalised intensity analysis against β-actin. MDCKII^mCh-EB2 cells showed 42% increase in γ-tubulin expression compared to MDCKII^mCh-EMPTY cells. More experiments are needed to determine significance. +/- 1 SE shown. n=2 western blots.
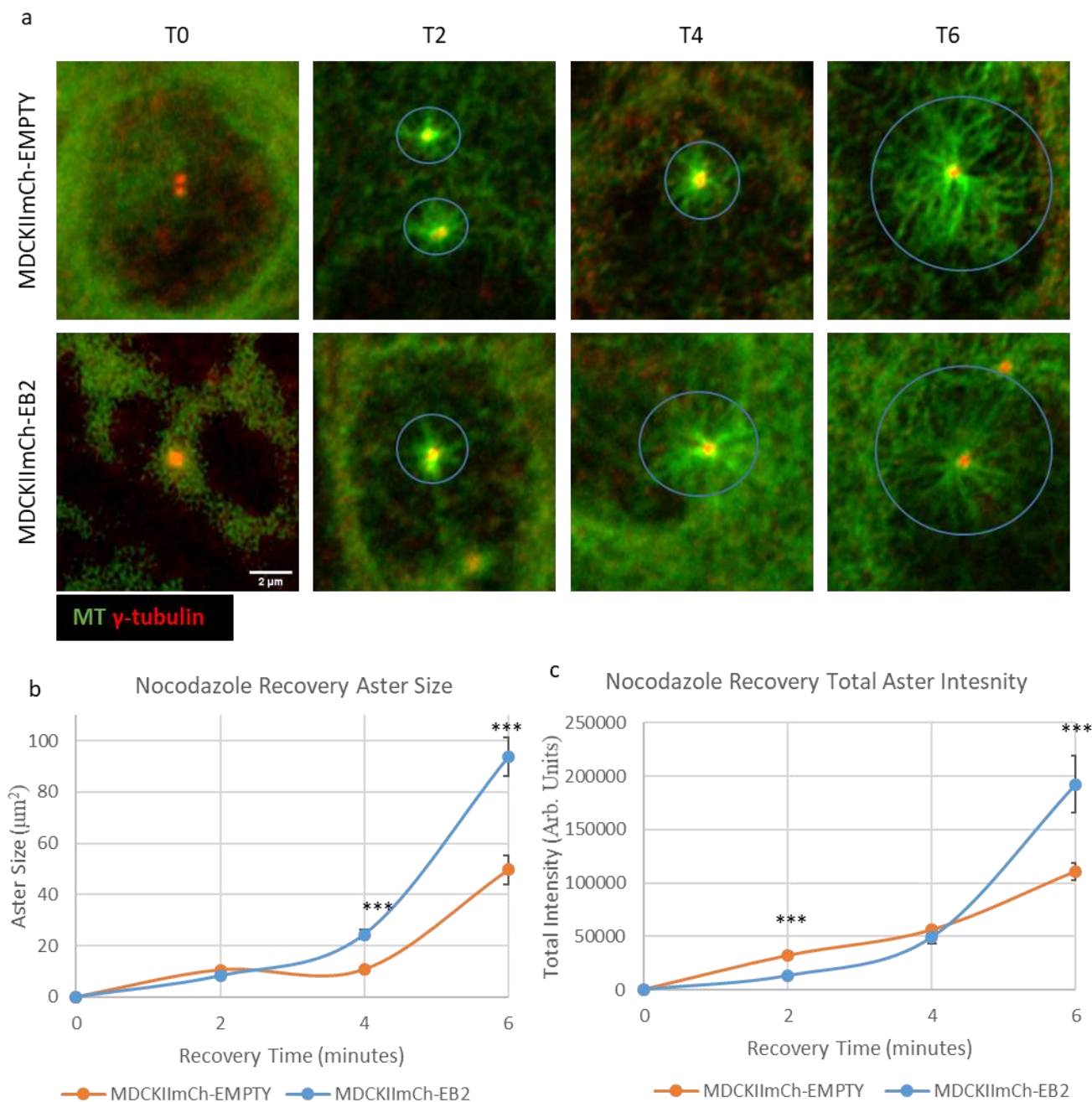
Figure 4.14 Analysis of microtubule nucleation and assembly using Nocodazole regrowth assay in MDCKII^mCh-EMPTY and MDCKII^mCh-EB2 cells. (a) MDCK cells seeded on glass and treated with Nocodazole to depolymerise MTs. Immunolabelling for γ-tubulin (red) and MTs (green) was carried out and images were taken using a widefield fluorescence microscope. Time points shown are with nocodazole (T0) and 2, 4 and 6 minutes (T2, T4 and T6) of recovery after Nocodazole washout. MT asters (blue circle) were quantified in terms of size (b) and fluorescence intensity (c) scale bar= 2μm. (b) Analysis of aster size show a significant increase in size only after 4 mins recovery in MDCKII^mCh-EB2 compared to MDCKII^mCh-EMPTY cells. (c) Analysis of the total fluorescence intensity of the asters reveal significant increases at 2 and 6 mins recovery but not at 4 mins in MDCKII^mCh-EB2 compared to MDCKII^mCh-EMPTY cells. +/- 1 SE shown. N= (MDCKII^mCh-EMPTY T2=14 asters, T4=23 asters, T6=12 asters), (MDCKII^mCh-EB2 T2=36 asters, T4=14 asters, T6=16 asters), 1 experiment.

Cep215 is a γ-tubulin accessory factor that greatly increases the nucleation activity of γ-tubulin and has been shown to anchor γ-tubulin to the centrosome and also move in EB1 dependent comets. This was analysed using Western blotting and fluorescent intensity measurements. However, the Cep215 antibody showed no reactivity in the Western blot, therefore only the fluorescence intensity analysis was carried out. This analysis showed no significant difference in intensity or staining area at the centrosome when analysing with a T test. Cep215 moves along MTs in distinct comets, the number of which were analysed (Fig. 4.16). Analysis was carried by immunolabelling for Cep215 with widefield fluorescence imaging, thresholding was then used in ImageJ to select the brightest pixels, these bright spots (comets) where then analysed using particle analysis again using ImageJ (Fig. 4.16b). This showed a drastic decrease of 57% in the number of Cep215 comets seen associated with MTs in the MDCKII$^{mCh-EB2}$ cells compared to the MDCKII$^{mCh-EMPTY}$ cells. This decrease in comet number was significant (p=<0.001) when using a T test. As Cep215 is transported via EB1, it made sense to study the effect of EB2 overexpression on EB1 comet number. This analysis showed that EB1 comet number was significantly increased in the MDCKII$^{mCh-EB2}$ cells by 34% compared to empty vector control cells (Fig. 4.17). Similarly, comet size and intensity were also significantly increased by 10% and 5% (p=<0.001) respectively with T test statistical testing (Fig. 4.17c,d). This suggests that these comets consist of a higher concentration and overall amount of EB1 protein. Additionally, comet circularity was significantly decreased by 5% in the MDCKII$^{mCh-EB2}$ cells (p= 0.003) although there was no significant difference in the ferret diameter (Fig. 4.17 e and f).

As well as MT nucleation, the centrosome also anchors MTs via the MT minus end anchoring protein ninein. To determine if EB2 expression influences the MT binding ability of the centrosome during differentiation, the effect of EB2 overexpression on ninein was analysed. Western blot analysis was used to measure total ninein expression and immunolabelling was carried out to determine ninein localisation at the centrosome. This analysis showed no significant difference in ninein intensity at the centrosome nor staining area at the centrosome (n=73 cell per group, 3 experiments). There was also no significant difference in ninein expression from the western blot analysis (n=1).

Pericentrin was also studied as it forms the scaffold of the PCM which many proteins including γ-tubulin bind to for their localisation at the centrosome. This was done as before using western blot and fluorescent intensity measurements. There was no significant difference in the intensity or area of the centrosome when labelling for pericentrin (n=64, 3 experiments). Similarly, there was no significant difference in overall pericentrin expression (n=3 experiments).
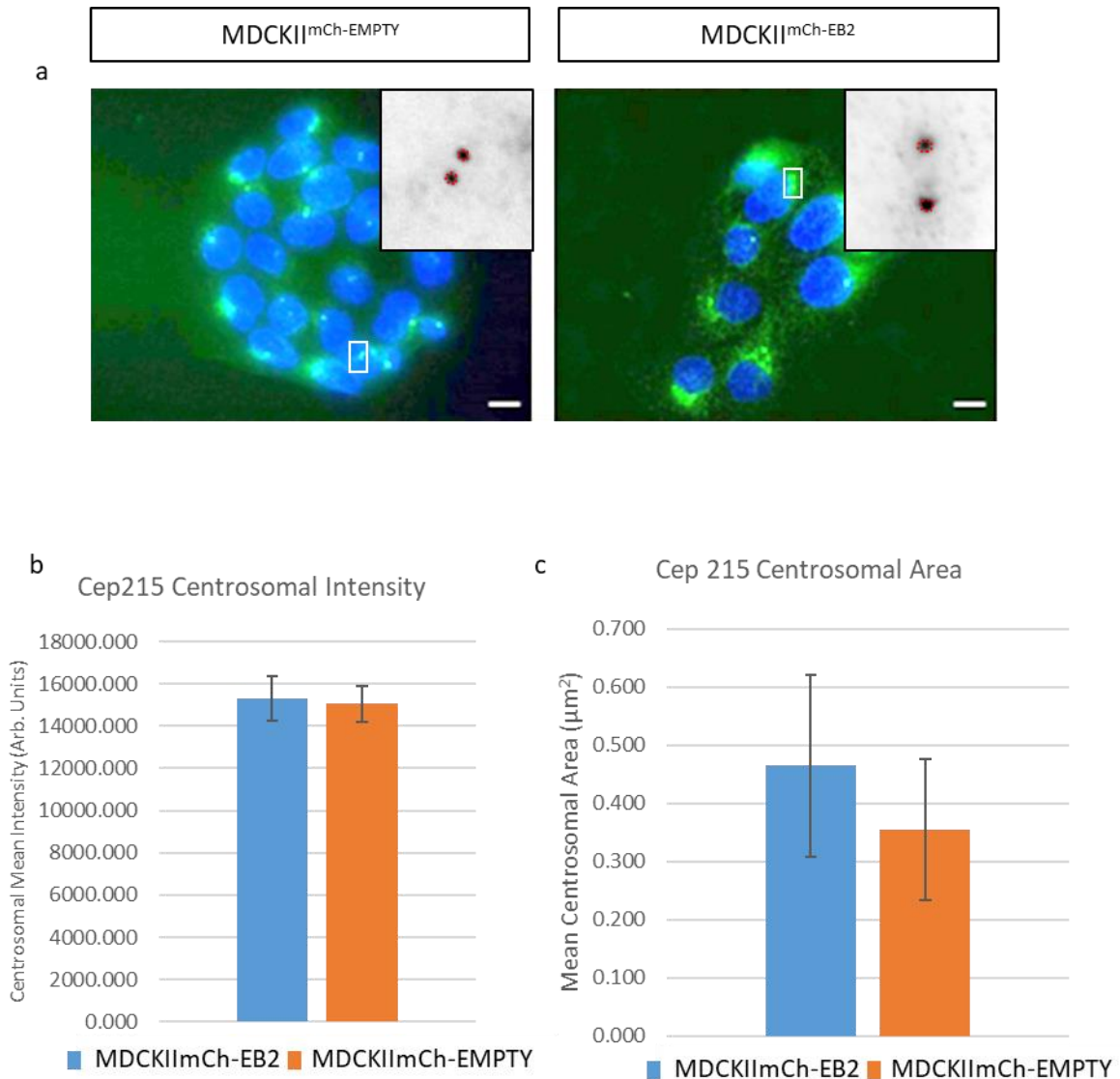
Figure 4.15 Centrosomal Cep215 analysis in MDCKII^{mCh-EMPTY} and MDCKII^{mCh-EB2} cells. (a) MDCKII cells seeded on glass and immunolabelled for Cep215, imaged using fluorescence widefield microscopy and analysed using ImageJ. (b) Quantification of Cep215 intensity at the centrosome. No significant difference in Cep215 intensity was seen at the centrosome between MDCKII^{mCh-EMPTY} and MDCKII^{mCh-EB2} cells. (c) Quantification of Cep215 staining area at the centrosome. No significant difference in Cep215 centrosomal area was seen between MDCKII^{mCh-EMPTY} and MDCKII^{mCh-EB2} cells. Scale bars= 10µm. n=65 cells, 3 experiments.
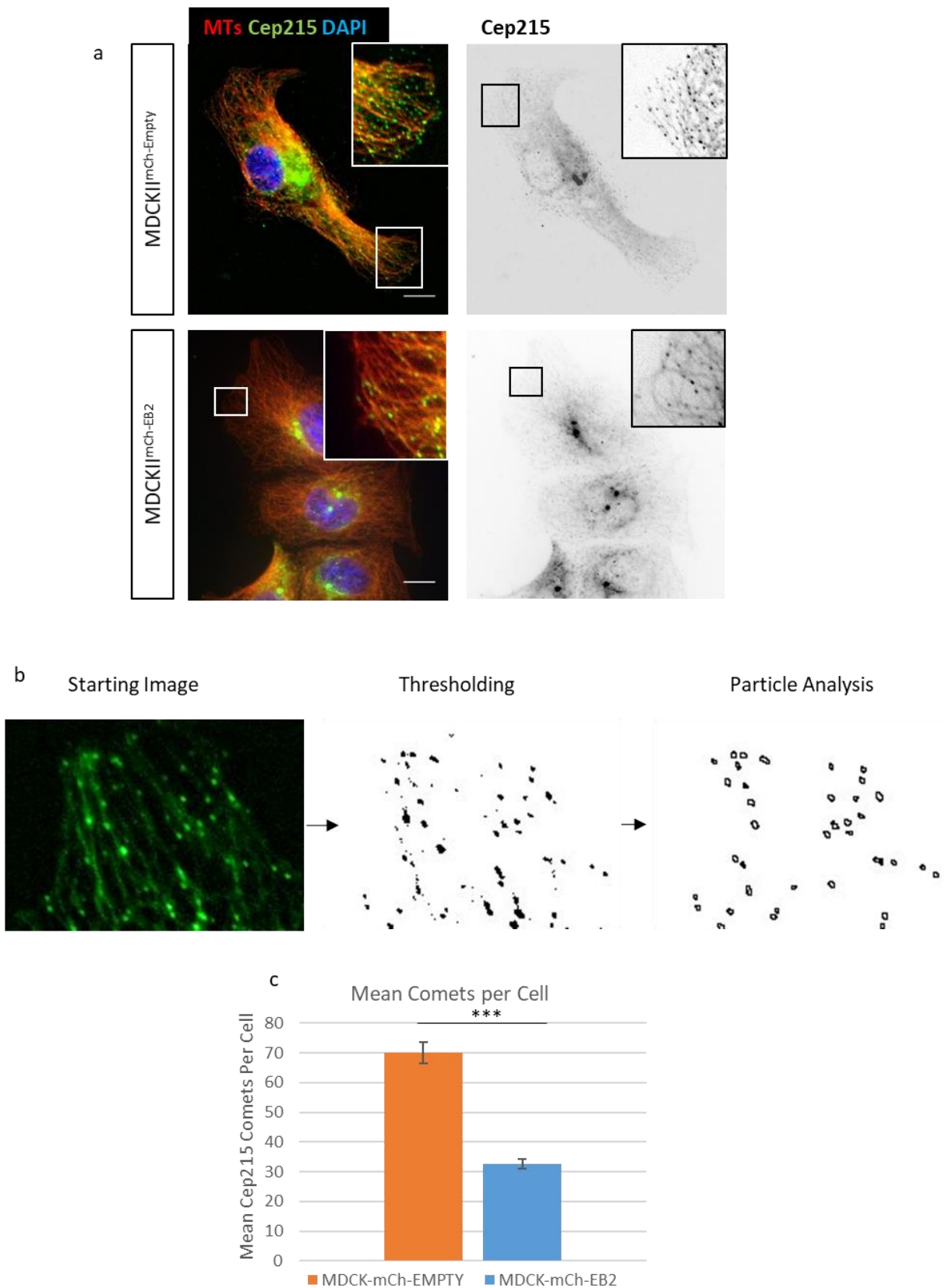
Figure 4.16 Cep215 microtubule comet analysis in MDCKII^mCh-EMPTY and MDCKII^mCh-EB2 cells. (a) MDCKII cells seeded on glass for 2 days, immunolabelled for CEP215 (green) and MTs (red) and visualised using widefield fluorescence microscopy. Scale bar= 10μm. (b) Example of image analysis work flow for comet measurement showing original image then thresholding based on pixel intensity and finally particle identification and measurment using ImageJ. (c) Analysis of Cep215 comet frequency per cell. MDCKIImCh-EB2 cells showed a significant decrease in mean comet number per cells of 53%. +/- 1 SE shown. P=<0.001. n=15 cells, 3 experiments.
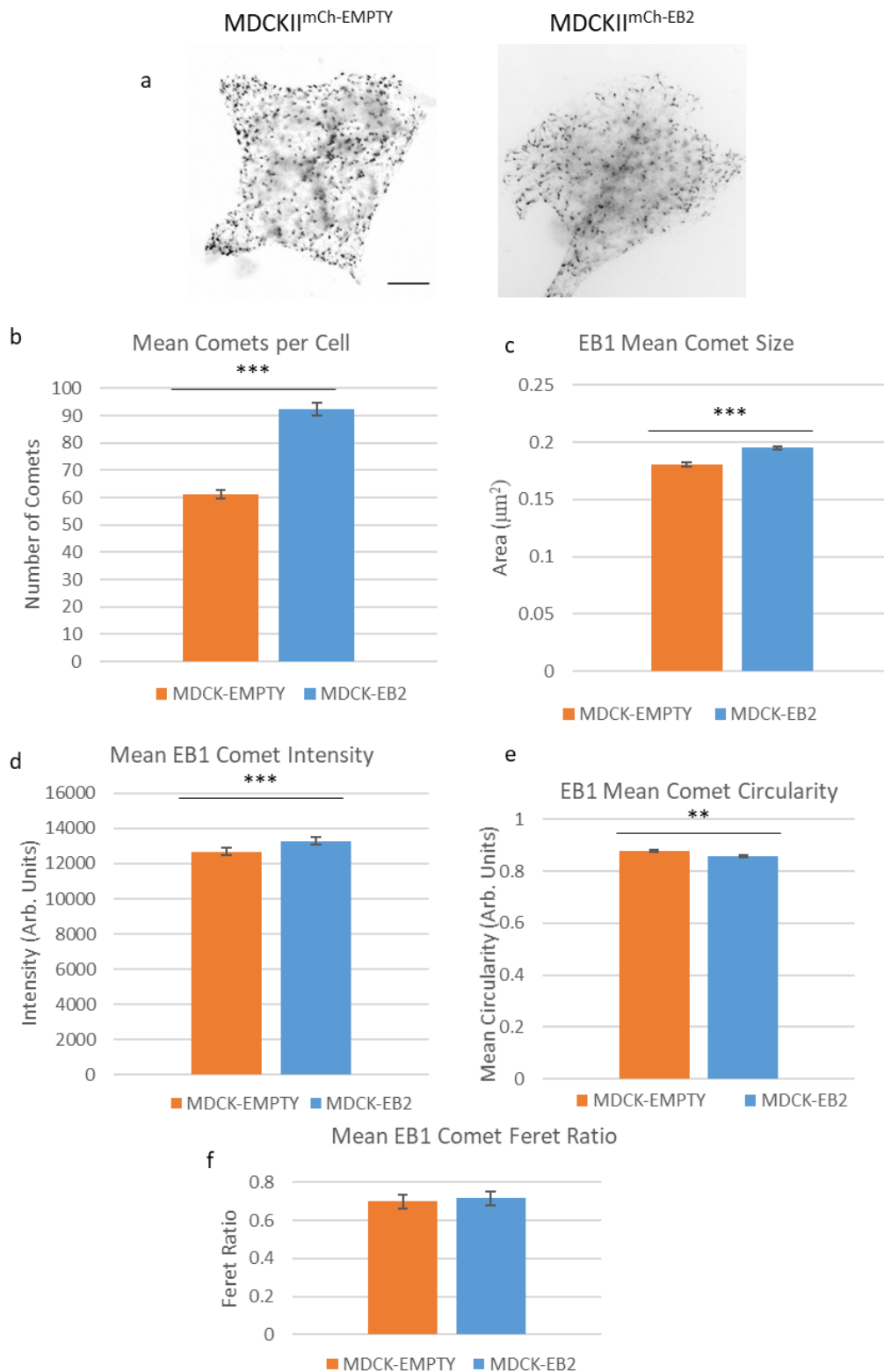
Figure 4.17 Analysis of EB1 microtubule comets in MDCKII^mCh-EMPTY and MDCKII^mCh-EB2 cells. (a) MDCKII cells seeded on glass and immunolabelled for EB1, imaged using fluorescent widefield microscopy. Scale bar= 10µm. (b-f) Quantification of EB1 analysis showing mean number of comets per cell (b), mean EB1 comet size (c), mean EB1 comet intensity (d), mean EB1 comet circularity (e) and Mean EB1 comet feret ratio (f). (b-d) Measures size, frequency and intensity of comets, (e and f) Measures circularity and ferret ratio which is used to determine if comets remain circular or become elongated which is shown by ferret ratio (the ratio between longest and shortest measurements). MDCKII^mCh-EB2 cells show significantly increased comet number per cell with increased comet size and intensity. The circularity of these comets was significantly decreased in MDCKII^mCh-EB2 cells with no difference in the ferret ratio. +/- 1 SE. n= mCh-EMPTY:54 cells, mCh-EB2:44 cells, frequency $p<0.001$, size $p<0.001$, intensity $p<0.001$, circularity $p=0.003$. 1 experiment.
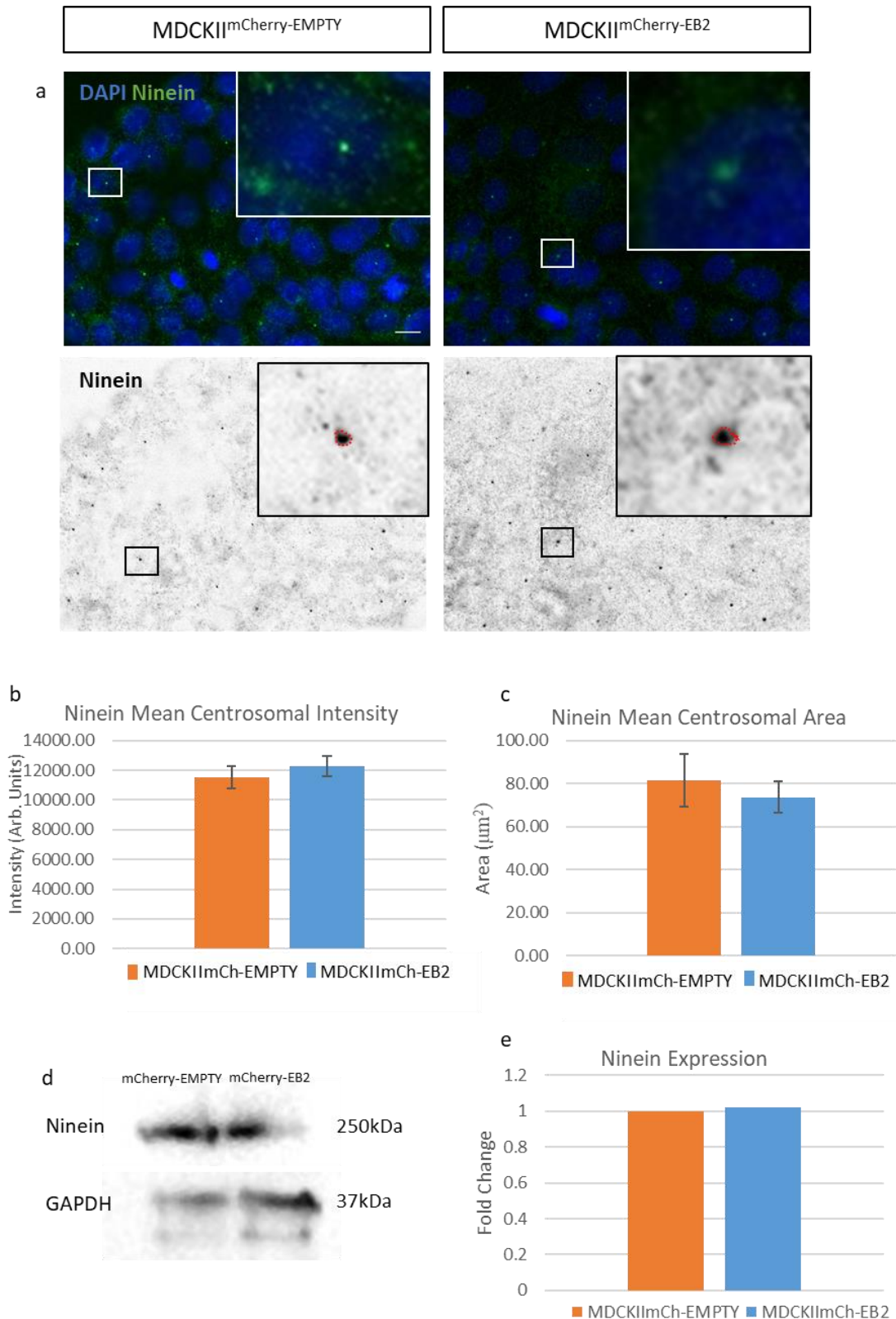
Figure 4.18 Analysis of ninein expression and localisation at the centrosome in MDCKII^{mCh-EMPTY} and MDCKII^{mCh-EB2} cells. (a) MDCKII cells seeded on glass, immunolabelled for ninein and imaged using widefield fluorescent microscopy. Enlargements show mother centriole with measurement area (red dotted line). (b) Analysis of mean ninein intensity within centrosomal measurement area. No significant difference was seen in centrosomal intensity between groups. +/- 1 SE shown. (c) Quantification of mean ninein staining area at the centrosome. No significant difference was seen in ninein staining area at the centrosome between groups. +/- 1 SE shown, n= 73 centrosomes, 3 repeats. (d) Western blot labelled for ninein and GAPDH as a loading control. (e) Quantification of western analysis showing normalised ninein expression. 1 western blot. +/- 1 SE shown.

116
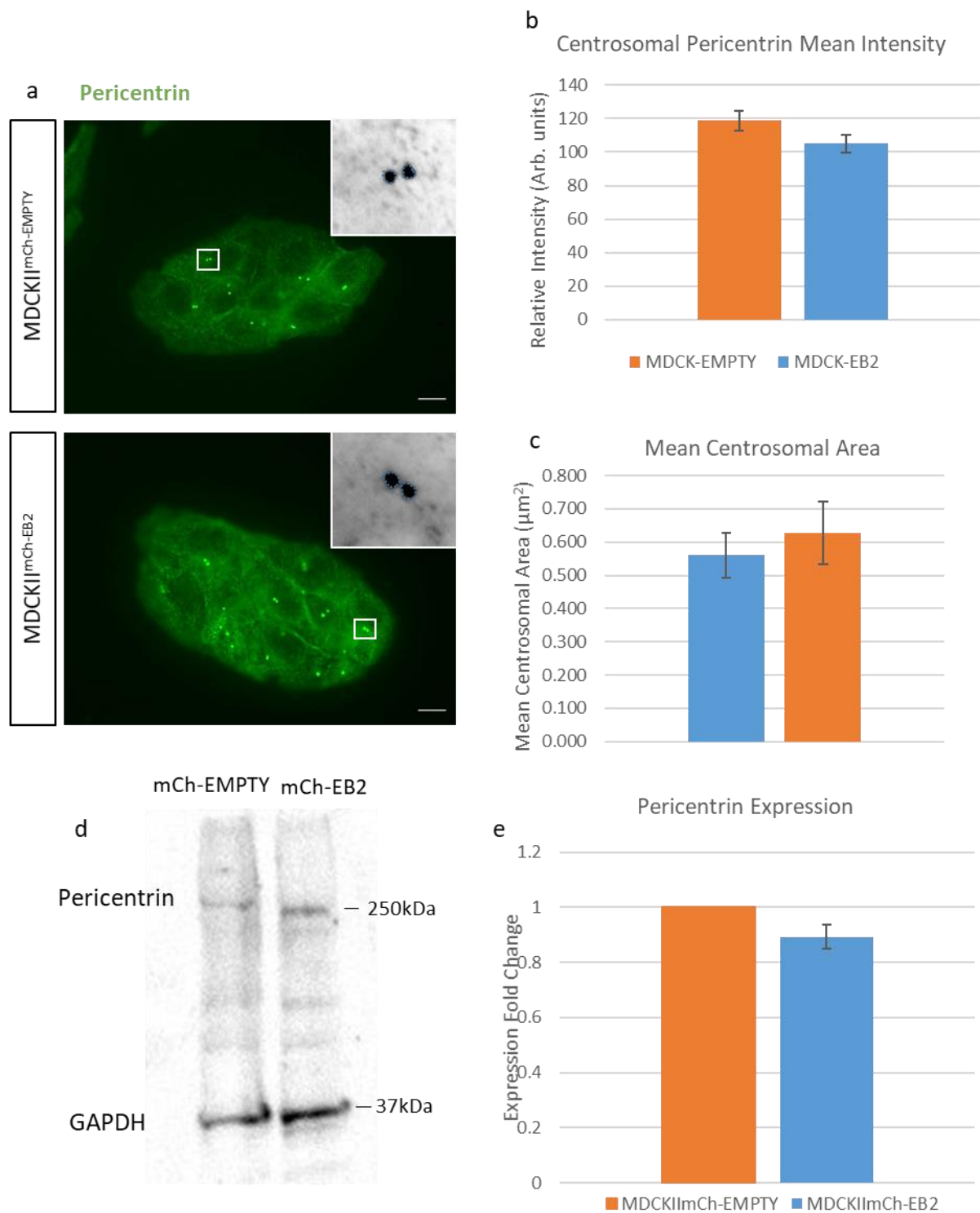
Figure 4.19 Analysis of pericentrin expression and accumulation at the centrosome in MDCKII[mCh-EMPTY] and MDCKII[mCh-EB2] cells. (a) MDCKII cells seeded on glass, immunolabelled for pericentrin and visualised using fluorescent widefield microscopy. (b) Analysis of mean pericentrin intensity at the centrosome. There was no significant difference in mean pericentrin intensity at the centrosome between groups. N=64 centrosomes per group, 3 experiments. +/- 1 SE shown. (c) Analysis of the mean pericentrin centrosomal area. There was no significant difference in pericentrin centrosomal area between groups. n=64 centrosomes per group, 3 experiments. +/- 1 SE shown. (d) Western blot labelling of pericentrin and GAPDH as the loading control. (e) Analysis of western blot analysis with normalisation based on GAPDH labelling. No significant difference in pericentrin expression was seen between groups. +/- 1 SE shown, n=3 western blots.

117

4.3.8 High EB2 expression lead to CAMSAP2 decorated Golgi in Panc-1 but not MDCKII cells

Previous research has shown that during differentiation, MTs detach from the centrosome and become organised at ncMTOCs. Here, CAMSAP2 may be used as a MT minus end marker to show where non-centrosomal MTs are anchored and organised. This was analysed in MDCKII$^{mCh-EB2}$ and MDCKII$^{mCh-EMPTY}$ cells and showed that there was no significant change in the area of the Golgi or colocalization of CAMSAP2 at the Golgi (Fig 4.20). Previous work from the Mogensen lab sub cloned Panc-1 cells to produce clones with varying levels of EB2 expression (Gadsby, Thesis). Two such clones, one with very high EB2 expression and one with very low EB2 expression were compared. Using these Panc-1 sub clones, CAMSAP2 association with the Golgi was analysed (Fig 4.21). This showed that 15% more CAMSAP2 decorated the Golgi in the high EB2 expressing Panc-1 clone compared to the low clone, although this was not significant due to the large variation seen in the results. Observation of CAMSAP2 staining shows that CAMSAP2 stretches (likely decorating MTs) can be seen far more widespread in the low EB2 expressing cell clone when compared high EB2 expressing clone. These stretches can be seen throughout the low EB2 cells whereas the high EB2 expressing cells show almost no CAMSAP 2 stretches except very close to the Golgi.
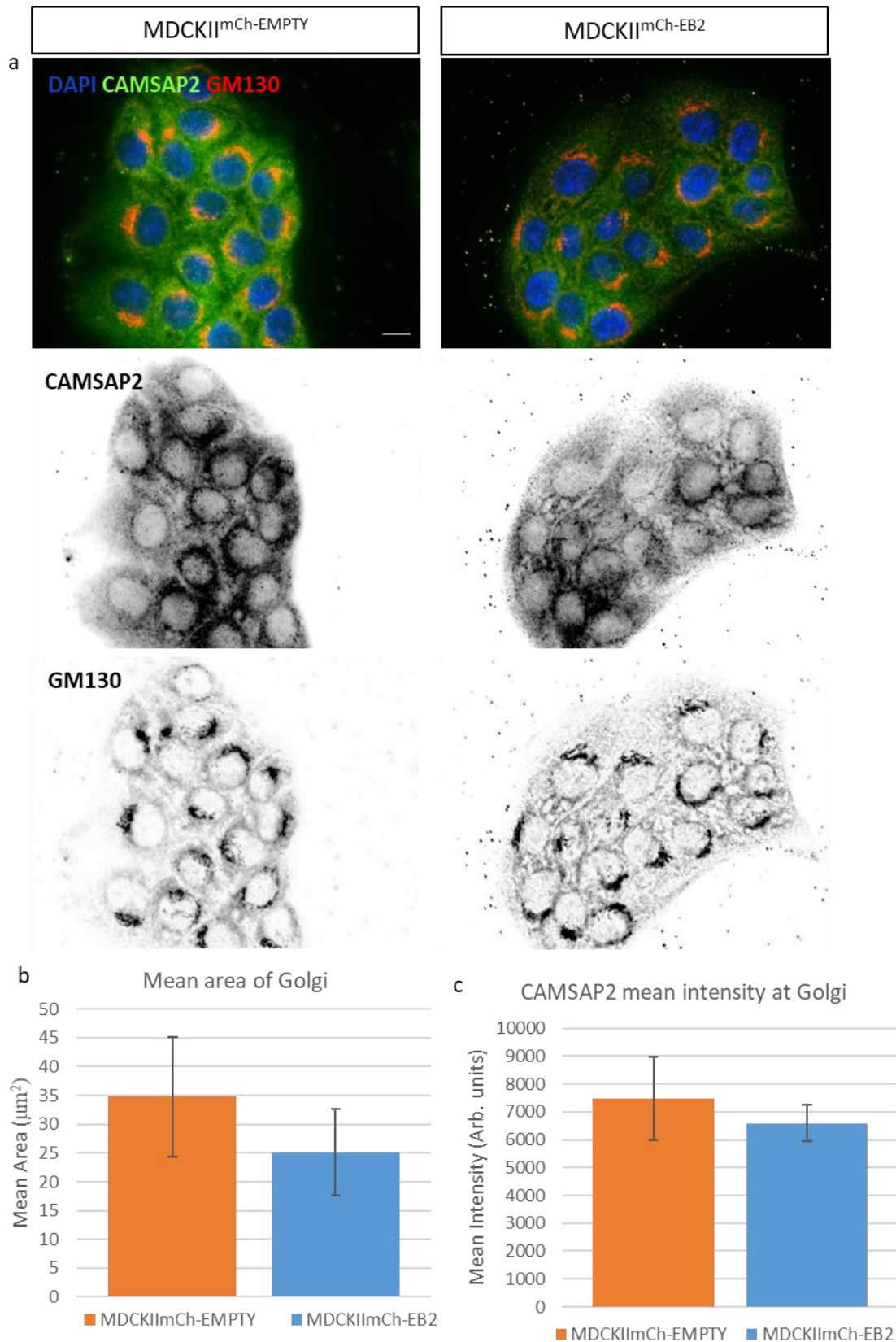
Figure 4.20 CAMSAP2 localisation at the Golgi in MDCKII^mCh-EMPTY and MDCKII^mCh-EB2 cells. (a) MDCKII cells seeded on glass, immunolabelled for CAMSAP2 (green) and GM130 (Golgi) (red), visualised via fluorescence widefield microscopy. (b) Analysis of Golgi size using GM10 as a marker. There was no significant difference in the area of the Golgi between groups. +/- 1 SE shown (c) Analysis of CAMSAP2 intensity at the Golgi. There was no significant difference in CAMSAP2 and GM130 colocalization between groups. +/- 1 SE shown. MDCK EB2 n=99 cells, MDCK EMPTY n=60 cells, 1 experiment.

119
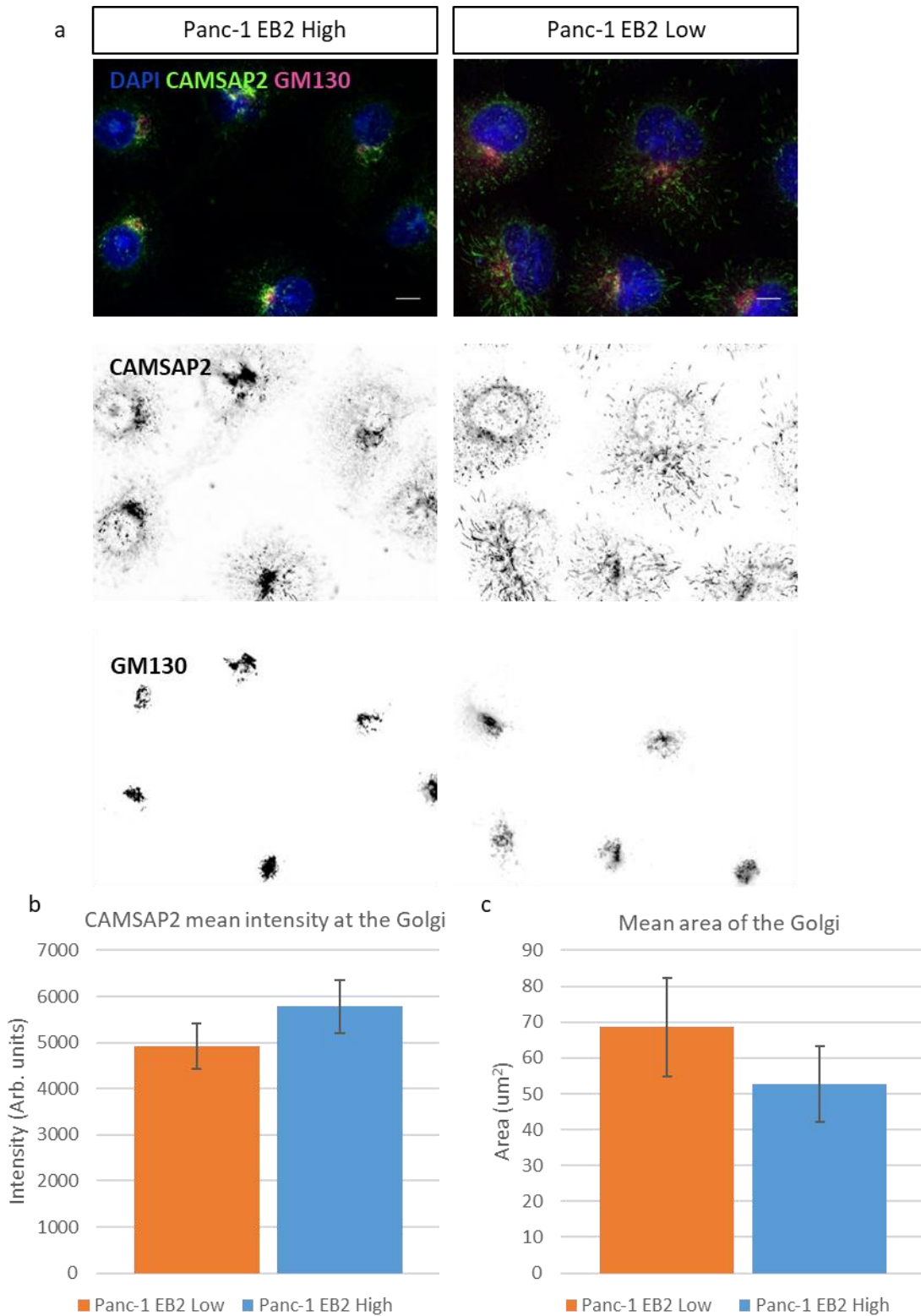
Figure 4.21 CAMSAP2 decoration at the Golgi in Panc-1 cells. (a) Panc-1 sub clones with a high or low expression of EB2 immunolabelled for GM130 (red) and CAMSAP2 (green), visualised using widefield fluorescence microscopy. Scale bars= 10µm. (b) Analysis of mean CAMSAP2 intensity at the Golgi. There was no significant difference in CAMSAP2 colocalization with GM130 between groups. +/- 1 SE shown. (c) Analysis of GM130 area at the Golgi. There was no significant difference in the area of the Golgi between groups. +/- 1 SE shown. n=78 cells, 1 experiment.

4.4 Discussion

4.4.1 MDCKII cells overexpressing mCherry-EB2 as a model of high EB2 expression

The generation of the MDCKII cells expressing the mCh-EB2/mCh-EMPTY vectors can be seen in detail in section 2.1. In brief, WT MDCKII cells were transfected with a vector containing mCherry unattached (EMPTY) or attached to mouse MAPRE2 (EB2) under the control of a highly active promoter (CMV) to ensure high expression. These cells were sub-cloned and clones with vector expression were maintained using G418 antibiotic selection, resistance for which was contained with the vector backbone. Use of the empty vector cell line as a control was a useful tool and rules out any unknown effects that expression of mCherry may have on these cells. A potential improvement that could be made to this is the inclusion of a WT MDCKII group for comparisons to the empty vector control cells. Although this is not essential as comparisons should always be made to the empty vector control cells rather than WT if included. It was shown that empty vector cells express 1.8 fold more mCherry compared to MDCKII^mC-EB2 cells which is not ideal as the same expression is desired to ensure that the potential effect of mCherry is accounted for. However, the fact that MDCKII^mCh-EMPTY cells express higher mCherry allows for comparisons to be made as any effect of mCherry would be observed in these cells.

Importantly MDCKII^mCh-EB2 cells showed the presence of exogenous EB2 expression when analysed using Western blot analysis. However, it was impossible to quantify the increase in EB2 expression using this analysis as the EB2 antibody showed no reactivity to canine EB2 when carrying out Western blotting. This is likely caused by antigen loss from protein denaturation as part of the Western blotting protocol as our anti EB2 antibody does show reactivity when used for immunolabelling of canine cells. This lack of antibody reactivity highlights an issue with using canine cells, less conserved proteins may show enough deviation to lose reactivity. Nonetheless, the presence of exogenous mouse EB2 was detected in MDCKII^mCh-EB2 cells showing that these cells can be used as a model for EB2 overexpression. Ideally endogenous EB2 would also be measured to confirm it remains unchanged although this was not possible in this study. The addition of exogenous EB2 to these cells means that this model compares a high EB2 expression to a 'normal' WT EB2 expression rather than comparing high to low expression. Therefore, this model is very useful for the study of the high EB2 expression seen in the early stages of some epithelial cell polarisation and elucidating the effect of this high expression.

MDCKII^mCh-EB2 cells were significantly larger than the MDCKII^mCh-EMPTY cells. The major effector of cell size is the length of time cells remain in interphase. The longer cells remain in these growth phases the larger they generally are (Bjorkland *et al.,* 2006). Here, to determine if these cells are larger due to increased growth phases, proliferation curves were collected over 72 hours. This growth curve

showed that MDCKII^mCh-EB2 cells did show a slight decrease in proliferation, which only became significant after 72 hours. This is likely because the difference was small enough to only become apparent at a later time period due to the exponential nature of cell growth. Therefore, this increase in cell size is likely caused or at least contributed to by an increase in interphase time caused by the EB2 overexpression. It is possible that the mitosis time is also increased due to high EB2 expression. Previous research has shown that EB2 is phosphorylated to reduce its affinity to MTs prior to mitosis. This effect was essential for mitosis to occur therefore overexpression of EB2 potentially disrupted this process (Limori *et al.,* 2006). Overexpression may led to some unphosphorylated EB2 remaining bound to MTs and preventing MT reorganisation during mitosis. Further exploration is needed to determine if increased EB2 expression causes a proportion of the EB2 to remain unphosphorylated to disrupt/prolong mitosis.

4.4.2 EB2 overexpression perturbs the normal localisation of the PAR3 polarity marker

Previous research has shown that EB2 expression changes in some epithelial tissues depending on the differentiation level of the cells in the system. Goldspink *et al*., (2013) showed this in isolated adult mouse small intestinal crypts where EB2 expression was very high in the base of the crypt. Very little expression of EB2 was seen in more differentiated cells containing bundles of MTs such as the transit amplifying cells and enterocytes. This suggests that loss of EB2 occurs in some differentiated cells that assemble bundles of MTs while undifferentiated cells such as stem cells that contain unbundled MTs require EB2 to maintain their specificity. Currently it is unknown what effect excess expression of EB2 has on cell polarisation, elongation and apico-basal MT organisation.

As there are many factors that determine cell polarisation it is unclear if EB2 expression modification alone is enough to affect this. To model increasing polarisation *in vitro*, MDCKII cells with or without EB2 overexpression were grown for varying time periods to study the effect of EB2. As time/confluences increases so does the differentiation/polarisation level of the cells. The prediction was that EB2 overexpression would reduce cell elongation and therefore height, likely due to EB2s effect on MT reorganisation and dynamics. Indeed, the MDCKII^mCh-EB2 cells were significantly shorter although only up until day 9 when there was no difference. This suggests that EB2 overexpression did not prevent epithelial cell polarisation although perturbed its development. This effect supports the prediction and previous research although confirms that overexpression alone is not enough to prevent these cell from elongating as normal in this system as cells ultimately reached the same maximum height. To explore the effect of EB2 and further determine its influence on polarisation, the polarity marker PAR3 was analysed as its localisation is a key event in the polarisation process. As

before the prediction was that EB2 overexpression would cause a detrimental effect to the normal apical junctional positioning of PAR3 in polarising cells. Accordingly, PAR-3 localisation revealed that it was greatly disrupted upon the overexpression of EB2 with less at the cell-cell contacts and a vast increase of a mis localised cytoplasmic fraction.

Expression loss of PAR3 has been previously studied as a promoter of tumour metastasis and EMT although little work has been carried out on the mis-localisation of PAR3. Some deductions can be made on the effect of this PAR3 disruption based on previous research. One such study that investigated the effect of PAR3 mis localisation was by Schumann *et al.,* (2011), this research showed that PAR3 was mis localised in duodenal biopsies taken from patients suffering from Coeliac disease. This work describes no change in PAR3 expression, but with an abnormal partially intracellular fraction as seen in our results. The aPKC protein (part of the PAR polarity complex) was also mis localised in their study. This suggests that EB2 overexpressing cells may also show this phenotype of mis localised aPKC as PAR3 recruits aPKC to apical junctional sites, although this was not tested (Ishiuchi and Takeichi., 2011, Hao *et al.,* 2010). No conclusion was made to the cause of this, but one suggestion was cytokine induction especially from transforming growth factor β (TGFβ). Indeed, treatment with TGFβ shows similar PAR3 aberrations as EB2 overexpression in our work but PAR3 expression is not lost (Wang *et al.,* 2008). TGFβ is known to induce EMT, this is a well-known characteristic of TGFβ and previous work in the Mogensen lab show that high EB2 expression increases invasiveness, a characteristic of EMT (Amodu., 2018). Recent research by Zhong *et al.,* (2021) studied the effect of EB2 in hepatocellular carcinoma and showed that high expression predicts poor prognosis. It was shown that high EB2 expression induced invasion and metastasis by Src and p-ERK1/2 activation. Again, this suggests that EB2 overexpression may be inducing EMT like behaviour in our system. Loss of PAR3 has also been shown to perturb cell-cell cohesion as it was required for E-cadherin junction stability (Xue *et al.,* 2012). Disruption of PAR3 localisation to the junctions may affect the E-cadherin accumulation here and therefore effect the ability of these cells to polarise/differentiate as junctional abnormalities are also seen in our results which is another marker of EMT. These results may suggest that the EMT inducing effect of EB2 overexpression may influence our results to such a degree that its function during apico-basal polarisation may be difficult to determine using this method. It is likely that the EMT inducing ability and its role in apico-basal are intrinsically linked and warrant further study.

Junction architecture was analysed in MDCKII$^{mCh-EMPTY}$ and MDCKII$^{mCh-EB2}$ cells grown at increasing time periods. The key difference in these results was seen at the later stages of differentiation/polarisation, particularly in MDCKII$^{mCh-EB2}$ cells at day 7 and 9 which are considered the most polarised time points. Here, peak intensity of E-cadherin was significantly decreased with more

adjacent intensity in MDCKII[mCh-EB2] cells. The question is why was E-cadherin localisation affected at these time points and not before (Fig 4.6)? One possibility is that mechanical forces differ within the cell layer at these later time points. Previous research shows that mechanical forces play critical roles in adherens junction composition and dynamics (Pinheiro and Bellaiche., 2019). Liu *et al.,* (2010) showed that force has a direct relationship with adheren junction size, increase in force caused an increase in junction size and *vice versa.* As MDCKII[mCh-EB2] cells show such an increase in adherens junction size although this is assumed from the diffuse E-caherin, traction forces are a potential cause of this. It should be noted that the averaged line profiles are not a good measurements of junction size and E-cadherin diffusion as irregular shaped junctions will be hidden due to the averaging effect. A better comparison of junction size and E-cadherin diffusion can be made from single representative plots such as those shown in figure 4.6 c and e (Liu *et al.,* 2010). Quantification of these plots was difficult as severe junction abnormalities could not be quantified by size, therefore reducing the difference seen between groups as shown in figure S4.

To explore this further, epithelial tugging forces were decreased via the use of blebbistatin (myosin inhibitor) and Y27632 (ROCK inhibitor). Tugging forces are applied to junctions via actin which is connected to the junctions by the catenin family that bind directly to the intracellular E-cadherin domain. The motor protein myosin II generates the forces that pulls on the junctions to influence cell movement, shape and morphogenesis (Lecuit and Lenne., 2007). Priya *et al.,* (2015) show that myosin II directed scaffolding of ROCK1 protects RhoA from suppression leading to maintenance of junction tension. Therefore, inhibition of activated myosin or ROCK would reduce junctional tension and reduce junction size and E-cadherin diffusion. The partial recovery of junctional width/size with blebbistatin treatment suggests that the increase in junction width in MDCKII[mCh-EB2] cells may be caused by increased tugging forces at the junctions or by decreased junction tension. Furthermore, treatment with Y27632 to antagonise cytoskeletal tension by inhibiting Rho kinase also appeared to reduce junction width in the MDCKII[mCh-EB2] cells, further suggesting that EB2 overexpression increases tugging forces/decreases junction tension and increasing junction size and E-cadherin diffusion. Activated myosin was the same between MDCKII[mCh-EMPTY] and MDCKII[mCh-EB2] which suggests that force was equivalent, suggesting that E-cadherin delivery/maintenance is affected rather than monolayer forces as it is myosin dependent tugging forces that regulate adherens junction assembly (Liu *et al.,* 2010). Although activated myosin is a small part of the process and many other factors such as mechanosensing by α-catenin/vinculin to modulate tugging forces at the junction (Dufour *et al.,* 2013).

To confirm that junction width measurements were not influenced by any differences in lateral membrane angle and irregularity, z-stack reconstructions were used. If enough lateral membrane deviation was present, then out of focus junction sections may be seen when imaging and

influence the results. This qualitative analysis showed that junctions remain at similar angles and without enough deviation to cause the results seen here. Some basal staining of E-cadherin was seen here which may contribute to the appearance of diffuse junctions although more work is needed to determine if this is E-cadherin staining or non-specific staining. Ideally to confirm the cause of these junctional changes, measurements of the forces within the cell monolayer would be made. This can be done in several ways reviewed by Pineiro and Bellaiche (2018), most commonly laser ablation is used at cell-cell contacts and the retraction of cells is measured from the ablation site. Unfortunately, due to time constraints this was not possible in our experiments.

Another possibility for the differences in junctions in MDCKII[mCh-EB2] is turnover of E-cadherin, lowering junction tension making them more prone to the forces applied and increasing the width and size of the junction and E-cadherin diffusion. Zhong *et al.,* (2021) recently discovered that high EB2 expression in hepatocellular carcinoma induced activation of Src, which in turn has been shown to cause the internalisation of E-cadherin from the junctions, suggesting that EB2 overexpression is reducing E-cadherin at junctions due to increased internalisation. This may also effect the changes in shape index seen and a lack of cell-cell adhesion may also explain an increase in cell size as contractile forces overcome tensile forces to pull cells in all directions, increasing size. Testing for E-cadherin turnover using fluorescent recovery after photobleaching (FRAP) would have been very useful in determining if E-cadherin delivery and turnover was affected. A good example of FRAP can be seen in Beco *et al.,* (2009) where it was shown that E-cadherin endocytosis is required for the maintenance of adherens junctions. Here E-cadherin at the junctions was bleached and a time series of GFP-E-cadherin recovery was tracked. If EB2 overexpression effects E-cadherin turnover, then it would be expected that after photobleaching of fluorescently tagged E-cadherin, recovery time would be increased in the MDCKII[mCh-EB2] cells. This was initiated but time did not permit these experiments to be completed. Fluorescent loss in photobleaching (FLIP) may also have been utilised which bleaches the pool of fluorescently tagged proteins and measures the loss of intensity at the site of interest, avoiding the damaging effect of the laser at this site. Biochemical approaches to study junctional E-cadherin such as biotinylation could also be used to identify the internalised pool of E-cadherin compared to the E-cadherin at the junction.

As a measure of the E-cadherin distribution, the fluorescence intensity of line profiles as a method worked well, capturing the diffuse nature of E-cadherin seen in the MDCKII[mCh-EB2] cells. The method was limited by the small measurement area as it only analysed a single line through the junction instead of the junction as a whole. Perhaps it would be better to measure total intensity measurements per field of view with the emphasis on the lower intensity pixels. This would better represent the diffused area of E-cadherin at junctions in MDCKII[mCh-EB2] cells. Widefield fluorescent

microscopy was used here to capture a larger area of the junction for analysis as confocal imaging would have been very selective and capture a smaller optical section. Ideally many optical sections would have been taken and reconstructed to examine the entirety of the E-cadherin staining at the junctions but this was not carried out due to time constraints.

There are of course other potential downstream effects of EB2 expression changes such as a change in MT dynamics. Previous research has shown that EB2 depletion decreases MT dynamics and produces relatively stable MTs. EB1 was shown to decorate the MT lattice in the absence of EB2 due to their competitive binding nature. The extended EB1 decoration was likely the reason for this MT stabilisation as it has the effect normally at the MT plus end (Goldspink *et al.,* 2013). Preliminary data on MT dynamics using plusTipTracker (Applegate et al., 2011) in MDCKII$^{mCh-EB2}$ and MDCKII$^{mCh-EMPTY}$ cells suggest that EB2 overexpression may affect MT dynamics with increased MT growth speed being evident (Amodu 2018, thesis). However, further analysis of MT dynamics using GFP-tubulin or SirTubulin will be needed to establish shrinkage and pausing events. Changes in MT dynamics may be the cause of the potential force changes seen in our experiments. MTs have the ability to generate force through the polymerisation/depolymerisation processes or from motor proteins such as dynein and the kinesin family (Kent and Lele., 2017). It is known that dynamic MTs are needed for the delivery of E-cadherin to adherens junction but excessive EB2 lattice binding may interfere with the delivery process (Stehbens *et al.,* 2006). The results from this study suggest that increased EB2 expression influences junction formation and maintenance most likely by perturbing E-cadherin localisation to adherens junctions.

Another aspect of apico-basal polarisation that may be affected by EB2 overexpression is the interaction between actin and MTs in bundles. As EB2 depletion causes ACF7 recruitment to MTs and actin co-alignment it is possible that overexpression prevents this bundling of actin and MT formation, perturbing polarisation (Goldspink *et al.,* 2013, Antonellis et al., 2014, May-Simera et al., 2016). This was not tested due to time constraints but labelling of ACF7 in this system may explore this further as Noordstra *et al.,* (2016) showed ACF7 was essential for the apical MT minus end organisation as knockout of EB2 leads to a more radial MT array. ACF7 therefore appears to act as a regulator of apico-basal polarisation.

Ultimately, abnormal PAR3 localisation suggests EMT may be induced by overexpression of EB2, E-cadherin downregulation is another characteristic of EMT (Sommariva and Gagliano., 2020). E-cadherin expression was not measured in this study but is another possibility for the difference in junctions and requires further exploration. Overexpression of EB2 may be inducing EMT rather than

modelling the difference seen during polarisation, analysis of cell jamming may shed some light on this.

4.4.3 EB2 overexpression caused unjamming in MDCKII cells

To further explore the effect of overexpression of EB2 on *in vitro* epithelial cells, the jamming/unjamming states of confluent MDCKII^mCh-EB2 and MDCKII^mCh-EMPTY cells were established. Described by Park *et al.,* (2015) the shape index may be used as a measurement of the transitional state or UJT of an epithelial layer. The shape index is used in the vertex model which mimics predicted cell characteristics, when cell adhesion is increased the shape index decreases as expected. Use of this model and the key transitional value of 3.813 can be used as a measure of cell epithelial stability, with shape index values below 3.813 being considered jammed and "healthy". The minimum shape index value is 3.5 and comes from a perfect circle and increasing deviation from a circle causes increasing shape index. Previous research using primary HBEC cells show shape index with time and cells become jammed (Park *et al.,* 2015). This model is superior to using cell area alone as this only quantifies difference in cell size and would not reflect jamming. Another option would be to calculate circularity although its relationship to unjamming is currently unclear, circularity is also a poor measure of shapes that greatly deviate from a circle, therefore this method loses definition in sever loss of circularity. An advantage of circularity is that it is unaffected by cell size changes and therefore does offer some advantages over shape index.

Currently the shape index is used as a measure of cell jamming and partial EMT (pEMT) which have subtle differences (see section 1.8.2). As described above and discussed here recent work has attempted to differentiate these two aspects of cell monolayers. Our work shows that as control MDCKII^mCh-EMPTY cells increase in confluence over time, the shape index decreases to a low of 3.81 after day 14. This is considered the point at which cells transition between jammed and unjammed states known as the UJT. A normal epithelial monolayer would usually be below this threshold, but as these cells were seeded onto glass in 2D, it is likely that this would have taken even longer. Seeding these cells onto semi-permeable layers or with external ECM most likely would achieve a shape index below the level seen here. Despite this, comparisons to EB2 overexpressing cells can still be made. This showed that EB2 overexpression consistently led to cells with a higher shape index at every time point, signifying a more unjammed state in these layers. The shape index means of these cells remained ~4 at every timepoint which suggests that time is not a factor here as shape index did not decrease as expected and as seen in control cells. Therefore, EB2 overexpression causes unjamming based on the shape index alone, however there is the question of pEMT. As explained in section 1.8.2, pEMT carries

several characteristics not identified in cell jamming. One characteristic is a partial loss of E-cadherin from junctions, likely replaced by N-cadherin as in EMT (Mitchel *et al.,* 2019). Total expression of E-cadherin was not tested in our work due to time constraints but would prove useful for detecting if EB2 is inducing EMT in these cells. EMT markers are another characteristic unique to pEMT and not UJT, again these were not tested but labelling for markers such as vimentin and N-cadherin may provide further answers.

The polarity marker PAR3 has been shown to be downregulated in EMT but not in unjamming, our experiments show loss of localisation at the junctions, instead PAR3 appears to remain more cytosolic in MDCKII^mCh-EB2 cells but expression was not quantified (Mitchel *et al.,* 2020, Wang *et al.,* 2008). The effect of pEMT has been attributed primarily due to diminished junctional tension, although this was not directly measured in our work. Increased junctional width suggests more tugging forces or a decrease in junctional tension or both. Although it should be mentioned that the migratory behaviour of pEMT induction in monolayers can also cause these junctional differences (Mitchel *et al.,* 2020). Based on these results it cannot be determined if EB2 overexpression is causing pEMT or UJT. To further study this, several characteristics should be examined such as the presence of EMT markers vimentin and N-cadherin. The presence of these would confirm the induction of EMT. Cell velocities should also be examined through live imaging as unjammed cells show increased motility as a whole compared to cells induced into pEMT (Mitchel *et al.,* 2019).

From these experiments it is unclear how EB2 overexpression causes increased shape index and unjamming/pEMT. More work is needed here to further explore the relationship between EB2, PAR3 localisation, junction structure and shape index. If EB2 overexpression causes UJT or pEMT should be elucidated to draw further conclusions. As shape index is affected by size and EB2 overexpressing cells show increased size, normalisation should be carried out in the future as the increase in cell size may cause the observed increase in shape index. Although the EB2 overexpressing cells shape index did not change over time which is the key result here, suggesting these cells are not jamming as control cells did. This difference also appeared to affect the number of cells per field of view as EB2 overexpression showed reduced numbers which would also decrease the jamming of cells, increasing the shape index.

4.4.4 EB2 overexpression leads to increased γ-yubulin and MT nucleation at the centrosome
The centrosome is another important aspect of epithelial apico-basal polarisation and several changes have been identified at the centrosome during polarisation. These changes include the redistribution of proteins such as ninein, NEDD1 and Cep215 to new ncMTOCs (Moss *et al.,* 2007,

Muroyama *et al.,* 2016). The full extent of these changes is yet to be elucidated. Positional changes also occur as the centrosome moves apically and then disappears or remains as a site for MT nucleation only depending on the cell type (see section 1.8) (Carvajal-Gonzalez *et al.,* 2016). As EB2 expression changes with differentiation in some apico-basal *in vivo* and *in vitro* epithelial cells it was important to determine if EB2 expression effected the composition and behaviour of the centrosome (Goldspink *et al.,* 2013). As EB2 is expressed highly by undifferentiated cells, it is predicted the EB2 overexpression studied here maintains nucleation and anchorage at the centrosome.

To assess if EB2 effects the centrosome composition the intensity of key functional and structural proteins was analysed. Here both the fluorescence intensity and area of immuno-labelled centrosomal proteins was analysed as an increased concentration of a particular protein could be seen through an increase in area at the centrosome or though fluorescence intensity. Analysis of γ-tubulin showed a significant increase in area in EB2 overexpressing cells compared to control cells suggesting a potential increase in MT nucleation at the centrosome. EB2 therefore potentially plays a role in the maintenance of nucleation at the centrosome via γ-tubulin.

To determine if this increase in γ-tubulin expression and centrosomal area in MDCKII$^{mCh-EB2}$ cells confers a change in MT nucleation behaviour, a nocodazole regrowth assay was carried out. Nocodazole regrowth assays can be used to determine the location of nucleation as well as the extent of MTs nucleation. As γ-tubulin was increased at the centrosome it was predicted that MT nucleation would be increased at the centrosome. MT outgrowth and therefore length is controlled by interactions at the plus tip, so this is not likely affected by changes in γ-tubulin. As expected, α-tubulin intensity at the asters was increased in the EB2 overexpressing cell line in the later stages of recovery after MT depolymerisation. This suggests that increased EB2 expression in undifferentiated and early differentiated cells maintains MT nucleation at the centrosome which is a property of these cells in the intestinal crypts for example. From these results it is unknown what relationship EB2 and γ-tubulin have, and further experimentation is needed to describe this. As EB2 has been shown to indirectly effect MT dynamics this may be the mechanism behind this relationship. Some recruiters of γ-tubulin rely on MTs for their transport and have been shown to move along MT during differentiation of some cells. One such protein is Cep215 which functions to anchor and localise γ-tubulin at the centrosome. Intensity and size analysis of Cep215 show no significant difference at the centrosome although again centrosomal area was increased with EB2 overexpression, as Cep215 recruits γ-tubulin it makes sense that these two measurements would be comparable. It is known that Cep215 moves along MTs in comets, these Cep215 comets were analysed. This analysis showed that overexpression of EB2 caused a drastic decrease in the number of Cep215 comets seen along MTs. This suggests that EB2 prevents

movement of Cep215 along MTs in undifferentiated cells to maintain γ-tubulin nucleation and the centrosome, but how does this potential effect occur.

EB1 has been shown to transport Cep215 along MTs in comets, as EB1 and EB2 show competitive binding at MTs, EB2 maybe exerting an effect by outcompeting EB1 (Fong *et al.,* 2017, Goldspink *et al.,* 2013). To study this hypothesis, EB1 comet analysis was carried out in MDCKII[mCh-EMPTY] and MDCKII[mCh-EB2] cells. It was predicted that EB1 comet number would be decreased in EB2 overexpressing cells due to this competition, but the opposite was true. MDCKII[mCh-EB2] cells showed significantly increased comet number with increased size and intensity suggesting more EB1 is present at the MT plus tip. This significant increase in EB1 comet size and intensity with EB2 overexpression would explain why increased MT outgrowth is seen in the later stages of the nocodazole regrowth assay but it is unclear how EB2 causes this increase in EB1 and more elucidation is needed. Zanic *et al.,* (2013) showed that synergy between the MT polymerising agent XMAP215 and EB1 increased MT growth. EB1 has also been shown to induce tubulin sheet closure, a marker of MT growth (Vitre *et al.,* 2008). One possibility is that high EB2 expression and the subsequent MT lattice decoration causes EB1 to decorate a more specific MT domain at the plus end, increasing its size and intensity here due to more free EB1 available, the GTP cap area may also be enriched where this EB1 binds. GTP decoration is a marker of MT stability that recruits EB1 to encourage outgrowth (Zanic *et al.,* 2009). This notion is supported by the decreased circularity of these comets as this would cause more elongated comets and the increased outgrowth. Measuring of the GTP cap could add evidence to this concept or a tubulin assay study could investigate the relationship of EB1 and EB2 along MTs. Measuring of the GTP cap is a difficult task, one possibility is to use an anti-GTP tubulin antibody and measuring fluorescence from immunolabelling although these antibodies are not commercially available. Commonly fluorescently tagged EB1 is used to measure the GTP cap but this may not be suitable in this work as EB2 and EB1 show competitive binding and may not represent GDP or GTP tubulin respectively (Brouhard and Sept., 2012).

As well as nucleation the centrosome is also responsible for MT anchorage, ninein is responsible for this at the sub distal appendage of the mother centriole (Mogensen *et al.,* 2000). It has also been shown to move along MTs and accumulate at ncMTOCs during apico-basal polarisation and differentiation and therefore is potentially affected by the differential EB2 expression seen with differentiation (Moss *et al.,* 2007, Goldspink *et al.,* 2017, Goldspink *et al.,* 2013). As no significant difference was seen in ninein at the centrosome or overall expression it is unlikely the EB2 expression level effects the distribution of ninein during apico-basal polarisation. Again, more work is needed here as this conclusion may change if analysis is undertaken when ninein is induced to move along MTs to ncMTOC sites (Goldspink *et al.,* 2017). Another functional protein studied here was pericentrin.

Pericentrin is the scaffold of the centrosome and anchors numerous proteins and protein complexes. Through these interactions, pericentrin contributes to a diverse number of fundamental processes including the anchorage of γ-tubulin (Dictenburg *et al.,* 1998). As overexpression of EB2 had no significant effect on pericentrin centrosomal size and area it is unlikely EB2 exerts an effect on centrosomal function through the modification of the centrosomal scaffold.

4.4.5 High EB2 expression caused dispersed CAMSAP2 decoration in Panc-1 but not MDCKIIs cells

To assess the effect of EB2 overexpression on MTOC organisation at the Golgi, CAMSAP2 and Golgi (GM130) labelling was carried out and used as a marker of MT minus end accumulation. Although CAMSAP2 presence does not guarantee the presence of MT anchorage it may suggest it as previous research has shown this at the Golgi (Wu *et al.,* 2016). Despite this there was no difference in the intensity of CAMSAP2 seen at the Golgi with the overexpression of EB2 in MDCKIIs. This was also true when examining Panc-1 sub clones exhibiting high or low EB2 expression. Despite this, qualitative analysis of CAMSAP2 distribution in these Panc-1 cells showed a much wider distribution of short stretches that likely are decorating MTs. This suggests that EB2 influences the localisation of MTs and high EB2 expression localises MTs close to the centrosome possibly still at the centrosome or Golgi, although this cannot be determined from these results. Work from the Mogensen lab has shown that more invasive breast cancer cell lines show higher EB2 expression (Amodu 2018, thesis). A characteristic of migratory cells is Golgi organised MTs and these results suggests EB2 overexpression induces this although MT decoration here must be confirmed (Miller *et al.,* 2009). Further work is needed to explore this effect of EB2 overexpression as it offers evidence that EB2 is causing pEMT rather than UJT by inducing characteristics of migratory cells.

4.5 Summary

In summary, experiments carried out showed that the overexpression of EB2 effects several characteristics of epithelial cells. These changes fit with the model of high EB2 expression as a marker and regulator of undifferentiated cells. The results showed that EB2 overexpression increased cell size and led to increased junction width and disorder and reduced localisation of the PAR3 polarity marker. This in combination with the decreased height and increased shape index suggest changes indicative of a lack of differentiation. Centrosomal changes that likely maintain nucleation at the centrosome were also found, a characteristic of undifferentiated/proliferating epithelial cells. In the future, experiments need to be carried out to further explore the role of EB2, another aspect of its behaviour may be the control of mitosis as it is phosphorylated and removed from MTs before mitosis is imitated (Limori *et al.,* 2016). More work is needed to identify how EB2 exerts these effects, is it simply through changes in MT dynamics or are the more complex interactions at play? Another aspect to look into is the argument of EB2 causing unjamming or pEMT as there is evidence for both, these aspects may be intrinsically linked and may become an exciting area of research.

Chapter V:

**Generation of a MDA-MB-231
MAPRE2 KO Cell Line using CRISPR
Cas9**

5.0 Chapter V: Generation of a MDA-MB-231 MAPRE2 KO Cell Line using CRISPR Cas9

5.1 Overview

Research from the Mogensen lab has identified EB2 as a protein implicated in both apico-basal polarisation and cell migration (Amodu, 2018). Here, a EB2 knock-out (KO) is generated in the highly invasive MDA-MB-231 cell line in order to create a model for studying loss of EB2 in cell migration. This includes validation of the EB2 mutation, loss of protein and mRNA expression. Finally, some cell characteristics were determined in the KO MDA-MB-231 cell line such as cell size and migration velocity to assess the effect of loss of EB2.

5.2 Introduction

MDA-MB-231 cells have been widely used as a model for cell migration in both 2D and 3D applications, particularly in regard to breast cancer. They are considered to be a highly invasive cell line with high expression of epithelial to mesenchymal transition (EMT) markers. They were isolated from human breast pleural effusion of a 51-year-old Caucasian female who had metastatic mammary adenocarcinoma (Cailleau *et al.,* 1974). MDA-MB-231 are triple negative, lacking the oestrogen receptor, progesterone receptor and amplification of human epidermal growth factor receptor 2. This cell line is known to express very low levels of E- and N-cadherin and have very high vimentin expression. (Blick *et al.,* 2008, Chavez *et al.,* 2010). They also have relatively high expression of EB2 and EB1 when compared to less invasive cell lines such as the MCF-7 breast cancer cell line as shown by research carried out in our lab (Tope Amodu, Thesis).
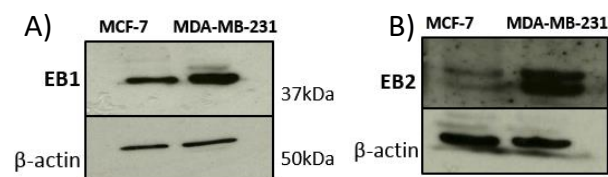
Western blot analyses showing the different expression levels of EB1 and EB2 in the MCF-7 and MDA-MB-31 cell lines. **A:** MDA-MB-231 shows greater expression levels of EB1 than MCF-7. B: Much higher level of EB2 expression is evident in MDA-MB-231 compared to MCF7 cells. Courtesy of Tope Amodu, Thesis (Amodu, 2018, thesis)

Very little is known about the function of EB2 and its effect on migration, preliminary work from our lab suggests that increased EB2 expression causes an increase in cell migration. Liu *et al.,* (2015) studied the interaction of EB2 with HAX1 and the subsequent effect on focal adhesion turnover, an important factor in cell migration. Using coimmunoprecipitation and immunolabelling HAX1 was found to localise at focal adhesions and EB2 recruited HAX1 to MTs for its delivery. Knock down of either EB2 or HAX1 caused reduce focal adhesion turnover which in turn reduce cell migration *in vitro*

and wound healing *in vivo* (Liu *et al.,* 2015). Yue *et al.,* (2014) also describes a role for EB2 in focal adhesion disassembly where MTs deliver MAP4K4 to focal adhesions via EB2 recruitment. This MAP4K4 localisation indirectly activates Arf6 which then enhances focal adhesion dissolution (Yue *et al.,* 2014).

Here, CRISPR-Cas9 technology was used to mutate and functionally KO EB2 in the MDA-MB231 cell line. Prior to the discovery and expansion of CRISPR, gene editing was far more complex, mainly relying on two techniques; transcription activator-like effector nuclease (TALEN) and zinc finger nucleases (ZFN). Genome editing using TALEN required the use of TAL effector DNA-binding domains which recognised specific DNA sequences, these were created in a modular fashion, composing of sequential proteins that each recognised a nucleotide. This DNA recognition domain was then combined with the nuclease domain to efficiently recognise and cleave DNA in a sequence specific manner (Wright *et al.,* 2014, Wei *et al.,* 2013). The ZFN genome editing system works in a similar manner, typically they contain between 3 and 6 individual zinc finger repeats which recognise 9-18 nucleotide pairs. This is also paired with the same nuclease used in TALEN which is the Fok1 endonuclease which is active as a dimer and therefore requires pairs of SFNs or TALENs binding to palindromic sequences (Gaj *et al.,* 2012, Granja *et al.,* 2014). The major drawback of these techniques is the complexities of creating these DNA recognising complexes, a time-consuming process which is usually validated even before genome editing is attempted. Transfection of these relatively large proteins may also be a challenge depending on the application. They also lack the cleavage efficiency seen with CRISPR with potentially more off target effects although this is disputed (Gaj *et al*., 2013, Zhang *et al* 2019).

Compared to these previous techniques, CRISPR is a simple, cost effective and rapid technique with increased efficiency. The prokaryotic CRISPR system was first described by Ishino *et al.,* (1987) where the repetitive sequences of CRISPR were accidentally amplified along with a different targeted gene, although the function of this sequence was unknown. It was not until 2012 when Jinek *et al.,* (2012) demonstrated the potential of this system in molecular biology. Here, two RNA structures were used to direct an endonuclease to cleave targeted DNA sequences. The first *in vitro* use of this system was described in 2013 in two research papers by Cong et al., (2013) and Mali *et al.,* (2013). Cong *et al.,* (2013) used human HEK 293FT cells transfected with the elements needed for CRISPR which will be described later. Co-transfection of these elements resulted in efficient cleavage of the target sequence. Similarly, Mali *et al.,* (2013), again using HEK293T used CRISPR to edit genomic DNA. Here, a GFP coding sequence was used that contained a stop codon within it. As a proof of concept, the CRISPR system was used to target this stop codon and via homologous recombination, restore the functionality of the GFP gene to act as a positive marker for genome editing. Furthermore, the AAVS1

locus was targeted and validated via next generation sequencing in HEK 293T, K5623 and PGP1 cells to show effective genome editing with efficiencies of 38% although this varied with cell type and guide sequence. Five years after these pioneering research papers were published there were 6,300 CRISPR-related publications listed on PubMed, showing the growth in popularity of the technique (Cong *et al.,* 2013, Mali *et al.,* 2013).

The CRISPR technique today has many variations with varying applications. The main components of this CRISPR are the Cas9 endonuclease and the guide RNA (gRNA) which targets this Cas9 endonuclease to the target site (Jinek *et al.,* 2012). The *Streptococcus pyogenes* Cas9 (SpCas9) is by far the most common Cas9 used in molecular biology, although many other variants are now available (Hu *et al.,* 2018). One major difference between these Cas9 proteins is the protospacer adjacent motif (PAM) sequence recognised by the Cas9. This PAM sequence is a short DNA sequence usually 2-6 base pairs in length that follows the target DNA sequence. The PAM sequence is recognised by the Cas9 protein and is independent of the guide sequence, therefore PAM sequences are a limiting factor for target availability, particularly when short sequences are the target (Kleinsteiver *et al.,* 2015). SpCas9 recognises the PAM NGG where N represents any nucleotide, therefore the targeted sequence must follow this NGG sequence, this in most cases is not a limiting factor due to the commonality of this short sequence. However, as the CRISPR technique is further understood and developed, less restrictive Cas9 proteins and subsequently PAMs have been developed. For example, a more recent Cas9 from the *Streptococcus canis* (ScCas9) has been discovered with high sequence similarity to SpCas9 (89.2%) and importantly has the PAM NNG (Xu *et al.,* 2020, Chatterjee *et al.,* 2018). Therefore, this Cas9 will recognise a larger number of potential sites across the genome which is of particular importance when target sequences are limited such as in the targeting of miRNAs. The PAM site is not the only consideration when choosing a Cas9 variant. Relatively recently several Cas9 proteins have been engineered as well as some new Cas proteins being discovered from other species (Burstein *et al.,* 2017).

Engineered Cas9 alternatives confer some advantages over the traditional SpCas9 protein. Nickases are one of the most commonly used alternatives to date, these Cas9 variants have been developed to create single strand breaks (nicks) as opposed to the usual double strand break created by the original Cas9 protein (Ran *et al.,* 2013). Therefore, two guides are used to recognise sequences of opposite strands at the target site to create the double strand break. The advantage of this system is that if off target sites exist, then only a nick will be created instead of a double strand break, nicks are usually repaired without mutation. Theoretically in this system for off target mutagenesis to occur then the two guides would need to recognise the same off target site, a very unlikely occurrence. Using this technique Cho *et al.,* (2014) was able to delete sequences of 1kb *in vitro* and could not

detect any off-target mutagenesis. Although they have higher fidelity, nickases show reduced efficiency compared to the traditional system as they require 2 guides to be delivered and reach their target sites. Here, two guides must be designed and validated with added cost and time (Cho *et al*., 2014). Many other variants exist such as a Cas9 that does not cleave but instead binds and temporarily silences target genes and more recently RNA editing Cas proteins such as Cas13 (Qi *et al.,* 2013, Dahlman *et al.,* 2015).

Guide design is a very important process that will ultimately determine the efficiency of the CRISPR technique. The first step in this process is the identification of the PAM site within the target gene. The PAM site limits the number of sites that can be targeted within the genome, although the NGG PAM most commonly used is a regular occurrence. The guide sequence will then begin 20 nucleotides 5' from the desired PAM and may be on either DNA strand, it is important to note that the PAM sequence is separate from the guide RNA (gRNA). An idiosyncrasy of guide design is that higher efficiencies has been achieved when guides begin with a G and have an A or T at position 17, it is currently unknown how this effects efficiency (Hsu *et al.,* 2013). Due to the differences seen in efficiencies of different gRNAs it is recommended to trial as many as possible to improve chances of genome editing. The guide must also contain sequences for docking with the Cas9 protein known as the CRISPR (crRNA) and trans-activating RNA (trRNA). Guides known as single gRNAs (sgRNAs) contain these sequences with the crRNA and trRNA sequence attached via a linker region. Alternatively, the trRNA may be separate but still part of the gRNA complex but without this loop region (Karvelis *et al.,* 2013). Karvelis *et al.,* (2013) showed that the trRNA is essential for DNA cleavage by Cas9 and that interaction between the crRNA and trRNA is mediated by the Cas9 nuclease.

Another consideration is which of the cell repair machinery is used to insert the desired mutation. There are two possibilities, non-homologous end joining (NHEJ) and homology directed repair (HDR). NHEJ involves the re-joining of two strands of DNA that have been broken by a double strand break. This process is very error prone and usually introduces insert/deletion (INDEL) mutations into the cut site (Weterings and Chen., 2008). Here, the ideal outcome is the introduction of frameshift mutations. These mutations not only disrupt the codon sequence within the target site but also disrupt the downstream reading frame. Additionally, if a blunt ended linear donor sequence is present, then these may be incorporated, these sequences often contain selection markers. HDR is more precise in its mutagenesis, it relies on the use of a repair template. The repair template is a double stranded DNA fragment that must first be produced, adding some complexity to the system. The repair template contains the desired mutation to be inserted, but it also contains homology arms. These homology arms are usually a minimum of 1kb in length and match either side of the site to be mutated. This reduces the chances of off target insertion which may occur with NHEJ and linear donors. The result

of this is the generation of a specific mutation rather than the random method used in NHEJ. As HDR requires the insertion of this repair template, it has lower efficiency then that of the NHEJ method (Ran *et al.,* 2013).

The gRNA target position within the gene to be mutated is another very important factor to be considered. Simply, the target should be close to the start codon but not within the first 20-50 nucleotides. Previous research has found that cells have the ability to use alternate ATG sites downstream of the annotated start codon, potentially skipping the target site during transcription if it is too near to the start. Due to splicing events the target should be within the exon rather than the intron. If the gene has several splice variants, then it is possible for exons to be removed during splicing. If the targeted exon is removed so is the mutation, therefore it is important to target exons present in all transcript variants to ensure full KO of the gene (Cui *et al.,* 2018). Induction of frameshift mutations may mitigate the need for some of the above consideration as all downstream sequences will be disrupted.

There are various ways to deliver the CRSPR elements into the cell each with their own efficiencies. The gRNA has been delivered as cDNA under the control of an RNA polymerase III (e.g. U6 or H1). This method includes the usual mRNA modifications of capping and tailing which has been shown reduce the efficiency of genome editing. However purified gRNA without these modifications have been used with higher efficiencies (Dang *et al*., 2015). The modified guides are combined with Cas9 protein to form ribonucleoprotein (RNP) complex's which are then delivered into the cell (Mout *et al.,* 2017). Alternatively, the modified guide has been transfected into a cell already constitutively expressing Cas9, this has the advantage of tissue specific genome editing *in vivo* by placing the Cas9 gene under a tissue specific promoter (Albain *et al.,* 2015). Delivery of these preformed elements exposes them to degradation by proteases and RNases without the replenishment that cDNA transfection provides. The simplest and long-lasting method is the delivery of cDNA sequences for both the gRNA and Cas9 nuclease which are often included within a single construct. Although this method has been shown to have reduced efficiency of preformed delivery, it arguably has a higher probability of success due to the increased longevity of the effect. Viral delivery is another option, Yin *et al.,* (2016) used viral and non-viral (nanoparticle) CRISPR delivery in an *in vivo* mouse model, correcting a human disease model within the mouse. Here, hereditary tyrosinemia was corrected with a 6% efficiency in hepatocytes. The model used may dictate the method of delivery as *in vivo* applications would require large scale organ or organism wide genetic engineering which viruses have been used to achieve with tragic consequences. *In vitro* applications are far easier with a wider variety of method available.

CRISPR shares the same disadvantages as any other genome editing techniques which is off-target genome editing events. Genomic sequences sharing similar sequences to that of the target have a high risk of editing. This is particularly problematic for use in therapeutics and an unacceptable risk in many of these cases. In molecular biology these off-targets are less of a problem but are still an important factor to consider as they have the potential to alter results. Of course, there are also ethical implication with the use of any genome editing technique, but the ease of use and efficiency of CRISPR makes this more relevant with this method.

Validation of CRISPR based results is focused on the effect at the target site and subsequent protein expression and the potential off-target effects. To date the gold standard for genetic validation of the effects of CRISPR is whole genome sequencing, analysing both the desired genetic aberration and any unintended, off target mutations. However, this technique is rarely carried out due to the increased cost and time required. Therefore, most analysis of the effects of CRISPR rely on sequencing of the target site, as well as the most likely off target sites determined by sequence similarity to the intended target site. The gene product must also be validated as mutations may be silent and therefore have no bearing on the functionality of the gene. This is achieved by analysis of the mRNA product(s) of the gene via techniques such as RT-PCR or RNA seq. Finally, protein expression can be quantified using mass spectrometry or antibody-based techniques such as immunofluorescence or western blotting.

Rationale and gaps in knowledge

- Modulation of EB2 appears to play a role in the maintenance of normal epithelial layers
- EB2 is important for focal adhesion turnover and therefore cell migration, and its expression appears to correlate with a cells ability to migrate
- Does EB2 overexpression cause the UJT transition or pEMT?
- Further study of this requires an EB2 KO/KD model in a known highly invasive cell line such as the MDA-MB-231 used

Hypothesis

EB2 KO/KD in the MDA-MB-231 cell line will cause a significant decrease in cell migration.

Aims

- The aim of this chapter is the generation of an MDA-MB-231 MAPRE2 (EB2) KO/KD cell line with genomic and proteomic validation. Specifically, validation of loss of EB2 protein expression along with MAPRE2 mRNA analysis and sequencing of the effected site

- Analyse the effect of EB2 KO/KD on MDA-MB-231 cell migration.

5.4 Results

An overview for the generation of EB2 KO MDA-MB-231 cells can be seen in figure 5.1. Briefly, single guides and a linear donor were transfected into MDA-MB-231 cells. These cells are then selected for the presence of the genome integrated linear donor via puromycin resistance and the presence of GFP. Sub cloning was then carried out in an attempt to isolate a single clonal population. These sub clones were then validated for the presence of the genome integrated linear donor and a decrease in EB2 protein expression as well as decreased mRNA expression.

5.4.1 Guide Design and Target Site Validation

Two predesigned and commercially available guides (Origene) were used in this study (Guide 1: AGCGGCCTATTGCCAATTCA and Guide 2: GCTAGTGAAAGGACGTTTCC), these guides were used individually rather than in combination. To ensure these designed guides were appropriate for the KO of MAPRE2 in MDA-MB-231, it was first essential to explore the characteristics of the MAPRE2 gene. Transcripts and exon positioning were analysed using the NCBI genome database and the Ensembl genome browser. The MAPRE2 gene is located on chromosome 18 (18q12.1-q12.2). The gene has 13 protein coding transcripts with 5 transcripts being validated under CCDS and several other incomplete coding sequences (undefined stop codon) or sequences with retained introns. The gene also has two functional ATG start sites with two promoter sites resulting in two points of transcript initiation which gives rise to two sets of transcripts if categorised by size. The two key functional domains, the CH and EBH C terminal domain are both contained within 3 different exons. The predesigned guides target an exon containing part of the CH domain which is the most 5' of the functional domains. The target exon for guide 1 is present in all protein coding transcripts and the same is true for guide 2 with the exception of one transcript (MAPRE2-206). This transcript is a truncated form of the MAPRE2 gene and does not contain the full MT binding CH domain nor does it contain the EBH and therefore has no MT binding ability and none of the usual MT binding partners (Fig. 5.2).

To confirm that the guide target sites were intact in the MDA-MB-231 cell line used in this study, PCR was carried out. This was achieved by using guides that annealed 5' and 3' of the guide sites and the product was band extracted and sent for sequencing. This sequencing confirmed that the guides target sites were present in the MDA-MB-231 cell line used here (Fig. 5.3).
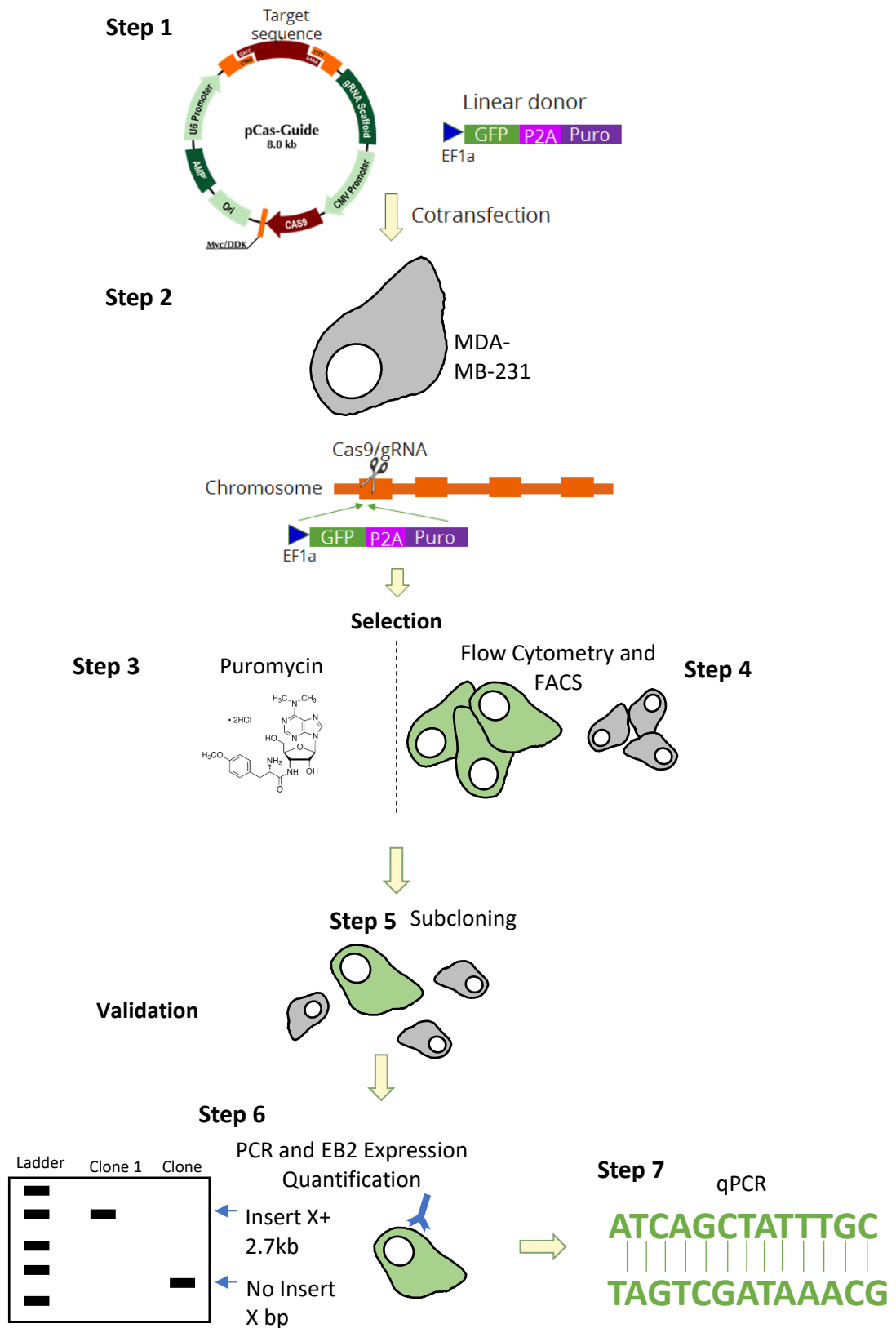
Figure 5.1 Method overview. (Step 1) sgRNA, Cas9 (pCas-Guide) and Linear donor are co-transfected into cells. (Step 2) Guides and Cas9 endonuclease induce DNA double strand breaks at the MAPRE2 target site and linear donor is integrated. (Step 3) Cells are selected by puromycin resistance to select only cells containing integrated linear donor. (Step 4) Cells are sorted to isolate larger GFP positives cells using FACS. (Step 5) Clones are sub cloned to isolate individual cells. (Step 6) EB2 expression in subclones was quantified via immunolabelling and western blot and linear donor integration was confirmed via PCR. (Step 7) qPCR quantification of MAPRE2 mRNA expression.

142
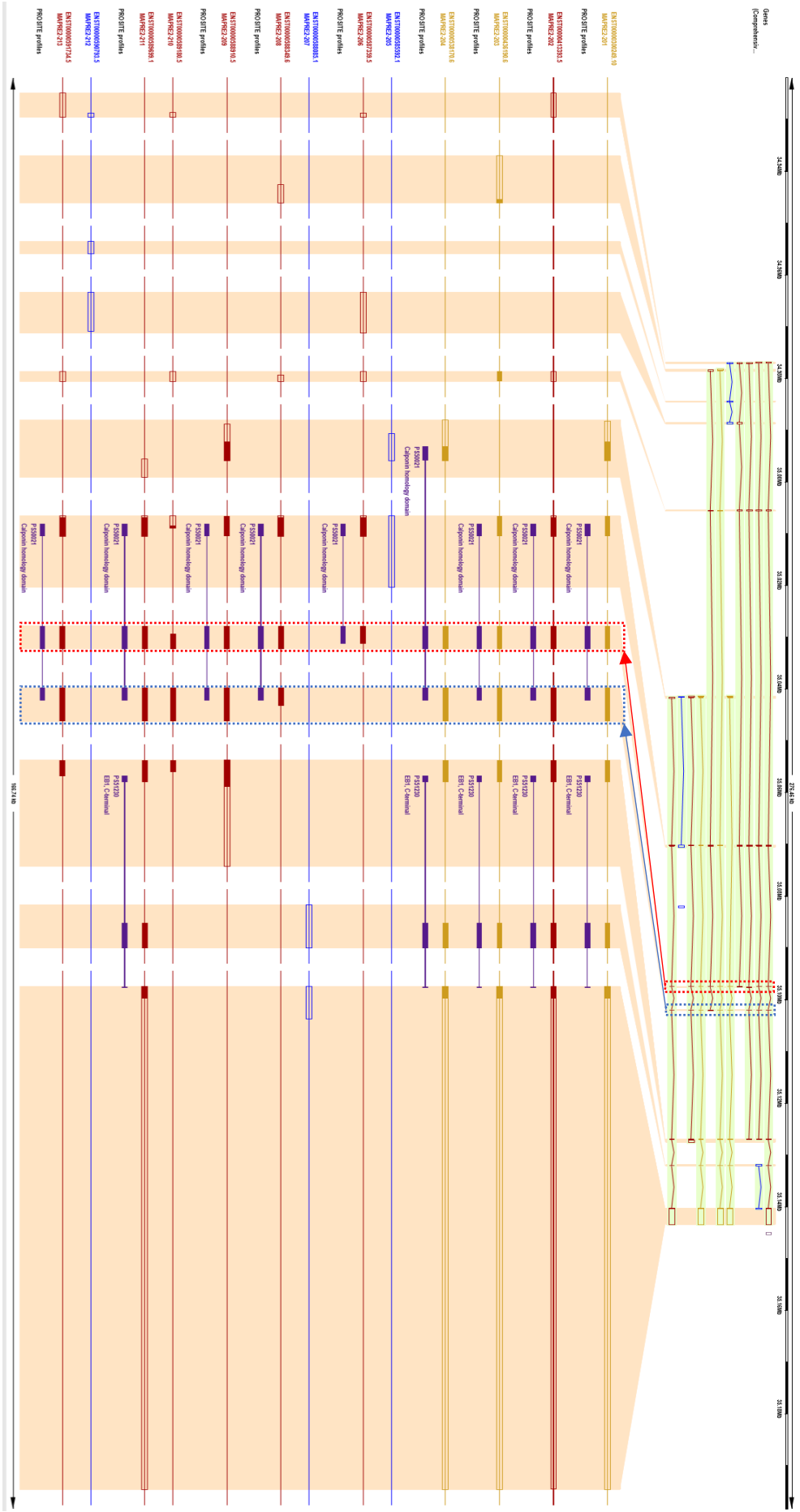
Figure 5.2 Analysis of MAPRE2 transcript variants. Diagram of transcripts produced by the MAPRE2 gene. The MAPRE 2 gene has 13 protein coding transcripts with several other incomplete coding sequences (undefined stop codon) or sequences with retained introns. The gene also has two functional ATG start sites with two promoter sites, resulting in two points of transcript initiation. This gives rise to two main sets of transcripts if categorised by size. Dotted boxes represent the targeted exons by guide 1 and guide 2. Guide 1 targets the red box whereas guide 2 targets the blue box. Data was collected from the ensembl genome browser database.

143

Guide 1:

AGCGGCCTATTGCCAATTCA
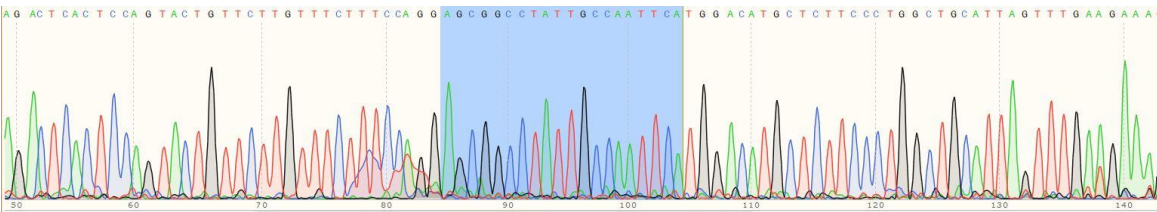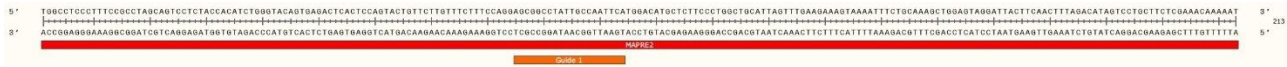
Guide 2:

GCTAGTGAAAGGACGTTTCC

■ MAPRE2 sequence (BLAST)

■ Guide sequence
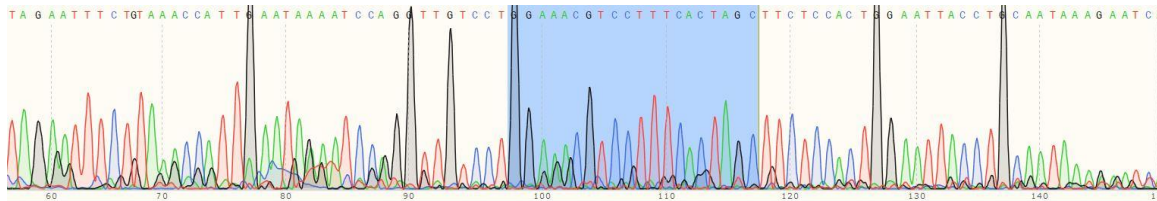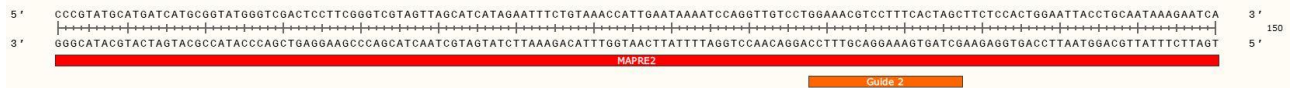
Figure 5.3 Target site validation in MDA-MB-231. Guide target sites were present in the MDA-MB-231 cell line. Using PCR, target sites were amplified and sequenced using next generation sequencing. Chromatagrams are shown and sequenced DNA was aligned to MAPRE2 2 (red) using BLASTn containing the guides target sites (orange).

5.4.2 Transfection of pCas-Guide 2 construct and linear donor yielded puromycin resistant cells

The sgRNA and Cas9 sequence were delivered into cells contained within the pCas-Guide construct. Two variations of these constructs were used, one containing guide 1 and the other containing guide 2. For the transfection of these constructs and the linear donor the lipofectamine 3000 (ThermoFisher) system was used, due to its high efficiency specifically in relation to the MDA-MB-231 cells line and its ability to transfect relatively large constructs. Transfection was then carried out as follows. Cells were seeded at 150,000 cells per well of a 24 well plate and incubated at 37°C, 5% CO_2 for 24 hours. Then 1μg of guide (1 or 2) (Origene) was mixed with 1μg of linear donor (Origene) and the transfection was carried out as per manufacturer's instructions. These transfected cells were then incubated with the transfection reagents and DNA at 37°C and 5% CO_2 for 4 days.

After this period, cells were subjected to 7 mg/ml puromycin treatment for 72 hours. This initial treatment yielded resistant cells in both the guide 1 and guide 2 treated MDA cells. These cells were then grown in normal media for 3 weeks to remove the unintegrated linear donor. The cells were then subjected to a second round of puromycin treatment at the same concentration, this resulted in complete cell death of guide 1 treated cells but yielded puromycin resistant cells treated with guide 2 (Fig. 5.4). Therefore, subsequent steps were carried out using the guide 2 treated cells only, with comparisons to wild type (WT) MDA-MB-231 were necessary.

5.4.3 Flow cytometry and FACS

As well as puromycin resistance, cells were also selected for both the presence of GFP and an increase in cell size. Increase in cell size is a known characteristic of EB2 depletion as siRNA of EB2 by Goldspink *et al.,* (2013) caused an increase in cell size by ~4 fold. This phenotype was rescued with the transfection of a construct containing mCherry-EB2 (Goldspink *at al.,* 2013). Initially cells were analysed using flow cytometry to assess the GFP expression levels within the guide 2 treated cell population and compared to WT control cells. Cells in suspension were analysed using the BD FACSAria II cell sorter (BD Biosciences) equipped with a 488 nm laser. Forward vs side scatter showed that CRISPR treated cells were also much larger with higher granularity (Fig. 5.5a). Flow cytometry analysis of WT and CRISPR treated cells also showed that CRISPR treated cells had 98% more GFP positive events compared to the WT cells (Fig. 5.5b). Plotting the cell size against green fluorescent intensity shows that a population of larger cell with increased GFP intensity existed within the population (Fig 5.5c). These larger GFP positive cells were gated (P1) using the BD FACSDiva by selecting cells around 4-fold larger than mean WT cell size and it was these larger cells that were sorted from the population (Fig. 5.5d). These cells were selected as Goldspink et al., (2013) show a 4-fold increase in cell size with

EB2 depletion. Observation of sorted cells showed an enrichment of larger cells although some smaller cells were still present in the population (data not shown).
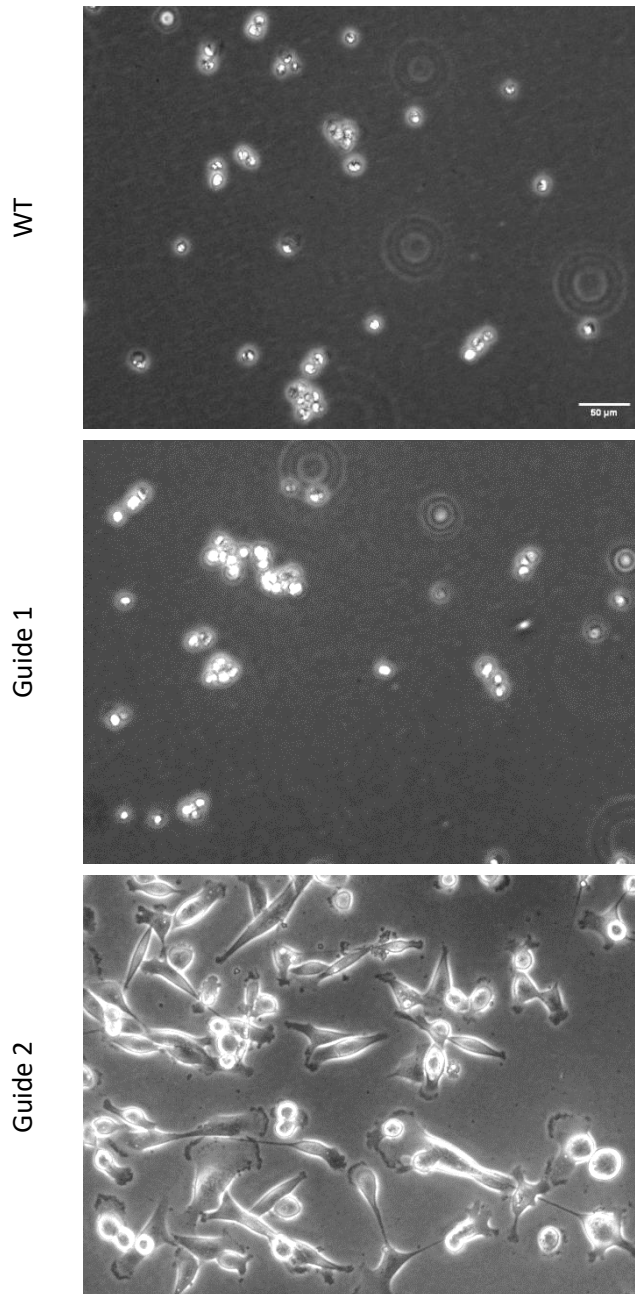
Figure 5.4 Puromycin selection of transfected MDA-MB-231 cells. Phase contrast imaging of MDA cells after puromycin treatment. Cells were treated with puromycin ($7\mu g/ml$) in T75 tissue culture flasks to select for the presence of the linear donor containing the puromycin resistance gene (pac). After three weeks of culturing only cells treated with guide 2 survived puromycin treatment. Scale bar= 50µm.
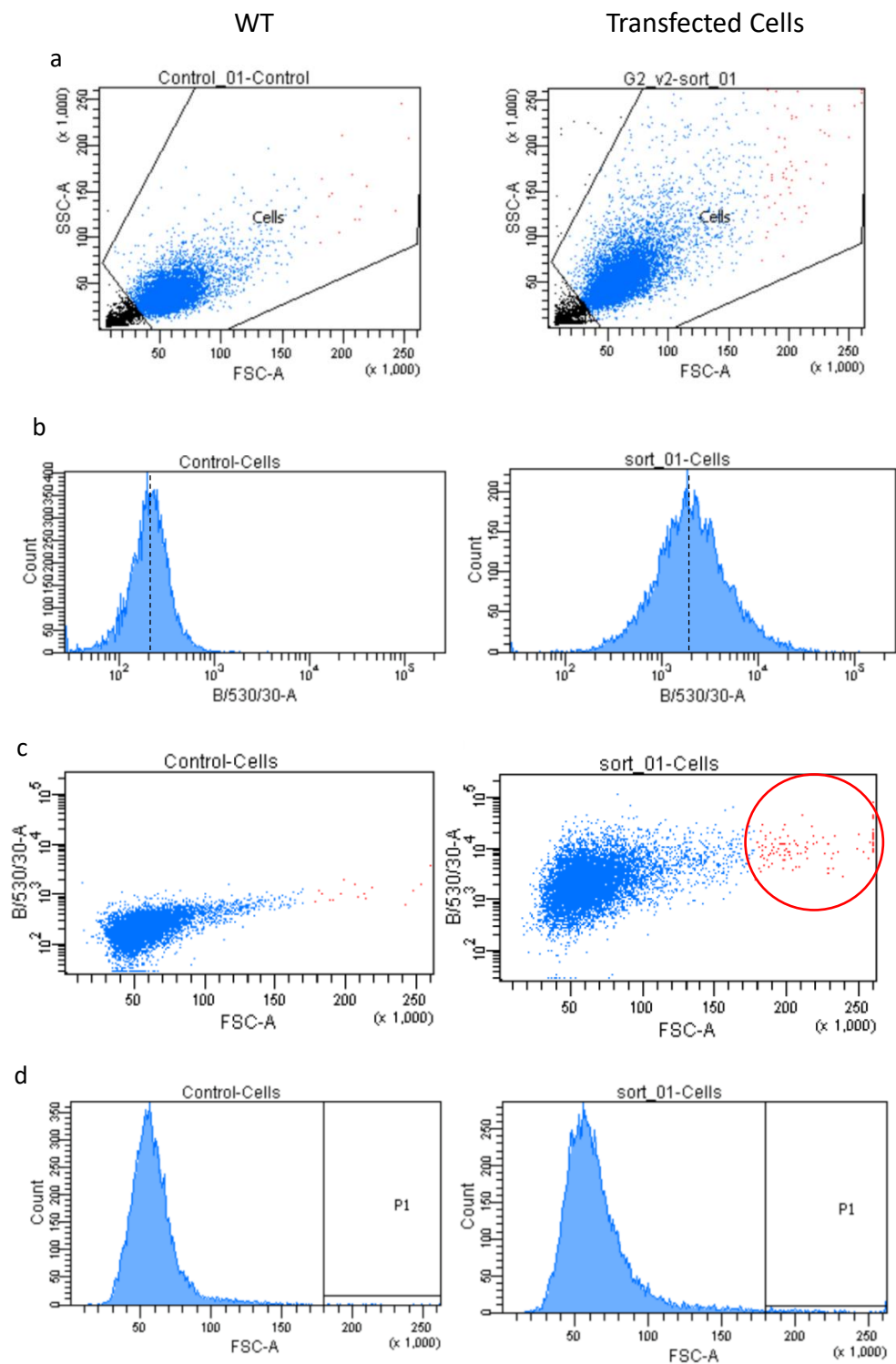
Figure 5.5 Flow cytometry analysis of guide 2 transfected MDA cells. (a) Forward versus side scatter of cell populations. A higher density of larger cells (events) were seen in transfected cells (red). (b) GFP (B/530/30-A) analysis in gated cells from (a). Transfected cells show higher GFP intensity compared to WT control (dotted lines show mean intensity). (c) Forward scatter versus GFP intensity showing GFP positives cells were larger than negative cells (red circle). Gated (P1) cells in red were sorted as shown in (d). (d) Forward scatter analysis shows gated region (P1) for selection of larger cells via FACS. ~11,500 events per group.

5.4.4 Sub Cloning of Sorted Cells

The aim was to generate a monoclonal population of KO cells to eliminate variation in future analysis due to any heterogeneity of EB2 expression within the cell population. To attempt this, two cloning methods were used. Firstly, serial dilutions were trialled, this cloning technique resulted in the presence of several wells containing a single cell when observed under a light microscope and several wells containing two or more cells (Fig.5.6). Cell survival was incredibly low with very few single large cells surviving 24 hours. Unfortunately, these large single cells which were the most desired failed to proliferate and were observed over a three-week period. These cells were known to be living as they regularly changed shape, although failed to proliferate and eventually died. To attempt to increase survival rate, media filtered from MDA cells was applied to isolated cells, but this had no beneficial effect. Additionally, to induce proliferation, the serum concentration was increased from 10% to 20% but this also failed to increase viability of these cells. Therefore, the selection of these cells was not possible. Wells that originally contained 2-4 cells that also proliferated were selected and expanded. The expansion of these cells into increasingly larger vessels up to a T75 took several weeks to achieve due to very slow proliferation. From now on these cultures are defined as numbered clones or sub clones but it should be noted that these are unlikely to be monoclonal populations.

A more selective method was also trialled where 5000 cells were seeded into 100mm petri dishes and individual cells were visualised using an inverted microscope and isolated and pipetted into individual wells of a 96 well plate (Fig. 5.6). Collagen coating and conditioned media was also used in this system. This method allowed for the selection of only the largest cells which were most likely the desired homozygous KOs. However, as these cells did not proliferate they could not be tested for EB2 expression. This method was very effective at isolating single cells. Unfortunately, this method also showed no cell survival of single cells when isolated. Comparison of CRISPR treated cells and WT MDA cells show WT cells show much higher survival rates compared to the treated cells. Blebbing was seen in CRISPR treated cells, large cells that did not die, failed to proliferate making them impossible to culture and therefore use in subsequent experiments (Fig. 5.7).
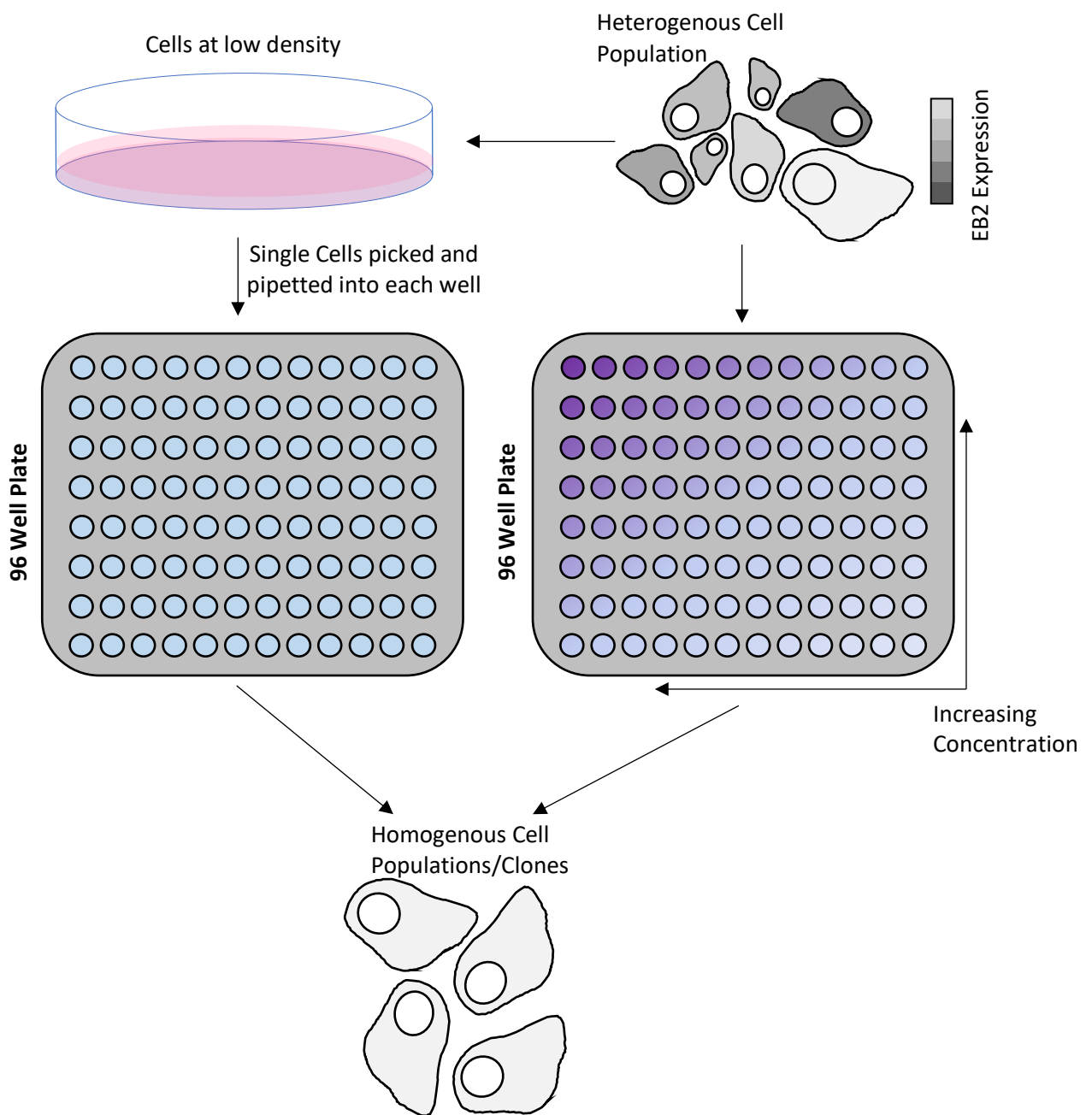
Figure 5.6 Diagram depicting the cloning methods used. In order to successfully isolate single cells, two methods were used. Left: cells were pipetted at extremely low density and single cells were picked and pipetted into 96 well plates. Right: traditional serial dilutions were carried out to give increasingly fewer cells in a 96 well plate.
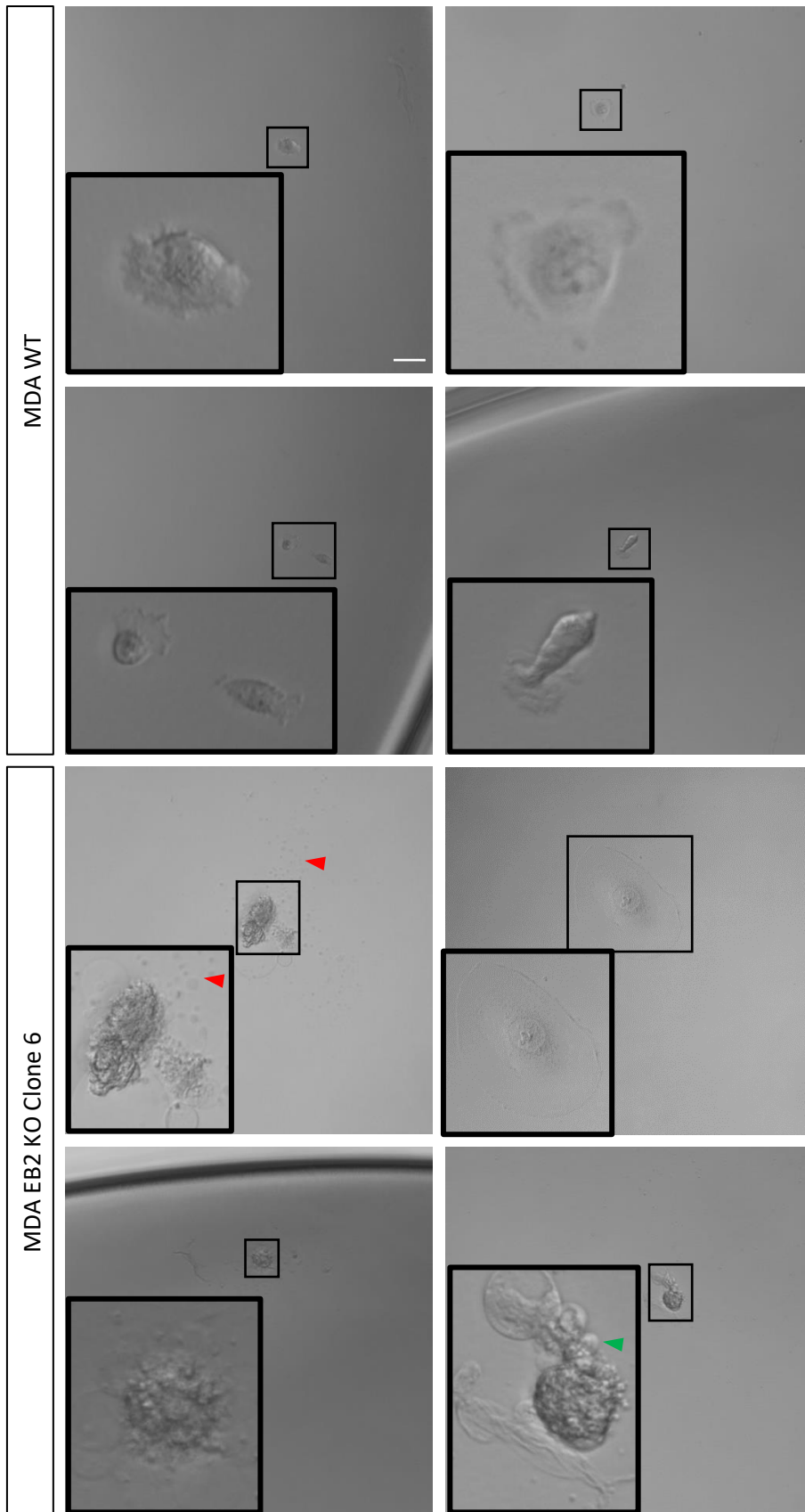
Figure 5.7 Transfected and sorted cells show low survivability when isolated. Light microscopy of recently isolated single cells, cells were isolated using the individual cell picking method. Blebbing (green arrow) can be seen in isolated MDA clone 6 cells which did not occur in WT MDA cells. Presumed apoptotic bodies (red arrow) also appear to be present in isolated clone 6 cells. Scale bar= 50μm.

5.4.5 Validation of Linear Donor Integration in two clones

Of the potential clones isolated from the puromycin selected and sorted cells, sub clone 3 and 6 looked the most promising morphologically. These clones appeared much larger and more homogenous then other clones although some smaller cells were still present. Genomic integration of the linear donor was verified in these sub clones. The gDNA from these cells was extracted and PCR was carried out as described above, the results were compared to WT gDNA. The guide site was amplified which would result in a small band if no insert was present or a band around 2.5kb bigger representing the insert plus the MAPRE2 region (Fig. 5.8). The WT PCR resulted in the amplification of the expected band of 622 bp which represents the presence of the intact guide 2 site within the MAPRE2 gene. The PCR of sub clone 3 resulted in amplifications identical to the WT control whereas the PCR of sub clone 6 showed amplification of a larger band of around 3+ kb along with the 622 bp amplification indicative of WT MAPRE2 and integrated linear donor amplification (Fig. 5.9). This suggests that WT MAPRE2 is present in both clone 3 and clone 6 but clone 6 also shows successful integration of the linear donor into this MAPRE2 site.

5.4.6 Analysis of MAPRE2 and EB2 expression

To test for expression of the EB2 protein in clone 6, immunolabelling and Western blotting was carried out. Several sub clones (1,3,4,5 and 6) were tested using these methods and clone 6 was shown to have the greatest reduction in EB2 expression. Firstly, EB2 expression was carried out by seeding cells on glass, methanol fixing and immunolabelling for EB2. Cells were then imaged using a widefield fluorescent microscope with a 63x objective ensuring that exposure times were kept consistent for comparisons to be made. Cells were then selected manually, and intensity measurements were made using ImageJ. This immunolabelling quantification of EB2 in clone 6 showed a 62% reduction in expression when measuring cell intensity (based on 1 experiment, Fig. 5.10). Similarly, Western blotting of clone 6 cells revealed a reduction of 68% in EB2 expression (Figure 5.11a). Western blotting was quantified using ImageJ by band intensity measurement with normalisation based on the GAPDH loading control, fold change and was then calculated and plotted (based on 1 experiment). Finally, MAPRE2 mRNA expression was quantified in clone 6 using qPCR. This analysis showed a 73% reduction in MAPRE2 mRNA expression (3 biological and 3 technical repeats, Fig. 5.11b).
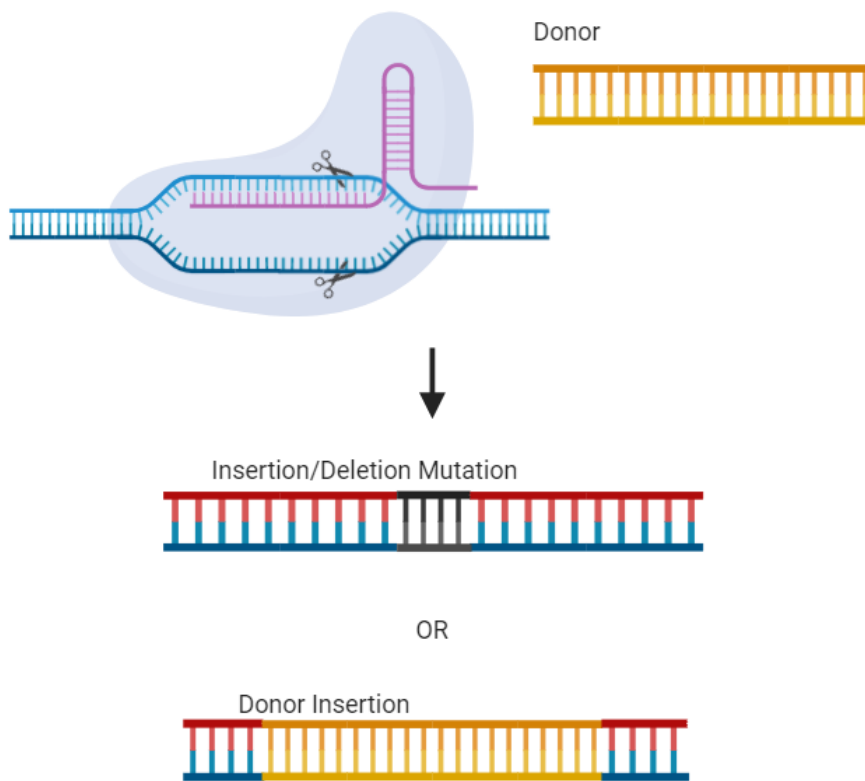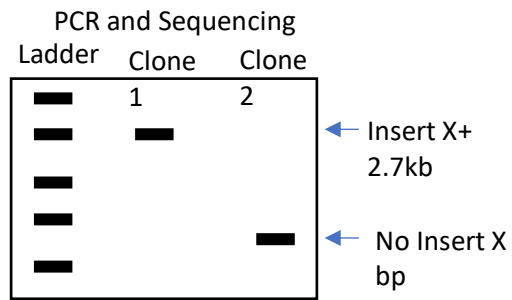
Figure 5.8 Overview of the validation strategy. Diagram showing the potential states of the MAPRE2 gene in sub clones. Sub clones may contain WT MAPRE2 or INDEL mutations at guide 2 with the linear donor expressed in its unintegrated form. The desired outcome is linear donor integrated into the MAPRE2 guide 2 target site.
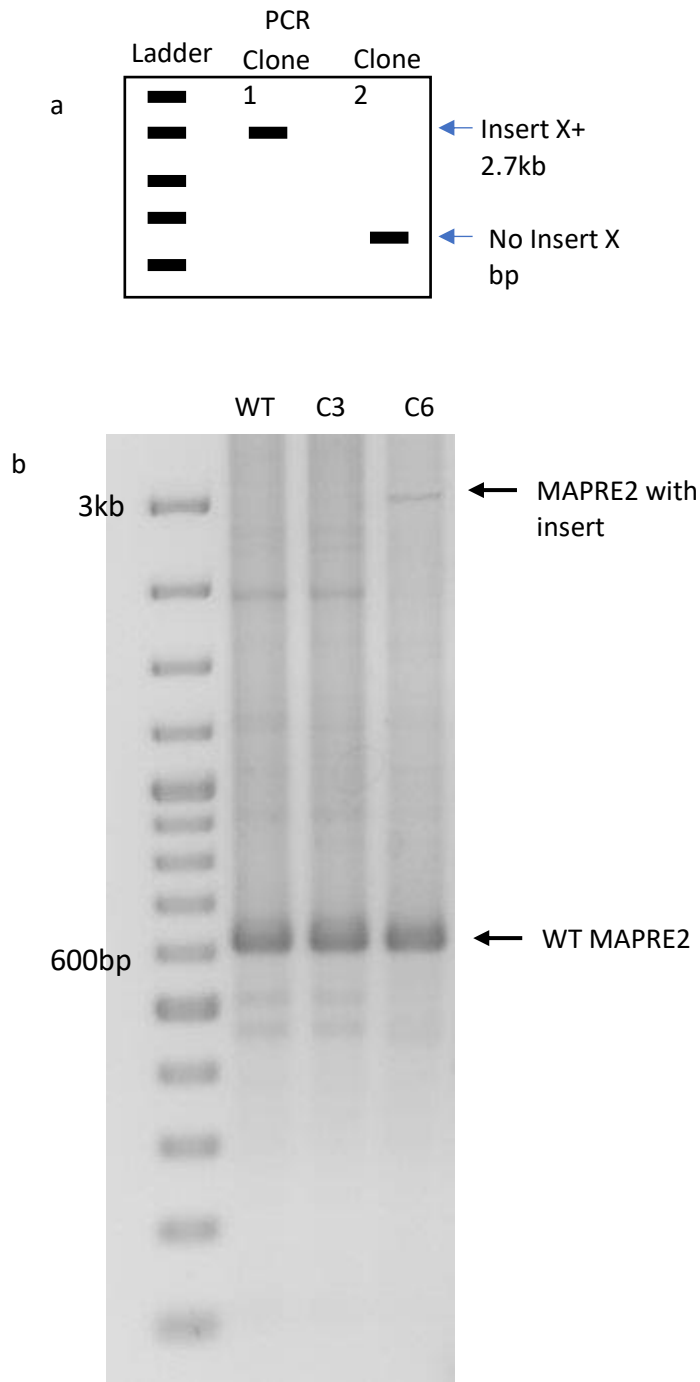
Figure 5.9 Amplification of guide 2 site containing linear donor. (a) Diagram showing the potential results from amplification of the guide 2 site. A smaller band of 600bp represents the WT MAPRE2 gene whereas a band of 3.1kb represents the same site except with linear donor integration. (b) Guide 2 target site was amplified using PCR. WT and clone 3 (C3) showed amplification of the WT MAPRE2 (600 bp) site. PCR of clone 6 (C6) amplified WT MAPRE2 but also a larger band (3.1 kb) likely containing the linear donor.
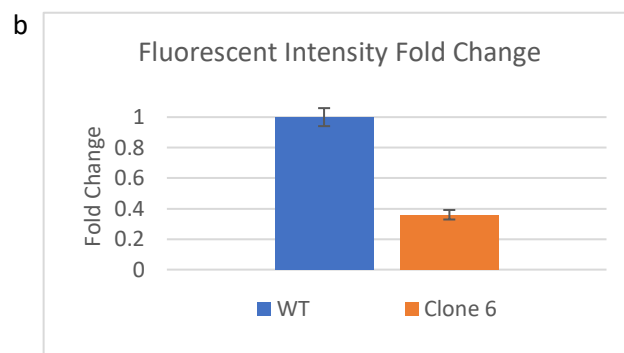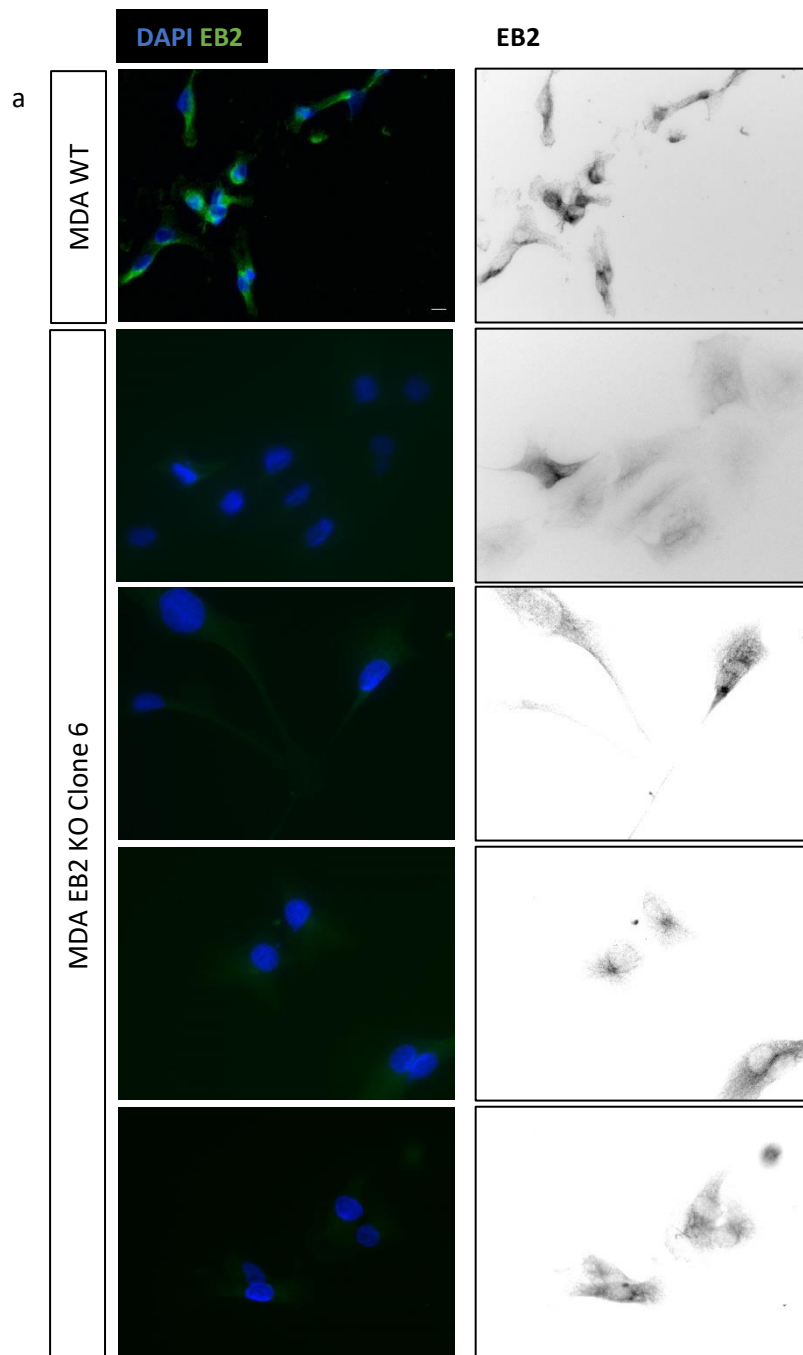
Figure 5.10 Analysis of EB2 expression via immunolabelling of clone 6.
Immunolabelling for EB2 in MDA clone 6 visualised with widefield microscopy. (a)
MDA cells immunolabelled for EB2 show decrease in intensity. (b) quantification of
mean intensity of Clone 6 compared to control. +/- 1 SE. Scale bar= 10 μm. WT n=29
cells, C6 n=11 cells from 1 experiment
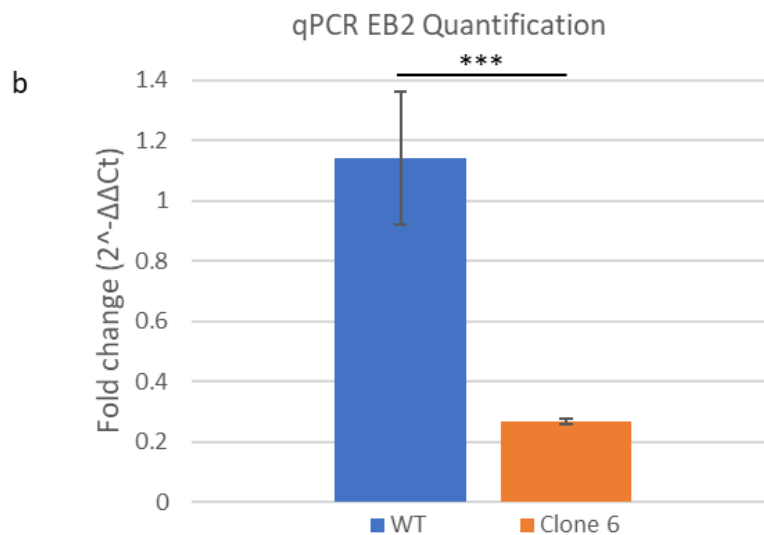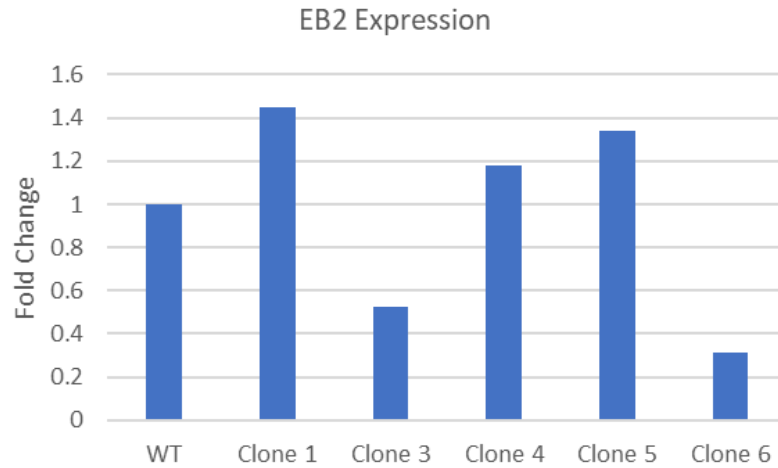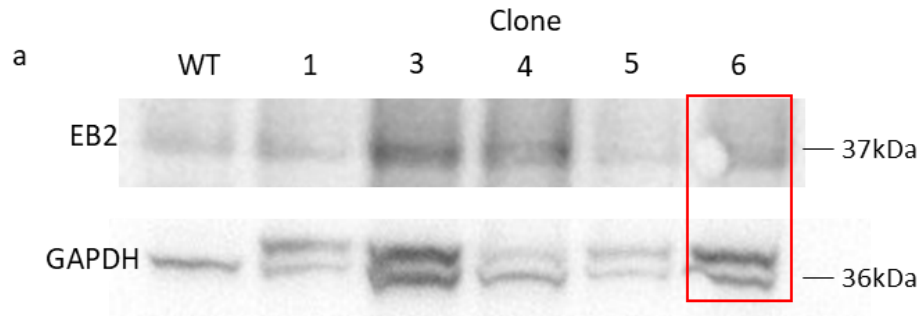
Figure 5.11 EB2/MAPRE2 expression quantification. (a) Quantification of western blot analysis of various clones isolated after puromycin treatment and FACS. Only Clone 3 and 6 show a reduction in EB2 expression. N=1 western blot. (b) Comparison of the relative gene expression of human MAPRE2 in WT MDA cells versus CRISPR-Cas9 + sgRNA transfected MDA cells for insertion mutation to disrupt MAPRE2. Expression represented as fold change. 73% decrease in MAPRE2 expression in Clone 6 seen normalised to expression of 18S housekeeping gene. +/- 1 SE shown n=9 samples from 3 experiments. P=<0.001.

5.4.7 Clone 6 shows increased size, reduce proliferation and reduced migration compared to WT MDA-MB-231

Cell size was quantified using immunolabelling and ImageJ freehand analysis tool to demarcate cells and measure area, this showed clone 6 cells were on average 3.5-fold larger than the WT controls (based on 32 cells, 3 experiments) (Fig. 5.12a). Cell proliferation was also measured by seeding cells at 50,00 cells per well of a 6 well plate, cells were then detached and counted using haemocytometer every 24 hours for 96 hours. Clone 6 cells also had reduced proliferation rates compared to the WT control, this difference increased with time (based on 3 biological repeats, Fig. 5.12b). A random migration experiment was carried out to assess the effect of reduced EB2 expression on cell migration. This was carried out by seeding 150,000 cells per well of a collagen I coated 6 well. Time lapse phase imaging was then carried out using a 10x objective, imaging every 10 minutes for 18 hours. This showed clone 6 had both significantly reduced migration speed and distance when analysed using image manual tracking and the Ibidi chemotaxis analysis tool (based on 30 cells each, 3 biological repeats, Fig. 5.13).

a | MDA WT | MDA Clone 6

b

Mean Cell Size

***

c

Cell Proliferation

*** *** *** ***
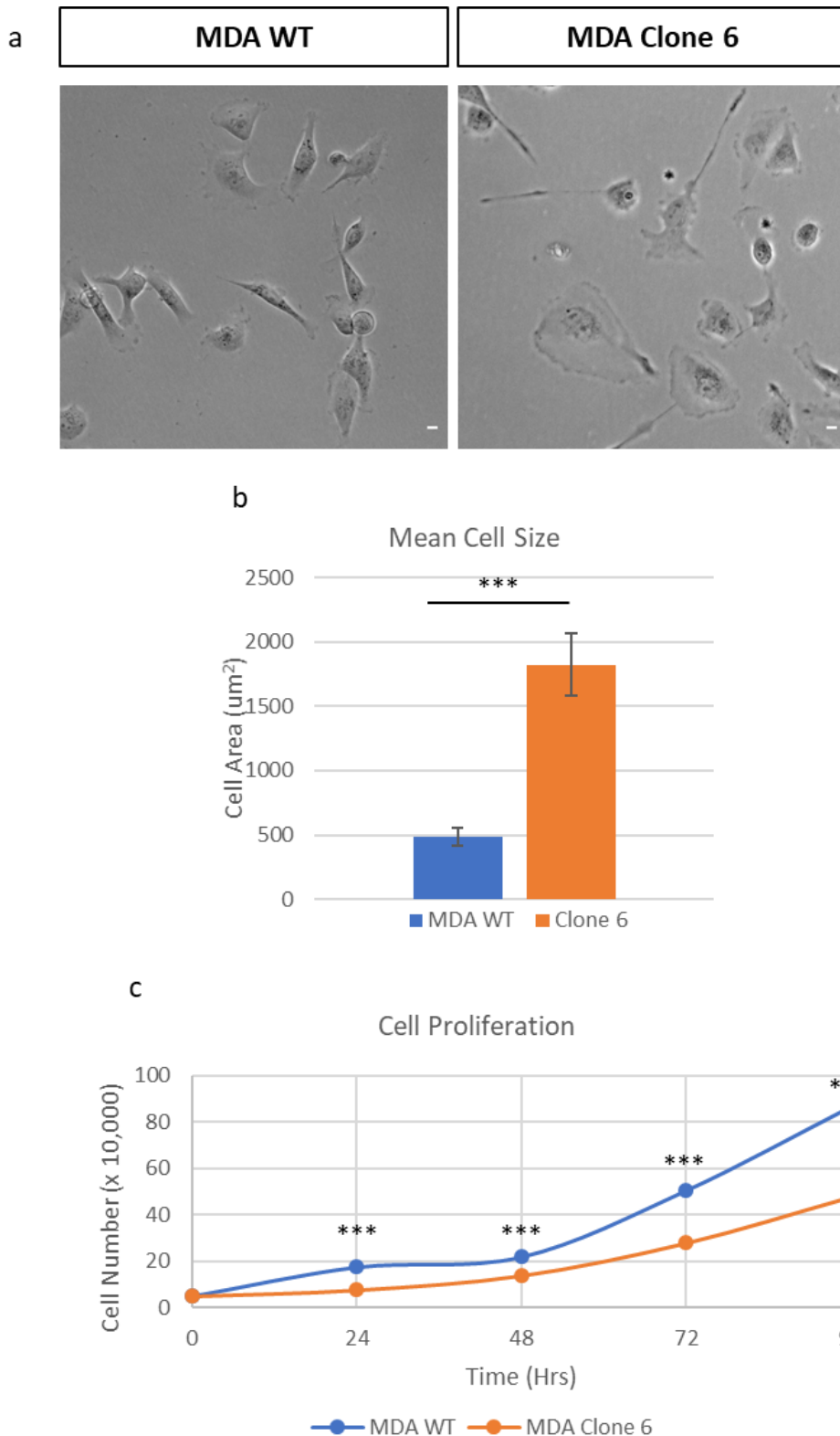
Figure 5.12 Cell size and proliferation analysis. (a) Example phase contrast images of MDA WT and clone 6 cells seeded onto collagen coated glass. Scale bars= 10μm. (b) quantification of cell size analysis. Cell size was determined using ImageJ to manually demarcate cells and cell area was then measured. Clone 6 showed an average increase of 3.5 fold in size. P= <0.001. n=32 cell per group, 3 experiments. +/- 1 SE shown. (c) Quantification of cell counts over time. Cells were counted every 24 hours using a hemocytometer. Clone 6 shows significantly reduced proliferation at all time points. P=<0.001. n=3 wells from 3 experiments. +/- 1 SE shown.
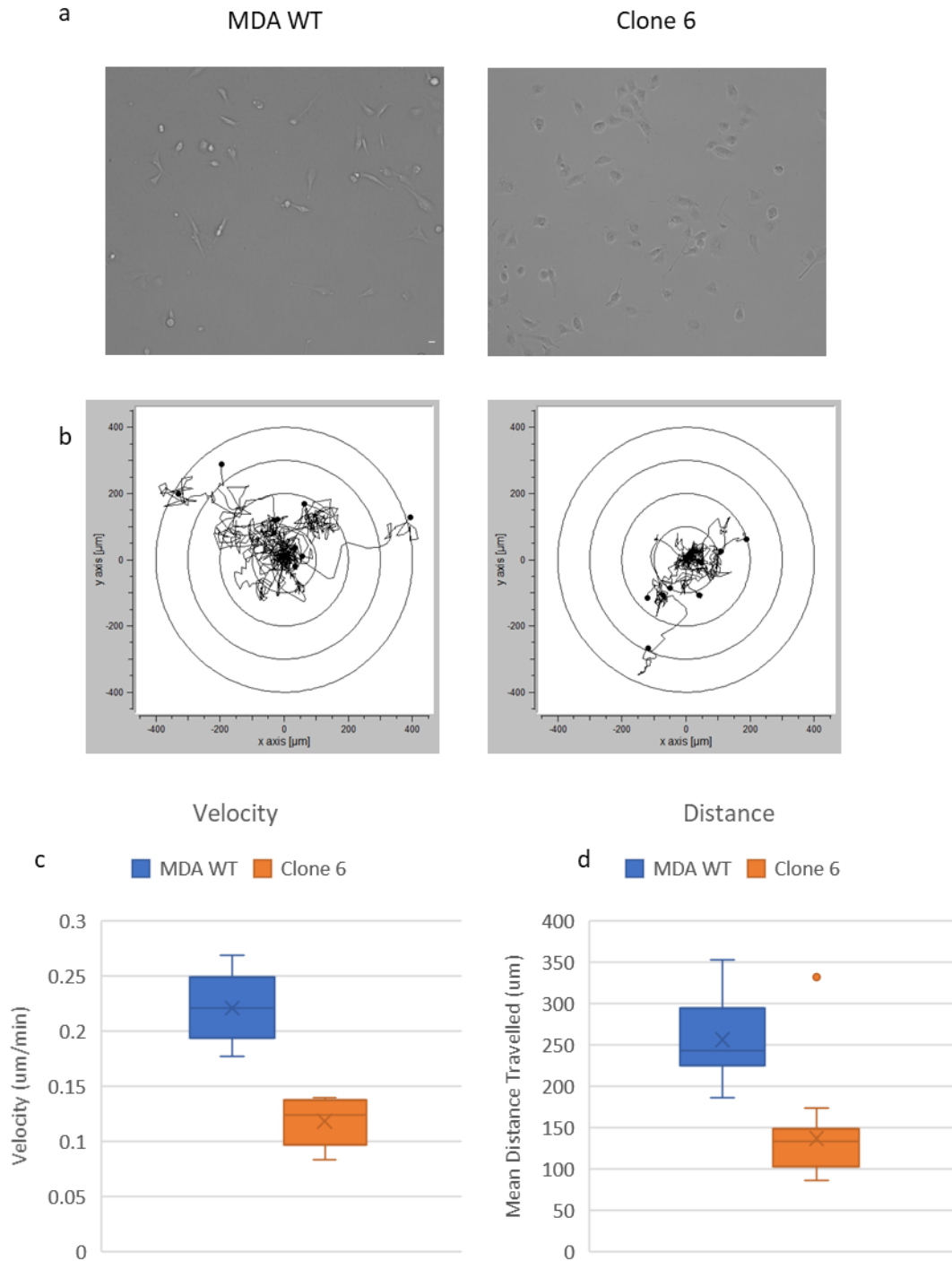
Figure 5.13 Random migration analysis of Clone 6 cells. (a) Random migration visualized by Phase contrast time-lapse microscopy. MDA WT and Clone 6 cells were seeded onto collagen I and allowed to randomly migrate (see supplementary for videos). (b) The spider diagrams show the overall tracking of cell movement during random migration assay. The spider graphs show 10 representative tracks each with single cell tracking done manually. (c) Quantification of cell velocity during random migration showing clone 6 cell exhibited both decreased migration distance (50%) and velocity (53%). (d) Quantification of total distance travelled during random migration assay. n=30 cells per group, 3 experiments.

5.5 Discussion

5.5.1 Guide RNAs target functional domains of the MAPRE2 gene and targets are present in the MDA-MB-231 cell line

As part of guide design protocols, the guide target site should be around 50 bp from the start site of the gene to increase the likelihood of generating a non-functional gene product (Mohr *et al.,* 2016). Due to the dual initiation sites within the MAPRE2 gene, the guides could not be targeted in close proximity to the 5' region of the transcripts. Additionally, many of the exons were not shared between transcripts, limiting the potential targeting locations. Due to these limiting factors it was essential to target upstream of the functional domains (CH and EBH C terminal). Both guides were designed to target the CH domain but in separate exons. Guide 1 targeted an exon present in all transcripts and guide 2 targeted an exon present in all but one transcript. The result of integration of the linear donor into either of these sites will be sufficient to disrupt MT binding of any potential proteins that may be produced. Also, if a frame shift mutation is created all downstream domains will be disrupted. Integration of the linear donor alone would ensure gene disruption as it contains a stop codon, resulting in the generation of a truncated protein conjugated to the puromycin resistance gene upon initiation of EB2 transcription. The linear donor is under the control of the EF1α promoter and will therefore be expressed separately of the MAPRE2 expression.

It was important to validate the presence of the guide sites within the MDA-MB-231 cell line as genetic variation within cells lines is common. Mitalipova *et al.,* (2005) showed that enzymatic dissociation of cells in culture induced chromosomal abnormalities by passage 23 in human embryonic stem cells, confirming the need to validate for the presence of guide target sites. The MDA-MB-231 is also transformed and therefore contains many mutations which may potentially effect guide site fidelity. Several primer pairs were designed to both validate the sequence integrity within this cell line but also to ensure that several working primers were developed to explore the mutated sequence within the CRISPR treated cells. It has been reported that CRISPR events can led to substantial disruption of the guide sites (>250 nucleotides), therefore several primers were developed that varied in distance from the predicted cut site (Thomas *et al.,* 2019). Using this method, it was confirmed that the target sites were intact and a viable option in this cell line.

5.5.2 CRISPR Cas9 treatment with guide 2 but not guide 1 yielded puromycin resistant cells

Transfection of the CRISPR components was carried out with subsequent puromycin selections. Initially it was impossible to select for the successful transfection of the pCas-Guide construct, as no mammalian selection marker existed within it. An improvement that could be made to this protocol is the addition of an alternative mammalian selection marker within the pCas-Guide

construct, to allow for the selection of both linear donor and pCas-Guide transfection using dual antibiotic selection. Adding this step would allow for the rapid selection of cells that contained all components (pCas-Guide + Linear Donor) needed for successful donor integration into the target site, greatly increasing the probability of selected cells being MAPRE2 KOs. Here, cells containing only the linear donor were selected for by treating with puromycin soon after transfection. The problem with this method is that the linear donor is expressed without genomic integration due to the presence of the EF1α promoter (Wang *et al.,* 2017). Although, this method does eliminate those cell that do not contain the linear donor, increasing the probability that these cells will have the linear donor integrated into the genome in the next experimental stages. Both guide 1 and guide 2 treated cells survived the first round of puromycin selection suggesting that the linear donor was successfully transfected into these cells. Cells containing unintegrated linear donor were eliminated by culturing for 3 weeks, passaging every 2-3 days. As the linear donor has no replication sequences it will only be replicated when integrated within the genome. Long term culture essentially diluted the presence of the linear donor in the cell population, which would led to a larger proportion of cells with integrated linear donors compared to the undesired unintegrated linear donor containing cells. Finally, to eliminate remaining cells that lose the linear donor through degradation during this long-term culturing, a final treatment with puromycin was carried out as before. This resulted in the total cell death in the guide 1 treated cells but yielded a puromycin resistant population in cells treated with guide 2.

Death of guide 1 treated cells may be due to several reasons. It was confirmed that the target site for guide 1 was present in the MDA-MB-231 cells which eliminates the possibility that guide 1 has no target site in this cell line. The efficiency of the guides is also a factor that will affect their ability to create double strand breaks, with some guides having a very low efficiency. Large variation in guide efficiency has been described and it is not currently fully understood which characteristics determine this (Moreno-Mateos *et al.,* 2015). Moreno-Mateos *et al.,* (2015) studied the effect of sgRNA nucleotide composition on target site mutagenic efficiency. The nucleotide sequence was varied, and subsequent efficiency was analysed. The most efficient sgRNAs contained an enrichment of guanine at positions 1-14 (distal to the PAM) and an enrichment of cytosine at positions 15-18 with a low occurrence of thymidine and adenine except at positions 9 and 10. A cytosine residue at position 3 was found to significantly lower the efficiency of the guide.

Table 5.1 Theoretical guide efficiency. Guide 1 contains 5 nucleotides at positions known to increase efficiency (green) but also contains a cytosine residue at position 3, a characteristic known to significantly reduce efficiency (red). Guide 2 however contains 6 nucleotides that fit the high efficiency model and does not contains the cytosine residue at position 3. *= position where cytosine residue significantly reduces efficiency.

Position	1	2	3	4	5	6	7	8	9	10	11	12	13	14	15	16	17	18	19	20
Efficient	G	G	G*	G	G	G	G	G	G	G	G	G	G	G	C	C	C	C	N	G
Guide 1	A	G	C*	G	G	C	C	T	A	T	T	G	C	C	A	A	T	T	C	A
Guide 2	G	C	T	A	G	T	G	A	A	A	G	G	A	C	G	T	T	T	C	C

Using this model as a predictor for the efficiency of the guides used in this study it is clear that guide 1 was less efficient than guide 2. Guide 1 had only 5 nucleotides in a position that increased efficiency and importantly contains a cytosine residue at position 3 which also severely decreases efficiency. This predicted low efficiency of guide 1 may explain its lack of function as DNA cleavage efficiency may not have been high enough to result in the incorporation of the linear donor. Linear donor integration has low efficiency and therefore relies on many cleavage events for its integration which guide 1 may not have been able to provide. Alternatively, transfection of the pCas-Guide construct containing guide 1 may not have been successful. This would result in the initial puromycin resistance, this resistance would then be lost as no linear integration would occur which was the case. To determine if the pCas-Guide transfected into the cells successfully PCR using primers for the construct could have been used, but as a puromycin resistant population of guide 2 treated cells was attained, this was not carried out due to time constraints. Moving forward, all subsequent work is carried out on guide 2 treated cells.

5.5.3 Guide 2 treated cells were larger when analysed via flow cytometry, a characteristic indicative of EB2 KO

Long term growth and puromycin selections of guide 2 treated cells resulted in a population of cells that appeared heterogenous for both size and morphology. This suggests that not all cells contained the linear donor integrated into the MAPRE2 gene although increased size is only predictor based on Goldspink *et al.,* (2013). Flow cytometry and FACS was therefore used to analyse and sort out a population of cells with increased size and that were GFP positive. As described previously, cells depleted of EB2 via siRNA were shown to be larger (Goldpink *et al.,* 2013). However, it should be noted that previous size analysis of EB2 depleted cells was carried out on 2D cells adhered to glass. The size of these cells was determined by adhesion behaviour, focal adhesion amount and distribution. These factors may be the main influences for cell size as a result of EB2 depletion, although this remains to be determined. Flow cytometry analysis and sorting of cells was carried out in suspension and

therefore volume rather than the 2D size/area is the characteristic being quantified and selected for. Currently it is unknown if these two measurements are mutual, but likely do have a close relationship. Another concern using this method is the possibility of multiple adhered cells clustered in suspension. These clumps of cells would give false positives for larger cells although this effect would be present in both groups nullifying any data skew. As large cells were isolated it was essential to reduce the number of adhered cells in suspension as to avoid the sorting of these undesired cells. To achieve this, both MDA cultures were treated with longer periods of trypsin and importantly with increased concentration of EGTA to separate cells. Other methods could also have been used to separate cell clusters such as mechanical sonic dissociation.

Flow cytometry analysis was first carried out to quantify the presence of GFP positive cells and the volumes of the untreated and CRISPR treated cells. Almost all (98%) CRISPR treated cells had increased 488nm fluorescence compared to the control which showed low signal intensity, most likely caused by background and autofluorescence of these cells. This suggests that almost all CRISPR (guide 2) treated cells contained the linear donor, although at this stage it was unclear if this linear donor was integrated at the desired position within the MAPRE2 gene. Analysis of cell volume was carried out using forward scatter (FSC) Vs side scatter (SSC) that showed an enrichment of larger cells in the CRISPR treated group compared to the untreated cells. Although it is normal for *in vitro* tissue cultures to contain some heterogeneity for size, as there was an enrichment of these larger cells, it is likely that these larger cells contain the linear donor inserted into the guide 2 target site, knocking out EB2.

5.5.4 Cells 3.5-fold larger than WT were sorted from the population of guide 2 treated cells and showed variation in EB2 expression

FACS was then carried out to sort the larger GFP cells from the population which likely contained the linear donor within the MAPRE2 gene. The desired outcome was a monoclonal population of cells with the linear donor integrated in a homozygous fashion. Although this could not be achieved at this stage, it was possible to select for larger cells, decreasing the heterogeneity of the population. This made downstream experiments to isolate desired cells more achievable. Using FACS, cells were sorted based on two gates. Firstly, all GFP positive cells were gated, these were larger than the GFP negative cells in the CRISPR treated group although there was some heterogeneity in this population. Within the GFP positive gated cells the largest cells were gated, and it was this combination of gates that was sorted from the cell suspension. Within the GFP positive population there were some outliers with substantially increased size of around 3.5x the peak of that of the GFP positive population. Goldspink *et al.,* (2013) found that EB2 KO caused a ~4x increase in cell size with EB2 siRNA depletion, therefore these large cells were also sorted from the population. Observation of

this population showed an enrichment for larger cells, but some smaller cells still remained. This was likely due to the inaccuracies of the FACS system but also because of cell doublets (clusters) being present in the suspension which gave false positive readings for cell size increase. Seen under a light microscope after sorting, these doublets were also present in the untreated controls so likely had little bearing on flow cytometry analysis but suggests future isolation of a homozygous clone will be more challenging due to the presence of these cells.

5.5.5 Sub cloning of CRISPR treated cells failed to yield monoclonal populations due to low survival rates

Cell cloning was carried out with the aim of isolating a monoclonal population of homozygous EB2 KOs. Unfortunately, isolated single cells showed extremely low survival rates even when using MDA conditioned media and collagen coating. To determine if the lack of single cell survivability was a feature of the MDA-MB-231 cell line or due to CRISPR treatment, single cells were isolated from both (Fig. 5.7). As MDA WT cells showed very good single cell survival and the CRISPR treated cells did not, this confirms that the apparent lack of EB2 was lethal to these cells in this environment. The majority of isolated cells from the CRISPR treated and sorted population showed extensive blebbing indicative of apoptosis. This could have been confirmed by labelling for apoptosis markers such as annexin V.

Elucidation of the low survival rates of these sub clones is beyond the scope of this study but several possibilities remain likely. Previous research by Yang *et al*., (2017) used CRISPR to KO EB2 but only in combination with EB1 and EB3 KO in Hela cells. EB2 KO was also attempted in the RPE1 and HT1080 cell lines in combination with EB1 and EB3 KO but KO of EB2 was unsuccessful. EB2 CRISPR KO was carried out in these cell lines with no observable effect, this suggests that depletion/KO of EB2 has no effect when EB1 and EB3 are also depleted/KO. These studies did not attempt the KO of EB2 alone and therefore it is unclear if cells are viable with KO of EB2 based on this previous literature, no other study has attempted EB2 KO alone. However, EB2 siRNA depletion studies by Goldspink et al (2013) revealed no effect after 96h but growth was slower after 120h. The low survival rate of sub clones with suspected EB2 KO in this study may be explained by the very high expression of EB1 in the MDA-MB-231 cell line, normally EB2 competes for MT binding and excludes EB1 from the MT lattice due to affinity competition (Yang *et al.,* 2017, Goldspink *et al.,* 2013). Knock down of EB2 via siRNA has been shown to result in EB1 association along the MT lattice, resulting in long straight MT bundles in the ARPE-19 cell line, which is a marker of MT stability (Goldspink *et al* 2013). Based on this research, KO of EB2 likely leads to a strong association of EB1 along the lattice, creating very stable and long MTs exacerbated by the high EB1 expression in the MDA-MB-231 cell line. MT remodelling is likely negatively affected by this accumulation of EB1 causing spindle abnormalities. These abnormalities

may be severe enough to prevent mitosis occurring as MT binding to kinetochores is a cell cycle checkpoint known as the spindle assembly checkpoint. McKinley and Cheeseman., (2017) showed dramatic spindle abnormalities in dividing cells with the KO of EB1 and EB3. Using CRISPR to KO EB1 and EB3, this study showed an increase in the frequency and severity of mitotic defects (McKinley and Cheeseman., 2017). The fact that large cell that did survive isolation, and in the current study, did not proliferate suggests that cells likely enter cell cycle arrest or apoptosis in response to a failed checkpoint during proliferation. Two clones (referred to as clones but likely consisting of several founding cells) were isolated numbered 3 and 6 which looked the most promising due to their increased size compared to WT and other clones.

5.5.6 Genomic integration of linear donor was confirmed in sub clone 6

To confirm that the linear donor containing the selection markers was inserted into the MAPRE2 guide 2 site, PCR was carried out with primers 5' and 3' of this target site. WT and clone 3 showed amplification of the WT MAPRE2 region and no amplification of the larger fragment indicating no linear integration in these cells. Clone 3 exhibited puromycin resistance and therefore either possess off target integration of the linear donor or the donor was expressed in its linear form without genome integration, two results that are undesirable for this study. Clone 3 potentially contained INDEL mutations within the MAPRE2 guide 2 site caused by CRISPR Cas9 treatment but without the successful integration of the donor. Donor integration has lower efficiency than simply inducing these INDEL mutations and therefore would occur more commonly. Work on this clone was halted due to the unknown location of the linear donor and risk of off-target effects which may affect cell behaviour in later experiments. On the other hand, clone 6 was more promising as it showed the amplification of a larger band around 2.5kb larger than that of the WT MAPRE2. This shows the presence of the linear donor within the cut site and confirms mutation of MAPRE2 in this clone. However, WT MAPRE2 was also amplified in this sub clone which suggests the cell population was heterozygous for this genomic integration or a heterogenous population of cells exists.

An attempt was made to sequence this 3+kb band via gel extraction and third party sanger sequencing. As traditional Taq polymerase has no proof reading ability and is considered too error prone for amplifications of this length, the OneTaq system (NEB) was used. This system uses Taq polymerase due to its high efficiency but also uses the DeepVent polymerase with 5x higher fidelity than Taq owing to its 3' to 5' proofreading exonuclease activity. Unfortunately, sequencing of this site proved difficult, time did not allow for the optimisation of this process. This may have been achieved by band extraction, purification and amplification followed by sequencing. Ideally nested PCR would

be used to further increase efficiency as primer binding to 5' or 3' extreme ends reduces reaction efficiency. Another method that could have been used was the use of primers that bind within the linear donor itself. This removes the reaction bias that exists in the amplification of the WT site as this is a shorter amplicon and would therefore have an exponentially higher rate of amplification.

5.5.7 EB2/MAPRE2 expression in clone 6

At this point, guide 2 treated cells have been selected for puromycin resistance and sorted for GFP expression and for increased size. An attempt was made to isolate single cells which proved difficult. Isolation of groups of 2 to 3 cells did prove more successful. Although not ideal this does dramatically decrease the possible heterogeneity seen in the population although it is likely EB2 expressing cells persist. Immunolabelling for EB2 was then carried out to determine the expression levels in these cells. EB2 immunolabelling confirmed clone 6 was the most promising of the clones with the lowest expression/intensity when quantified, with a reduction of 62%. Clone 6 did show some EB2 staining suggesting it may be present in the population. This reaffirms that this is likely a heterogenous population, consisting of heterozygous knockouts with the potential of having homozygous KOs present. Further evidence of this comes from western blot analysis of EB2 in clone 6. This showed an expression decrease similar to that seen in immunolabelling showing the presence of some WT EB2. Clone 3 cells showed little difference in EB2 expression from quantification of immunolabelling (data not shown).

However, the use of antibodies as a measure of gene expression had the potential to under report the proportion of cells with EB2 KO. MAPRE2 mutations induced by CRISPR Cas9 treatment may have produced non-functional forms of the EB2 protein yet still maintain reactivity to the antibodies used. It is therefore important to understand where the epitope site is on the antigen and the potential effects on this site which depend on the site being targeted within the target gene. Unfortunately, the epitope site for the EB2 antibody used in this study is currently unknown and it is therefore impossible to predict whether non-functional, antibody reactive products are produced. Immunolabelling for EB2 showed a mixed culture with some showing normal expression when compared to control and others showing an almost complete loss of EB2 with little fluorescence presumably because of non-specific binding. This suggests that the sorted cell population was heterogenous for the expression of EB2 although this is based on antibody testing which may be overreporting it presence.

To overcome this potential problem, qPCR was carried out to quantify the expression of MAPRE2 (EB2) mRNA in clone 6. As predicted qPCR analysis showed a more significant knock down of 73% suggesting that antibody quantification was slightly overreporting its presence. This again

confirms that some WT EB2 remains in the clone 6 population and is therefore not a knockout cell line but instead is a model for reduced EB2 expression.

5.5.8 Depleted EB2 expression caused several morphological changes in MDA cells (clone 6)

To determine the functional effect of depletion of EB2 several characteristics were studied such as size, proliferation and migration. EB2 siRNA depletion has previously been shown to led to an increase in cells size (Goldspink *et al.,* 2017) and this was also the case for this current CRISPR EB2 KO study. The Goldspink et al (2013) study showed a 4 fold increase in cell size which is close to the 3.5 fold size increase seen here. This supports the success of EB2 depletion in this sub clone although the large variation suggests a heterogenous population as evidenced previously. Although it should be noted that these larger cell were sorted out of the population which may contribute to this increase in size. None the less, larger cells were enriched in guide 2 treated cells showing it as an effect of EB2 depletion. EB2 depletion also reduced the proliferation rate when compared to controls suggesting influence on the cell cycle. Most likely, EB2 KO caused an increased stabilisation of MTs, preventing efficient reorganisation for mitotic spindle formation. Previous unpublished work from the Mogensen lab show that MDA-MB-231 have relatively high EB1 expression as well as high EB2 expression (Amodu, 2018). This would have the added effect of further stabilising MTs and may be the reason for the lack of survival of single KO cells. It is known that EB2 depletion does led to less dynamic MTs, supporting this theory (Goldspink *et al.,* 2017). Based on further experiments from the Mogensen lab it was also predicted that depletion of EB2 would have a detrimental effect on cell migration (Amodu, 2018). Indeed, this was also found to be the case in clone 6 cells. It was not possible to explain this effect based on these experiments, but it is likely dependent on the turnover of focal adhesions as suggested by work carried out in the Mogenesen lab as well as published work (Liu *et al.,* 2015, Yue *et al.,* 2014). This work showed that EB2 depletion reduces the turnover of focal adhesions through its association with HAX1 and MAP4K4, an essential process in the progression of cell migration. However Balcerak *et al.,* (2019) show that HAX1 depletion impacts collective cell migration of layers but not of single cells suggesting that HAX1 has a greater role in maintenance of cell-cell junctions and substrate adhesion. This work attributed the effects of HAX1 on actomyosin contractility via RhoA and septin signalling. This not only warrants further study in EB2 knockdown cells but also hints at the possible effects of EB2 in the maintenance of epithelial architecture studied within this thesis.

5.6 Summary

The aim of this chapter was to generate an EB2 KO/KD monoclonal cell line for use in further experiments for the study of EB2. Based on the presence of both WT MAPRE2 and EB2 in clone 6, only a knock down was achieved rather than the more desirable knock out of EB2. Despite this, clone 6 is a good model for reduced EB2 expression of 62-73% although with one major flaw. It is unclear if any homozygous KOs are present in the population and therefore results taken from this cell line should always be complimented with EB2 quantification as some cells likely express higher levels of EB2. Further exploration is needed into the low survival rates of desired cells, depletion of EB1 in these cells may increase survival but of course results may then be affected by loss of EB1. Ultimately, it may not be possible completely to KO EB2 in this cell line due to this high EB1 expression. None the less if this cell line is to be used further validation is needed, such as sequencing of the linear donor in the guide 2 site and also verification of potential off-target sites.

Chapter VI:

General Discussion

6.0 Chapter VI: General Discussion

6.1 Introduction

Understanding the intricacies of epithelial formation and maintenance is of great importance for the development of new treatments for diseases such as cancer. In fact, 90% of all cancers derive from epithelial tissue, a process that ultimately leads to epithelial tissue dysregulation. Understanding how this tissue is maintained as a polarised 'healthy' layer may prove very useful for the development of therapeutics or identification of early abnormal changes. In this study the effects of centrosome elimination on apico-basal polarisation/elongation, cyst formation and tissue architecture were analysed in MDCKII cells. Currently the role and importance of the centrosome in the formation of apico-basally polarised cells is unknown and requires further elucidation. The role of the MT plus tip binding protein EB2 was also studied to determine its effects during apico-basal polarisation. The MT cytoskeleton likely plays an important role in the results seen in this work as the centrosome and EB2 are important regulators of the MT network. MTs are important in many cellular processes such as mitosis, protein trafficking, migration, polarity and differentiation. Importantly for this work, MTs play an important role in apico-basal polarity where they are anchored by their minus-ends to apical ncMTOCs and extend basally. An apico-basal MT pattern allows for the bi-directional transport of cargo across the epithelial barrier. Exactly what role the MT binding protein EB2 and its expression level has on apico-basal polarisation in epithelial cells is not fully understood. Published data suggest that EB2 expression is required for the initial MT reorganisation as its depletion prevents MT reorganisation and cell elongation (Goldspink et al 2013). Here the effects of EB2 overexpression on cell polarisation/elongation and tissue architecture were studied in the MDCKII epithelial cell model. In addition, a MAPRE2 knock-down cell clone with reduced EB2 expression was generated using CRISPR/Cas9 in the highly invasive MDA-MB-231 breast cancer cell line and the consequences for cell proliferation, size and migration were analysed.

6.2 The centrosome is important for ncMTOC formation, apico-basal polarisation and 3D cyst formation

The centrosome is the main MTOC of most symmetrical animal cells, responsible for the nucleation and anchorage of MTs. Distinct changes occur to the centrosome upon apico-basal polarisation such as its relocation to the cell apex and change in function, as well as compositional changes. It is not known if the centrosome in an essential player in apico-basal polarisation and the formation of ncMTOCs in epithelial systems. The limited work that has been carried out in C. elegans suggests that the centrosome is essential for the redistribution of γ-tubulin to ncMTOC but whether lack of a centrosome prevents apico-basal polarisation is not known (Feldman and Priess., 2012). Some

cell types such as *Drosophila* wing cells do not require the centrosome for the reorganisation of MTs and the establishment of new ncMTOCs at the apical membrane. In this system the centrosome is present during pupal development where some MT reorganisation to the junctions occurs, but during very late pupal development the centrosome is lost and a ncMTOC occurs (Mogensen *et al.,* 1987, Mogensen *et al.,* 1989, Tillery *et al.,* 2018).

The findings in this study suggests that the centrosome is essential for the proper localisation of many key proteins involved in the formation of apico-basal polarised cells. Amongst these proteins is the relatively new CAMSAP family which was characterised in MDCKIIs for the first time here. As expected likely due to the primary peripheral MT organisation in MDCKIIs, CAMSAP3 was found at these peripheral MTOC sites in polarised cells as previously reported in other cell lines (Meng *et al.,* 2008, Toya *et al.,* 2016). Additionally, CAMSAP2 was found to be localised in puncta at apical sites in these polarised cells with some co-localisation with CAMSAP3. These puncta most likely represents sites for MT minus-end binding as apical organised MTs have been seen in MDCKII as well as other cell types such as enterocytes (Meads and Schroer,. 1995, Jiang *et al.,* 2014). Our findings show that the centrosome is essential for the normal distribution of CAMSAP2 and CAMSAP3 as centrosome removal ablated the peripheral and apical localisation of these proteins. Toya *et al.,* (2015) shows that functional loss of CAMSAP3 led to a loss of apico-basal arrays *in vivo* and a perturbed epithelial architecture. Therefore, the loss of CAMSAP3 localisation alone in this study likely confers a lack of polarisation in acentrosomal MDCKII cells. Analysis of the polarity marker PAR3 shows a distinct reduction in it localisation to the junctions with distinct cytosolic staining in this acentrosomal cells. This suggests that 2D partial polarisation was perturbed in the absence of the centrosome. The next logical step was to study these characteristics in 3D as this system is closer to the *in vivo* system, functionally and morphologically. However, acentrosomal cells showed a complete failure in the formation of cysts and therefore little data could be collected from this technique. This does however highlight the importance of the centrosome in 3D cyst formation, it is possible that the disruption to PAR3 and CAMSAP2/3 seen in acentrosomal 2D cells were enough to prevent 3D polarisation. More work is needed here to study why this cyst formation fails, imaging at much earlier time points instead of the ten days used in this study may provide some answers. A summary of results from chapter III can be seen in figure 6.1.

Why does removal of the centrosome cause these aberrations and what effect is this likely to have on normal cell behaviour? The mechanisms of ncMTOC formation are still not fully understood but the basic principles are the formation and activation of ncMTOC with an attenuation of the centrosome. One theory to the formation of ncMTOCs is that MTs transport nucleation and anchoring factors directly to these sites, indeed this has been shown to occur for ninein (Sanchez and Feldman.,

2017, Goldspink *et al.,* 2017). The loss of proper PAR3 is likely the cause of this lack of ncMTOC formation as PAR3 has been shown to recruit proteins such as γ-tubulin to the adherens junctions showing that PAR3 localisation acts upstream the formation of these sites. This is likely to effect CAMSAP2 and CAMSAP3 localisation as CAMSAP localisation here occurs after the formation of the adherens junction as CAMSAP3 is recruited to PLEKHA7 at this site (Meng *et al.,* 2015). Exactly how PAR3 becomes localised to the junctional and apical sites is currently unclear but dynein mediated MT transport has been shown to be important and essential for its positioning suggesting that centrosome removal may perturb MT organisation and thus misdeliver PAR3 (Jouette *et al.,* 2019). More work is needed into the examination of the MT network that forms in the absence and how this network interacts with the periphery and how protein transport is affected.

A limitation of this work is the use of centrinone B to prevent centrosome replication rather than the use of a method that actively removes the centrosome (Wong *et al.,* 2015). This method results in a few centrosomes always present in a population of cells which may affect results. Although it was confirmed that centrinone B treatment drastically reduced the proportion of cells containing a centrosome, centrosome labelling was not carried out in every experiment. Centrinone B treatment also caused a significant increase in cell size which may also have affected the cells ability to polarise normally. The reason for this increase in cell size could not be determined, this increase in size raises concerns about the health of the cells during these experiments and more work is needed to elucidate the cause of this and potential downstream effects on polarisation. Inhibition of PLK4 may also have undesirable effects as PLK4 is involved in cytokinesis, Press *et al.,* (2019) showed that PLK4 is found at the cleavage furrow of cytokinesis stage cells. PLK4 inhibition in HCT-116 cells showed that cell abcission could not occur and daughter cells were not produced (Press *et al.,* 2019). Due to these potential issues, more than one method should be used such as laser ablation and the results compared to those seen here with centrinone B treatment. More work is also needed to elucidate the survivability of these cells with centrinone B treatment, it is possible that centrinone B treatment is selecting a sub set of MDCKII cells containing mutations for survival without a centrosome such as p53 mutations. Finally, the use of the CAMSAPs as a marker of MT minus-end localisation should be used in combination with MT staining to confirm the co-localisation. CAMSAP localisation may not necessarily always confer MT organisation although the literature suggests it.
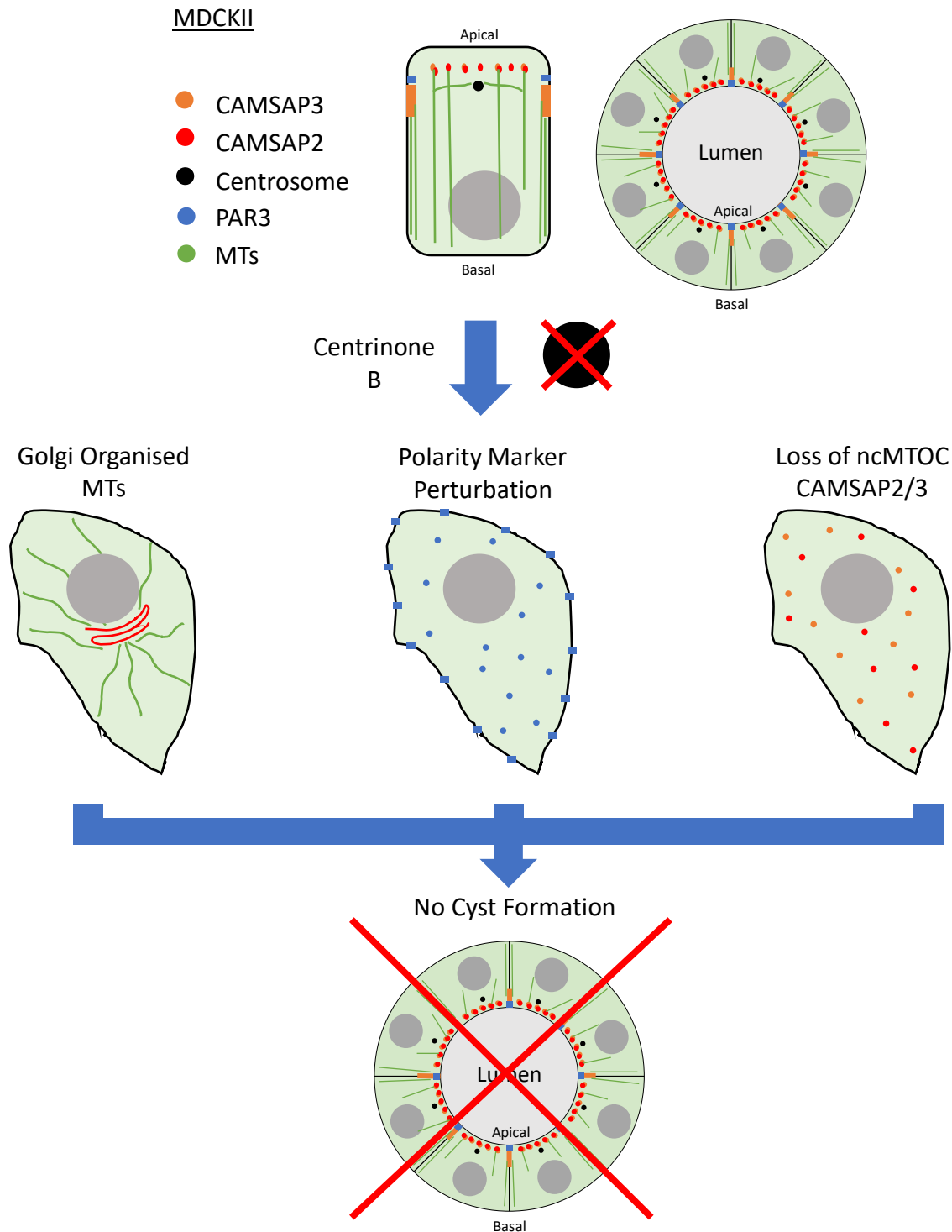
Figure 6.1 Summary diagram of a possible model for chapter III results. In 2D, centrosome removal led to loss of normal CAMSAP2 and CAMSAP3 localisation and PAR3 polarity marker with a change in MT pattern. Diagram shows MTs likely became organised at the Golgi, the PAR3 polarity marker decoration of cell-cell contacts was perturbed and CAMSAP2 and CAMSAP3 decoration of known ncMTOCs was lost. Taken together these results suggest a reason for the inability of cells to form 3D cysts as these effects may have prevented cyst formation in 3D as acentrosomal cells did not form cysts although this needs further examination.

6.3 Increased EB2 expression mimics characteristics of undifferentiated cells

Little research has been carried out on EB2 and its function in epithelial apico-basal polarisation. Previous published work identified a relatively high expression of EB2 in undifferentiated cells both *in vitro* and *in vivo*, this expression decreased as differentiation/polarisation proceeded (Goldspink *et al.,* 2013). Based on this evidence EB2 appears to be a regulator of epithelial cell differentiation and polarisation. Our work explored the effects of too much EB2 on epithelial cell polarisation, elongation and tissue architecture using EB2 overexpression in MDCKII cells as a model.

Our results revealed that overexpression of EB2 caused several characteristics indicative of early differentiated cells. This included a decrease in cell height in these EB2 overexpressing cells compared to the empty vector control cells. Increase in cell height is a marker of increased polarisation and differentiation and as such a reduction indicates EB2 perturbs this process. This fits with previous research showing less differentiated cells show increased EB2 expression (Goldspink *et al.,* 2013). Exploring this further it was shown that the polarity marker PAR3 had reduced staining at the cell-cell contacts. As PAR3 is essential for the establishment of apico-basal cell polarity, a lack of proper localisation further suggests that overexpression of EB2 perturbs polarisation and differentiation (Malt *et al.,* 2019). A relatively new method for the analysis of epithelial monolayers is shape index which compares the perimeter and area of cells in a layer to define a value against a threshold value (UJT), representing jammed or unjammed layers (Park *et al.,* 2015). Using this analysis method, it was shown that EB2 overexpressing cells presented an increased shape index that did not decrease with time. Again, this adds to the evidence which further supports the notion that EB2 perturbs normal tissue maintenance and architecture in these cells. The observation that EB2 overexpression effects junctions suggests that changes cell-cell contact may be influencing cell jamming or pEMT. Although Ilina *et al.,* (2020) shows cell density and its regulation by 3D tissue boundaries physically control collective movement and jamming irrespective of the composition and stability of the cell-cell contacts. This work suggests that jamming–unjamming transitions are jointly controlled by cell–cell and cell–matrix interactions and cell slippage. More work is therefore needed to examine the effect on the external environment of cells and how cell interactions with their environment effect jamming and pEMT Ilina *et al.,* (2020).

As shown by this work, the centrosome is very important for polarisation. As EB2 is a MT binding protein it stands to reason that it likely has some effect on the centrosome. Indeed, this work showed that overexpression of EB2 increased γ-tubulin retention at the centrosome likely increasing MT nucleation at this site. It is well known that γ-tubulin is released from the centrosome and becomes localised to the apical membrane in some cell lines during apico-basal polarisation (Feldman and Priess, 2012). Therefore, an increase in γ-tubulin at the centrosome likely indicates that high EB2

expression perturbs the formation of ncMTOC nucleation sites as γ-tubulin redeployment has been seen in MDCKII cells (Bre *et al.,* 1990). PAR3 has been shown to be responsible for this γ-tubulin localisation, the abnormal PAR3 labelling in EB2 overexpressing cells may therefore suggest a mechanism for this abnormal γ-tubulin retention (Feldman and Priess, 2012). PAR3 relies on dynein for its localisation, dynein is a MT motor protein that has many known interactions with EB1 (Jayatilaka *et al.,* 2018, Hendricks *et al.,* 2012). As EB2 and EB1 have been shown to have a competitive binding relationship this is a further area that warrants further explanation (Goldspink *et al.,* 2013). Despite these exciting results it is still unclear exactly how EB2 induces this lack of polarisation and differentiation. Goldspink *et al.,* (2013) show siRNA treatment of EB2 reduces MT dynamics significantly. Therefore, EB2 maybe exerting these effects through a change in MT dynamics. A summary of results from chapter IV can be seen in figure 6.2.

This work displays the potential importance of EB2 on the control of apico-basal epithelial tissue. This has implications not only for the development of these tissues but also for the further understanding of diseases affecting the epithelium. Isrie *et al.,* (2015) showed that mutations in MAPRE2 are a cause of circumferential skin creases kuze type disease, a congenital development disorder. It was shown that MAPRE2 mutations caused increased MT binding affinity with increased dwell time on MTs causing the phenotypes (Isrie *et al.,* 2015, Thues *et al.,* 2021). EB2 may have a role in early development of many biological systems that require the establishment of polarisation. Our work also implicates EB2 as a potential effector of cancer progression. Based on these results, high EB2 expression in fully differentiated epithelial cells likely causes some degree of reversion in the form of EMT. As work from our lab shows high EB2 expression increases invasiveness *in vitro* this is a very exciting area of research (Amodu 2018, Thesis). More work is needed to establish whether EB2 overexpression causes UJT or EMT as there is evidence for both in this work.

One of the main limitations of this work regarding the EB2 overexpression results, is that our model compares EB2 overexpression to a normal EB2 expression. As a reduction in EB2 is seen upon differentiation, it is likely it has concentration dependent effect and the endogenous EB2 expression of MDCKII cells may mask or limit effects of its overexpression. A more fitting model would compare an absolute high to low EB2 expression level. Another problem with this model is the fact that endogenous EB2 expression could not be quantified likely due to the loss of antigen when using the western blot. Alternatively, EB2 could have been quantified using qRT-PCR with probes designed for canine housekeeping genes as controls. Although it is likely that endogenous EB2 expression remains the same in the MDCKII[mCh-EMPTY] and MDCKII[mCh-EB2] cells this must be confirmed for future work. Improvements are also needed to some of the quantification methods used here such as the junction comparisons. Although carried out blind this is a very selective process that would be greatly improved

with automation and whole junction measurements to remove potential bias from the system. Additionally, much of this work relies on quantification of fluorescent intensities, which is sometimes regarded as a semi-quantitative method due to its potential high variability. Replacing these measurement with force measurements for studying the junctions and FRAP type experiments looking at E-cadherin junctional turnover would prove very useful. This would help elucidate if EB2 is in fact effecting cellular forces or E-cadherin turnover. Additionally, more work is needed to determine if the diffuse E-cadherin staining seen in MDCKII^mCh-EB2 confers an increase in junction size or a cytoplasmic faction of E-cadherin. Analysis of cell jamming was very limited in this study; further exploration of cell movement and behaviour should also have been carried out. This would further define the state of these monolayers and help differentiate cell jamming from pEMT. Finally, more repeats are needed for many experiments to ideally ensure at least three biological repeats are completed.
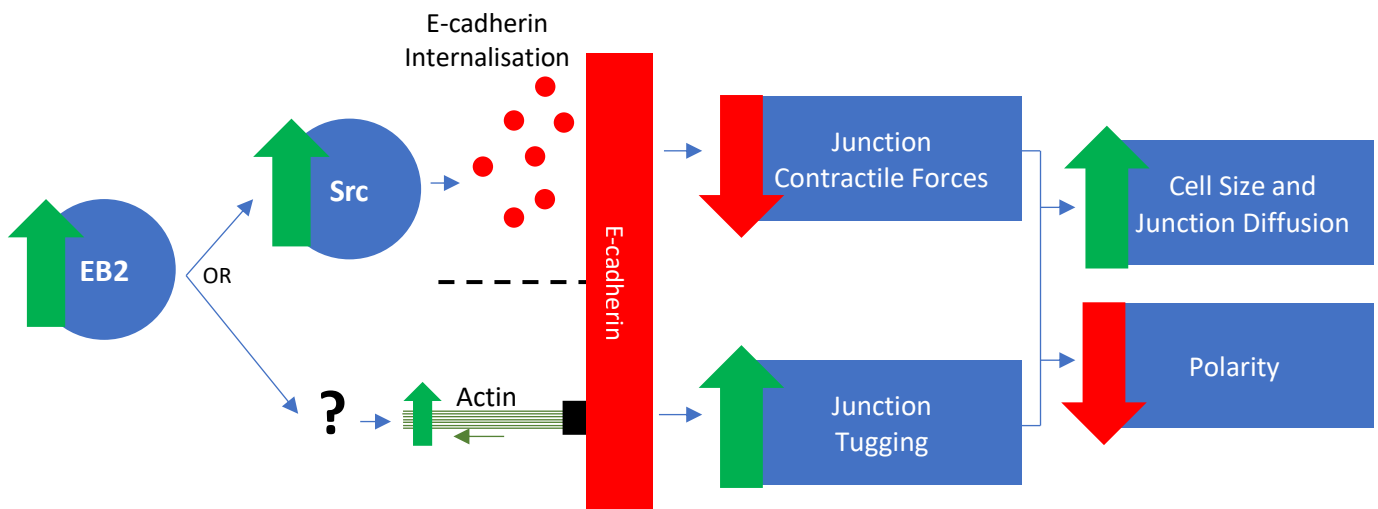
Figure 6.2 Summary diagram of a possible model for chapter IV results. The mechanism behind the junctional phenotype upon overexpression could not be fully elucidated in this work. Although it is likely that EB2 either increases tugging forces at the junction or decreases junction contractility by causing increased internalisation of E-cadherin via the activation of Src which is a known characteristic of high EB2 expression. Ultimately, this loss of junction stability may cause irregular cell shape by reducing order within the system which may also increase cell size as cells are stretched due to this increased tugging or reduction in resistance to this force. This also likely effects cell polarity as junction formation and maintenance is essential to apico-basal cell polarity.

6.4 CRISPR-Cas9 knock down of EB2 reduced cell migration in MDA-MB-231 cells

In order to elucidate the effect of EB2 in an invasive cell line, CRISPR-Cas9 KO of MAPRE2 was attempted in the MDA-MB-231 cell line. This work resulted in a heterogenous population of MDA-MB-231 cells with reduced expression of EB2/MAPRE2. The target sites for our predesigned guides were validated to be present in the MDA-MB-231 cell line. Transfection of guide 1 and 2, Cas9 and a linear donor containing GFP and a puromycin resistance yielded guide 2 puromycin resistant cells only. Suggesting that guide 1 treatment failed to produce genomic integration of the linear donor possibly due to low efficiency of guide 1 directed genomic cleavage. Flow cytometry analysis show these cells were larger and GFP positive compared to WT control cell, this increase in cell size was a phenotype seen from previous siRNA knock down of EB2 (Goldspink *et al.,* 2013). One potential problem here is that Goldspink *et al.,,* (2013) took cell size measurements from adhered cells whereas flow cytometry analysis deals with cells in suspension. Adhered cells are heavily influenced by surface attachments such as focal adhesion therefore sorting cells based on size when in suspension may not be advantageous. Furthermore, previous research has shown that EB2 is essential for focal adhesion turnover as it recruits HAX1 and MAP4K4 to MTs for its delivery to the focal adhesions and untimely increases their turnover. It was not suggested if this would affect cell size and warrants further study if EB2 KO cells are generated in the future (Liu *et al.,* 2015, Tue *et al.,* 2014).

Another desirable characteristic was GFP expression as this indicated the presence of the linear donor, although there is a possibility that this comes from expression of the unintegrated linear donor with no mutation. These larger GFP positive cells were sorted from the population. Single cell isolation of these cells proved impossible, raising questions about the survivability of these cells and it is suggested that the high EB1 expression in the MDA-MB-231 is responsible for this due to perturbed MT reorganisation. Despite this a sub clone was collected although this subclone likely consisted of several parental cells. Western blot and immunolabelling for EB2 show significant reduction in clone 6 cells. PCR amplification of the guide 2 MAPRE2 target site showed increased band size indicative of linear genome integration but some WT MAPRE2 amplification was also seen in these cells. Concordantly, RT-q-PCR showed a similar reduction of MAPRE2 expression although again a full knockout was not seen. Random migration analysis of these cells showed that a reduction in EB2 expression caused a significant decrease in the invasiveness of these cells. A summary of results from chapter V can be seen in figure 6.3.

Clone 6 showed the most promise from this work with the greatest reduction of EB2/MAPRE2 expression. However, these cells consist of a mixed population, the genetics of which is unknown. The presence of some WT EB2 suggest cell are heterozygous for linear donor integration although it is not known if some homozygous KO cells are present. Additionally, the linear donor could not be

sequenced within the MAPRE2 gene, although increased size at this site suggests the linear donor has been integrated, this must be confirmed via sequencing. Sequencing of the MAPRE2 gene within these cells may elucidate what effect CRISPR-Cas9 treatment has had at this site and help determine the heterogeneity of these cells.
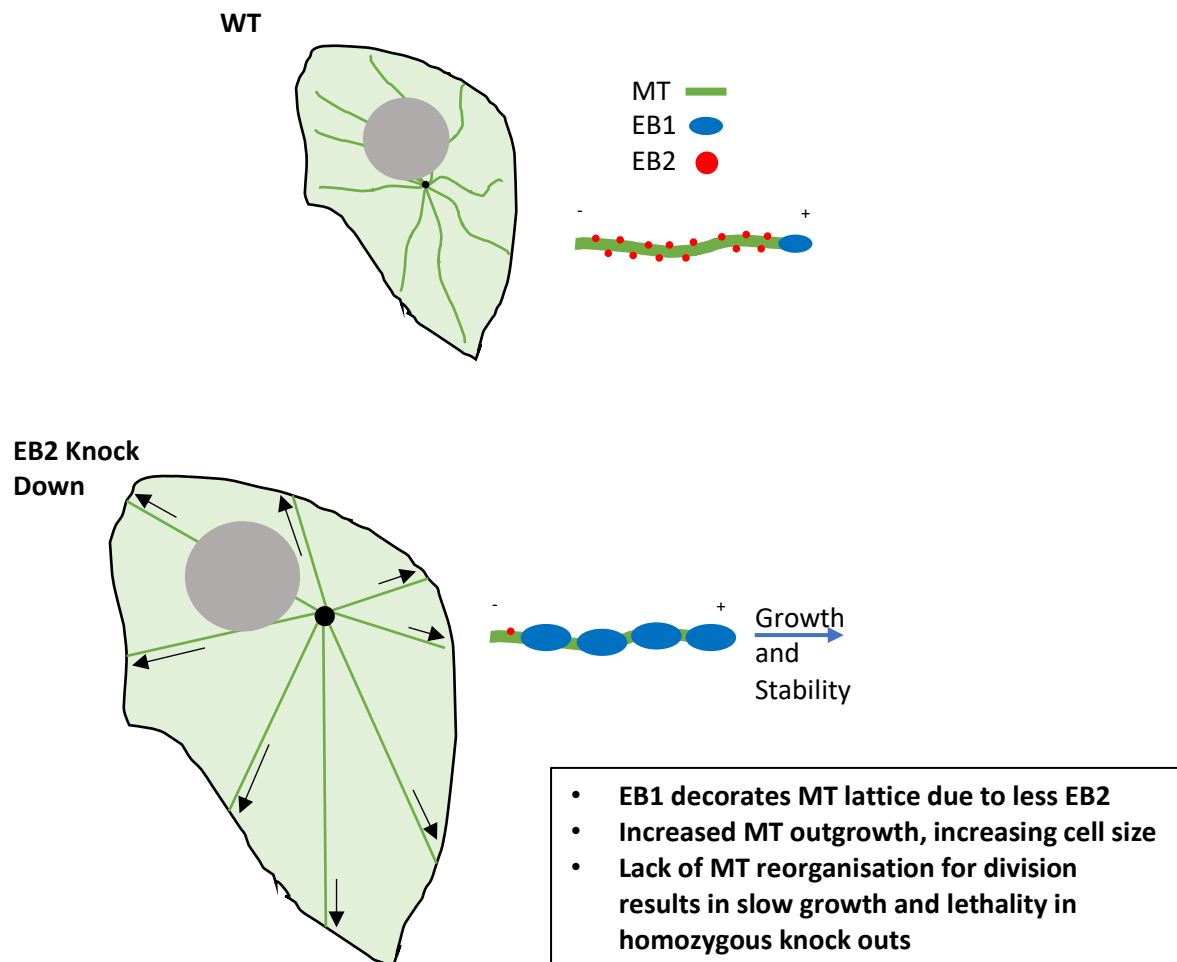
Figure 6.3 Summary diagram of a possible model for chapter V results. Previous research has shown that EB2 knockdown causes EB1 to decorate the MT lattice, increasing MT stability and bundle formation and ultimately cell size (Goldspink *et al.,* 2013). This likely explains several of the results in this work such as the lack of homozygous knockouts as these cells most likely cannot divide due to very stable MTs that cannot reorganise. These stable MTs likely increase the cell size and reduce the migration ability of these cells, again by inhibiting MT reorganisation.

6.5 Summary

Key findings of this project include:

1. Centrosome removal causes several aberrations of apico-basal polarisation events. These include loss of CAMSAP2 and CAMSAP3 localisation from the apical surface and cell junctions respectively. Centrosome loss also caused aberrant PAR3 localisation, a key marker of polarity. Finally, the centrosome appeared more important for polarisation of 3D samples as acentrosomal cells did not form cyst structures.

2. Overexpression of EB2 appears to mimic characteristics of undifferentiated cells in MDCKII cells. This includes a reduction in cell height, decreased PAR3 localisation to cell-cell contacts, increased shape index and increased γ-tubulin localisation at the centrosome.

3. CRISPR/Cas9 knock-down of EB2 in the highly invasive MDA-MB-231 cell line significantly reduced migration speed and distance.

6.6 Future work

These results suggest the centrosome is important for many aspects of apico-basal polarisation. Although very little is still known about the function of the centrosome in this process. A key finding here was loss of proper CAMSAP 2 and CAMSAP 3 localisation, suggesting the centrosome is important for defining ncMTOC sites. Further exploration is needed into the functional cause of the aberrations observed following centrosome removal in this system. As centrosome removal likely has many downstream effects more elucidation is needed to determine it effects. Study of MT dynamics in acentrosomal cell may explain the apparent loss of ncMTOC formation as previous research has shown that dynamics MT are essential for junction maintenance (Stehbens *et al.,* 2006). Detailed study of MT organisation is also needed to observe their anchorage and interactions at ncMTOCs. It is unknown what effect centrosome removal has on MT organisation and the transport of centrosomal proteins along them. This would also include studying MTs at ncMTOCs to confirm loss of organisation at these sites. Live imaging experiments would prove very useful for the study of many apico-basal events such as the movement and organisation of MTs. Labelling of MTs with dyes such as SiR-tubulin would elucidate MT organisation in acentrosomal cells and show their behaviour at ncMTOCs.

The results seen from the overexpression of EB2 in MDCKII cells gives rise to many exciting questions about its role in this process. Future work is needed to explore this area and elucidate how EB2 exerts the effects seen in this study. Key work will include examining the effect of EB2 on MT dynamics and how this effects apico-basal cell characteristics such as shape index and polarity marker

positioning. More work is needed into the relationship of EB1 and EB2 at the level of the MT to determine if EB2s effects are imparted through control of EB1 binding to MTs. An *in vivo* model of polarisation would be very useful for the study of the effect of EB2 on apico-basal polarisation. In particular, future work should explore this in an organoid system such as using gut organoids. This *in vitro* system combined with EB2 KO or overexpression would give great insight into the effect of EB2. Intestinal organoids show the differentiation of intestinal stem cells to terminally differentiated enterocytes and therefore EB2 modification could be visualised in this process (Fair *et al.,* 2018). As EB2 expression has been identified in some cancers to increase invasiveness, EB2 may also have an oncogenic property (Amodu 2018, thesis). Further exploration should include analysis of EMT markers such as vimentin and N-cadherin in the MDCKII$^{mCh-EB2}$ cells as well as studying cell velocity in these layers. This effect is potentially linked to the results seen from EB2 overexpression on apico-basal polarised cells. Loss of epithelial architecture and an increase in invasiveness are properties of EMT and warrant further investigation. It is likely that the expression level of EB2 needs to be finely balanced during development and tissue maintenance and that deviations may led to diseases such as cancer and circumferential skin creases (Goldspink et al, 2013; Thues et al 2021). Future work should also elucidate if EB2 overexpression causes a change in force distribution in the cell monolayer or a change in E-cadherin delivery at the junctions. This could be achieved by using FRAP with fluorescently tagged E-cadherin and looking at E-cadherin turnover at the junctions. Junctional laser ablation could also be carried out to measure the retraction of the layer to quantify the forces present within the cell layer (Liang *et al.,* 2016).

The EB2 knock-down cell line generated in this work require further validation. This includes validation for off target mutations and also sequencing of the linear donor integrated into MAPRE2 gene target site to ensure successful integration. Off-target mutation sites can be predicted based on complementarity to the guides used for MAPRE2 mutation, the most likely off-target sites should be identified and sequenced to ensure no mutation is present. Ultimately these studies will further enhance the results seen in this work and explore there meaning in this exciting area. To circumvent the possible failure of cell division in the absence of EB2 an inducible knockout cell line could be generated, this would be particularly useful when studying the effect of EB2 during polarisation. Using the Cre ER system, cell could be allowed to multiply then the knockout could be induced when suitable cell numbers are present.

Chapter VII:

Appendices

7.0 Appendices

7.1 Appendix: Supplementary Data

mCherry-EB2
Mouse EB2 (variant 3) in pmCherry-C1 (Clontech)

Multiple Cloning Site
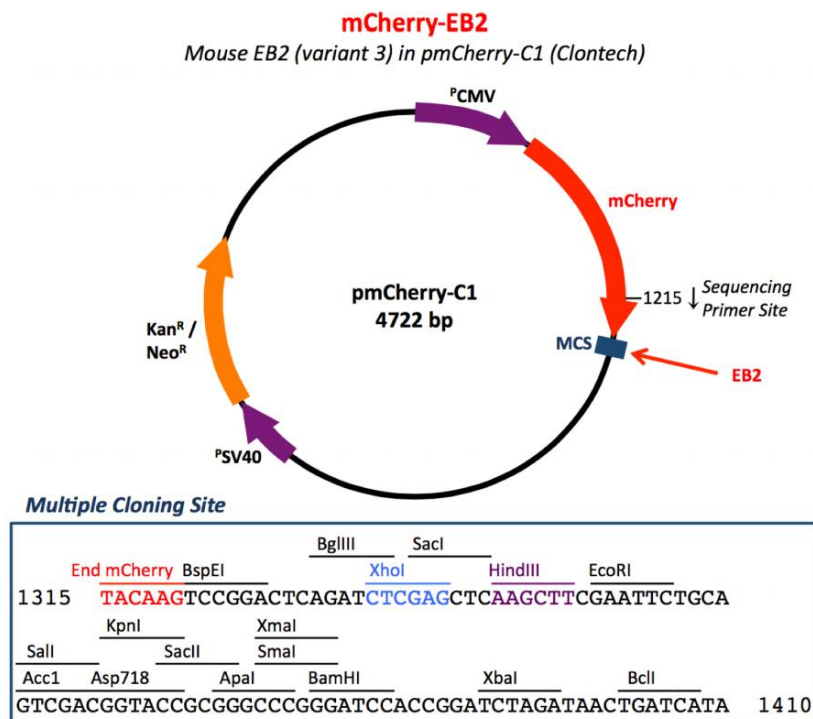
Figure S1 Construct map of pmCherry-C1. Generation of EB2 overexpressing cells was achieved using the pmCherry-C1 construct containing EB2 at the MCS. Mouse MAPRE2 was cloned into the MCS using the XhoI and HindII restriction sites. Kindly gifted by P.Powell, University of East Anglia.
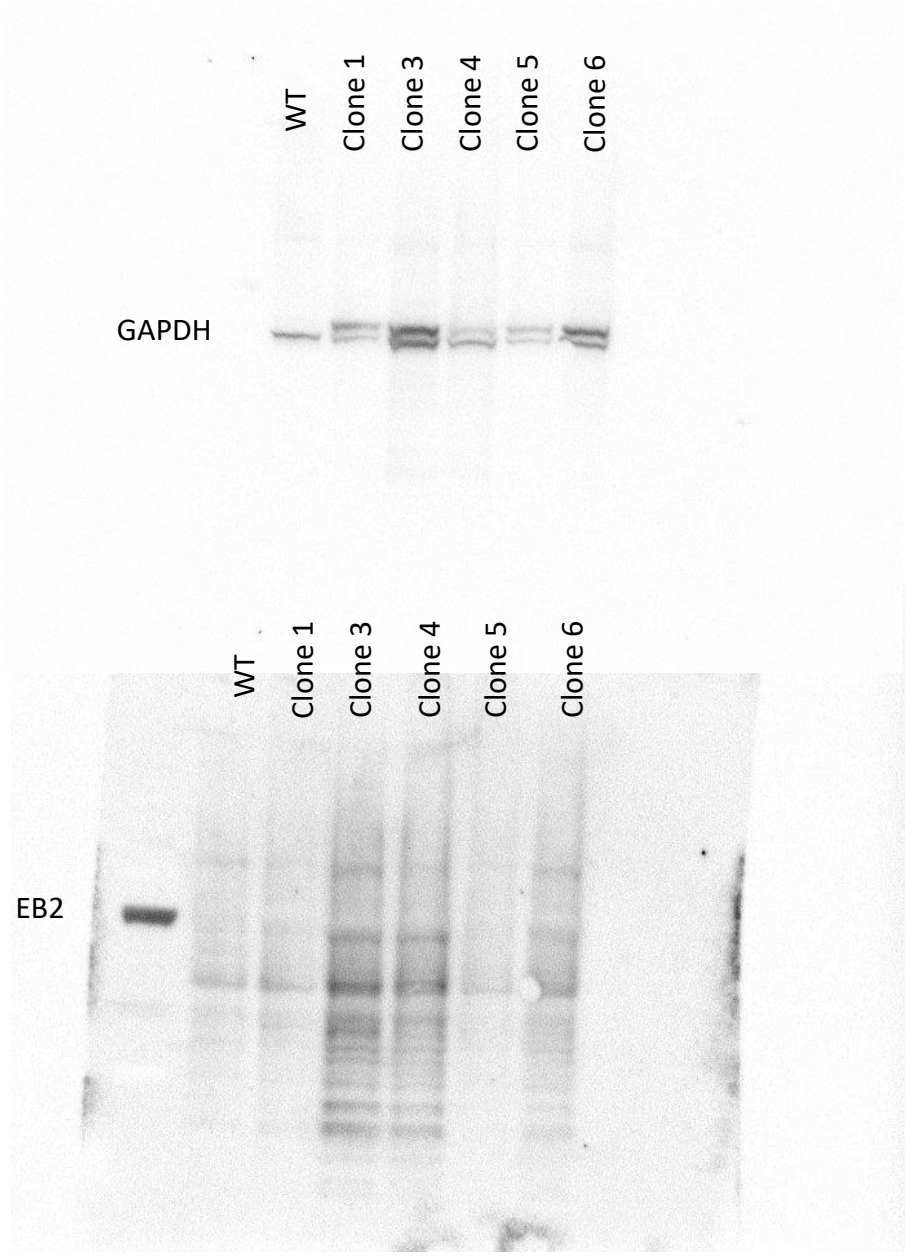
Figure S2 Full blots of EB2 expression in CRISPR treated clones
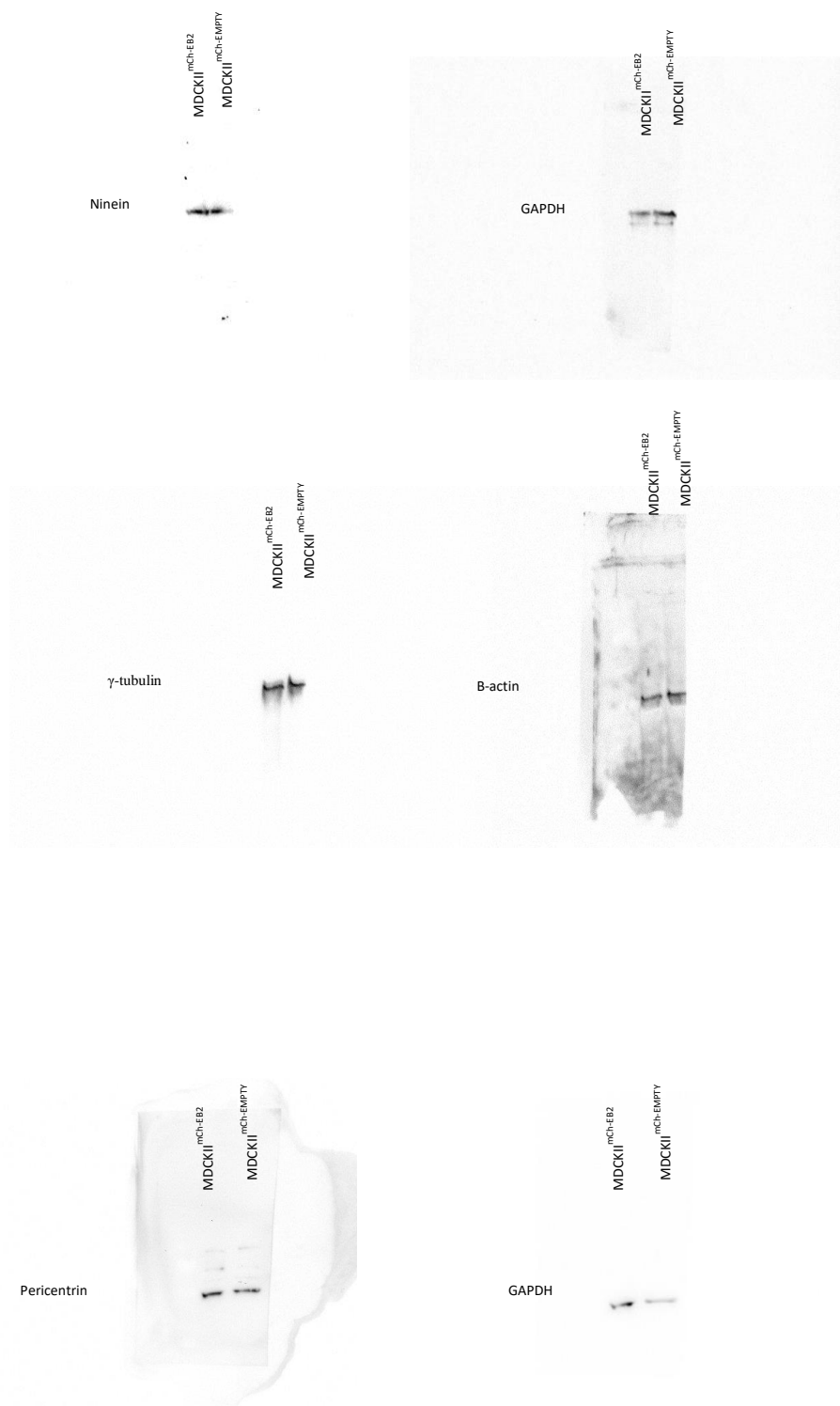
Figure S3 Full blots of Ninein, γ-tubulin and pericentrin expression with loading controls in MDCKII^{mCh-EB2} and MDCKII^{mCh-EMPTY} cells.

Junction Size (Blebbistatin)

Junction Size (Y27362)
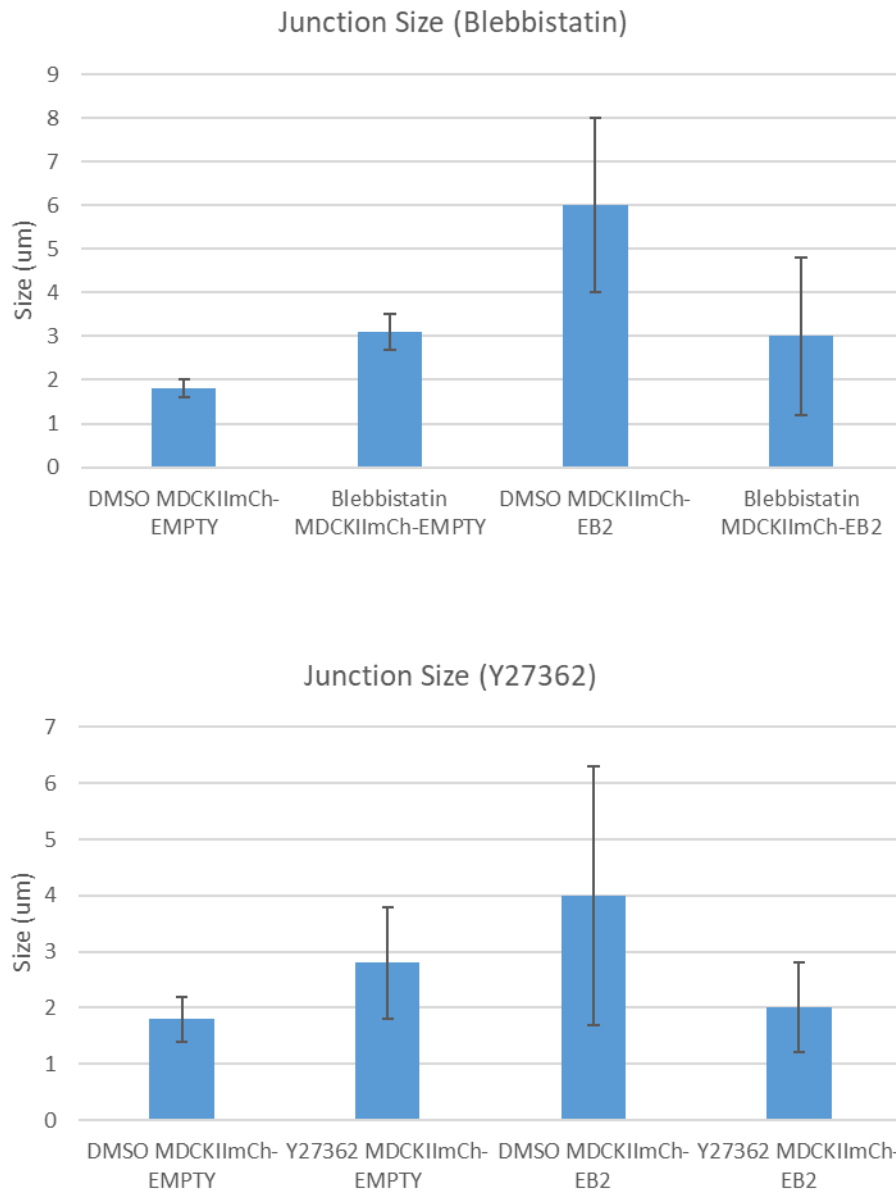
Figure S4 Quantification of junction diffusion with DMSO/blebbistatin/Y27362 treatment. Quantification based on thresholding of pixel intensities and measurements of junction diffusion using ImageJ. N=8 junction line profiles per group. +/- 1 SD shown.
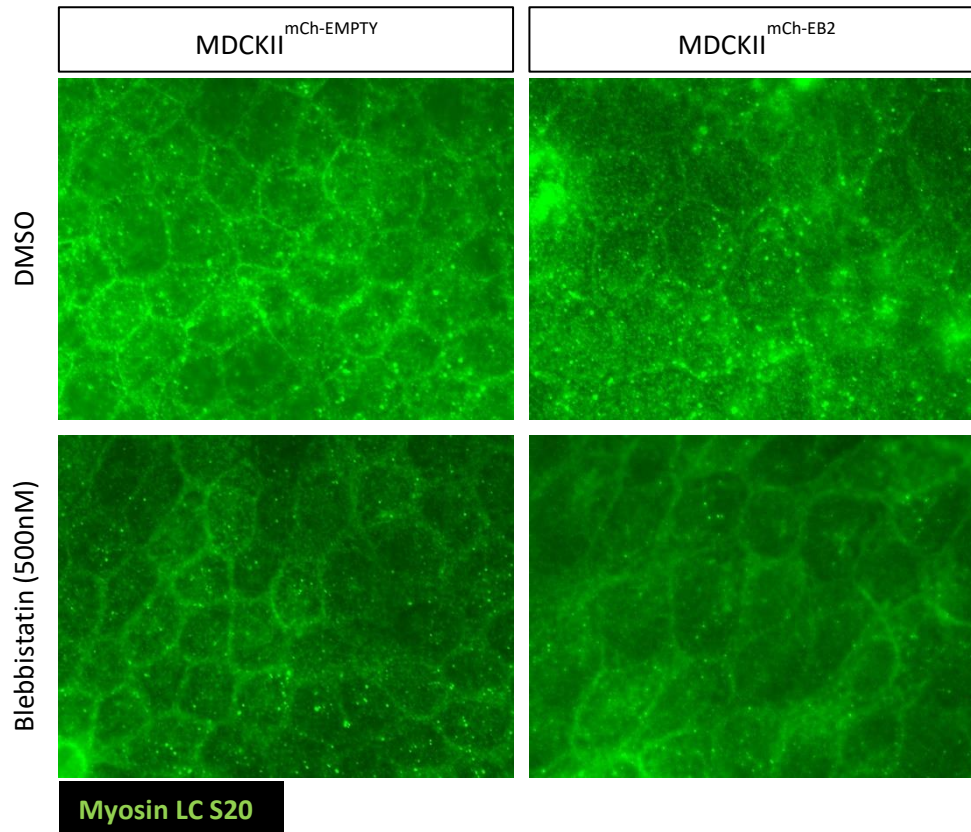
Figure S5 Activated myosin with blebbistatin treatment. Immunolabelling shows reduced intensity of activated myosin (Myosin LC S20) with blebbistatin treatment compared to DMSO control. Measurements shown in figure 4.9.

| | 0 Hours | 3 Hours | 6 Hours | 9 Hours |

WT
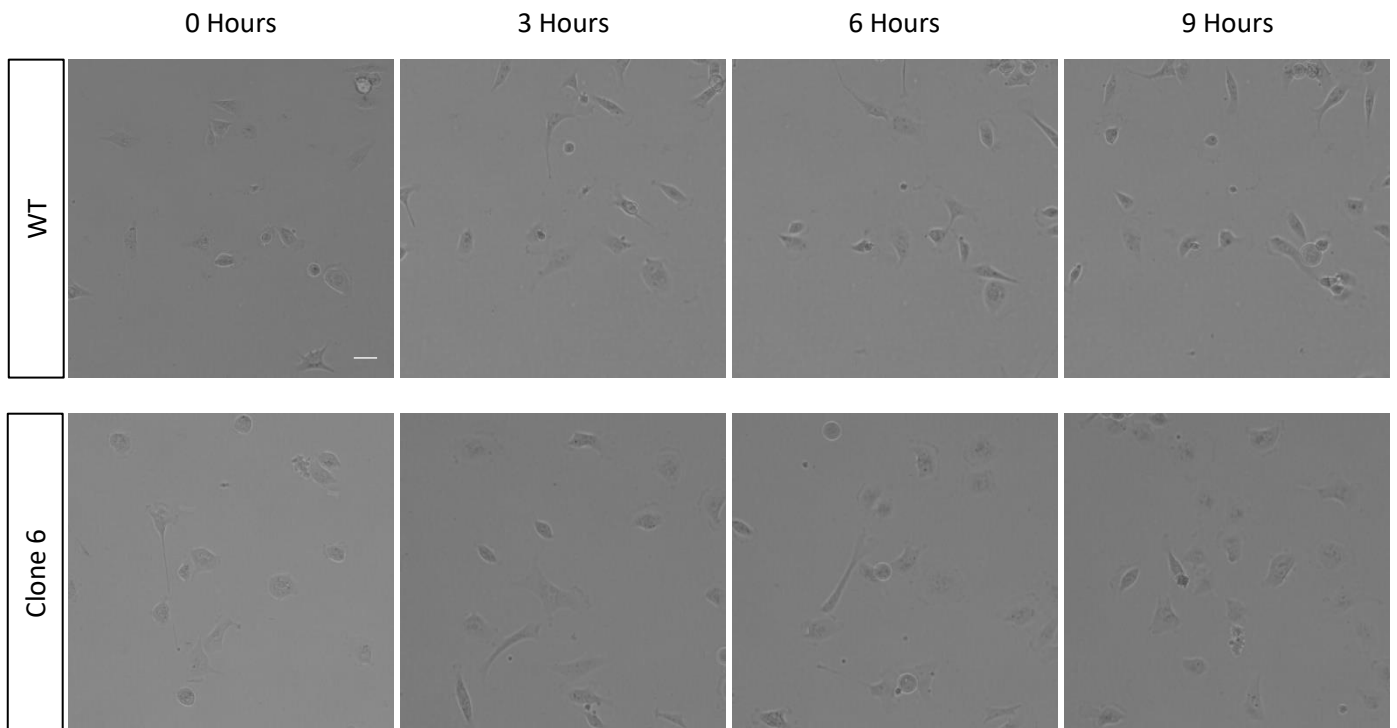
Clone 6

Figure S6 Random migration assay. MDA and CRISPR treated clone 6 cells seeded onto collagen coated plastic and imaged over 9 hours. Speed and distance of CRISPR treated clone 6 cells can be seen to migrate far less with quntifcation seen in figure 5.13.
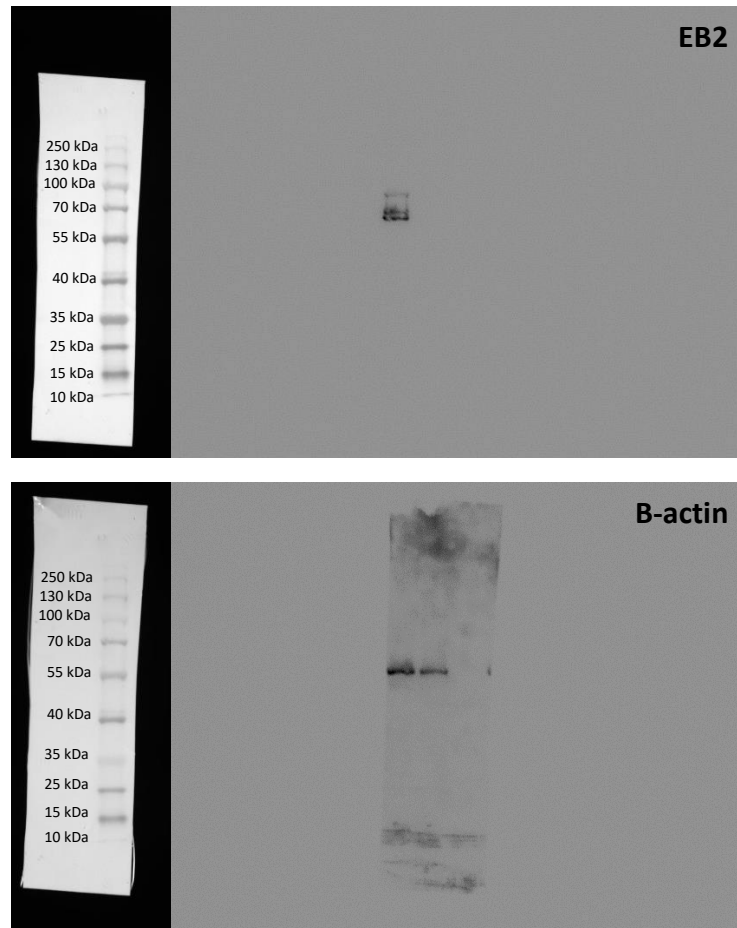
Figure S7 Full unaltered western blots showing EB2 and β-actin labelling in MDCKII^{mCh-EMPTY} (left) and MDCKII^{mCh-EB2} (right) cells.
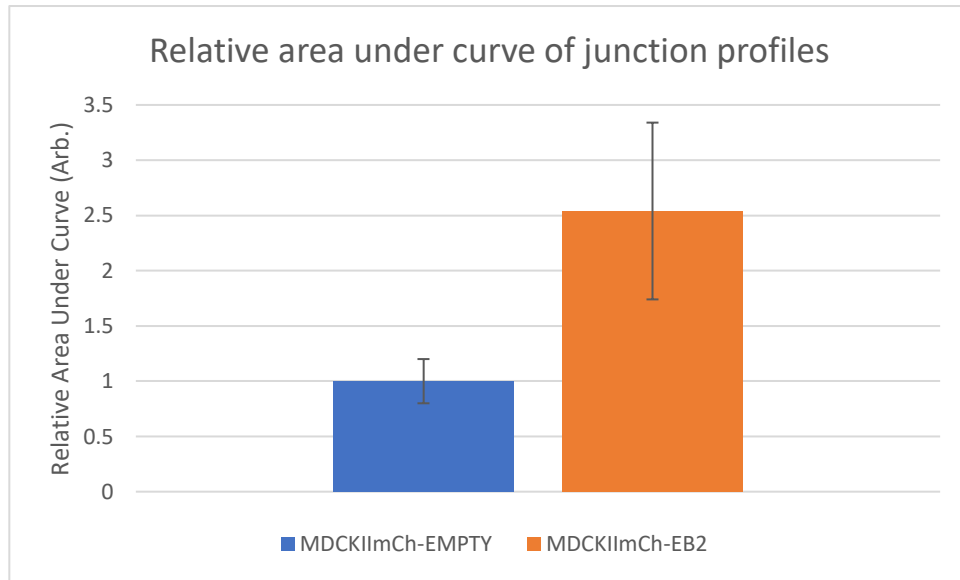
Figure S7 Relative Area under the curve of E-cadherin junctional intensity profile. Area under the curve relating to figure 4.5b shows that more junctional E-cadherin diffusion is present with MDCKII$^{mCh-EB2}$ cells which is confirmed by measuring area under the curve. Area under the curve was calculated using the common integration method.

Chapter VIII:

References

8.0 References

Ablain, J., Durand, E.M., Yang, S., Zhou, Y. and Zon, L.I., 2015. A CRISPR/Cas9 vector system for tissue-specific gene disruption in zebrafish. *Developmental cell*, *32*(6), pp.756-764.

Aillaud, C., 2017. *Modifications post-traductionnelles de la tubuline: identification des tubulines carboxypeptidases et découverte de nouveaux variants* (Doctoral dissertation, Université Grenoble Alpes).

Akhmanova, A., Hoogenraad, C.C., Drabek, K., Stepanova, T., Dortland, B., Verkerk, T., Vermeulen, W., Burgering, B.M., De Zeeuw, C.I., Grosveld, F. and Galjart, N., 2001. Clasps are CLIP-115 and-170 associating proteins involved in the regional regulation of microtubule dynamics in motile fibroblasts. *Cell*, *104*(6), pp.923-935.

Akhmanova, A. and Steinmetz, M.O., 2015. Control of microtubule organization and dynamics: two ends in the limelight. *Nature reviews Molecular cell biology*, *16*(12), pp.711-726.

Amodu T. A. 2018. Microtubules and end-binding proteins in epithelial remodeling and breast cancer invasion. Thesis. UEA

Antonellis, P.J., Pollock, L.M., Chou, S.W., Hassan, A., Geng, R., Chen, X., Fuchs, E., Alagramam, K.N., Auer, M. and McDermott, B.M., 2014. ACF7 is a hair-bundle antecedent, positioned to integrate cuticular plate actin and somatic tubulin. *Journal of Neuroscience*, *34*(1), pp.305-312.

Arora, P., Dongre, S., Raman, R. and Sonawane, M., 2020. Stepwise polarisation of developing bilayered epidermis is mediated by aPKC and E-cadherin in zebrafish. *Elife*, *9*, p.e49064.

Atia, L., Bi, D., Sharma, Y., Mitchel, J.A., Gweon, B., Koehler, S.A., DeCamp, S.J., Lan, B., Kim, J.H., Hirsch, R. and Pegoraro, A.F., 2018. Geometric constraints during epithelial jamming. *Nature physics*, *14*(6), pp.613-620.

Au, F.K., Jia, Y., Jiang, K., Grigoriev, I., Hau, B.K., Shen, Y., Du, S., Akhmanova, A. and Qi, R.Z., 2017. GAS2L1 is a centriole-associated protein required for centrosome dynamics and disjunction. *Developmental cell*, *40*(1), pp.81-94.

Azimzadeh, J. and Bornens, M., 2007. Structure and duplication of the centrosome. *Journal of cell science*, *120*(13), pp.2139-2142.

Balcerak, A., Trebinska-Stryjewska, A., Wakula, M., Chmielarczyk, M., Smietanka, U., Rubel, T., Konopinski, R., Macech-Klicka, E., Zub, R. and Grzybowska, E.A., 2019. HAX1 impact on collective cell migration, cell adhesion, and cell shape is linked to the regulation of actomyosin contractility. *Molecular biology of the cell*, *30*(25), pp.3024-3036.

Bartolini, F. and Gundersen, G.G., 2006. Generation of noncentrosomal microtubule arrays. *Journal of cell science*, *119*(20), pp.4155-4163.

Bearce, E.A., Erdogan, B. and Lowery, L.A., 2015. TIPsy tour guides: how microtubule plus-end tracking proteins (+ TIPs) facilitate axon guidance. *Frontiers in cellular neuroscience*, *9*, p.241.

de Beco, S., Gueudry, C., Amblard, F. and Coscoy, S., 2009. Endocytosis is required for E-cadherin redistribution at mature adherens junctions. *Proceedings of the National Academy of Sciences*, *106*(17), pp.7010-7015.

Bellett, G., Carter, J.M., Keynton, J., Goldspink, D., James, C., Moss, D.K. and Mogensen, M.M., 2009. Microtubule plus-end and minus-end capture at adherens junctions is involved in the assembly of apico-basal arrays in polarised epithelial cells. *Cell motility and the cytoskeleton*, *66*(10), pp.893-908.

Bertran, M.T., Sdelci, S., Regué, L., Avruch, J., Caelles, C. and Roig, J., 2011. Nek9 is a Plk1-activated kinase that controls early centrosome separation through Nek6/7 and Eg5. *The EMBO journal*, *30*(13), pp.2634-2647.

Bi, D., Lopez, J.H., Schwarz, J.M. and Manning, M.L., 2015. A density-independent rigidity transition in biological tissues. *Nature Physics*, *11*(12), pp.1074-1079.

Bieling, P., Kandels-Lewis, S., Telley, I.A., van Dijk, J., Janke, C. and Surrey, T., 2008. CLIP-170 tracks growing microtubule ends by dynamically recognizing composite EB1/tubulin-binding sites. *The Journal of cell biology*, *183*(7), pp.1223-1233.

Björklund, M., Taipale, M., Varjosalo, M., Saharinen, J., Lahdenperä, J. and Taipale, J., 2006. Identification of pathways regulating cell size and cell-cycle progression by RNAi. *Nature*, *439*(7079), pp.1009-1013.

Blick, T., Widodo, E., Hugo, H., Waltham, M., Lenburg, M.E., Neve, R.M. and Thompson, E.W., 2008. Epithelial mesenchymal transition traits in human breast cancer cell lines. Clinical & experimental metastasis, 25(6), pp.629-642.

Bobinnec, Y., Khodjakov, A., Mir, L.M., Rieder, C.L., Edde, B. and Bornens, M., 1998. Centriole disassembly in vivo and its effect on centrosome structure and function in vertebrate cells. *The Journal of cell biology*, *143*(6), pp.1575-1589.

Bornens, M., 2021. Centrosome organization and functions. *Current Opinion in Structural Biology*, *66*, pp.199-206.

Bosch Grau, M., Gonzalez Curto, G., Rocha, C., Magiera, M.M., Marques Sousa, P., Giordano, T., Spassky, N. and Janke, C., 2013. Tubulin glycylases and glutamylases have distinct functions in stabilization and motility of ependymal cilia. *Journal of Cell Biology*, *202*(3), pp.441-451.

Bossinger, O., Fukushige, T., Claeys, M., Borgonie, G. and McGhee, J.D., 2004. The apical disposition of the Caenorhabditis elegans intestinal terminal web is maintained by LET-413. *Developmental biology*, *268*(2), pp.448-456.

Brabletz, T., Kalluri, R., Nieto, M.A. and Weinberg, R.A., 2018. EMT in cancer. *Nature Reviews Cancer*, *18*(2), pp.128-134.

Bré, M.H., Kreis, T.E. and Karsenti, E., 1987. Control of microtubule nucleation and stability in Madin-Darby canine kidney cells: the occurrence of noncentrosomal, stable detyrosinated microtubules. *The Journal of cell biology*, *105*(3), pp.1283-1296.

Bre, M.H., Pepperkok, R., Hill, A.M., Levilliers, N., Ansorge, W., Stelzer, E.H. and Karsenti, E., 1990. Regulation of microtubule dynamics and nucleation during polarization in MDCK II cells. *The Journal of cell biology*, *111*(6), pp.3013-3021.

Brodu, V., Baffet, A.D., Le Droguen, P.M., Casanova, J. and Guichet, A., 2010. A developmentally regulated two-step process generates a noncentrosomal microtubule network in Drosophila tracheal cells. *Developmental cell*, *18*(5), pp.790-801.

Brouhard, G. and Sept, D., 2012. Microtubules: sizing up the GTP cap. *Current biology*, *22*(18), pp.R802-R803.

Bryant, D.M., Datta, A., Rodríguez-Fraticelli, A.E., Peränen, J., Martín-Belmonte, F. and Mostov, K.E., 2010. A molecular network for de novo generation of the apical surface and lumen. *Nature cell biology*, *12*(11), pp.1035-1045.

Bu, W. and Su, L.K., 2001. Regulation of microtubule assembly by human EB1 family proteins. *Oncogene*, *20*(25), pp.3185-3192.

Buey, R.M., Mohan, R., Leslie, K., Walzthoeni, T., Missimer, J.H., Menzel, A., Bjelić, S., Bargsten, K., Grigoriev, I., Smal, I. and Meijering, E., 2011. Insights into EB1 structure and the role of its C-terminal domain for discriminating microtubule tips from the lattice. *Molecular biology of the cell*, *22*(16), pp.2912-2923.

Burstein, D., Harrington, L.B., Strutt, S.C., Probst, A.J., Anantharaman, K., Thomas, B.C., Doudna, J.A. and Banfield, J.F., 2017. New CRISPR–Cas systems from uncultivated microbes. *Nature*, *542*(7640), pp.237-241.

Cailleau, R., Young, R., Olive, M. and Reeves Jr, W.J., 1974. Breast tumor cell lines from pleural effusions. *Journal of the National Cancer Institute*, *53*(3), pp.661-674.

Carvajal-Gonzalez, J.M., Mulero-Navarro, S. and Mlodzik, M., 2016. Centriole positioning in epithelial cells and its intimate relationship with planar cell polarity. *Bioessays*, *38*(12), pp.1234-1245.

Caudron, F., Andrieux, A., Job, D. and Boscheron, C., 2008. A new role for kinesin-directed transport of Bik1p (CLIP-170) in Saccharomyces cerevisiae. Journal of cell science, 121(9), pp.1506-1513.

Chatterjee, P., Jakimo, N. and Jacobson, J.M., 2018. Minimal PAM specificity of a highly similar SpCas9 ortholog. *Science advances*, *4*(10), p.eaau0766.

Chavez, K.J., Garimella, S.V. and Lipkowitz, S., 2010. Triple negative breast cancer cell lines: one tool in the search for better treatment of triple negative breast cancer. *Breast disease*, *32*(1-2), p.35.

Chen, X., Kojima, S.I., Borisy, G.G. and Green, K.J., 2003. p120 catenin associates with kinesin and facilitates the transport of cadherin–catenin complexes to intercellular junctions. *The Journal of cell biology*, *163*(3), pp.547-557.

Cho, S.W., Kim, S., Kim, Y., Kweon, J., Kim, H.S., Bae, S. and Kim, J.S., 2014. Analysis of off-target effects of CRISPR/Cas-derived RNA-guided endonucleases and nickases. *Genome research*, *24*(1), pp.132-141.

Clevers, H., 2013. The intestinal crypt, a prototype stem cell compartment. *Cell*, *154*(2), pp.274-284.

Conduit, P.T., Brunk, K., Dobbelaere, J., Dix, C.I., Lucas, E.P. and Raff, J.W., 2010. Centrioles regulate centrosome size by controlling the rate of Cnn incorporation into the PCM. *Current Biology*, *20*(24), pp.2178-2186.

Conduit, P.T., Feng, Z., Richens, J.H., Baumbach, J., Wainman, A., Bakshi, S.D., Dobbelaere, J., Johnson, S., Lea, S.M. and Raff, J.W., 2014. The centrosome-specific phosphorylation of Cnn by Polo/Plk1 drives Cnn scaffold assembly and centrosome maturation. *Developmental cell*, *28*(6), pp.659-669.

Cong, L., Ran, F.A., Cox, D., Lin, S., Barretto, R., Habib, N., Hsu, P.D., Wu, X., Jiang, W., Marraffini, L.A. and Zhang, F., 2013. Multiplex genome engineering using CRISPR/Cas systems. *Science*, *339*(6121), pp.819-823.

Cui, Y., Xu, J., Cheng, M., Liao, X. and Peng, S., 2018. Review of CRISPR/Cas9 sgRNA design tools. *Interdisciplinary Sciences: Computational Life Sciences*, *10*(2), pp.455-465.

Dahlman, J.E., Abudayyeh, O.O., Joung, J., Gootenberg, J.S., Zhang, F. and Konermann, S., 2015. Orthogonal gene knockout and activation with a catalytically active Cas9 nuclease. *Nature biotechnology*, *33*(11), p.1159.

Dang, Y., Jia, G., Choi, J., Ma, H., Anaya, E., Ye, C., Shankar, P. and Wu, H., 2015. Optimizing sgRNA structure to improve CRISPR-Cas9 knockout efficiency. *Genome biology*, *16*(1), p.280.

Delgehyr, N., Sillibourne, J. and Bornens, M., 2005. Microtubule nucleation and anchoring at the centrosome are independent processes linked by ninein function. *Journal of cell science*, *118*(8), pp.1565-1575.

Dictenberg, J.B., Zimmerman, W., Sparks, C.A., Young, A., Vidair, C., Zheng, Y., Carrington, W., Fay, F.S. and Doxsey, S.J., 1998. Pericentrin and γ-tubulin form a protein complex and are organized into a novel lattice at the centrosome. *The Journal of cell biology*, *141*(1), pp.163-174.

Dong, C., Xu, H., Zhang, R., Tanaka, N., Takeichi, M. and Meng, W., 2017. CAMSAP3 accumulates in the pericentrosomal area and accompanies microtubule release from the centrosome via katanin. *Journal of cell science*, *130*(10), pp.1709-1715.

Doxsey, S., Zimmerman, W. and Mikule, K., 2005. Centrosome control of the cell cycle. *Trends in cell biology*, *15*(6), pp.303-311.

Dudka, D., Castrogiovanni, C., Liaudet, N., Vassal, H. and Meraldi, P., 2019. Spindle-length-dependent HURP localization allows centrosomes to control kinetochore-fiber plus-end dynamics. Current Biology, 29(21), pp.3563-3578.

Dufour, S., Mège, R.M. and Thiery, J.P., 2013. α-catenin, vinculin, and F-actin in strengthening E-cadherin cell–cell adhesions and mechanosensing. *Cell adhesion & migration*, *7*(4), pp.345-350.

Dujardin, D.L. and Vallee, R.B., 2002. Dynein at the cortex. *Current opinion in cell biology*, *14*(1), pp.44-49.

Dupin, I., Sakamoto, Y. and Etienne-Manneville, S., 2011. Cytoplasmic intermediate filaments mediate actin-driven positioning of the nucleus. *Journal of cell science*, *124*(6), pp.865-872.

Errico, A., Claudiani, P., D'Addio, M. and Rugarli, E.I., 2004. Spastin interacts with the centrosomal protein NA14, and is enriched in the spindle pole, the midbody and the distal axon. *Human molecular genetics*, *13*(18), pp.2121-2132.

Eshun-Wilson, L., Zhang, R., Portran, D., Nachury, M.V., Toso, D.B., Löhr, T., Vendruscolo, M., Bonomi, M., Fraser, J.S. and Nogales, E., 2019. Effects of α-tubulin acetylation on microtubule structure and stability. *Proceedings of the National Academy of Sciences*, *116*(21), pp.10366-10371.

Evans, W.H. and Martin, P.E., 2002. Gap junctions: structure and function. *Molecular membrane biology*, *19*(2), pp.121-136.

Fair, K.L., Colquhoun, J. and Hannan, N.R., 2018. Intestinal organoids for modelling intestinal development and disease. *Philosophical Transactions of the Royal Society B: Biological Sciences*, *373*(1750), p.20170217.

Fant, X., Srsen, V., Espigat-Georger, A. and Merdes, A., 2009. Nuclei of non-muscle cells bind centrosome proteins upon fusion with differentiating myoblasts. *PLoS One*, *4*(12), p.e8303.

Feldman, J.L. and Priess, J.R., 2012. A role for the centrosome and PAR-3 in the hand-off of MTOC function during epithelial polarization. *Current Biology*, *22*(7), pp.575-582.

Fletcher, G.C., Lucas, E.P., Brain, R., Tournier, A. and Thompson, B.J., 2012. Positive feedback and mutual antagonism combine to polarize Crumbs in the Drosophila follicle cell epithelium. *Current Biology*, *22*(12), pp.1116-1122.

Fong, K.W., Au, F.K., Jia, Y., Yang, S., Zhou, L. and Qi, R.Z., 2017. Microtubule plus-end tracking of end-binding protein 1 (EB1) is regulated by CDK5 regulatory subunit-associated protein 2. *Journal of Biological Chemistry*, *292*(18), pp.7675-7687.

Forth, S. and Kapoor, T.M., 2017. The mechanics of microtubule networks in cell division. *Journal of Cell Biology*, *216*(6), pp.1525-1531.

Fredberg, J., Mitchel, J., Kim, J.H. and Park, J.A., 2016. Unjamming and cell shape in the asthmatic airway epithelium. *The FASEB Journal*, *30*, pp.1296-2.

Friend, D.S. and Gilula, N.B., 1972. Variations in tight and gap junctions in mammalian tissues. *The Journal of cell biology*, *53*(3), pp.758-776.

Fukata, M., Watanabe, T., Noritake, J., Nakagawa, M., Yamaga, M., Kuroda, S., Matsuura, Y., Iwamatsu, A., Perez, F. and Kaibuchi, K., 2002. Rac1 and Cdc42 capture microtubules through IQGAP1 and CLIP-170. *Cell*, *109*(7), pp.873-885.

Fukuhara, A., Irie, K., Nakanishi, H., Takekuni, K., Kawakatsu, T., Ikeda, W., Yamada, A., Katata, T., Honda, T., Sato, T. and Shimizu, K., 2002. Involvement of nectin in the localization of junctional adhesion molecule at tight junctions. Oncogene, 21(50), pp.7642-7655.

Fukuhara, A., Irie, K., Yamada, A., Katata, T., Honda, T., Shimizu, K., Nakanishi, H. and Takai, Y., 2002. Role of nectin in organization of tight junctions in epithelial cells. Genes to Cells, 7(10), pp.1059-1072.

Gaj, T., Gersbach, C.A. and Barbas III, C.F., 2013. ZFN, TALEN, and CRISPR/Cas-based methods for genome engineering. *Trends in biotechnology*, *31*(7), pp.397-405.

Galjart, N., 2005. CLIPs and CLASPs and cellular dynamics. *Nature reviews Molecular cell biology*, *6*(6), pp.487-498.

Galjart, N., 2010. Plus-end-tracking proteins and their interactions at microtubule ends. *Current Biology*, *20*(12), pp.R528-R537.

Garcin, C. and Straube, A., 2019. Microtubules in cell migration. *Essays in biochemistry*, *63*(5), pp.509-520.

Gardner, M.K., Zanic, M., Gell, C., Bormuth, V. and Howard, J., 2011. The depolymerizing kinesins Kip3 (kinesin-8) and MCAK (kinesin-13) are catastrophe factors that destabilize microtubules by different mechanisms. *Cell*, *147*(5), pp.1092-1103.

Geyer, E.A., Burns, A., Lalonde, B.A., Ye, X., Piedra, F.A., Huffaker, T.C. and Rice, L.M., 2015. A mutation uncouples the tubulin conformational and GTPase cycles, revealing allosteric control of microtubule dynamics. *Elife*, *4*, p.e10113.

Gheiratmand, L., Coyaud, E., Gupta, G.D., Laurent, E.M., Hasegan, M., Prosser, S.L., Gonçalves, J., Raught, B. and Pelletier, L., 2019. Spatial and proteomic profiling reveals centrosome-independent features of centriolar satellites. *The EMBO journal*, *38*(14), p.e101109.

Goldspink, D.A., Gadsby, J.R., Bellett, G., Keynton, J., Tyrrell, B.J., Lund, E.K., Powell, P.P., Thomas, P. and Mogensen, M.M., 2013. The microtubule end-binding protein EB2 is a central regulator of microtubule reorganisation in apico-basal epithelial differentiation. *Journal of cell science*, *126*(17), pp.4000-4014.

Goodwin, S.S. and Vale, R.D., 2010. Patronin regulates the microtubule network by protecting microtubule minus ends. *Cell*, *143*(2), pp.263-274.

Goshima, G., Mayer, M., Zhang, N., Stuurman, N. and Vale, R.D., 2008. Augmin: a protein complex required for centrosome-independent microtubule generation within the spindle. *The Journal of cell biology*, *181*(3), pp.421-429.

Grego, S., Cantillana, V. and Salmon, E.D., 2001. Microtubule treadmilling in vitro investigated by fluorescence speckle and confocal microscopy. *Biophysical Journal*, *81*(1), pp.66-78.

Grimaldi, A.D., Maki, T., Fitton, B.P., Roth, D., Yampolsky, D., Davidson, M.W., Svitkina, T., Straube, A., Hayashi, I. and Kaverina, I., 2014. CLASPs are required for proper microtubule localization of end-binding proteins. *Developmental cell*, *30*(3), pp.343-352.

Gruber, J., Harborth, J., Schnabel, J., Weber, K. and Hatzfeld, M., 2002. The mitotic-spindle-associated protein astrin is essential for progression through mitosis. *Journal of Cell Science*, *115*(21), pp.4053-4059.

Guillot, C. and Lecuit, T., 2013. Mechanics of epithelial tissue homeostasis and morphogenesis. *Science*, *340*(6137), pp.1185-1189.

Guizzunti, G. and Seemann, J., 2016. Mitotic Golgi disassembly is required for bipolar spindle formation and mitotic progression. Proceedings of the National Academy of Sciences, 113(43), pp.E6590-E6599.

Gundersen, G.G., Gomes, E.R. and Wen, Y., 2004. Cortical control of microtubule stability and polarization. *Current opinion in cell biology*, *16*(1), pp.106-112.

Hao, Y., Du, Q., Chen, X., Zheng, Z., Balsbaugh, J.L., Maitra, S., Shabanowitz, J., Hunt, D.F. and Macara, I.G., 2010. Par3 controls epithelial spindle orientation by aPKC-mediated phosphorylation of apical Pins. *Current Biology*, *20*(20), pp.1809-1818.

Hashimoto, M., Shinohara, K., Wang, J., Ikeuchi, S., Yoshiba, S., Meno, C., Nonaka, S., Takada, S., Hatta, K., Wynshaw-Boris, A. and Hamada, H., 2010. Planar polarization of node cells determines the rotational axis of node cilia. *Nature cell biology*, *12*(2), pp.170-176.

Hatch, E.M., Kulukian, A., Holland, A.J., Cleveland, D.W. and Stearns, T., 2010. Cep152 interacts with Plk4 and is required for centriole duplication. *Journal of Cell Biology*, *191*(4), pp.721-729.

Hayashi, I. and Ikura, M., 2003. Crystal structure of the amino-terminal microtubule-binding domain of end-binding protein 1 (EB1). Journal of Biological Chemistry, 278(38), pp.36430-36434.

He, X.C., Zhang, J., Tong, W.G., Tawfik, O., Ross, J., Scoville, D.H., Tian, Q., Zeng, X., He, X., Wiedemann, L.M. and Mishina, Y., 2004. BMP signaling inhibits intestinal stem cell self-renewal through suppression of Wnt–β-catenin signaling. *Nature genetics*, *36*(10), pp.1117-1121.

Hendershott, M.C. and Vale, R.D., 2014. Regulation of microtubule minus-end dynamics by CAMSAPs and Patronin. *Proceedings of the National Academy of Sciences*, *111*(16), pp.5860-5865.

Hesse, M., Magin, T.M. and Weber, K., 2001. Genes for intermediate filament proteins and the draft sequence of the human genome: novel keratin genes and a surprisingly high number of pseudogenes related to keratin genes 8 and 18. *Journal of cell science*, *114*(14), pp.2569-2575.

Hinchcliffe, E.H., Miller, F.J., Cham, M., Khodjakov, A. and Sluder, G., 2001. Requirement of a centrosomal activity for cell cycle progression through G1 into S phase. *Science*, *291*(5508), pp.1547-1550.

Hinck, L. and Näthke, I., 2014. Changes in cell and tissue organization in cancer of the breast and colon. *Current opinion in cell biology*, *26*, pp.87-95.

Howard, J. and Hyman, A.A., 2003. Dynamics and mechanics of the microtubule plus end. *Nature*, *422*(6933), pp.753-758.

Hsu, P.D., Scott, D.A., Weinstein, J.A., Ran, F.A., Konermann, S., Agarwala, V., Li, Y., Fine, E.J., Wu, X., Shalem, O. and Cradick, T.J., 2013. DNA targeting specificity of RNA-guided Cas9 nucleases. *Nature biotechnology*, *31*(9), p.827.

Hu, J.H., Miller, S.M., Geurts, M.H., Tang, W., Chen, L., Sun, N., Zeina, C.M., Gao, X., Rees, H.A., Lin, Z. and Liu, D.R., 2018. Evolved Cas9 variants with broad PAM compatibility and high DNA specificity. *Nature*, *556*(7699), pp.57-63.

Hubbert, C., Guardiola, A., Shao, R., Kawaguchi, Y., Ito, A., Nixon, A., Yoshida, M., Wang, X.F. and Yao, T.P., 2002. HDAC6 is a microtubule-associated deacetylase. *Nature*, *417*(6887), pp.455-458.

Hunter, A.W., Caplow, M., Coy, D.L., Hancock, W.O., Diez, S., Wordeman, L. and Howard, J., 2003. The kinesin-related protein MCAK is a microtubule depolymerase that forms an ATP-hydrolyzing complex at microtubule ends. *Molecular cell*, *11*(2), pp.445-457.

Hurd, T.W., Gao, L., Roh, M.H., Macara, I.G. and Margolis, B., 2003. Direct interaction of two polarity complexes implicated in epithelial tight junction assembly. *Nature cell biology*, *5*(2), pp.137-142.

Ilina, O., Gritsenko, P.G., Syga, S., Lippoldt, J., La Porta, C.A., Chepizhko, O., Grosser, S., Vullings, M., Bakker, G.J., Starruß, J. and Bult, P., 2020. Cell–cell adhesion and 3D matrix confinement determine jamming transitions in breast cancer invasion. *Nature cell biology*, *22*(9), pp.1103-1115.

Indra, I., Hong, S., Troyanovsky, R., Kormos, B. and Troyanovsky, S., 2013. The adherens junction: a mosaic of cadherin and nectin clusters bundled by actin filaments. *Journal of Investigative Dermatology*, *133*(11), pp.2546-2554.

Ishino, Y., Shinagawa, H., Makino, K., Amemura, M. and Nakata, A., 1987. Nucleotide sequence of the iap gene, responsible for alkaline phosphatase isozyme conversion in Escherichia coli, and identification of the gene product. *Journal of bacteriology*, *169*(12), pp.5429-5433.

Ishiuchi, T. and Takeichi, M., 2011. Willin and Par3 cooperatively regulate epithelial apical constriction through aPKC-mediated ROCK phosphorylation. *Nature cell biology*, *13*(7), pp.860-866.

Ishiyama, N., Tanaka, N., Abe, K., Yang, Y.J., Abbas, Y.M., Umitsu, M., Nagar, B., Bueler, S.A., Rubinstein, J.L., Takeichi, M. and Ikura, M., 2013. An autoinhibited structure of α-catenin and its implications for vinculin recruitment to adherens junctions. *Journal of Biological Chemistry*, *288*(22), pp.15913-15925.

Isrie, M., Breuss, M., Tian, G., Hansen, A.H., Cristofoli, F., Morandell, J., Kupchinsky, Z.A., Sifrim, A., Rodriguez-Rodriguez, C.M., Dapena, E.P. and Doonanco, K., 2015. Mutations in either TUBB or MAPRE2 cause circumferential skin creases Kunze type. *The American Journal of Human Genetics*, *97*(6), pp.790-800.

Jiang, K., Faltova, L., Hua, S., Capitani, G., Prota, A.E., Landgraf, C., Volkmer, R., Kammerer, R.A., Steinmetz, M.O. and Akhmanova, A., 2018. Structural basis of formation of the microtubule minus-end-regulating CAMSAP-katanin complex. *Structure*, *26*(3), pp.375-382.

Jiang, T., McKinley, R.A., McGill, M.A., Angers, S. and Harris, T.J., 2015. A Par-1-Par-3-centrosome cell polarity pathway and its tuning for isotropic cell adhesion. *Current Biology*, *25*(20), pp.2701-2708.

Jiang, K., Hua, S., Mohan, R., Grigoriev, I., Yau, K.W., Liu, Q., Katrukha, E.A., Altelaar, A.M., Heck, A.J., Hoogenraad, C.C. and Akhmanova, A., 2014. Microtubule minus-end stabilization by polymerization-driven CAMSAP deposition. *Developmental cell*, *28*(3), pp.295-309.

Jimbo, T., Kawasaki, Y., Koyama, R., Sato, R., Takada, S., Haraguchi, K. and Akiyama, T., 2002. Identification of a link between the tumour suppressor APC and the kinesin superfamily. *Nature cell biology*, *4*(4), pp.323-327.

Jinek, M., Chylinski, K., Fonfara, I., Hauer, M., Doudna, J.A. and Charpentier, E., 2012. A programmable dual-RNA–guided DNA endonuclease in adaptive bacterial immunity. *science*, *337*(6096), pp.816-821.

Jouette, J., Guichet, A. and Claret, S.B., 2019. Dynein-mediated transport and membrane trafficking control PAR3 polarised distribution. *Elife*, *8*, p.e40212.

Kaltschmidt, J.A. and Brand, A.H., 2002. Asymmetric cell division: microtubule dynamics and spindle asymmetry. *Journal of cell science*, *115*(11), pp.2257-2264.

Kardon, J.R. and Vale, R.D., 2009. Regulators of the cytoplasmic dynein motor. *Nature reviews Molecular cell biology*, *10*(12), pp.854-865.

Karvelis, T., Gasiunas, G., Miksys, A., Barrangou, R., Horvath, P. and Siksnys, V., 2013. crRNA and tracrRNA guide Cas9-mediated DNA interference in Streptococcus thermophilus. *RNA biology*, *10*(5), pp.841-851.

Kaul, N., Soppina, V. and Verhey, K.J., 2014. Effects of α-tubulin K40 acetylation and detyrosination on kinesin-1 motility in a purified system. *Biophysical journal*, *106*(12), pp.2636-2643.

Keating, T.J., Peloquin, J.G., Rodionov, V.I., Momcilovic, D. and Borisy, G.G., 1997. Microtubule release from the centrosome. *Proceedings of the National Academy of Sciences*, *94*(10), pp.5078-5083.

Kent, I.A. and Lele, T.P., 2017. Microtubule-based force generation. *Wiley Interdisciplinary Reviews: Nanomedicine and Nanobiotechnology*, *9*(3), p.e1428.

Khanal, I., Elbediwy, A., Fletcher, G.C. and Thompson, B.J., 2016. Shot and Patronin polarise microtubules to direct membrane traffic and biogenesis of microvilli in epithelia. *Journal of cell science*, *129*(13), pp.2651-2659.

Khodjakov, A., Cole, R.W., Oakley, B.R. and Rieder, C.L., 2000. Centrosome-independent mitotic spindle formation in vertebrates. *Current Biology*, *10*(2), pp.59-67.

Kim, J.H., Pegoraro, A.F., Das, A., Koehler, S.A., Ujwary, S.A., Lan, B., Mitchel, J.A., Atia, L., He, S., Wang, K. and Bi, D., 2020. Unjamming and collective migration in MCF10A breast cancer cell lines. *Biochemical and biophysical research communications*, *521*(3), pp.706-715.

Kleinstiver, B.P., Prew, M.S., Tsai, S.Q., Topkar, V.V., Nguyen, N.T., Zheng, Z., Gonzales, A.P., Li, Z., Peterson, R.T., Yeh, J.R.J. and Aryee, M.J., 2015. Engineered CRISPR-Cas9 nucleases with altered PAM specificities. *Nature*, *523*(7561), pp.481-485.

Kodama, A., Karakesisoglou, I., Wong, E., Vaezi, A. and Fuchs, E., 2003. ACF7: an essential integrator of microtubule dynamics. *Cell*, *115*(3), pp.343-354.

Komarova, Y.A., Akhmanova, A.S., Kojima, S.I., Galjart, N. and Borisy, G.G., 2002. Cytoplasmic linker proteins promote microtubule rescue in vivo. *The Journal of cell biology*, *159*(4), pp.589-599.

Komarova, Y., De Groot, C.O., Grigoriev, I., Gouveia, S.M., Munteanu, E.L., Schober, J.M., Honnappa, S., Buey, R.M., Hoogenraad, C.C., Dogterom, M. and Borisy, G.G., 2009. Mammalian end binding proteins control persistent microtubule growth. *Journal of Cell Biology*, *184*(5), pp.691-706.

Komarova, Y., Lansbergen, G., Galjart, N., Grosveld, F., Borisy, G.G. and Akhmanova, A., 2005. EB1 and EB3 control CLIP dissociation from the ends of growing microtubules. *Molecular biology of the cell*, *16*(11), pp.5334-5345.

Kratz, A.S., Bärenz, F., Richter, K.T. and Hoffmann, I., 2015. Plk4-dependent phosphorylation of STIL is required for centriole duplication. *Biology open*, *4*(3), pp.370-377.

Kubota, H., Miyazaki, M., Ogawa, T., Shimozawa, T., Kinosita Jr, K. and Ishiwata, S.I., 2017. Biphasic effect of profilin impacts the formin mDia1 force-sensing mechanism in actin polymerization. *Biophysical journal*, *113*(2), pp.461-471.

Lacroix, B., Letort, G., Pitayu, L., Sallé, J., Stefanutti, M., Maton, G., Ladouceur, A.M., Canman, J.C., Maddox, P.S., Maddox, A.S. and Minc, N., 2018. Microtubule dynamics scale with cell size to set spindle length and assembly timing. *Developmental cell*, *45*(4), pp.496-511.

Leblond, C.P. and Inoue, S., 1989. Structure, composition, and assembly of basement membrane. American Journal of Anatomy, 185(4), pp.367-390.

Lecuit, T. and Lenne, P.F., 2007. Cell surface mechanics and the control of cell shape, tissue patterns and morphogenesis. *Nature reviews Molecular cell biology*, *8*(8), pp.633-644.

Le Droguen, P.M., Claret, S., Guichet, A. and Brodu, V., 2015. Microtubule-dependent apical restriction of recycling endosomes sustains adherens junctions during morphogenesis of the Drosophila tracheal system. *Development*, *142*(2), pp.363-374.

Lessard, D.V., Zinder, O.J., Hotta, T., Verhey, K.J., Ohi, R. and Berger, C.L., 2019. Polyglutamylation of tubulin's C-terminal tail controls pausing and motility of kinesin-3 family member KIF1A. *Journal of Biological Chemistry*, *294*(16), pp.6353-6363.

Li, D., Kuehn, E.W. and Prekeris, R., 2014. Kinesin-2 mediates apical endosome transport during epithelial lumen formation. *Cellular logistics*, *4*(2), p.e28928.

Li, Z., Wang, L., Hays, T.S. and Cai, Y., 2008. Dynein-mediated apical localization of crumbs transcripts is required for Crumbs activity in epithelial polarity. *The Journal of cell biology*, *180*(1), pp.31-38.

Li, D., Xie, S., Ren, Y., Huo, L., Gao, J., Cui, D., Liu, M. and Zhou, J., 2011. Microtubule-associated deacetylase HDAC6 promotes angiogenesis by regulating cell migration in an EB1-dependent manner. *Protein & cell*, *2*(2), pp.150-160.

Liang, X., Michael, M. and Gomez, G.A., 2016. Measurement of mechanical tension at cell-cell junctions using two-photon laser ablation. *Bio-protocol*, *6*(24).

Liu, J.J., 2017. Regulation of dynein-dynactin-driven vesicular transport. *Traffic*, *18*(6), pp.336-347.

Liu, Z., Tan, J.L., Cohen, D.M., Yang, M.T., Sniadecki, N.J., Ruiz, S.A., Nelson, C.M. and Chen, C.S., 2010. Mechanical tugging force regulates the size of cell–cell junctions. *Proceedings of the National Academy of Sciences*, *107*(22), pp.9944-9949.

Liu, H., Yue, J., Huang, H., Gou, X., Chen, S., Zhao, Y. and Wu, X. (2015). Regulation of Focal Adhesion Dynamics and Cell Motility by the EB2 and Hax1 Protein Complex. Journal of Biological Chemistry, 290(52), pp.30771-30782.

Ligon, L.A., Karki, S., Tokito, M. and Holzbaur, E.L., 2001. Dynein binds to β-catenin and may tether microtubules at adherens junctions. *Nature cell biology*, *3*(10), pp.913-917.

Ligon, L.A., Shelly, S.S., Tokito, M.K. and Holzbaur, E.L., 2006. Microtubule binding proteins CLIP-170, EB1, and p150Glued form distinct plus-end complexes. *FEBS letters*, *580*(5), pp.1327-1332.

Lin, T.C., Neuner, A. and Schiebel, E., 2015. Targeting of γ-tubulin complexes to microtubule organizing centers: conservation and divergence. *Trends in cell biology*, *25*(5), pp.296-307.

Mali, P., Yang, L., Esvelt, K.M., Aach, J., Guell, M., DiCarlo, J.E., Norville, J.E. and Church, G.M., 2013. RNA-guided human genome engineering via Cas9. *Science*, *339*(6121), pp.823-826.

Malt, A.L., Dailey, Z., Holbrook-Rasmussen, J., Zheng, Y., Hogan, A., Du, Q. and Lu, X., 2019. Par3 is essential for the establishment of planar cell polarity of inner ear hair cells. *Proceedings of the National Academy of Sciences*, *116*(11), pp.4999-5008.

Man, X., Megraw, T.L. and Lim, Y.P., 2015. Cep68 can be regulated by Nek2 and SCF complex. *European journal of cell biology*, *94*(3-4), pp.162-172.

Mandelkow, E. and Mandelkow, E.M., 1994. Microtubule structure. *Current opinion in Structural Biology*, *4*(2), pp.171-179.

Mardin, B.R. and Schiebel, E., 2012. Breaking the ties that bind: new advances in centrosome biology. *Journal of Cell Biology*, *197*(1), pp.11-18.

Margolis, B. and Borg, J.P., 2005. Apicobasal polarity complexes. *Journal of cell science*, *118*(22), pp.5157-5159.

Matsuzawa, K., Akita, H., Watanabe, T., Kakeno, M., Matsui, T., Wang, S. and Kaibuchi, K., 2016. PAR3-aPKC regulates Tiam1 by modulating suppressive internal interactions. *Molecular biology of the cell*, *27*(9), pp.1511-1523.

May-Simera, H.L., Gumerson, J.D., Gao, C., Campos, M., Cologna, S.M., Beyer, T., Boldt, K., Kaya, K.D., Patel, N., Kretschmer, F. and Kelley, M.W., 2016. Loss of MACF1 abolishes ciliogenesis and disrupts apicobasal polarity establishment in the retina. *Cell reports*, *17*(5), pp.1399-1413.

McKinley, K.L. and Cheeseman, I.M., 2017. Large-scale analysis of CRISPR/Cas9 cell-cycle knockouts reveals the diversity of p53-dependent responses to cell-cycle defects. *Developmental cell*, *40*(4), pp.405-420.

McNally, F.J., Okawa, K., Iwamatsu, A. and Vale, R.D., 1996. Katanin, the microtubule-severing ATPase, is concentrated at centrosomes. *Journal of cell science*, *109*(3), pp.561-567.

Meads, T. and Schroer, T.A., 1995. Polarity and nucleation of microtubules in polarized epithelial cells. *Cell motility and the cytoskeleton*, *32*(4), pp.273-288.

Meiring, J.C., Shneyer, B.I. and Akhmanova, A., 2020. Generation and regulation of microtubule network asymmetry to drive cell polarity. *Current opinion in cell biology*, *62*, pp.86-95.

Meitinger, F., Anzola, J.V., Kaulich, M., Richardson, A., Stender, J.D., Benner, C., Glass, C.K., Dowdy, S.F., Desai, A., Shiau, A.K. and Oegema, K., 2016. 53BP1 and USP28 mediate p53 activation and G1 arrest after centrosome loss or extended mitotic duration. *Journal of Cell Biology*, *214*(2), pp.155-166.

Meng, W., Mushika, Y., Ichii, T. and Takeichi, M., 2008. Anchorage of microtubule minus ends to adherens junctions regulates epithelial cell-cell contacts. *Cell*, *135*(5), pp.948-959.

Mennella, V., Agard, D.A., Huang, B. and Pelletier, L., 2014. Amorphous no more: subdiffraction view of the pericentriolar material architecture. *Trends in cell biology*, *24*(3), pp.188-197.

Meraldi, P., Lukas, J., Fry, A.M., Bartek, J. and Nigg, E.A., 1999. Centrosome duplication in mammalian somatic cells requires E2F and Cdk2–cyclin A. Nature cell biology, 1(2), pp.88-93.

Merino, F., Pospich, S., Funk, J., Wagner, T., Küllmer, F., Arndt, H.D., Bieling, P. and Raunser, S., 2018. Structural transitions of F-actin upon ATP hydrolysis at near-atomic resolution revealed by cryo-EM. *Nature structural & molecular biology*, *25*(6), pp.528-537.

Mierke, C.T (2018) *Microtubules during migration and matrix invasion. Physics of Cancer, Volume 2 (Second Edition)* [Online]. Available at: *https://iopscience.iop.org/book/978-0-7503-2117-4/chapter/bk978-0-7503-2117-4ch9* (Accessed: 6th March 2021).

Miller, P.M., Folkmann, A.W., Maia, A.R., Efimova, N., Efimov, A. and Kaverina, I., 2009. Golgi-derived CLASP-dependent microtubules control Golgi organization and polarized trafficking in motile cells. *Nature cell biology*, *11*(9), pp.1069-1080.

Mimori-Kiyosue, Y. and Tsukita, S., 2003. "Search-and-capture" of microtubules through plus-end-binding proteins (+ TIPs). *Journal of biochemistry*, *134*(3), pp.321-326.

Mitalipova, M.M., Rao, R.R., Hoyer, D.M., Johnson, J.A., Meisner, L.F., Jones, K.L., Dalton, S. and Stice, S.L., 2005. Preserving the genetic integrity of human embryonic stem cells. *Nature biotechnology*, *23*(1), pp.19-20.

Mitchel, J.A., Das, A., O'Sullivan, M.J., Stancil, I.T., DeCamp, S.J., Koehler, S., Butler, J.P., Fredberg, J.J., Nieto, M.A., Bi, D. and Park, J.A., 2019. The unjamming transition is distinct from the epithelial-to-mesenchymal transition. *bioRxiv*, p.665018.

Mitchel, J.A., Das, A., O'Sullivan, M.J., Stancil, I.T., DeCamp, S.J., Koehler, S., Ocaña, O.H., Butler, J.P., Fredberg, J.J., Nieto, M.A. and Bi, D., 2020. In primary airway epithelial cells, the unjamming transition is distinct from the epithelial-to-mesenchymal transition. *Nature communications*, *11*(1), pp.1-14.

Mogensen, M.M., 1999. Microtubule release and capture in epithelial cells. Biology of the Cell, 91(4-5), pp.331-341.

Mogensen, M.M., Malik, A., Piel, M., Bouckson-Castaing, V. and Bornens, M., 2000. Microtubule minus-end anchorage at centrosomal and non-centrosomal sites: the role of ninein. *Journal of cell science*, *113*(17), pp.3013-3023.

Mogensen, M.M. and Tucker, J.B., 1987. Evidence for microtubule nucleation at plasma membrane-associated sites in Drosophila. *Journal of cell science*, *88*(1), pp.95-107.

Mogensen, M.M., Tucker, J.B. and Stebbings, H., 1989. Microtubule polarities indicate that nucleation and capture of microtubules occurs at cell surfaces in Drosophila. *The Journal of cell biology*, *108*(4), pp.1445-1452.

Mohr, S.E., Hu, Y., Ewen-Campen, B., Housden, B.E., Viswanatha, R. and Perrimon, N., 2016. CRISPR guide RNA design for research applications. *The FEBS journal*, *283*(17), pp.3232-3238.

Moreno-Mateos, M.A., Vejnar, C.E., Beaudoin, J.D., Fernandez, J.P., Mis, E.K., Khokha, M.K. and Giraldez, A.J., 2015. CRISPRscan: designing highly efficient sgRNAs for CRISPR-Cas9 targeting in vivo. *Nature methods*, *12*(10), pp.982-988.

Moritz, M., Braunfeld, M.B., Guénebaut, V., Heuser, J. and Agard, D.A., 2000. Structure of the γ-tubulin ring complex: a template for microtubule nucleation. *Nature cell biology*, *2*(6), pp.365-370.

Moss, D.K., Bellett, G., Carter, J.M., Liovic, M., Keynton, J., Prescott, A.R., Lane, E.B. and Mogensen, M.M., 2007. Ninein is released from the centrosome and moves bi-directionally along microtubules. *Journal of cell science*, *120*(17), pp.3064-3074.

Mout, R., Ray, M., Yesilbag Tonga, G., Lee, Y.W., Tay, T., Sasaki, K. and Rotello, V.M., 2017. Direct cytosolic delivery of CRISPR/Cas9-ribonucleoprotein for efficient gene editing. *ACS nano*, *11*(3), pp.2452-2458.

Murakami, K., Yasunaga, T., Noguchi, T.Q., Gomibuchi, Y., Ngo, K.X., Uyeda, T.Q. and Wakabayashi, T., 2010. Structural basis for actin assembly, activation of ATP hydrolysis, and delayed phosphate release. *Cell*, *143*(2), pp.275-287.

Muroyama, A., Seldin, L. and Lechler, T., 2016. Divergent regulation of functionally distinct γ-tubulin complexes during differentiation. *Journal of Cell Biology*, *213*(6), pp.679-692.

Nashchekin, D., Fernandes, A.R. and St Johnston, D., 2016. Patronin/Shot cortical foci assemble the noncentrosomal microtubule array that specifies the Drosophila anterior-posterior axis. *Developmental cell*, *38*(1), pp.61-72.

Nawrotek, A., Knossow, M. and Gigant, B., 2011. The determinants that govern microtubule assembly from the atomic structure of GTP-tubulin. *Journal of molecular biology*, *412*(1), pp.35-42.

Nejsum, L.N. and Nelson, W.J., 2007. A molecular mechanism directly linking E-cadherin adhesion to initiation of epithelial cell surface polarity. *The Journal of cell biology*, *178*(2), pp.323-335.

Ning, W., Yu, Y., Xu, H., Liu, X., Wang, D., Wang, J., Wang, Y. and Meng, W., 2016. The CAMSAP3-ACF7 complex couples noncentrosomal microtubules with actin filaments to coordinate their dynamics. *Developmental Cell*, *39*(1), pp.61-74.

Nirschl, J.J., Magiera, M.M., Lazarus, J.E., Janke, C. and Holzbaur, E.L., 2016. α-Tubulin tyrosination and CLIP-170 phosphorylation regulate the initiation of dynein-driven transport in neurons. *Cell reports*, *14*(11), pp.2637-2652.

Nishimura, T., Yamaguchi, T., Kato, K., Yoshizawa, M., Nabeshima, Y.I., Ohno, S., Hoshino, M. and Kaibuchi, K., 2005. PAR-6–PAR-3 mediates Cdc42-induced Rac activation through the Rac GEFs STEF/Tiam1. *Nature cell biology*, *7*(3), pp.270-277.

Nogales, E., 1999. A structural view of microtubule dynamics. *Cellular and Molecular Life Sciences CMLS*, *56*(1), pp.133-142.

Nogales, E., 2015. An electron microscopy journey in the study of microtubule structure and dynamics. *Protein Science*, *24*(12), pp.1912-1919.

Noordstra, I., Liu, Q., Nijenhuis, W., Hua, S., Jiang, K., Baars, M., Remmelzwaal, S., Martin, M., Kapitein, L.C. and Akhmanova, A., 2016. Control of apico–basal epithelial polarity by the microtubule minus-end-binding protein CAMSAP3 and spectraplakin ACF7. *Journal of cell science*, *129*(22), pp.4278-4288.

Oakley, B.R., Oakley, C.E., Yoon, Y. and Jung, M.K., 1990. γ-Tubulin is a component of the spindle pole body that is essential for microtubule function in Aspergillus nidulans. *Cell*, *61*(7), pp.1289-1301.

Oakley, C.E. and Oakley, B.R., 1989. Identification of γ-tubulin, a new member of the tubulin superfamily encoded by mipA gene of Aspergillus nidulans. *Nature*, *338*(6217), pp.662-664.

Oakley, B.R., Paolillo, V. and Zheng, Y., 2015. γ-Tubulin complexes in microtubule nucleation and beyond. *Molecular biology of the cell*, *26*(17), pp.2957-2962.

Ohi, R. and Zanic, M., 2016. Ahead of the curve: new insights into microtubule dynamics. *F1000Research*, *5*.

Palamidessi, A., Malinverno, C., Frittoli, E., Corallino, S., Barbieri, E., Sigismund, S., Beznoussenko, G.V., Martini, E., Garre, M., Ferrara, I. and Tripodo, C., 2019. Unjamming overcomes kinetic and proliferation arrest in terminally differentiated cells and promotes collective motility of carcinoma. *Nature materials*, *18*(11), pp.1252-1263.

Paoletti, A., Moudjou, M., Paintrand, M., Salisbury, J.L. and Bornens, M., 1996. Most of centrin in animal cells is not centrosome-associated and centrosomal centrin is confined to the distal lumen of centrioles. Journal of cell science, 109(13), pp.3089-3102.

Park, J.A., Atia, L., Mitchel, J.A., Fredberg, J.J. and Butler, J.P., 2016. Collective migration and cell jamming in asthma, cancer and development. *Journal of cell science*, *129*(18), pp.3375-3383.

Park, J.A., Kim, J.H., Bi, D., Mitchel, J.A., Qazvini, N.T., Tantisira, K., Park, C.Y., McGill, M., Kim, S.H., Gweon, B. and Notbohm, J., 2015. Unjamming and cell shape in the asthmatic airway epithelium. *Nature materials*, *14*(10), pp.1040-1048.

Pelham, R.J. and Chang, F., 2002. Actin dynamics in the contractile ring during cytokinesis in fission yeast. *Nature*, *419*(6902), pp.82-86.

Perez, F., Diamantopoulos, G.S., Stalder, R. and Kreis, T.E., 1999. CLIP-170 highlights growing microtubule ends in vivo. *Cell*, *96*(4), pp.517-527.

Petry, S., Groen, A.C., Ishihara, K., Mitchison, T.J. and Vale, R.D., 2013. Branching microtubule nucleation in Xenopus egg extracts mediated by augmin and TPX2. *Cell*, *152*(4), pp.768-777.

Petry, S. and Vale, R.D., 2015. Microtubule nucleation at the centrosome and beyond. *Nature cell biology*, *17*(9), pp.1089-1093.

Pickett, M.A., Naturale, V.F. and Feldman, J.L., 2019. A polarizing issue: diversity in the mechanisms underlying Apico-Basolateral polarization in vivo. *Annual review of cell and developmental biology*, *35*, pp.285-308.

Pinheiro, D. and Bellaïche, Y., 2018. Mechanical force-driven adherens junction remodeling and epithelial dynamics. *Developmental cell*, *47*(1), pp.3-19.

Pongrakhananon, V., Saito, H., Hiver, S., Abe, T., Shioi, G., Meng, W. and Takeichi, M., 2018. CAMSAP3 maintains neuronal polarity through regulation of microtubule stability. *Proceedings of the National Academy of Sciences*, *115*(39), pp.9750-9755.

Portran, D., Schaedel, L., Xu, Z., Théry, M. and Nachury, M.V., 2017. Tubulin acetylation protects long-lived microtubules against mechanical ageing. *Nature cell biology*, *19*(4), pp.391-398.

Press, M.F., Xie, B., Davenport, S., Zhou, Y., Guzman, R., Nolan, G.P., O'Brien, N., Palazzolo, M., Mak, T.W., Brugge, J.S. and Slamon, D.J., 2019. Role for polo-like kinase 4 in mediation of cytokinesis. *Proceedings of the National Academy of Sciences*, *116*(23), pp.11309-11318.

Priya, R., Gomez, G.A., Budnar, S., Verma, S., Cox, H.L., Hamilton, N.A. and Yap, A.S., 2015. Feedback regulation through myosin II confers robustness on RhoA signalling at E-cadherin junctions. *Nature cell biology*, *17*(10), pp.1282-1293.

Qi, L.S., Larson, M.H., Gilbert, L.A., Doudna, J.A., Weissman, J.S., Arkin, A.P. and Lim, W.A., 2013. Repurposing CRISPR as an RNA-guided platform for sequence-specific control of gene expression. *Cell*, *152*(5), pp.1173-1183.

Ran, F.A., Hsu, P.D., Wright, J., Agarwala, V., Scott, D.A. and Zhang, F., 2013. Genome engineering using the CRISPR-Cas9 system. *Nature protocols*, *8*(11), p.2281.

Ravichandran, Y., Goud, B. and Manneville, J.B., 2020. The Golgi apparatus and cell polarity: Roles of the cytoskeleton, the Golgi matrix, and Golgi membranes. *Current opinion in cell biology*, *62*, pp.104-113.

Reed, N.A., Cai, D., Blasius, T.L., Jih, G.T., Meyhofer, E., Gaertig, J. and Verhey, K.J., 2006. Microtubule acetylation promotes kinesin-1 binding and transport. *Current biology*, *16*(21), pp.2166-2172.

Reilein, A., Yamada, S. and Nelson, W.J., 2005. Self-organization of an acentrosomal microtubule network at the basal cortex of polarized epithelial cells. *The Journal of cell biology*, *171*(5), pp.845-855.

Riga, A., Castiglioni, V.G. and Boxem, M., 2020. New insights into apical-basal polarization in epithelia. *Current opinion in cell biology*, *62*, pp.1-8.

Robin, F., Van Gorp, A. and Véber, A., 2021. The role of mode switching in a population of actin polymers with constraints. *Journal of Mathematical Biology*, *82*(3), pp.1-43.

Román-Fernández, A. and Bryant, D.M., 2016. Complex polarity: building multicellular tissues through apical membrane traffic. *Traffic*, *17*(12), pp.1244-1261.

Roostalu, J. and Surrey, T., 2017. Microtubule nucleation: beyond the template. *Nature Reviews Molecular Cell Biology*, *18*(11), pp.702-710.

Roostalu, J., Thomas, C., Cade, N.I., Kunzelmann, S., Taylor, I.A. and Surrey, T., 2020. The speed of GTP hydrolysis determines GTP cap size and controls microtubule stability. *Elife*, *9*, p.e51992.

Ross, J.L., Ali, M.Y. and Warshaw, D.M., 2008. Cargo transport: molecular motors navigate a complex cytoskeleton. *Current opinion in cell biology*, *20*(1), pp.41-47.

Roth, D., Fitton, B.P., Chmel, N.P., Wasiluk, N. and Straube, A., 2019. Spatial positioning of EB family proteins at microtubule tips involves distinct nucleotide-dependent binding properties. *Journal of cell science*, *132*(4).

Rübsam, M., Mertz, A.F., Kubo, A., Marg, S., Jüngst, C., Goranci-Buzhala, G., Schauss, A.C., Horsley, V., Dufresne, E.R., Moser, M. and Ziegler, W., 2017. E-cadherin integrates mechanotransduction and EGFR signaling to control junctional tissue polarization and tight junction positioning. *Nature communications*, *8*(1), pp.1-16.

Ruch, T.R., Bryant, D.M., Mostov, K.E. and Engel, J.N., 2017. Par3 integrates Tiam1 and phosphatidylinositol 3-kinase signaling to change apical membrane identity. *Molecular biology of the cell*, *28*(2), pp.252-260.

Sanchez, A.D. and Feldman, J.L., 2017. Microtubule-organizing centers: from the centrosome to non-centrosomal sites. *Current opinion in cell biology*, *44*, pp.93-101.

Salisbury, J.L., Suino, K.M., Busby, R. and Springett, M., 2002. Centrin-2 is required for centriole duplication in mammalian cells. *Current Biology*, *12*(15), pp.1287-1292.

Salomon, J., Gaston, C., Magescas, J., Duvauchelle, B., Canioni, D., Sengmanivong, L., Mayeux, A., Michaux, G., Campeotto, F., Lemale, J. and Viala, J., 2017. Contractile forces at tricellular contacts modulate epithelial organization and monolayer integrity. *Nature communications*, *8*(1), pp.1-18.

Sato, T., Fujita, N., Yamada, A., Ooshio, T., Okamoto, R., Irie, K. and Takai, Y., 2006. Regulation of the assembly and adhesion activity of E-cadherin by nectin and afadin for the formation of adherens junctions in Madin-Darby canine kidney cells. *Journal of Biological Chemistry*, *281*(8), pp.5288-5299.

Schmidt, T.I., Kleylein-Sohn, J., Westendorf, J., Le Clech, M., Lavoie, S.B., Stierhof, Y.D. and Nigg, E.A., 2009. Control of centriole length by CPAP and CP110. *Current biology*, *19*(12), pp.1005-1011.

Schöckel, L., Möckel, M., Mayer, B., Boos, D. and Stemmann, O., 2011. Cleavage of cohesin rings coordinates the separation of centrioles and chromatids. *Nature cell biology*, *13*(8), pp.966-972.

Schroeder, T.E., 1973. Actin in dividing cells: contractile ring filaments bind heavy meromyosin. *Proceedings of the National Academy of Sciences*, *70*(6), pp.1688-1692.

Schumann, M., Günzel, D., Buergel, N., Richter, J.F., Troeger, H., May, C., Fromm, A., Sorgenfrei, D., Daum, S., Bojarski, C. and Heyman, M., 2012. Cell polarity-determining proteins Par-3 and PP-1 are involved in epithelial tight junction defects in coeliac disease. *Gut*, *61*(2), pp.220-228.

Scott, L.E., Griggs, L.A., Narayanan, V., Conway, D.E., Lemmon, C.A. and Weinberg, S.H., 2020. A hybrid model of intercellular tension and cell–matrix mechanical interactions in a multicellular geometry. *Biomechanics and modeling in mechanobiology*, pp.1-17.

Shahbazi, M.N., Megias, D., Epifano, C., Akhmanova, A., Gundersen, G.G., Fuchs, E. and Perez-Moreno, M., 2013. CLASP2 interacts with p120-catenin and governs microtubule dynamics at adherens junctions. *Journal of Cell Biology*, *203*(6), pp.1043-1061.

Simon, D.B., Lu, Y., Choate, K.A., Velazquez, H., Al-Sabban, E., Praga, M., Casari, G., Bettinelli, A., Colussi, G., Rodriguez-Soriano, J. and McCredie, D., 1999. Paracellin-1, a renal tight junction protein required for paracellular Mg2+ resorption. *Science*, *285*(5424), pp.103-106.

Sir, J.H., Pütz, M., Daly, O., Morrison, C.G., Dunning, M., Kilmartin, J.V. and Gergely, F., 2013. Loss of centrioles causes chromosomal instability in vertebrate somatic cells. *Journal of Cell Biology*, *203*(5), pp.747-756.

Sirajuddin, M., Rice, L.M. and Vale, R.D., 2014. Regulation of microtubule motors by tubulin isotypes and post-translational modifications. *Nature cell biology*, *16*(4), pp.335-344.

Slep, K.C., 2010. Structural and mechanistic insights into microtubule end-binding proteins. Current opinion in cell biology, 22(1), pp.88-95.

Snider, N.T. and Omary, M.B., 2014. Post-translational modifications of intermediate filament proteins: mechanisms and functions. *Nature reviews Molecular cell biology*, *15*(3), pp.163-177.

Sonnen, K.F., Gabryjonczyk, A.M., Anselm, E., Stierhof, Y.D. and Nigg, E.A., 2013. Human Cep192 and Cep152 cooperate in Plk4 recruitment and centriole duplication. *Journal of cell science*, *126*(14), pp.3223-3233.

Stehbens, S.J., Paterson, A.D., Crampton, M.S., Shewan, A.M., Ferguson, C., Akhmanova, A. and Parton, R.G., 2006. Dynamic microtubules regulate the local concentration of E-cadherin at cell-cell contacts. *Journal of cell science*, *119*(9), pp.1801-1811.

Svenson, I.K., Kloos, M.T., Jacon, A., Gallione, C., Horton, A.C., Pericak-Vance, M.A., Ehlers, M.D. and Marchuk, D.A., 2005. Subcellular localization of spastin: implications for the pathogenesis of hereditary spastic paraplegia. *Neurogenetics*, *6*(3), pp.135-141.

Takeda, Y., Kuroki, K., Chinen, T. and Kitagawa, D., 2020. Centrosomal and non-centrosomal functions emerged through eliminating centrosomes. *Cell structure and function*, *45*(1), pp.57-64.

Tanaka, N., Meng, W., Nagae, S. and Takeichi, M., 2012. Nezha/CAMSAP3 and CAMSAP2 cooperate in epithelial-specific organization of noncentrosomal microtubules. *Proceedings of the National Academy of Sciences*, *109*(49), pp.20029-20034.

Theys, J., Jutten, B., Habets, R., Paesmans, K., Groot, A.J., Lambin, P., Wouters, B.G., Lammering, G. and Vooijs, M., 2011. E-Cadherin loss associated with EMT promotes radioresistance in human tumor cells. *Radiotherapy and oncology*, *99*(3), pp.392-397.

Thiery, J.P., Acloque, H., Huang, R.Y. and Nieto, M.A., 2009. Epithelial-mesenchymal transitions in development and disease. *cell*, *139*(5), pp.871-890.

Thomas, M., Burgio, G., Adams, D.J. and Iyer, V., 2019. Collateral damage and CRISPR genome editing. *PLoS genetics*, *15*(3), p.e1007994.

Tillery, M.M., Blake-Hedges, C., Zheng, Y., Buchwalter, R.A. and Megraw, T.L., 2018. Centrosomal and non-centrosomal microtubule-organizing centers (MTOCs) in Drosophila melanogaster. *Cells*, *7*(9), p.121.

Toya, M., Kobayashi, S., Kawasaki, M., Shioi, G., Kaneko, M., Ishiuchi, T., Misaki, K., Meng, W. and Takeichi, M., 2016. CAMSAP3 orients the apical-to-basal polarity of microtubule arrays in epithelial cells. *Proceedings of the National Academy of Sciences*, *113*(2), pp.332-337.

Toya, M. and Takeichi, M., 2016. Organization of non-centrosomal microtubules in epithelial cells. *Cell structure and function*, p.16015.

Tran, A.D.A., Marmo, T.P., Salam, A.A., Che, S., Finkelstein, E., Kabarriti, R., Xenias, H.S., Mazitschek, R., Hubbert, C., Kawaguchi, Y. and Sheetz, M.P., 2007. HDAC6 deacetylation of tubulin modulates dynamics of cellular adhesions. *Journal of cell science*, *120*(8), pp.1469-1479.

Turner, C.M. and Adler, P.N., 1998. Distinct roles for the actin and microtubule cytoskeletons in the morphogenesis of epidermal hairs during wing development in Drosophila. *Mechanisms of development*, *70*(1-2), pp.181-192.

Uetake, Y., Loncarek, J., Nordberg, J.J., English, C.N., La Terra, S., Khodjakov, A. and Sluder, G., 2007. Cell cycle progression and de novo centriole assembly after centrosomal removal in untransformed human cells. *The Journal of cell biology*, *176*(2), pp.173-182.

Vaart, B.V.D., Akhmanova, A. and Straube, A., 2009. Regulation of microtubule dynamic instability. *Biochemical Society Transactions*, *37*(5), pp.1007-1013.

van Breugel, M., Hirono, M., Andreeva, A., Yanagisawa, H.A., Yamaguchi, S., Nakazawa, Y., Morgner, N., Petrovich, M., Ebong, I.O., Robinson, C.V. and Johnson, C.M., 2011. Structures of SAS-6 suggest its organization in centrioles. *Science*, *331*(6021), pp.1196-1199.

Van Dijk, J., Rogowski, K., Miro, J., Lacroix, B., Eddé, B. and Janke, C., 2007. A targeted multienzyme mechanism for selective microtubule polyglutamylation. *Molecular cell*, *26*(3), pp.437-448.

van Haren, J., Charafeddine, R.A., Ettinger, A., Wang, H., Hahn, K.M. and Wittmann, T., 2018. Local control of intracellular microtubule dynamics by EB1 photodissociation. *Nature cell biology*, *20*(3), pp.252-261.

van Leen, E.V., Di Pietro, F. and Bellaïche, Y., 2020. Oriented cell divisions in epithelia: from force generation to force anisotropy by tension, shape and vertices. *Current opinion in cell biology*, *62*, pp.9-16.

Vasileva, E. and Citi, S., 2018. The role of microtubules in the regulation of epithelial junctions. *Tissue barriers*, *6*(3), p.1539596.

Verhey, K.J. and Hammond, J.W., 2009. Traffic control: regulation of kinesin motors. *Nature reviews Molecular cell biology*, *10*(11), pp.765-777.

Vicente-Manzanares, M., Webb, D.J. and Horwitz, A.R., 2005. Cell migration at a glance. Journal of cell science, 118(21), pp.4917-4919.

Vitre, B., Coquelle, F.M., Heichette, C., Garnier, C., Chrétien, D. and Arnal, I., 2008. EB1 regulates microtubule dynamics and tubulin sheet closure in vitro. *Nature cell biology*, *10*(4), pp.415-421.

Wall, K., Bobak, T., Tilden, S., Hawkins, T. and Hough, L., 2018. Effects of tubulin post-translational modification on microtubule bending rigidity and C-terminal tails. In *APS March Meeting Abstracts* (Vol. 2018, pp. F51-007).

Wang, X., Nie, J., Zhou, Q., Liu, W., Zhu, F., Chen, W., Mao, H., Luo, N., Dong, X. and Yu, X., 2008. Downregulation of Par-3 expression and disruption of Par complex integrity by TGF-β during the process of epithelial to mesenchymal transition in rat proximal epithelial cells. *Biochimica et Biophysica Acta (BBA)-Molecular Basis of Disease*, *1782*(1), pp.51-59.

Wang, J., Xu, H., Jiang, Y., Takahashi, M., Takeichi, M. and Meng, W., 2017. CAMSAP3-dependent microtubule dynamics regulates Golgi assembly in epithelial cells. *Journal of Genetics and Genomics*, *44*(1), pp.39-49.

Wang, X., Xu, Z., Tian, Z., Zhang, X., Xu, D., Li, Q., Zhang, J. and Wang, T., 2017. The EF-1α promoter maintains high-level transgene expression from episomal vectors in transfected CHO-K1 cells. *Journal of cellular and molecular medicine*, *21*(11), pp.3044-3054.

Watanabe, T., Noritake, J., Kakeno, M., Matsui, T., Harada, T., Wang, S., Itoh, N., Sato, K., Matsuzawa, K., Iwamatsu, A. and Galjart, N., 2009. Phosphorylation of CLASP2 by GSK-3β regulates its interaction with IQGAP1, EB1 and microtubules. Journal of cell science, 122(16), pp.2969-2979.

Watanabe, T., Wang, S., Noritake, J., Sato, K., Fukata, M., Takefuji, M., Nakagawa, M., Izumi, N., Akiyama, T. and Kaibuchi, K., 2004. Interaction with IQGAP1 links APC to Rac1, Cdc42, and actin filaments during cell polarization and migration. *Developmental cell*, *7*(6), pp.871-883.

Wehrle-Haller, B., 2012. Structure and function of focal adhesions. *Current opinion in cell biology*, *24*(1), pp.116-124.

Weng, M. and Wieschaus, E., 2017. Polarity protein Par3/Bazooka follows myosin-dependent junction repositioning. *Developmental biology*, *422*(2), pp.125-134.

Weterings, E. and Chen, D.J., 2008. The endless tale of non-homologous end-joining. *Cell research*, *18*(1), pp.114-124.

Werner, S., Pimenta-Marques, A. and Bettencourt-Dias, M., 2017. Maintaining centrosomes and cilia. *Journal of cell science*, *130*(22), pp.3789-3800.

Wieczorek, M., Urnavicius, L., Ti, S.C., Molloy, K.R., Chait, B.T. and Kapoor, T.M., 2020. Asymmetric molecular architecture of the human γ-tubulin ring complex. *Cell*, *180*(1), pp.165-175.

Wong, Y.L., Anzola, J.V., Davis, R.L., Yoon, M., Motamedi, A., Kroll, A., Seo, C.P., Hsia, J.E., Kim, S.K., Mitchell, J.W. and Mitchell, B.J., 2015. Reversible centriole depletion with an inhibitor of Polo-like kinase 4. *Science*, *348*(6239), pp.1155-1160.

Wu, J., De Heus, C., Liu, Q., Bouchet, B.P., Noordstra, I., Jiang, K., Hua, S., Martin, M., Yang, C., Grigoriev, I. and Katrukha, E.A., 2016. Molecular pathway of microtubule organization at the Golgi apparatus. *Developmental cell*, *39*(1), pp.44-60.

Xu, G.K., Liu, Y. and Li, B., 2015. How do changes at the cell level affect the mechanical properties of epithelial monolayers?. *Soft Matter*, *11*(45), pp.8782-8788.

Xu, Z., Schaedel, L., Portran, D., Aguilar, A., Gaillard, J., Marinkovich, M.P., Théry, M. and Nachury, M.V., 2017. Microtubules acquire resistance from mechanical breakage through intralumenal acetylation. *Science*, *356*(6335), pp.328-332.

Xue, B., Krishnamurthy, K., Allred, D.C. and Muthuswamy, S.K., 2013. Loss of Par3 promotes breast cancer metastasis by compromising cell–cell cohesion. *Nature cell biology*, *15*(2), pp.189-200.

Yamada, T., Kuramitsu, K., Rikitsu, E., Kurita, S., Ikeda, W. and Takai, Y., 2013. Nectin and junctional adhesion molecule are critical cell adhesion molecules for the apico-basal alignment of adherens and tight junctions in epithelial cells. *Genes to Cells*, *18*(11), pp.985-998.

Yamaguchi, H. and Condeelis, J., 2007. Regulation of the actin cytoskeleton in cancer cell migration and invasion. Biochimica et Biophysica Acta (BBA)-Molecular Cell Research, 1773(5), pp.642-652.

Yang, C., Wu, J., De Heus, C., Grigoriev, I., Liv, N., Yao, Y., Smal, I., Meijering, E., Klumperman, J., Qi, R.Z. and Akhmanova, A., 2017. EB1 and EB3 regulate microtubule minus end organization and Golgi morphology. *Journal of Cell Biology*, *216*(10), pp.3179-3198.

Yang, Z., Zimmerman, S., Brakeman, P.R., Beaudoin, G.M., Reichardt, L.F. and Marciano, D.K., 2013. De novo lumen formation and elongation in the developing nephron: a central role for afadin in apical polarity. *Development*, *140*(8), pp.1774-1784.

Yin, H., Song, C.Q., Dorkin, J.R., Zhu, L.J., Li, Y., Wu, Q., Park, A., Yang, J., Suresh, S., Bizhanova, A. and Gupta, A., 2016. Therapeutic genome editing by combined viral and non-viral delivery of CRISPR system components in vivo. *Nature biotechnology*, *34*(3), pp.328-333.

Yue, J., Xie, M., Gou, X., Lee, P., Schneider, M. and Wu, X. (2014). Microtubules Regulate Focal Adhesion Dynamics through MAP4K4. Developmental Cell, 31(5), pp.572-85.

Zanic, M., Stear, J.H., Hyman, A.A. and Howard, J., 2009. EB1 recognizes the nucleotide state of tubulin in the microtubule lattice. *PloS one*, *4*(10), p.e7585.

Zanic, M., Widlund, P.O., Hyman, A.A. and Howard, J., 2013. Synergy between XMAP215 and EB1 increases microtubule growth rates to physiological levels. *Nature cell biology*, *15*(6), pp.688-693.

Zenker, J., White, M.D., Templin, R.M., Parton, R.G., Thorn-Seshold, O., Bissiere, S. and Plachta, N., 2017. A microtubule-organizing center directing intracellular transport in the early mouse embryo. *Science*, *357*(6354), pp.925-928.

Zhang, D., Grode, K.D., Stewman, S.F., Diaz-Valencia, J.D., Liebling, E., Rath, U., Riera, T., Currie, J.D., Buster, D.W., Asenjo, A.B. and Sosa, H.J., 2011. Drosophila katanin is a microtubule depolymerase that regulates cortical-microtubule plus-end interactions and cell migration. *Nature cell biology*, *13*(4), pp.361-369.

Zhong, F., Li, Y, Xu., Sun, B., Wang., J, Yang, L. 2021. EB2 promotes hepatocellular carcinoma proliferation and metastasis via MAPK/ERK pathway by modulating microtubule dynamics. Clin Sci (Lond) 2021; CS20201500. doi: https://doi.org/10.1042/CS20201500

Zilberman, Y., Ballestrem, C., Carramusa, L., Mazitschek, R., Khochbin, S. and Bershadsky, A., 2009. Regulation of microtubule dynamics by inhibition of the tubulin deacetylase HDAC6. *Journal of cell science*, *122*(19), pp.3531-3541.

Zimmerman, W.C., Sillibourne, J., Rosa, J. and Doxsey, S.J., 2004. Mitosis-specific anchoring of γ tubulin complexes by pericentrin controls spindle organization and mitotic entry. *Molecular biology of the cell*, *15*(8), pp.3642-365